Vacuolar chloride transport in the extreme halophyte *Mesembryanthemum crystallinum*

Frank Wissing

Wolfson College

Thesis submitted for the degree of D.Phil.

Hilary Term 1999



Vacuolar chloride transport in the extreme halophyte *Mesembryanthemum crystallinum*

Frank Wissing, Wolfson College

Abstract of a thesis submitted for the degree of D.Phil., Hilary Term 1999

The halophyte *Mesembryanthemum crystallinum* L. accumulates high concentrations of NaCl (up to 1 M) in its leaf cells as a response to soil salinity. While there is evidence that vacuolar sodium transport is mediated by a tonoplast Na^+/H^+ antiporter (Barkla *et al.*, 1995), little is known about the transport of Cl^- into the vacuole. So far, it has been uncertain whether secondary active transport (e.g. H^+/Cl^- antiporter) is involved or whether a passive mechanism (Cl^- channel) is sufficient to mediate Cl^- accumulation in the vacuole of *M. crystallinum*.

This thesis describes the use of tonoplast vesicles from leaf mesophyll cells of *M. crystallinum* to study vacuolar Cl^- transport. Cl^- uptake into the vesicles was measured using the Cl^--sensitive fluorescent dye lucigenin (*N,N'*-dimethyl-9,9'-bisacridinium dinitrate). This work was complemented by a patch-clamp study of ionic currents of leaf-mesophyll vacuoles from *M. crystallinum*.

Cl^- transport into tonoplast vesicles showed saturation-type kinetics with an apparent K_m between 10 and 36 mM and a maximum initial change of the intravesicular Cl^- concentration of 4.8 mM min^{-1}, corresponding to an estimated Cl^- flux of 31 nmol m^2 s^{-1}. Vacuolar chloride transport was not affected by sulphate, malate, or nitrate, indicating a high specificity of this transport process for chloride over other anions. By imposing inside-positive membrane potentials using a K^+/valinomycin clamp revealed a sigmoidal voltage-dependent relationship with the steepest increase in vacuolar Cl^- uptake around +30 mV. Only under severe salt treatment with 500 mM NaCl for 3 weeks did 9-week-old *M. crystallinum* plants show a significant increase (63%) of vacuolar Cl^- uptake, along with an increased V-type H^+-ATPase hydrolytic activity (up to 65%). The apparent K_m of vacuolar Cl^- uptake was also increased from 27 mM to 44 mM under these conditions.

An inside-acid pH gradient, generated by a K^+/nigericin clamp, reduced the initial rate of chloride transport into tonoplast vesicles of *M. crystallinum*. External Cl^-, in contrast to external Na^+, did not dissipate an inside-acidic ΔpH generated by various techniques. This is strong evidence against a proton-driven antiport mechanism.

The patch-clamp study of ionic currents of whole vacuoles and excised vacuolar membrane patches from *M. crystallinum* leaf-mesophyll cells revealed a number of cation channels. At cytosolic free Ca^{2+} concentrations of 1 µM and above, ubiquitous slow-vacuolar type cation currents could be observed. In excised patches, eleven different single channel types, with conductances ranging from 2 up to 200 pS, could be described. However, no clear Cl^- conductance could be identified. The lack of observed vacuolar Cl^- channel activities is discussed in the light of possible lack of Cl^--channel activation due to the loss of a cytosolic factor.

The results obtained from the biochemical work on tonoplast vesicles support the hypothesis that a passive transport mechanism (i.e. channel) is sufficient to mediate vacuolar chloride transport in *M. crystallinum*. The observed upregulation of vacuolar Cl^- transport under severe salt stress shows that it plays an important role in the salt adaptation of this halophytic plant.

Acknowledgements

I would like to thank my supervisor Prof. J.A.C. Smith (Department of Plant Sciences, University of Oxford) for his support, the fruitful discussions and the nights he spent reading my thesis. I would also like to thank my second supervisor Dr C.A.R. Boyd (Department of Human Anatomy, University of Oxford) for his very knowledgeable support.

I big "Thank you!" goes to all of my colleagues for their advice, assistance and the never ending tea breaks: Paul Bailey, Dolores Bartholomew, Chris Cheffings, Renato Coelho, Anna Edwards-Stuart, Vicky Evetts, Emmanuelle Gratia, Fran Harper, Joe Holtum, Karin Köhl, Ute Krämer, Rachel Leighton, Andreas Meyer, Vakkas Tekin and Miltos Tsiantis. Special thanks go to Fran Harper for her time and enthusiasm to discuss my work and for the occasional skive to do some bird watching.

This list would certainly not be complete without all those who gave me excellent technical assistance in the department: I would like to thank Vakkas Tekin and Cristine Surman for their help to keep my ice plants happy. I would also like to acknowledge Doug Morris, Tony Probitts and all other members of the departmental workshop for their very skilled and swift support.

I am very grateful to Anna Amtmann (Department of Biology, University of York) for discussing my work and the time she spent to introduce me into the secrets of the patch-clamp technique. I would also like to thank Christoph Korbmacher (Department of Physiology, University of Oxford) and his lab for their help and support with the electrophysiology. For assistance with the electron microscopy I am indebted to Prof. J. Morris (Department of Human Anatomy, University of Oxford).

This work would not have been possible without the funding from the BBSRC, the Gottlieb-Daimler und Karl-Benz Stiftung, Ladenburg, Germany, and the generosity of the EPA-Cephalosporin Fund, Oxford. I am very grateful for their non-bureaucratic support.

Finally I would like to thank my wife Andrea and my daughters Lily and Hannah for their love, patience and support at all times. I am also very grateful to my parents for their encouragement and for supporting my move to Oxford.

Contents

Abstract 1

Acknowledgements 3

Contents 4

Abbreviations 8

Chapter 1 Introduction 11

1.1 Aim of thesis 11

1.2 The physiology of salt tolerance in halophytic plants 12

1.2.1 General overview 12

1.2.2 The role of vacuolar ion transport in salt tolerance 15

1.2.3 The halophyte *Mesembryanthemum crystallinum* as a model for studying salt tolerance 17

1.3 Methods for studying Cl^- transport 22

1.4 Cl^- transport in plants 26

1.4.1 Active Cl^- transport in plants 26

1.4.2 Plant Cl^- channels 28

1.4.2.1 Cl^- channels in the plasma membrane 29

1.4.2.2 Cl^- channels in the vacuolar membrane 35

1.4.2.3 Anion channels in other organelles 39

1.5 Cl^- channels in other systems 40

1.6 Structure of thesis 42

Chapter 2 Materials and methods 43

2.1 Materials 43

2.1.1 Chemicals 43

2.1.2 Plant material 43

2.2 Tonoplast vesicles 44
2.2.1 Isolation of tonoplast vesicles 44
2.2.2 Protein assays 45
2.2.3 H^+-ATPase hydrolytic activity assays 46
2.2.4 Electron microscopy 46
2.3 Fluorescence quenching studies 47
2.3.1 Dye loading of tonoplast vesicles 47
2.3.2 Measurements of the initial Cl^- transport 48
2.3.3 Calculating the initial Cl^- transport rate 50
2.4 Generating a $\Delta\psi$ 51
2.4.1 Oxonol-V fluorescence studies 51
2.5 Proton gradient experiments 52
2.5.1 K^+/nigericin clamp 52
2.5.2 pH-jump experiments 53
2.5.3 Energisation *via* the vacuolar H^+-ATPase 53
2.5.4 Measuring the ΔpH using BCECF 53
2.6 Inhibitor studies 55
2.7 Patch-clamp studies 55
2.7.1 Isolation of mesophyll protoplasts 55
2.7.2 Electrophysiological recordings 56
2.7.3 Recording solutions 58

Chapter 3 Properties of the Cl^- indicators and tonoplast vesicles 59

3.1 Introduction 59
3.2 Results 59
3.2.1 Properties of SPQ 59
3.2.2 Characterisation of the fluorescent dye lucigenin 60
3.2.2.1 Spectral properties 61
3.2.2.2 Sensitivity and specificity 61
3.2.2.3 Effect of pH 63

3.2.3 General properties of tonoplast vesicles of *M. crystallinum* 64
3.2.3.1 Hydrolytic H^+-ATPase activity as a marker for tonoplast membrane 64
3.2.3.2 Vesicle size 66
3.3 Discussion 67
3.3.1 Lucigenin as a Cl^- indicator 67
3.3.2 The vesicle preparation 70

Chapter 4 Chloride transport into tonoplast vesicles studied using lucigenin 73

4.1 Introduction 73
4.2 Results 74
4.2.1 Cl^- transport shows saturation kinetics 74
4.2.2 Voltage dependence of vacuolar Cl^- transport 76
4.2.2.1 Validity of the K^+/valinomycin clamp 77
4.2.2.2 Cl^- transport under varying membrane potentials 78
4.2.3 Inhibition of the vacuolar Cl^- transport 79
4.2.4 Selectivity of the vacuolar Cl^--transport system 83
4.2.5 Vacuolar Cl^- transport under salt stress 84
4.3 Discussion 88

Chapter 5 Testing for active Cl^- transport in tonoplast vesicles 101

5.1 Introduction 101
5.2 Results 102
5.2.1 Effect of ATP on Cl^- uptake in tonoplast vesicles 102
5.2.2 pH-jump experiments 102
5.2.3 Forming a ΔpH using the K^+/nigericin clamp 104
5.2.3.1 Validity and calibration of the K^+/nigericin clamp 105
5.2.3.2 No dissipation of the ΔpH by Cl^- 107
5.2.3.3 Effect of ΔpH on Cl^- transport 108

5.2.4 Energising vesicles using vacuolar H^+-ATPase pump activity 109

5.3 Discussion 111

Chapter 6 Electrophysiological studies of vacuolar ion currents 117

6.1 Introduction 117

6.2 Results 119

6.2.1 Patch-clamping large vacuoles of

Mesembryanthemum crystallinum 119

6.2.2 Recordings in KCl-based solutions 122

6.2.2.1 Macropatch recordings with high cytosolic Ca^{2+} 122

6.2.2.2 Single channels with high cytosolic free Ca^{2+} 125

6.2.2.3 Whole-vacuole recordings with 1 μM free cytosolic Ca^{2+} 129

6.2.2.4 Whole-vacuolar-current oscillations observed

with 1 μM free Ca^{2+} 130

6.2.2.5 Single channels with 1 μM cytosolic free Ca^{2+} 134

6.2.2.6 Recordings with 100 nM cytosolic Ca^{2+} 138

6.2.3 Patch-clamp recordings with NMDG-Cl-based solutions 140

6.3 Discussion 142

Chapter 7 General discussion 153

References 160

Abbreviations

9-AC	anthracene-9-carboxylic acid
ABC-transporter	ATP-binding-cassette (transporter)
ATP	adenosine 5'-triphosphate
ATPase	adenosine 5'-triphosphatase
BCECF	2',7'-bis-(2-carboxyethyl)-5-(6)-carboxyfluorescein
BSA	bovine serum albumin
BTP	1,3-bis[tris(hydroxymethyl)methylamino]propane
Bumetamide	3-[aminosulphonyl]-5-[butylamino]-4-phenoxybenzoic acid
C_3	plants in which the first product of photosynthesis is a 3-carbon compound
CAM	crassulacean acid metabolism
cAMP	adenosine 3',5' cyclic-monophosphate
CDPK	Ca^{2+}-activated protein kinase
CFTR	cystic fibrosis transmembrane conductance regulator
ClC	chloride channel family
C_m	membrane capacitance
co	cytosolic-side-out
DIDS	4,4'-di*iso*thiocyanatostilbene-2,2'-disulphonic acid
DIOA	R(+)-[(2-*n*-butyl-6,7-dichloro-2-cycolpentyl-2,3-dihydro-1-oxo-1H-inden-5-yl)oxy]acetic acid
DMSO	dimethylsulphoxide
DNDS	4,4'-dinitrostilbene-2,2'-disulphonic acid
DTT	dithiothreitol
EDTA	ethylenediaminetetraacetate
EGTA	ethylene glycol-bis(β-aminoethylether)-*N,N,N',N'*-tetraacetic acid
E	electrical potential
$E_{K,Cl,Ca}$	Nernst potentials for K^+, Cl^-, or Ca^{2+}
F	fluorescence intensity (or Faraday constant when indicated)
F_0	fluorescence intensity without quenching ion
$F_{external}$	external fluorescence intensity
F_{in}	intravesicular fluorescence intensity
Furosemide	5-[aminosulphonyl]-4-chloro-2[{furanylmethyl}-amino]benzoic acid

FV	fast-activating vacuolar (channel)
g	acceleration due to gravity
GCAC1	guard cell anion channel 1
GEF1	glycerol/ethanol Fe-requiring yeast mutant
GHK	Goldman-Hodgkin-Katz
Hepes	*N*-[2-hydroxethyl]piperazine-*N*'-[2-ethanesulphonic acid]
I	current amplitude
k	Boltzmann constant
K_m	Michaelis-Menten constant
KS	K^+ conducting "sleeper" (channel)
K_{SV}	Stern-Volmer constant
KVI	voltage independent K^+ (channel)
KVIH	voltage independent K^+ (channel) at high cytosolic $[Ca^{2+}]$
LOR	Large outward rectifying (channel)
Lucigenin	*N,N*'-dimethyl-9,9'-bisacridinium dinitrate
Mes	2-[*N*-morpholino]ethanesulphonic acid
Mops	3-[*N*-morpholino]propanesulphonic acid
N-EM	*N*-ethylmaleimide
NPPB	5-nitro-2-(3-phenylpropylamino)benzoic acid
ORH	Outward rectifying channel at high cytosolic $[Ca^{2+}]$
Oxonol-V	bis-(3-phenyl-5-oxo*iso*oxazol-4-yl)pentamethine oxonol
ψ	electrochemical potential
P	probability OR permeability with a subscript assigning ion
*p*CMBS	*p*-chloromercuribenzene sulphonate
pH	negative logarithm of the proton concentration
PKA	protein kinase A
pK_a	pH of half dissociation of an acid
PP_i	inorganic pyrophosphate
PPase	pyrophosphatase
PVP-40	polyvinylpyrrolidone (molecular weight 40 000)
Pyranine	8-hydroxypyrene-1,3,6-trisulphonic acid
Quinacrine	6-chloro-9-[(4-diethylamino)-1-methylbutyl]amino-2-methoxyacridine dihydrochloride

R	gas constant (or fluorescence ratio where indicated)
R-type	rapid-type (guard-cell anion-channel)
R_a	access resistance (resistance of the measuring electrode)
R_m	membrane resistance
R_s	series resistance (sum of all resistances in series with R_m)
R_{total}	total resistance ($R_{total} = R_m + R_s$)
s.e.m.	standard error of mean
S-type	slow-type (guard-cell anion-channel)
SITS	4-acetamido-4'-*iso*thiocyanatostilbene-2,2'-disulphonic acid
SPQ	6-methoxy-*N*-(3-sulphopropyl)quinolinium
SV	slow-activating vacuolar (channel)
T	absolute temperature
t	time
τ	time constant
Tricine	*N*-[2-hydroxy-1,1-bis(hydroxymethyl)ethyl]glycine
Tris	tris(hydroxymethyl)aminoethane
V	voltage
$V_{½}$	voltage of half-maximal activation
V-ATPase	V-type ATPase
VK	vacuolar K^+ (channel)
V_{max}	maximal velocity
vo	vacuolar-side-out
v/v	volume per volume
wv	whole vacuole
w/v	weight per volume
z	charge of an ion

Chapter 1

Introduction

1.1 Aim of thesis

Under salt stress, *Mesembryanthemum crystallinum* L. is known to accumulate up to 1 M NaCl within the cell, with 95 to 99% of the cell volume being occupied by the vacuole (Adams *et al.*, 1998). Therefore, most of the NaCl will be found in the vacuole. The aim of this work was to characterise the vacuolar Cl^- uptake mechanism in leaf mesophyll cells of *Mesembryanthemum crystallinum*. Of particular physiological interest is the question whether passive transport would be sufficient, or whether active transport is required, to explain the accumulation of vacuolar Cl^- concentrations of around 700 mM in mesophyll cells and up to 1 M in epidermal bladder cells *in vivo*.

No attempts have been made so far to characterise vacuolar Cl^- transport in *M. crystallinum*, and studies of vacuolar Cl^- transport in other plants are also rare. In the present work, Cl^- uptake into tonoplast vesicles from *M. crystallinum* was studied directly using the Cl^--sensitive fluorescent dye lucigenin. Since this is the first use of lucigenin in a Cl^--transport study on plants, the methodology had to be adapted for this use and was critically assessed. Using the lucigenin-based biochemical assay, vacuolar Cl^- uptake was characterised, with special emphasis on the question of passive *versus* active transport. This work was complemented by electrophysiological studies on whole vacuoles and excised tonoplast patches in order to detect vacuolar Cl^- currents and single Cl^- channels. Since the activities of vacuolar transport systems for H^+ and

Na^+ are upregulated under salt stress in *M. crystallinum* (Barkla *et al.*, 1995; Tsiantis *et al.*, 1996), the effect of growing plants under high salt conditions on vacuolar Cl^- uptake was tested.

This characterisation of vacuolar Cl^- transport in the extreme halophyte *M. crystallinum* and in particular the determination of its energisation and regulation under salt stress was intended to provide insight into the role of vacuolar Cl^- transport in salt tolerance in plants.

1.2 The physiology of salt tolerance in halophytic plants

1.2.1 General overview

Excess salinity is one of the most common causes of reduction in plant growth (O'Leary, 1985). Although many areas of the world are naturally saline, salt build-up frequently occurs in irrigated soils as a result of high rates of evapotranspiration of water which leaves behind residual mineral ions. It is estimated that as much as one-third of all irrigated agricultural land suffers from an accumulation of salts sufficient to impair plant growth (Hall, 1976).

Salinity has several adverse effects on plants that lead to growth reduction or death:

- High concentrations of NaCl are toxic to many metabolic processes
- High solute concentrations lower soil water potential, thereby impairing water uptake into the plant
- Competitive inhibition of uptake of essential nutrients can occur, e.g. Na^+ may inhibit K^+ uptake

- Soil structure can be degraded by salt crystals sticking soil particles together

Most plants, including many crops, are highly sensitive towards soil salinity and are sometimes called glycophytes. However, a number of plants, known as halophytes, have evolved the ability to grow on naturally saline soils. These plants could therefore be very useful models for understanding the cellular and molecular basis of salt tolerance.

A number of physiological and morphological adaptations can be found in various halophytes that appear to play a role in salt tolerance (extended from Crawford, 1989):

- Exclusion of NaCl from the root
- Highly specific uptake of essential ions
- Excretion of excess NaCl from tissue by special organs (salt glands)
- Succulence to lower salt concentrations in the tissue by dilution
- Passive removal of NaCl, e.g. shedding of leaves with high salt content
- Synthesis of cytoplasmic compatible solutes
- Intracellular compartments with different NaCl concentrations

Often several, but not all, of these mechanisms can be found in one species, along with further adaptations. Some mangroves and grasses, such as salt-tolerant *Puccinella* species, maintain relatively low salt concentrations (albeit still slightly above soil concentrations) in the tissue by actively pumping Na^+ out of the xylem, as well as by maintaining a highly impermeable double epidermis (Greenway and Munns, 1980). In parallel, K^+ is selectively taken up *via* active transport, thereby maintaining a high K^+/Na^+ ratio (Yeo, 1998).

Excretion of salt from specialised glands in the shoot is found in a number of plant families. Specialised trichomes, such as in *Atriplex*, accumulate Na^+, and to a lesser extent Cl^-, to high concentrations until the cells rupture and release excess ions from the plant. Many dicotyledonous halophytes, especially those that do not possess salt-excreting organs, show some degree of succulence. For example, in *Mesembryanthemum crystallinum* the parenchymatous mesophyll cells increase in volume with increasing salinity, with the vacuole occupying more than 90% of the total cell volume. Additionally, the intracellular spaces are very small, besides other morphological changes (Adams *et al.*, 1998). The succulence not only reduces the surface area to volume ratio of the shoot, thereby lowering water loss, but also dilutes vacuolar NaCl concentrations.

Fast-growing tissue might be less affected by salinity, due to its rapidly expanding volume accommodating for the influx of NaCl (Munns, 1993). In fully expanded tissues however, continued salt influx leads to a build-up of salt, which eventually becomes toxic. This is particularly important for perennial species. Shedding of mature leaves with high salt contents, especially in autumn, leads to passive removal of excess salt from the plants.

Most salt-tolerant species show accumulation of organic osmolytes with salinity. These compatible solutes, such as sugars or polyols, are responsible for the osmotic balance of the cytoplasm while being compatible with the cell's metabolism. Other compatible solutes, such as the zwitterionic glycine-betaine, have additional protein-stabilising functions under dehydration stress (Yeo, 1998). It has also been suggested that another function of osmolyte accumulation under salt stress is to

provide increased buffering capacity of the intracellular redox potential (Hare *et al.*, 1998).

A number of studies has shown that most metabolic enzymes of halophytes are not intrinsically more salt tolerant than their glycophytic counterparts (Flowers *et al.*, 1977). Concentrations of NaCl above 100 to 200 mM inhibit many metabolic functions, so low cytosolic NaCl concentrations need to be maintained *via* ion compartmentation (Munns, 1993; Flowers and Yeo, 1995). NaCl is predominantly sequestered in the vacuolar lumen, which takes up most of the total cell volume in succulent halophytes. In the cytoplasm, where most metabolic processes take place, much lower NaCl concentrations are maintained, and the osmotic balance is, at least partly, maintained by compatible solutes (Bohnert *et al.*, 1995; Hare *et al.*, 1998). Reliable measurements on intracellular NaCl compartmentation in halophytes are sparse. Under salt stress, cytoplasmic NaCl concentrations are estimated to be 150 mM or less, while the vacuolar concentrations can reach 500 mM to 1000 mM (Munns, 1993; Yeo, 1998). To accomplish this compartmentation, efficient transport of Na^+ and Cl^- out of the cytoplasm is essential.

1.2.2 The role of vacuolar ion transport in salt tolerance

An essential mechanism of salt tolerance in many halophytes is the ability to compartmentalise NaCl within the cell. Transport of NaCl from the cytoplasm into the vacuole therefore has to be efficient and NaCl has to be retained in the vacuole to allow accumulation.

According to current models, ion accumulation in the central vacuole of plant cells is primarily energised by two inwardly directed H^+ pumps at the vacuolar

membrane: an H^+-ATPase, and an H^+-PPase (Rea and Sanders, 1987; Yamashita *et al.*, 1994; Ayala *et al.*, 1996; Rausch *et al.*, 1996; Davies, 1997). These pumps generate an inside-acid pH and an electrical potential difference (cytosolic-side-negative) across the vacuolar membrane [according to Bertl *et al.* (1992), tonoplast membrane potentials are measured as the potential on the cytoplasmic side with reference to the vacuolar side]. This electrochemical gradient can be used to drive the transport of other solutes into the vacuole *via* other transport proteins. The H^+ gradient is utilised by the Na^+/H^+ antiporter, accumulating Na^+ in the vacuole against its electrochemical gradient. Under salt stress, both H^+-pump activity and Na^+/H^+-antiport activity are enhanced in many species (Barkla *et al.*, 1995; Wilson and Shannon, 1995; Rausch *et al.*, 1996; Ballesteros *et al.*, 1997). However, while the V-ATPase plays a dominant role in older tissues, H^+-PPase activities are generally much higher in developing tissues, and might therefore play only a small role in the adaptation to salt stress in mature leaves (Bremberger and Lüttge, 1992; Davies, 1997).

While Na^+ is transported against its electrochemical gradient *via* a secondary active mechanism, vacuolar Cl^- influx could be mediated by passive flux through anion-selective channels (Kaestner and Sze, 1987; Pope and Leigh, 1987). Hence, Cl^- would be equilibrated across the tonoplast according to its electrochemical potential.

But as yet the corresponding pathway for Cl^- transport into the vacuole remains unknown. The current lack of precise thermodynamic data leaves the question open to whether chloride transport (in contrast to sodium transport) is energetically downhill, which would make a channel mechanism plausible. Since sodium and chloride tend to accumulate in the vacuole of halophytes in approximately equal

amounts (Binzel *et al.*, 1988; Hajibagheri and Flowers, 1989; Adams *et al.*, 1998), such an electrogenic Cl^--transport system would play a very important role in maintaining charge balance. On the other hand, if the intracellular distribution of Cl^- is far from its thermodynamic equilibrium, an active Cl^--pump or a H^+/Cl^- antiport mechanism has to be postulated.

1.2.3 The halophyte *Mesembryanthemum crystallinum* as a model for studying salt tolerance

The common ice plant, *Mesembryanthemum crystallinum* L. (Aizoaceae), has become well established as a model system for studies of salt tolerance in higher plants. Furthermore, this species shows a drought-induced shift from C_3 photosynthesis to crassulacean acid metabolism (CAM) that has been extensively studied (Winter, 1973; Adams *et al.*, 1992; Lüttge, 1993; Adams *et al.*, 1998). *M. crystallinum* is native to coastal areas of southern and eastern Africa, and has been introduced into many other parts of Africa, North and South America, Western Australia and the Mediterranean (Adams *et al.*, 1998).

According to Adams *et al.* (1998), five distinct growth phases describe the life cycle of the individual plant:

(1) In its native habitat, the seeds germinate after a short rain season. In the germination phase, while only cotelydons are present, CAM is not inducible.

(2) Seven leaf pairs develop along the primary axis during the juvenile stage. At this stage, the plant has no side shoots or flowers and shows C_3 photosynthesis. CAM is not inducible.

(3) In the adult phase, side shoots with secondary leaves develop while the primary leaves senescence. CAM becomes inducible.

(4) Flowers develop at the terminus of the primary axis and in the axils of secondary leaves. Epidermal bladder cells become more obvious. CAM is always induced.

(5) In the final, seed-forming phase, seed capsules are the only viable part of the plant. No water is taken up and the epidermal bladder cells are prominent.

In its native habitat, progressive drought stress, accompanied by increased salinity, sets in after the rainy season and the initial juvenile stage of the plant (Winter and Lüttge, 1979). The distinct phases of the life cycle reflect the adaptations of this species to water and salt stress. The induction of CAM, coupled with the succulence of the plant, allows for more effective water usage. Specialised trichomes form large epidermal bladder cells up to 2 mm in diameter provide additional reservoirs for water storage. Progressive salinity leads to the accumulation of increasing amounts of NaCl in the shoot, with up to 1 M NaCl being measured in the bladder cells (Adams *et al.*, 1992). While *M. crystallinum* is a facultative halophyte and grows well even at low NaCl concentrations, its optimum salinity for growth is between 150 mM and 200 mM NaCl (Adams *et al.*, 1998).

Considerable progress has been made in studies of the molecular basis of the CAM induction and of the increased production of compatible solutes during salt stress (for a review see Cushman and Bohnert, 1997). Another study has shown an increase in the activities of three different isoforms of superoxide dismutase under salt

stress, indicating an increase in oxidative stress during salinity (Miszalski *et al.*, 1998).

The role of the vacuolar V-type H^+-ATPase in salt tolerance has been studied extensively in *M. crystallinum*. Under physiological conditions the V-ATPase catalyses the transport of H^+ from the cytosol into the vacuole, energised by the hydrolysis of ATP to ADP and P_i. Since this mechanism provides the primary energisation for many secondary transport processes across the tonoplast, it is a key component for the regulation of intracellular ion concentrations. The V-type H^+-ATPase is a high-abundance protein, with the head region of the protein complex covering about 12% and 26% of the tonoplast surface area in the C_3 and in the salt-induced CAM state, respectively. Similarly it comprises about 17% (C_3) and 31% (CAM) of the total amount of tonoplast protein (Ratajczak *et al.*, 1995). This increase in absolute amounts of V-type ATPase protein, as well as other studies demonstrating the qualitative and quantitative changes at the transcriptional and translational level (Ratajczak *et al.*, 1994; Rockel *et al.*, 1998), indicate the importance of a high H^+-pump activity during salt stress. Interestingly, similar changes at the transcript level could also be mimicked by the plant growth regulator ABA, suggesting its possible involvement in the signal-transduction pathway of salt response (Tsiantis *et al.*, 1996).

Under salt stress, the hyperaccumulation of NaCl to values of 700 mM to 1 M in the shoot tissue and epidermal bladder cells is a key feature of *M. crystallinum* (Lüttge *et al.*, 1978; Adams *et al.*, 1992; Vera-Estrella *et al.*, 1997). In contrast to salt-excreting glands like those in *Atriplex*, giant epidermal bladder cells of *M. crystallinum* do not provide a pathway for accumulation of NaCl away from photosynthetic tissue. Rather, the salt concentrations found in the giant bladder cells

are very similar to those found in the mesophyll tissue (Lüttge *et al.*, 1978). Since Cl^- is accumulated to almost the same level as Na^+, other anions have to charge balance the remaining cations, such as K^+ and Ca^{2+}. Large quantities of free oxalate are found in the bladder cells, as well as Ca-oxalate crystals in leaf and stem cells of *M. crystallinum* (Adams *et al.*, 1992).

Na^+ uptake and its allocation to the shoot in *M. crystallinum* are strongly upregulated by *myo*-inositol, a substrate for the production of compatible solutes (Nelson *et al.*, 1999). Given the steep Na^+ inward gradient, uptake is thought to be mediated by a passive mechanism. No pathway for Na^+ uptake has yet been identified in *M. crystallinum*. In glycophytes, cation channels have been found in the plasma membrane that can mediate uptake of both Na^+ and K^+ with different selectivities, thereby providing a flexible discrimination of cation influx (Amtmann *et al.*, 1997). Carrier-mediated Na^+ transport can provide further mechanism for uptake at the root level (Schachtman *et al.*, 1997).

To maintain low cytosolic Na^+ concentrations, Na^+ must be actively transported out across the plasma membrane or the tonoplast. In *M. crystallinum*, no Na^+/H^+ antiporter has yet been reported to actively exclude Na^+ from the cell. But the existence of this type of transporter in other plants, including halophytes, makes such a mechanism likely (Niu *et al.*, 1995). In contrast, the equivalent vacuolar Na^+/H^+ antiporter has been identified and described in *M. crystallinum* at a physiological level (Barkla *et al.*, 1995). The transport of Na^+ in exchange for H^+ is energised by the steep pH difference across the tonoplast generated by the V-type ATPase. Under salt stress, Na^+/H^+-antiport activity of tonoplast vesicles was found to increase two-fold (Barkla *et al.*, 1995). As yet the molecular basis for vacuolar Na^+/H^+ antiport in plants has not

been described, but the molecular identification of a number homologous animal and yeast Na^+ transporters should reveal valuable targets for molecular cloning strategies in plants. For example, the overexpression of AtNhx1, an *Arabidopsis thaliana* homologue of the yeast Na^+/H^+ antiporter Nhx1, in a *nhx1* mutant yeast strain suppressed some of the mutant phenotype, and the transcript level of *AtNhx1* was also shown to be increased by NaCl (Gaxiola *et al.*, 1999). This indicates the close structural and functional similarity between the Na^+/H^+ antiporters from fungi and plants.

In *M. crystallinum*, no work has been done up to now to identify possible Cl^- transport mechanisms. Studies on ion transport and localisation have so far focused on the shoot, particularly on the giant bladder cells. With volumes of up to 20 µl, the ionic contents of these specialised cells can be sampled easily (Adams *et al.*, 1998). Nothing is known about ion transport in roots of *M. crystallinum*. In bladder and lamina cells of *M. crystallinum*, membrane potentials measured with microelectrodes were very low, between -10 mV to -40 mV (Lüttge *et al.*, 1978). If Cl^- were at thermodynamic equilibrium, these small membrane potentials could account for cytoplasmic Cl^- concentrations between 1.5 and 4-fold lower than in the apoplast. Or, assuming an external concentration of around 700 mM Cl^-, the cytosolic Cl^- would be between 175 and 460 mM. Such high Cl^- concentrations are likely to be toxic. Hence, additional active transport would be needed to lower the cytosolic Cl^-. However, these measurements of the membrane potential showed large variability, and for lamina cells only single measurements from salt-treated plants were obtained. Furthermore, no account was taken of the intracellular localisation of the microelectrode tip. These low membrane potentials might rather reflect the difference between the tonoplast

potential against the external potential. Since the vacuole can constitute over 90% of the total cell volume, impalements of the vacuole are very likely. This might also explain the rather low membrane potentials observed, since the trans-tonoplast potential difference is believed also to be negative. On the basis of these measurements, neither the existence of passive, nor a requirement for active, Cl^- transport out of the cell can be inferred. Similar considerations apply for the accumulation of Cl^- in the vacuole.

1.3 Methods for studying Cl^- transport

For the study of Cl^- transport, a number of different approaches have been used in the past. Direct uptake or release of Cl^- can be measured using the radioactive isotope $^{36}Cl^-$ (Martinoia *et al.*, 1986). This method is non-invasive, and uptake can be measured at the whole-plant level, with protoplasts and also with isolated vacuoles. However, due to the low specific radioactivity of $^{36}Cl^-$, this method has relatively poor sensitivity.

Micro-sampling of tissue or cell sap (Fricke *et al.*, 1994) and the subsequent analysis of ion contents, for example *via* capillary zone electrophoresis (Bazzanella *et al.*, 1998), can provide reasonable spatial resolution down to the contents of single cells, but usually at the expense of lower sensitivity. Furthermore, this approach does not provide any temporal resolution and can only describe the static distribution of solutes. It is therefore not adequate for cellular transport studies.

A more sensitive method is the use of Cl^--selective microelectrodes. Cells can be directly impaled with these microelectrodes, and the Cl^- activities can be determined with high temporal and spatial resolution (Felle, 1994; for a general

review see Miller, 1995). By using triple-barrelled electrodes (i.e. a Cl^--sensitive combined with a pH-sensitive electrode and an electrode to measure the membrane potential), this method can provide exact thermodynamic data for the free cytosolic and vacuolar Cl^- activities, as well as the pH gradient and transmembrane potential (Trebacz *et al.*, 1994; Bethmann *et al.*, 1995). Similar approaches have been used to study the thermodynamic requirements of nitrate or K^+ accumulation (Miller and Smith, 1992; Miller *et al.*, 1995). A major disadvantage of this method is the fact that Cl^--selective electrodes are not very selective for Cl^- at all, but show significant deviations in the presence of nitrate. Therefore, such Cl^- measurements can only be reliably performed in species known to have only low nitrate concentrations (Trebacz *et al.*, 1994), or fixed nitrate concentrations have to be assumed for the correction (Felle, 1994).

Electrophysiological studies have provided the most detailed information on Cl^- transport so far. Using microelectrodes, changes in the membrane potential with changing external chloride concentrations can be measured, which can give an indication of the Cl^- fluxes involved (Brearley *et al.*, 1997). Similarly, measurements of electrical currents can be obtained in the voltage-clamp configuration, using either microelectrodes or the patch-clamp technique. The temporal resolution of these methods is very high, and currents can be detected down to the level of single channels with the patch-clamp technique (Sakmann and Neher, 1995). The patch-clamp technique can also be used to study ionic currents of subcellular organelles, such as vacuoles or thylakoids (Keller and Hedrich, 1992). The main disadvantage of this technique is that it measures the charge movement of all ions present in the system, so it is not selective for Cl^-. Therefore, special protocols and defined ionic

conditions have to be applied to dissect the total current to reveal the Cl^--current component. In solutions with complex ionic compositions this can be a complicated procedure. Patch-clamp recordings therefore tend to use a limited the number of different ions, often using solutions far removed from actual physiological conditions, in order to obtain quantitative results.

The last decade has seen the development of a number of Cl^--sensitive fluorescent dyes. The first and most widely used fluorescent dye is SPQ [6-methoxy-*N*-(3-sulphopropyl)quinolinium: Figure 1.1.A]. This has been used to study Cl^- transport into animal cells as well as isolated membrane vesicles (Illsley and Verkman, 1987; Verkman *et al.*, 1989; Chao *et al.*, 1990). SPQ was also used by Pope and Leigh (1988) to study the uptake of Cl^- into tonoplast vesicles from red beet and from barley. SPQ fluorescence, measured with an excitation wavelength of 350 nm and an emission wavelength of 440 nm, is readily quenched by low millimolar concentrations of halides. The quenching of the fluorescence intensity F is due to a collisional mechanism that follows the Stern-Volmer relation $F_0/F = 1 + K_{SV}$ [Q], with F_0 being the fluorescent intensity in the absence of the quenching ion Q and K_{SV} is the Stern-Volmer quenching constant. A pivotal structural feature for the Cl^- sensitivity of SPQ and all other Cl^--sensitive probes is a positively charged quaternary nitrogen in a heterocyclic ring (Verkman and Biwersi, 1995).

Only few organic ions have the ability to quench SPQ fluorescence, for example citrate, albeit with much lower efficiency. The fluorescence of SPQ and its Cl^- sensitivity are pH-independent (Pope and Leigh, 1988), but a recent study has shown that a number of organic buffer ions can quench the SPQ fluorescence when they become de-protonated (Vasseur *et al.*, 1993).

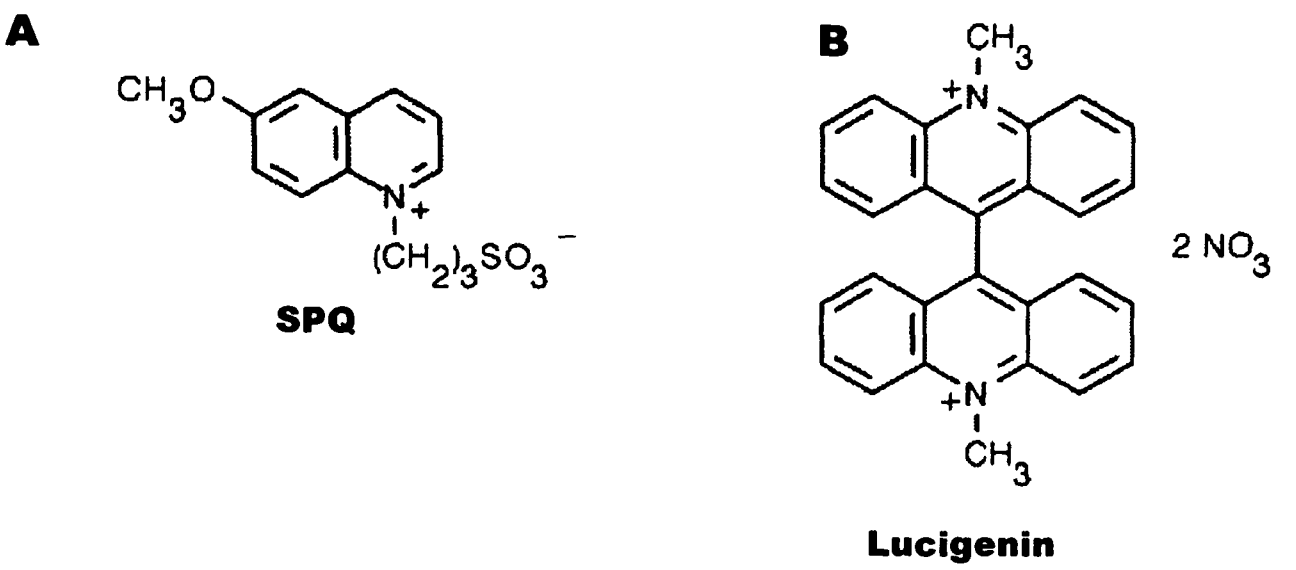


Figure 1.1. Chemical structures of (**A**) SPQ [6-methoxy-*N*-(3-sulphopropyl)quinolinium] and (**B**) lucigenin [*N,N'*-dimethyl-9,9'-bisacridinium dinitrate]

Several derivatives of SPQ have been developed in recent years with improved optical characteristics or higher sensitivity towards halides (Verkman and Biwersi, 1995). Furthermore, a Cl^--insensitive, membrane-permeable form [6-methoxy-*N*-ethyl-1,2-dihydroxyquinolinium (diH-MEQ)] was developed that is readily oxidised in the cell, thereby gaining Cl^--sensitivity and improved cell retention (Biwersi and Verkman, 1991). All these quinolinium-based compounds have rather short excitation wavelengths below 400 nm. This makes them rather susceptible to signal noise and to cellular auto-fluorescence effects.

The search for Cl^--sensitive fluorescent indicators with longer-wavelength characteristics has led to the discovery of lucigenin (*N,N'*-dimethyl-9,9'-bisacridinium dinitrate: Figure 1.1.B). Lucigenin has been hitherto used as a probe for the luminescent detection of O_2^- (Jabs *et al.*, 1997), a function independent of its Cl^--sensitivity. It was shown to have an excitation wavelength of up to 455 nm and an emission wavelength of 506 nm (Biwersi *et al.*, 1994). Also, it has much improved sensitivity towards Cl^- and shows brighter fluorescence than SPQ and its derivatives. However, a major drawback of lucigenin and similar acridine-based compounds is that they are readily converted into a Cl^--insensitive product in living cells, due to nucleophilic attack at the 9-position (Biwersi *et al.*, 1994). Although this means that lucigenin cannot be used to study Cl^- transport in intact living cells, membrane systems such as isolated vesicles or liposomes have no such restriction. Because of this limitation, lucigenin has so far only been used in one study to measure Cl^- transport (Biwersi *et al.*, 1994). However, its greater Cl^--sensitivity and improved optical properties make it preferable to SPQ when studying Cl^- transport in isolated membrane systems.

The potential advent of new Cl^--sensitive dual-wavelength dyes that are also cell permeable (Jayaraman *et al.*, 1998) will allow more accurate ratiometric measurements of intracellular Cl^--concentrations.

1.4 Cl^- transport in plants

Chloride is a freely soluble ion ubiquitous in nature. Since it is almost always present in the soil, it is rarely deficient. In plants, it is required for the oxygen-evolving reactions of photosynthesis. Additionally, its availability and high mobility makes it an important counterion for maintaining charge balance across membranes, as well as functioning as an osmotically active solute. In guard cells, efflux of Cl^- across the plasmalemma is essential for stomatal closure (MacRobbie, 1998). In *Chara*, chloride influx is important for osmoregulation (MacRobbie and Burman, 1989) and as a component of the action potentials observed in this alga (Gradmann *et al.*, 1993; Gradmann and Hoffstadt, 1998). Furthermore, Cl^- efflux is important for charge-balancing positive H^+-pump currents to maintain cytosolic pH (Johannes *et al.*, 1998). Even in non-halophytes, Cl^- is readily taken up and often accumulated above the external concentrations and in excess of the minimal requirements of the plant (Trebacz *et al.*, 1994).

1.4.1 Active Cl^- transport in plants

Since the membrane potential across the plant plasma membrane is usually very negative, often with several hundred millivolts, active Cl^- uptake into plant cells has been postulated (Sanders, 1994). Such an active transport across the plasma membrane, utilising the steep ΔpH generated by H^+ pumps in the form of a H^+/Cl^-

symport, has been well documented in characean cells and the reaction kinetics have been extensively modelled (Sanders, 1980, 1994; Beilby and Walker, 1981). In higher plants, Cl^--dependent depolarisations, coupled with cytoplasmic acidification and an increase in extracellular pH also indicate the presence of a nH^+/Cl^- symport, with $n >$ 1 (Ullrich and Novacky, 1990). Further compelling evidence comes from a study on root-hair cells from *Sinapsis alba*. Using ion-selective microelectrodes, Felle (1994) measured changes in the intracellular pH, cytosolic [Cl^-] and the membrane potential upon changing extracellular Cl^- concentrations. The observed changes were again consistent with nH+/Cl^- symport, with $n > 1$. Furthermore, Felle (1994) showed that Cl^- transport was kinetically coupled with the ΔpH rather than the membrane potential. Further studies on higher plants have not yet been performed, and the exact coupling factor n of the plasma membrane nH^+/Cl^- symport still needs to be determined.

In plant vacuoles, the existence of H^+-driven Cl^- transport is less clear. Measurements of the electrochemical Cl^- gradient, the ΔpH and the membrane potential across the tonoplast of the green fresh water algae *Eremosphaera viridis* (Bethmann *et al.*, 1995) have shown that passive vacuolar Cl^- uptake would not be sufficient for the observed vacuolar Cl^- accumulation in this species. The measured tonoplast membrane potential was only 0 mV, while the electrochemical potential gradient for Cl^- was -26 mV (2.9 mM cytosolic Cl^-, 8.2 mM vacuolar Cl^- concentration). In contrast, the steep pH gradient of 2.3 units would be sufficient to drive H^+/Cl^- antiport. Experiments on the liverwort *Conocephalum conicum*, an intermediate between algae and higher plants, suggest qualitatively similar conditions, with no detectable tonoplast potential and about 5-fold accumulation of Cl^- in the

vacuole (Trebacz *et al.*, 1994). However, in these measurements the intracellular position of the microelectrode tip was not well defined. Furthermore, Cl^--selective microelectrodes are notorious for their sensitivity for nitrate, which can reach high intracellular concentrations of almost 200 mM in some species (Adams *et al.*, 1992). Further measurements using different techniques are needed, especially in higher plants, to confirm these findings.

Another line of evidence for H^+-coupled vacuolar Cl^- transport comes from the work of Schumaker and Sze (1987). In isolated tonoplast vesicles from oat roots, they showed that Cl^- could dissipate an imposed inside-acid ΔpH. By short-circuiting electrical currents using a K^+/valinomycin clamp, they demonstrated that the dissipation was not due to an electrical coupling of H^+ and Cl^- fluxes. However, these experiments did not allow a distinction to be made between H^+/Cl^- symport or antiport, so the question of a putative vacuolar H^+/Cl^- antiport remains open

1.4.2 Plant Cl^- channels

So far, plant anion channels have been characterised mainly at the functional level, while the molecular basis for these channels is still largely unknown. Only one report exists of the functional expression of a plant chloride channel, ClC-Nt1, a homologue of the animal ClC chloride channel family, in oocytes (Lurin *et al.*, 1996). However, the elicited currents closely resemble endogenous oocyte chloride currents. Similar currents can also be elicited by the heterologous expression of other integral membrane proteins or non-functional animal ClC-type mutants (Weber *et al.*, 1995; Hechenberger *et al.*, 1996). An unambiguous demonstration of the molecular basis of plant anion-channel function is still needed. Also, it remains to be shown whether

plant homologues of animal ABC-type transporters such as CFTR (for review see Rea *et al.*, 1998) or Band 3 anion transporters (Rosenberg *et al.*, 1997) exhibit anion-channel functions.

In general, plant anion channels show similar, or even higher, permeabilities for NO_3^- over Cl^- (for a review, see Hedrich, 1994), and very low permeabilities for cations. Therefore, under physiological conditions anion channels might also play a role in the efflux of NO_3^- (Schmidt and Schroeder, 1994). Malate, which plays an important role in the regulation of the guard cell response to CO_2 and also serves as a storage for CO_2 during the CAM cycle, seems to be transported *via* specific channels with low Cl^- permeability (Iwasaki *et al.*, 1992; Pantoja *et al.*, 1992b; Cerana *et al.*, 1995; Cheffings *et al.*, 1997).

Many early studies on plant Cl^- transport focused on the green alga *Chara* because of the relative ease of electrophysiological and tracer flux measurements on its large internodal cells ("the green squid giant axon"). In higher plants, only stomatal guard cells have been studied in sufficient detail to provide a detailed picture of the function and regulation of Cl^- fluxes in the context of other ion fluxes. The summary given here therefore reflects a bias towards these two cell systems.

1.4.2.1 Cl^- channels in the plasma membrane

Anion channels have been well characterised in the plasma membrane of characean and other algal cells (Beilby, 1982; Coleman, 1986). A transient increase of Cl^- permeability of the plasma membrane of *Chara corallina* leads to brief depolarisations described as action potentials (Thiel, 1995; Kourie, 1996). Two types of Ca^{2+}-dependent Cl^- channels with conductances of 17 pS and 38 pS could be shown

to activate at depolarising membrane potentials (Thiel *et al.*, 1993). The distinct nature of the transient Cl^- current amplitudes observed in the cell-attached configuration suggests activation of these currents by a quantal release of a gating factor, most likely Ca^{2+}, from intercellular stores located close to the plasma membrane (Thiel and Dityatev, 1998). A Cl^- channel activated by hyperpolarisation with several conductance levels, the smallest being 7 pS, was described by Coleman (1986). The complex transitions observed between the different levels did not reveal whether this was due to the presence of a large conductance channel with several substates, or due to a highly synchronised set of separate channels with small conductances.

Two types of anion channel behaviour have been identified in the plasma membrane of guard cells, a slow and a fast type. In *Vicia faba*, the slow-activating S-type (Schroeder and Keller, 1992) is activated by Ca^{2+}. Phosphorylation is also a requirement for its activation over a wide voltage range up to +60 mV (Schmidt *et al.*, 1995). The activation of this channel type by elevated cytosolic Ca^{2+} is thought to cause a prolonged depolarisation. This leads to net salt efflux from the guard cell and thereby to stomatal closure (Schroeder, 1995). The S-type channel shows long opening times upon activation and remains activated for longer than 1 h (Linder and Raschke, 1992; Schroeder *et al.*, 1993). The plant hormone ABA (abscisic acid), involved in water stress related signalling, directly activates S-type single-channel activity in tobacco and *Arabidopsis* (Schwartz *et al.*, 1995; Pei *et al.*, 1997; Grabov *et al.*, 1997). This is consistent with the direct involvement of this anion channel in the closure of stomata upon water stress. The actual signalling intermediates have not yet been resolved, and the evidence suggests that they might be significantly different

between species (Grabov *et al.*, 1997; Pei *et al.*, 1997; MacRobbie, 1998). As was shown recently, protein farnesylation, a post-translational modification process, is also involved in ABA signalling in *Arabidopsis* (Pei *et al.*, 1998). Inhibition of farnesyltransferase or deletion of the corresponding gene leads to a marked increase in ABA-induced anion currents. However, the actual target of the farnesyltransferase within the ABA signalling-cascade is still unknown.

The second type of Cl^- channel observed in the guard-cell plasma membrane is of the rapid R-type (also called GCAC1). This rapid type is activated within 50 ms upon depolarisation and also deactivates much more rapidly than the S-type (for a review, see Hedrich, 1994). A detailed study of anion permeation has revealed a multi-ion pore with a diameter between 5 to 7 nm, with propionate being the largest permeant ion (Dietrich and Hedrich, 1998). Also, the channel is gated directly by external anions. In the presence of extracellular malate, the amplitude of the rapid currents is increased and the currents activate at more negative membrane potentials (Hedrich *et al.*, 1994). Malate release from neighbouring mesophyll cells due to rising CO_2 in the tissue could therefore trigger stomatal closure. Alternatively, release of malate from the guard cell itself could provide a positive feedback mechanism for further depolarisation (Schroeder, 1995).

The S-type and the R-type anion channels of guard cells show very distinct characteristics in terms of their kinetics, their regulation by effectors such as malate, and also their inhibitor sensitivity (Hedrich, 1994; Schroeder, 1995). On the other hand, some studies have suggested that these channel types could in fact be two different states of the same channel protein. As Dietrich and Hedrich (1994) have shown in *Vicia faba*, the excision of membrane patches containing R-type channels

led to the interconversion of the kinetics from fast flickering openings towards more prolonged channel openings and less voltage dependence, similar to the S-type, within a few minutes. Also, after this "interconversion" the channel current showed different sensitivity towards inhibition by stilbene derivatives, while the selectivity and conductance were not affected. Given the complex gating with multiple subconductance states (Schmidt and Schroeder, 1994), a more detailed statistical or molecular analysis of this large shift in single-channel properties needs to be conducted to determine the underlying mechanism.

Channels similar to the R-type, originally recorded only in guard cells, have recently been described in other cells. In protoplasts from tobacco cell-suspensions, similar interconversions were seen from rapid, strongly voltage-dependent to slow, less voltage-dependent kinetics, regulated by the intracellular phosphorylation status (Zimmermann *et al.*, 1994). Hypocotyl epidermis and parenchyma protoplasts from *Arabidopsis* also show this distinct channel type with an ATP-dependent interconversion (Thomine *et al.*, 1995). This indicates a widespread distribution of this type of channel, which might play a role in elicitor-induced responses in many cell types (Zimmermann *et al.*, 1998).

Elzenga and Van Volkenburgh (1997a) also reported whole-cell anion currents in pea mesophyll cells with characteristics similar to the R-type currents described above. However, the activation and deactivation kinetics, with time constants from 100 to 400 ms, were somewhat slower than those observed in guard cells. Regulation by ATP and activation by Ca^{2+}, which increases during illumination, might suggest a role for these currents in the cell's response to light, where transient depolarisations involving anion efflux can be recorded (Elzenga and Van Volkenburgh, 1997a).

Whether the inactivation of the anion currents upon elevation of ATP concentrations observed in pea is also due to an interconversion between different single-channel states still needs to be determined at the single-channel level. In the same cells, a light-controlled putative anion channel with complex gating involving several substates was described by Elzenga and Van Volkenburgh (1997b) which might underlie the observed light-induced anion currents. The changes in single-channel characteristics are reminiscent of the interconversions seen in R-type channels described above. The response to light could only be observed in the cell-attached configuration after several minutes, whereas in excised patches no light-dependent regulation of a prominent anion channel could be observed. The anion channel characterised by Elzenga and Van Volkenburgh (1997b) in the excised plasma-membrane patches from pea mesophyll cells was activated by high cytosolic Ca^{2+} and showed only weak voltage dependence. More detailed studies are needed to characterise this interesting light-dependent activation process.

A different type of anion channel was shown to play an important role in the response of *Arabidopsis* seedlings to blue light, which leads to an immediate growth inhibition of the hypocotyl. Upon illumination of dark-grown seedlings with blue light, anion-current induced depolarisations can be observed in growing cells. These depolarisations can be potently inhibited by the Cl^--channel blocker NPPB (Cho and Spalding, 1996). It was shown that NPPB not only selectively and potently inhibited a blue-light activated single channel residing in the plasma membrane, but also reduced the blue-light-induced growth inhibition. Furthermore, NPPB prevented the upregulation of parts of the biosynthetic pathway for anthocyanins, pigments that usually accumulate upon blue-light exposure (Noh and Spalding, 1998). Other parts of

this pathway were not affected by NPPB, but rather by genetically deleting a different blue-light receptor (Noh and Spalding, 1998). This suggests the direct involvement of blue-light activated anion channels in the selective regulation of protein expression.

Other anion channel types observed in the plasma membrane of various plants have been characterised in much less detail (for an overview, see Hedrich, 1994). In general, two classes of voltage-activated anion channels can be distinguished: inward-rectifiers and outward-rectifiers, with conductances ranging from 1 pS (Schroeder and Keller, 1992) up to 200 pS (Terry *et al.*, 1991). Most of these anion channels are subject to tight physiological control. For example, the 200 pS inward-rectifying anion channel from *Amaranthus* was shown to shift its voltage activation towards less negative membrane potentials and lose its voltage dependence with high cytosolic Ca^{2+} or low ATP, as well as being activated by low external pH (Terry *et al.*, 1991; Tyerman, 1992).

An outward-rectifying anion channel was found in protoplasts derived from wheat roots, and its physiological role might be the uptake of Cl^- at elevated soil salinity (Skerrett and Tyerman, 1994). This fast-activating channel with a conductance of around 4 pS has similar permeabilities for NO_3^- and Cl^-, shows multi-ion pore behaviour, and is gated by the permeant anion. Also, an increase in intracellular Ca^{2+} leads to a significant increase in the number of channel observations (Skerrett and Tyerman, 1994).

In the plasma membranes of the marine seagrass *Zostera muelleri,* two different types of anion channels have been observed (Garrill *et al.*, 1994). A low-conductance channel of 20 pS and a large channel showing distinct substates, with a main open state of 80 pS, and most transitions occurring between the mid- and the

main open-state. Unfortunately these channels have not been characterised further, but they might play a role in the osmoregulation of the plant in its saline environment (Garrill *et al.*, 1994).

A number of anion channels characterised in plant plasma membranes are mechanically activated (Falke *et al.*, 1988; Cosgrove and Hedrich, 1991). In *Vicia faba* guard cells, stretch-activated anion channels show multiple substates with conductances up to 27 pS, and together with stretch-activated cation channels might provide a fine control for the turgor regulation occurring in this osmotically highly active cell type (Cosgrove and Hedrich, 1991).

This overview emphasises the importance of anion channels found in plant plasma membranes in many physiological processes. Cl^--induced depolarisations play a key role in cellular signal transduction, not only for stomatal closure and osmoregulatory processes, but also for light-induced responses and action potentials.

1.4.2.2 Cl^- channels in the vacuolar membrane

Physiological studies on vacuolar Cl^- transport using isolated tonoplast vesicles have so far been inconclusive about the mechanism of transport involved. Several studies have shown the ability of extravesicular Cl^- and NO_3^- to dissipate $\Delta\psi$ (Bennett and Spanswick, 1983; Kaestner and Sze, 1987; Pope and Leigh, 1987). This indicates electrogenic Cl^- uptake and suggests a passive Cl^--transport mechanism. By measuring Cl^- uptake into tonoplast vesicles directly using the Cl^--sensitive dye SPQ and by characterising the voltage and Cl^--concentration dependence of this uptake, Pope *et al.* (1990) showed that a three-state reaction-kinetic model of passive Cl^- transport was sufficient to describe the data. But whether this passive transport was

channel- or carrier-mediated could not be determined, and an electrophysiological approach is needed to resolve this question.

In contrast to cation channels in the vacuole, much less is known about vacuolar Cl^- channels. Given the large efflux of K^+ and Cl^- from the guard cells during ABA-induced stomatal closure, the existence of vacuolar Cl^--channels has been suggested (MacRobbie, 1998). Earlier studies on vacuolar ion channels have ascribed a considerable Cl^- conductance to the slow-activating vacuolar (SV) cation channel (Hedrich and Kurkdjian, 1988; Schulz-Lessdorf and Hedrich, 1995). However, recent work has unequivocally shown that SV channels are highly selective for cations, with permeabilities for Ca^{2+}, Mg^{2+} and K^+, but hardly any anion permeability (Allen and Sanders, 1996; Pei *et al.*, 1996; Pottosin *et al.*, 1997).

Compelling evidence for vacuolar Cl^- channels in guard cells comes from the work of Pei *et al.* (1996). Under initial recording conditions, only small currents could be observed in *Arabidopsis* guard cell vacuoles. However, addition of a native Ca^{2+}-dependent protein kinase (CDPK) combined with Ca^{2+} and ATP activated large, fast-activating whole-vacuolar inward-currents carried by Cl^-. Furthermore, the authors showed that in the presence of a constitutively active mutated form of this serine/threonine protein kinase, $CDPK^*$, no cytosolic Ca^{2+} was needed to activate vacuolar Cl^- currents, but the presence of ATP remained a requirement. This activation was rather specific for the native CDPK, as another, non-native serine/threonine kinase (protein kinase A, PKA) could only elicit small (but still significant) activation of Cl^- currents. Flickery Cl^- channels, activated by CDPK, could only be observed at negative membrane potentials and showed a 34 pS conductance. Interestingly, similar Cl^- inward currents could also be activated in red beet storage

vacuoles by the *Arabidopsis* CDPK. This indicates that this type of serine/threonine-kinase activated vacuolar Cl^- channel might be widespread in plants. The fact that this channel shows strong inward rectification suggests a role in vacuolar Cl^- uptake, a function which is necessary in many cell types, not only guard cells.

When Cl^- was substituted by malate in all recording media, CDPK still activated inward currents in guard cells, albeit with much slower kinetics (Pei *et al.*, 1996). Whether malate permeates the same channel as Cl^- has not been determined. Similar slow-activating inward currents carried by malate have been seen in other plant vacuoles without CDPK activation, generally with higher permeability for malate than for Cl^- (Plant *et al.*, 1994; Cerana *et al.*, 1995; Cheffings *et al.*, 1997).

Another report describing vacuolar Cl^- channels was made by Ping *et al.* (1992). Studying ion channels in tobacco cell suspension vacuoles, they regularly observed a short-lasting Cl^--selective channel at negative membrane potentials. It had a single-channel conductance of 110 pS, but no selectivities were tested due to its short-lasting presence after excision, so its physiological relevance remains speculative.

In *Chara*, an anion channel was found in the membrane surrounding cytoplasmic droplets which is likely to be of tonoplast origin, with the vacuolar side facing outward (Tyerman and Findlay, 1989). With symmetrical Cl^- concentrations this channel did not rectify and had a 21 pS conductance. While commonly observed in cell-attached patches, this channel was rarely observed in excised patches. Only in the absence of Ca^{2+} could recordings of this channel from cytosolic-side-out patches be obtained. Even then the channel could be observed only for a short while, sufficient to allow solution changes showing higher permeability for NO_3^- than for Cl^-.

However, NO_3^- also reduced the channel open time, so net NO_3^- fluxes might not be larger than Cl^- fluxes under physiological conditions.

A mechano-sensitive channel which might confer a vacuolar Cl^- conductance has been shown in red beet vacuoles (Alexandre and Lassalles, 1991; Ramahaleo *et al.*, 1996). A 20 pS channel which showed an increased open probability with pressures between 3 and 9 kPa was only weakly selective for K^+ over Cl^- (~3:1). Interestingly, when an osmotic gradient was imposed instead of applying direct pressure, the actual unitary conductance was doubled. Ramahaleo *et al.* (1996) suggested an osmoelastic model for this effect, which would allow the rapid detection of osmotic changes with signalling speeds much faster than ionic diffusion. However, the physiological relevance of such a fast signalling pathway remains unclear.

The few reports that exist of plant vacuolar Cl^- channels have in common that these channels are subject to tight physiological control and seem to be activated *via* cytosolic factors, e.g. CDPK. It appears that during the isolation of vacuoles, i.e. removal of the plasma membrane and cytosol, these factors are lost. This leads to Cl^- channels being inactive, or showing rapid "run-down" (Tyerman and Findlay, 1989; Ping *et al.*, 1992). It might also explain the very low number of vacuolar anion channels reported to date, despite numerous attempts to characterise tonoplast ion channels. The finding by Pei *et al.* (1996) that serine/threonine kinases, such as CDPK or PKA, activate vacuolar anion currents in different cell types from different plants is promising and suggests that we will soon be able to determine characteristics and functions of vacuolar Cl^- channels from various plants. Since the inward rectifying anion channel described by Pei *et al.* (1996) could only account for vacuolar Cl^- uptake, other regulatory mechanism might exist that activate vacuolar Cl^- efflux. The

vacuolar Cl^- channel found in *Chara* is not intrinsically rectifying, so it could function as such an efflux channel in this organism. It would be interesting to find the factors that prevent the loss of activity of this channel after its removal from the cytosolic face.

1.4.2.3 Anion channels in other organelles

In the thylakoid membrane of chloroplasts, a voltage-dependent Cl^- channel with conductances around 100 pS has been characterised (Schönknecht *et al.*, 1988; Pottosin and Schönknecht, 1995). This channel showes a bell-shaped open-probability distribution with a maximum around 0 mV. Thylakoid anion-channels might function to charge-balance the transthylakoid membrane potential generated by the chloroplastic H^+-pumps, thereby facilitating the generation of a ΔpH. The outer envelope of chloroplasts also contains several anion-selective channels with conductances ranging from 50 to 150 pS (Fuks and Homble, 1995; Heiber *et al.*, 1995). It was shown recently that some of these anion channels may actually form the protein-conducting pores of the chloroplastic protein-import machinery (Hinnah *et al.*, 1997; Van den Wijngaard and Vredenberg, 1997). Interestingly, an anion channel sharing 22% amino-acid identity with a chloroplast outer-membrane channel was found in the outer membrane cyanobacteria and showed high affinity for polyamines and peptides (Bolter *et al.*, 1998). This suggests that parts of the protein-import machinery of chloroplasts were derived from anion channels from a putative endosymbiontic predecessor of cyanobacteria. Also, porin-like voltage-dependent anion channels with conductances of more than 500 pS are found in the inner and outer chloroplast envelope of plastids, as well as mitochondria (Fischer *et al.*, 1994;

Fuks and Homble, 1995). All these large pore-forming channels are likely to play a major role in the transport of large organic molecules across endomembranes rather than in Cl^--specific transport, but might nevertheless provide a major pathway for Cl^- uptake into plant organelles.

1.5 Cl^- channels in other systems

In animals and humans, a large number of chloride channels have been characterised, some also at the molecular level. In epithelia they play major roles in salt absorption or secretion and they are also important for the excitability of muscle cells. CFTR (cystic fibrosis transmembrane conductance regulator), an ABC-type transporter with Cl^--channel function, plays a key role in the cystic fibrosis disease (for a review, see Begenisich and Melvin, 1998). It is activated by cAMP, and channel opening also requires phosphorylation. CFTR has a single channel conductance of 8 pS and shows a linear current-voltage relationship. In addition to its role as Cl^- channel, expression of CFTR also regulates other channel functions. For example, a separate outward-rectifying Cl^- channel is activated and an epithelial Na^+ channel inhibited by CFTR (Schwiebert *et al.*, 1998).

A well characterised family of voltage-regulated Cl^- channels are the ClC-type channels. Currently, at least nine different subtypes have been identified, some of them with functions still unknown (Jentsch *et al.*, 1995; Jentsch and Günther, 1997). ClC-0, found in the electrical organ from *Torpedo*, forms homodimers containing two chloride-conducting pores (Ludewig *et al.*, 1996; Middleton *et al.*, 1996). The dimers dominantly show fast, independent gating of the individual pores (~8 pS), and some minor slow gating as a function of both pores (Ludewig *et al.*, 1997). Its predicted

molecular weight is around 90 kDa, and it is proposed to have 12 membrane-spanning α-helices (Jentsch and Günther, 1997).

What makes this chloride-channel family particularly interesting is the fact that one homologue (GEF1) exists in *Saccharomyces cerevisiae*, according to the yeast genome project (Davis-Kaplan *et al.*, 1998). Furthermore, at least four different homologues exist in *Arabidopsis* (Hechenberger *et al.*, 1996), and one in tobacco (Lurin *et al.*, 1996). Deletion mutants of *GEF1* (for glycerol/ethanol Fe-requiring), show an unexpected requirement for iron due to impaired iron uptake. The putative Cl^- channel GEF1 is located in the Golgi, where it seems to play an important role in pH regulation and Cl^- homeostasis (Gaxiola *et al.*, 1998; Schwappach *et al.*, 1998). As Davis-Kaplan *et al.* (1998) have shown, chloride is an allosteric effector of copper assembly for the yeast multicopper oxidase which takes place in the Golgi. This oxidase plays an important role as ferroxidase in the uptake of Fe. It was shown that not only was the loading of this enzyme with copper favoured by acidic pH, but that the presence of Cl^- in the millimolar range was an absolute requirement for copper loading, explaining the Fe requirement of *gef1* mutants. This supports the role of GEF1 as a putative Cl^- channel in yeast. Furthermore, expression of the *Torpedo ClC-0*, as well as *Arabidopsis ClC-c* and *-d*, genes in *gef1* mutants restored the wild-type phenotype (Hechenberger *et al.*, 1996; Gaxiola *et al.*, 1998). This suggests that ClC must have evolved relatively early during evolution and remained functionally highly conserved in eukaryotes. The fact that GEF1 is localised in endomembranes could explain the lack of success in expressing *Arabidopsis* ClC-homologues in oocytes (Hechenberger *et al.*, 1996), since this type of channel might not be targeted to the plasma membrane. The *Arabidopsis* ClC-homologues are most closely related to the mammalian ClC-6 and -7 type (Hechenberger *et al.*, 1996), and recent work has shown ClC-6 to be localised at the endoplasmic reticulum (Buyse *et al.*, 1998). This

makes the *Arabidopsis* ClC-homologues strong candidates for intracellular Cl^- channels.

1.6 Structure of thesis

The characterisation of vacuolar Cl^- transport presented in this work is based on two different approaches: (a) a physiological study of Cl^- uptake in isolated tonoplast vesicles from *M. crystallinum*, and (b) an electrophysiological characterisation of ion currents in whole vacuoles and small membrane patches.

The following chapter describes the methods and materials used in this work. Since the use of the fluorescent dye lucigenin to study Cl^- transport in tonoplast vesicles is the first time this dye has been used with plants, an assessment of the methodology and of the dye properties is provided in Chapter 3. Chapter 4 describes a general physiological characterisation of vacuolar Cl^- transport in vesicles based on the lucigenin assay. Cl^--sensitivity, specificity, voltage dependence and the effect of salt treatment of *M. crystallinum* plants on vacuolar Cl^- transport will be addressed in that chapter. The subsequent chapter analyses whether vacuolar Cl^- uptake might be mediated *via* an H^+/Cl^- antiporter. Finally, Chapter 6 will give an account of the properties of ionic currents of vacuoles from *M. crystallinum* mesophyll cells obtained by patch-clamping whole vacuoles, as well as isolated membrane patches. The general conclusions regarding vacuolar Cl^- transport in *M. crystallinum* derived from the results obtained in this work and its role in salt tolerance in plants will be discussed in the final chapter.

Chapter 2

Materials and methods

2.1 Materials

2.1.1 Chemicals

Unless otherwise specified, chemicals were purchased from Sigma (Poole, UK) or BDH (Poole, UK) and were of analytical grade.

2.1.2 Plant material

Seeds of *Mesembryanthemum crystallinum* L. were derived from material originally collected in Caesarea, Israel, by Dr. K. Winter (Winter and Lüttge, 1979). They were germinated in a propagation tray and after about 3 weeks transferred to single pots of 10 cm diameter containing general purpose compost (Goundrey & Son, Oxford). Plants were regularly watered with tap water and were maintained in a glasshouse with natural illumination supplemented by sodium-vapour lamps providing a 12-h photo period. Temperatures ranged between 25°C and 35°C in the light period and averaged 15°C during the dark period.

Initially, salt treatment was carried out following the protocol of Barkla *et al.* (1995). After 6 weeks, at the onset of the adult phase (phase 3, see section 1.2.3), plants were watered with increasing NaCl concentrations (increments of 50 mM per day) until a final concentration of 200 mM was reached, which was maintained until the end of the experiment. Control plants continued to be supplied with tap water only. In later experiments, salt treatment was performed according to Struve *et al.*

(1985), or Adams *et al.* (1998), where a final concentration of 400 mM and 500 mM was reached, respectively, in daily increments of 50 mM NaCl. Leaves (≥ 40 mm in length) were collected 2 weeks (Struve *et al.*, 1985; Barkla *et al.*, 1995) or 3 weeks (Adams *et al.*, 1998) after onset of the salt treatment, as well as from the control plants, for further experiments. All plants used in this study were 8 to 9 weeks old at the time of sampling.

Where indicated, 4-week-old plants were transferred to a reverse-phase growth room with illumination provided by a combination of fluorescent tubes and tungsten lamps (Philips TLD 50 W/83HF and Philips RS 60 W, respectively; Philips, Croydon, UK) for 12 h daily at a photosynthetic photon flux density of 200 µmol m^{-2} s^{-1} at mid-plant height. The air temperature was maintained at 25°C in the light period and 14°C in the dark period.

2.2 Tonoplast vesicles

2.2.1 Isolation of tonoplast vesicles

Tonoplast vesicles were isolated according to a method modified from Barkla *et al.* (1995). Leaves from *M. crystallinum* were harvested and sliced into small pieces after removal of major veins. The leaf material (between 40 and 80 g, depending on leaf size) was homogenised in 200 ml of ice-cold homogenisation solution using a commercial blender. This buffer solution contained 400 mM mannitol, 0.5% (w/v) PVP-40, 0.1% (w/v) BSA (bovine serum albumin), 10 mM Na_2EDTA, 5 mM $MgSO_4$, 0.5 mM butylated hydroxytoluene, 26 mM potassium metabisulphite, 2 mM

DTT and 10 mM Tricine, adjusted to pH 7.4 with bis-tris propane (BTP). For salt-treated plants, the mannitol concentration was increased to 600 mM.

All subsequent steps were performed at 4°C. The homogenate was filtered through two layers of cheese-cloth and centrifuged at 13 000 *g* for 15 min, using a Sorvall SS-34 fixed-angled rotor. The resulting pellets were discarded and the supernatant was centrifuged at 80 000 *g* for 50 min (Sorvall TFT50.38 fixed-angle rotor, Beckman L8-M ultracentrifuge). The microsomal pellet thereby obtained was resuspended using a paintbrush in resuspension buffer (1100 mM glycerol, 1 mM Na_2EDTA, 10 mM BTP-Tricine, pH 7.4, 2 mM DTT) and layered on top of a 23% (w/v) sucrose cushion made up in resuspension buffer. This was centrifuged at 100 000 *g* for 2 h using a Beckman SW-28 swinging-bucket rotor. Tonoplast-enriched membranes at the 0/23% interface were removed with a Pasteur pipette, diluted in resuspension buffer and sedimented at 100 000 *g* for 1 h (Sorvall TFT50.38 fixed-angle rotor). The final pellet was resuspended in 400 µl of resuspension medium and aliquots of 100 µl were frozen immediately in liquid nitrogen and stored at -80°C.

2.2.2 Protein assays

To quantify the amount of vesicles, the protein content of the preparations was measured according to the method of Bradford (1976). As an adjustment to this method, the detergent Triton X-100 was added to a final concentration of 0.038% (w/v) to solubilise the proteins prior to the assay, thereby increasing the assay sensitivity. BSA was used as the protein standard.

2.2.3 H^+-ATPase hydrolytic activity assays

To determine the purity of the isolated tonoplast vesicles, the hydrolytic activity of the V-type H^+-ATPase was measured as a marker enzyme. Two to 4 µg of vesicle preparation were incubated for 60 min (30°C) in a reaction medium containing 3 mM ATP, 3 mM $MgSO_4$, 0.1 mM Na_2EDTA, 50 mM Tricine/Tris, pH 8.0 and 0.15 mg ml^{-1} Brij-58. Subsequently the amount of inorganic phosphate was determined after Chifflet *et al.* (1988). The amount of V-type H^+-ATPase in the total ATPase activity was determined in triplicate by measuring enzymatic activity either in the absence of any ATPase inhibitor (total activity), with 0.1 mM molybdate, 0.2 mM azide, and 0.1 mM vanadate combined (to inhibit non-specific phosphatase, mitochondrial F-ATPase and P-type ATPases), or these inhibitors combined with 50 mM nitrate (to inhibit all ATPase activity). The level of inhibition gave an estimate of the relative amount of V-type and non-V-type H^+-ATPase activity.

2.2.4 Electron microscopy

To measure the size of the tonoplast vesicles, a preparation of vesicles from non-salt-stressed plants was examined under an electron microscope. About 100 µg of tonoplast vesicles were pelleted at 100 000 *g* for 15 min (TLA 100.3 fixed angle rotor in a TL-100 tabletop ultracentrifuge) and the supernatant discarded. The pellet was then resuspended and fixed in 5% (v/v) glutaraldehyde in resuspension medium (see section 2.2.1). Again, the vesicles were pelleted for 15 min at 100 000 *g*, and after discarding the supernatant, a 2% (v/v) solution of aqueous osmium tetroxide (in resuspension buffer) was added. The pellet was resuspended by repeatedly taking it up with a blue P1000 plastic Gilson pipette tip and transferred to an Eppendorf tube, where it was left to blacken in a fume hood for 1 h at room temperature. After this

osmium coating, the vesicles were centrifuged at 7000 *g* in a bench-top centrifuge for 5 min. The supernatant was discarded and the pellet resuspended in distilled water and left for 10 min at room temperature. The suspension was then centrifuged and resuspended in distilled water three times to give a thorough wash. To dehydrate the vesicles, a similar cycle was repeated six times with increasing ethanol concentrations (70%, 80%, 90%, 3 times 100%). The dehydrated vesicles were embedded in equal volumes of Spurr resin (Spurr, 1969) and 100% ethanol overnight at room temperature. They were then transferred to 100% Spurr resin the next morning, and after 4 h transferred to a further solution of 100% Spurr resin. The following morning the vesicles were transferred to a final 100% Spurr resin and incubated at 60°C until the resin had hardened. The samples were sectioned by Sarah Rogers (Dept. of Human Anatomy and Genetics, Oxford) into sections with a final thickness of 50 to 60 nm. The sections were put onto a copper grid and stained with a 2% (w/v) solution of uranyl acetate and lead citrate.

Finally, the sections were viewed and photographed together with Prof. J. Morris (Dept. of Human Anatomy and Genetics, Oxford) under a J.E.O.L. 1010 electron microscope at 80 kV (Japanese Electronics Optics Ltd., Welwyn Garden City, UK).

2.3 Fluorescence quenching studies

2.3.1 Dye loading of tonoplast vesicles

For loading the vesicles with fluorescent dyes, a method based on that of Pope and Leigh (1988) was used, with slight modifications as follows. Unless otherwise

stated, all steps were performed on ice using ice-cold media. After thawing frozen aliquots of tonoplast vesicles on ice, the membranes were pelleted at 370 000 *g* for 15 min (4°C, TLA-100.3 fixed-angle rotor). The supernatant was discarded and the pellet resuspended in a medium containing 1 mM Na_2EDTA, 10 mM BTP-Tricine (pH 7.4), 1 mM DTT and either 20 mM SPQ (6-methoxy-*N*-(3-sulpho-propyl)quinolinium) or 10 mM lucigenin (*N,N'*-dimethyl-9,9'-bisacridinium dinitrate; both from Fluka Chemicals, Gillingham, UK). Sufficient mannitol was added to maintain a total osmolality of 500 mosmol kg^{-1}, as determined using a cryoscopic osmometer (Osmomat 030, Gonotec, Berlin, Germany). To load vesicles with different potassium concentrations, K_2SO_4 was added in appropriate amounts. The vesicle suspension was incubated for 30 min at 38°C to allow equilibration of the internal volume with the outside medium (Pope and Leigh, 1990). After keeping the vesicles on ice for 10 min, external dye was removed by washing three times with dye-free washing medium (as above but without fluorescent dye). For this, the vesicles were pelleted at 370 000 *g* for 15 min (4°C, TLA-100.3 fixed-angle rotor) and the supernatant removed. After resuspending the vesicles in washing medium, the washing step was repeated two further times. After storing the vesicles on ice for more than 3 h an increase in external dye concentration could be detected again, so loaded vesicles were used within 3 h of the last washing step.

2.3.2 Measurements of the initial Cl^- transport

Most measurements of Stern-Volmer constants for a range of substances and the effect of pH changes on lucigenin fluorescence were made using a fluorescence plate reader (Perkin Elmer, Beaconsfield, UK). Stern-Volmer constants were determined using either aqueous solutions or a buffer containing 500 mM mannitol,

10 mM BTP-Tricine (pH 7.4) and 1 mM DTT. The effect of pH on lucigenin fluorescence was studied using various buffer systems adjusted to pH 7.4 and pH 8.0 using two different buffer ions. This ensured a constant total amount of buffering ions. The pH was then changed using sulphuric acid or potassium hydroxide to vary the pH of the test buffer. All Stern-Volmer constants used for calculating Cl^- transport rates were measured more accurately in cuvettes at a controlled temperature of 25°C.

Cl^--transport measurements were performed at 25°C in a 0.5 ml cuvette which was either stirred manually after solute addition or stirred using a small magnetic stirrer. Fluorescence intensities where measured using a Perkin-Elmer Luminescence Spectrometer LS50B. For SPQ fluorescence measurements an excitation wavelength of 350 nm and an emission wavelength of 430 nm were used (both slit width 5 nm for vesicle studies). Lucigenin fluorescence measurements were performed at 433 nm and 506 nm wavelength for excitation and emission, respectively (both slits at 5 nm).

Unless otherwise stated, assays were performed using 10 mM BTP-Tricine (pH 7.4), 5 µM valinomycin (from 1 mM stock in 100% ethanol) and sufficient mannitol to maintain iso-osmolarity with the vesicles (500 ± 5 mosmol kg^{-1}). KCl or BTP-Cl (pH 7.4) was used to vary the Cl^- concentration. When KCl was used, an appropriate amount of K_2SO_4 was added to maintain a constant potassium concentration. Unless otherwise stated, the total concentration of K^+ was kept at 50 mM inside and outside the vesicles to keep the membrane potential clamped to 0 mV in the presence of valinomycin. To impose K^+-diffusion potentials, the internal and external concentrations of K_2SO_4 were varied accordingly and the resulting membrane potential was calculated from the Nernst equation ($E = RT/zF \times \ln([K^+]_{out}/[K^+_{in}])$), on the basis of the ionic activities. Activities were calculated using the GEOCHEM-PC

2.0 software (Parker *et al.*, 1995). All solutions were filtered using disposable filter units (0.45 µm, Sigma) to reduce noise in the recordings. Also, care had to be taken that prior to starting transport experiments the temperature of the cuvette and the medium were the same as indicated above to avoid a drift in the baseline.

Cl^- transport was initiated by adding 20 µg of vesicles loaded with the fluorescent dye to the assay medium. An IBM compatible 486 microcomputer was used to record the time course of the fluorescence quenching using FL Data Manager software (Perkin Elmer).

2.3.3 Calculating the initial Cl^- transport rate

A falling exponential was fitted to the first 30 s of the curve (Figure 2.1) using the simplex algorithm by the program clampfit (part of the pClamp 6 software package, Axon Instruments, Foster City, CA, USA). The parameters obtained were used to calculate the initial rate of change of intravesicular Cl^- concentration ($d[Cl^-]/dt$ for $t = 0$) following the procedure of Pope and Leigh (1988). Michaelis-Menten kinetics were fitted using a least squares algorithm and the 'solver' function in Excel (Microsoft Corporation, Redmond, USA).

Pope and Leigh (1988) gave the following equation to describe the initial Cl^- flux:

$$\frac{d[Cl^-]_i}{dt}(t=0) = -\frac{1}{K_{SV}} * \frac{1}{F_{in}} * \frac{dF}{dt}(t=0)\ ;\ \text{mM min}^{-1},$$

with the luminal Cl^- concentration $[Cl^-]$, the Stern-Volmer constant (K_{SV}), the internal fluorescence (F_{in}) in the absence of luminal Cl^- and the initial change in fluorescence (dF/dt at $t = 0$, in min^{-1}), which was obtained by fitting a single

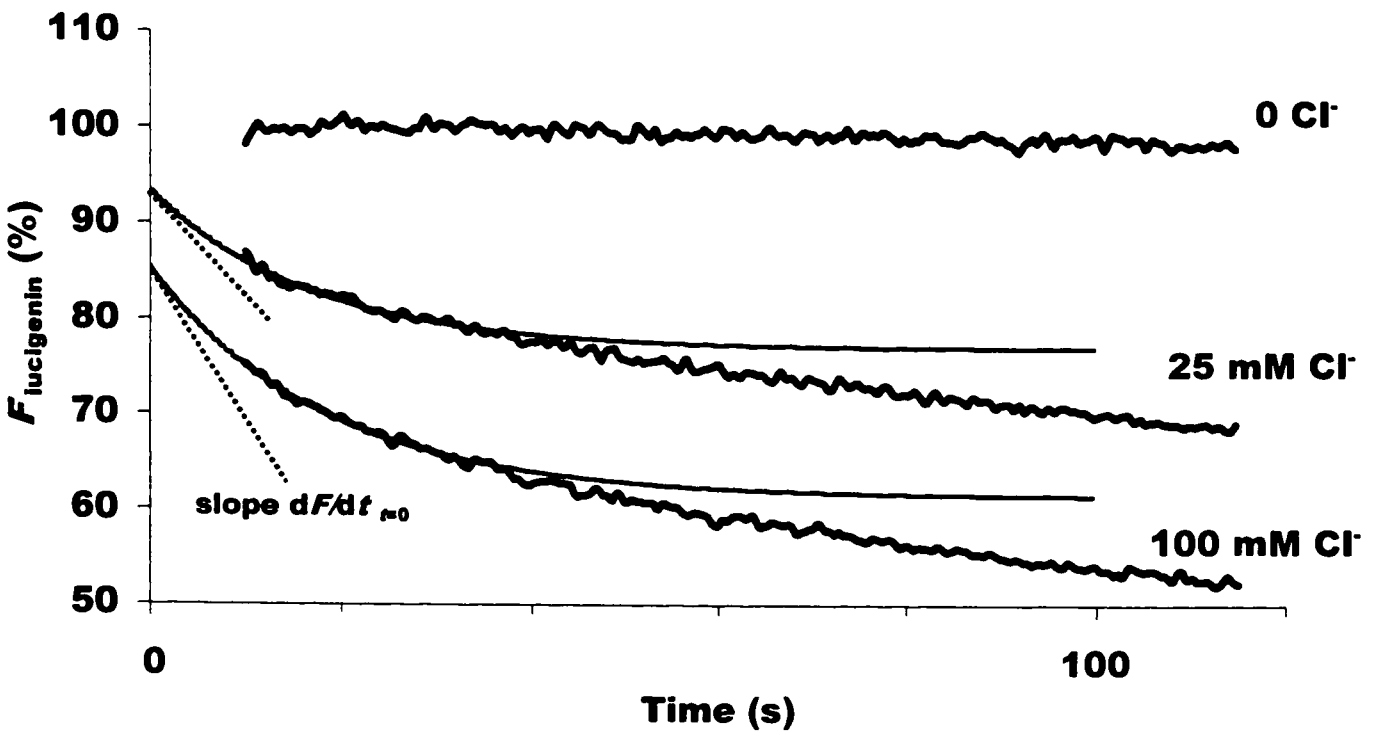


Figure 2.1. Measuring the initial change in lucigenin fluorescence. In the absence of Cl^- the fluorescence remains constant (F_0), while in the presence of Cl^- the fluorescence intensity decreases with time. A single exponential function was fitted to the first 30 s of the curve and the slope of the fitted curve at time point zero was determined

exponential to the first part of the traces. Addition of vesicles to the assay medium determined the time point zero (t_0). The internal fluorescence could be calculated from

$$F_{in} = F_0 - (F_0 - F) * \frac{1 + K_{SV} * [Cl^-]_o}{K_{SV} * [Cl^-]_o},$$

with F_0 being the normalised total fluorescence (in percent) in the absence of external Cl^- $[Cl^-]_o$, and F the normalised fluorescence at t = 0. Concentrations were calculated in mM. Calculations were performed using Excel 5.0 (Microsoft).

All results presented in this work are averages of several measurements with the corresponding standard error of mean. Statistical significance was evaluated with an appropriate version of Student's *t*-test.

2.4 Generating a $\Delta\psi$

2.4.1 Oxonol-V fluorescence studies

To test the K^+/valinomycin clamp, the potentiometric membrane dye oxonol-V (Fluka) was used. Oxonol-V (bis(3-phenyl-5-oxo*iso*xazol-4-yl)pentamethine oxonol) was first dissolved as a 10 mM stock solution in 100% ethanol with a trace of KOH. To define intravesicular conditions, vesicles were incubated for 30 min at 37°C in loading buffer additionally containing 2.5 mM K_2SO_4. The assays were performed using an excitation wavelength of 610 nm and an emission wavelength of 639 nm. Prior to each assay, 20 µg of vesicles were incubated for about 4 min in assay medium containing 10 mM BTP-Tricine (pH 7.4), 1 mM DTT, 2.5 mM K_2SO_4, mannitol to adjust osmolality and BTP-Cl as indicated. Additionally, the assay buffer contained 8 µM oxonol-V and 5 µM valinomycin. As a control 0.5% (v/v) ethanol (final

concentration) was used. Fluorescence changes were recorded after addition of aliquots of 500 mM K_2SO_4 to impose an electrochemical gradient across the vesicle membrane.

2.5 Proton gradient experiments

2.5.1 K^+/nigericin clamp

To impose an inside-acidic pH gradient, the potassium selective ion exchanger nigericin (Sigma; Figure 2.2) was used according to the protocol of Schumaker and Sze (1987). Vesicles were incubated in loading buffer (see above) containing 100 mM K_2SO_4, 2.5 mM BTP-Tricine (pH 7.4), mannitol to adjust the osmolality to 500 mosmol kg^{-1} and either lucigenin or the fluorescent dye SPQ. SPQ was used in some experiments instead of lucigenin since its shorter wavelength characteristics did not overlap with the wavelengths of the pH-sensitive dye quinacrine (6-chloro-9-[(4-diethylamino)-1-methylbutyl]amino-2-methoxyacridine dihydrochloride). To measure the formation and dissipation of the generated pH gradient, quinacrine fluorescence intensity was measured at an excitation of 427 nm and an emission of 495 nm. To start the experiment, vesicles were diluted 200 fold into assay buffer containing 5 µM nigericin, 25 mM BTP-Tricine (pH 7.4) and mannitol to adjust osmolality. After ΔpH formation, aliquots of ionic solutions were added as indicated. Triton X-100 (final concentration 0.03%, v/v) was added to disrupt the vesicle membrane and thereby abolish the ΔpH.

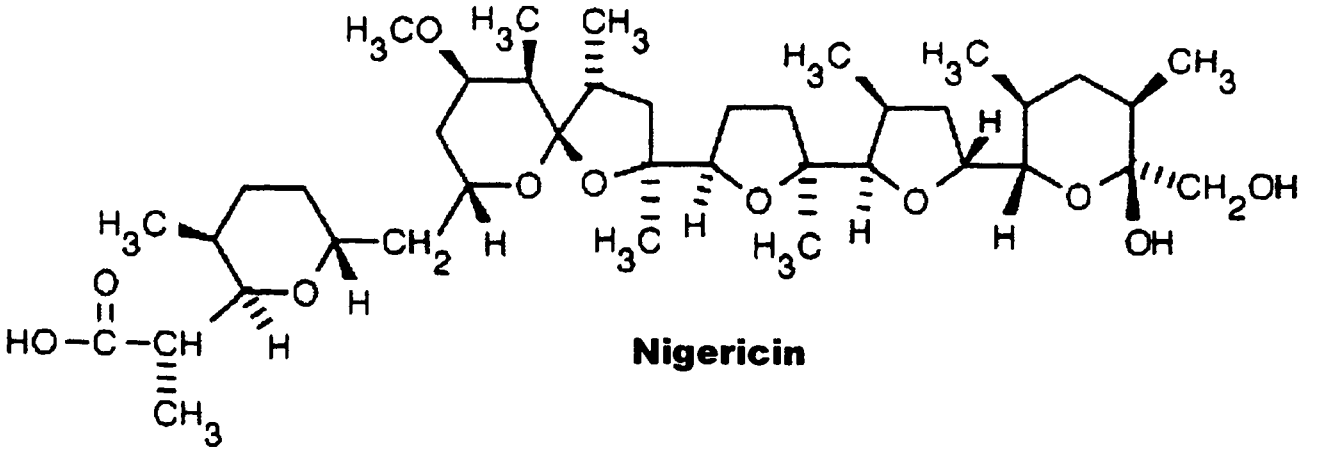


Figure 2.2. Chemical structure of nigericin. Note the high numbers of oxygens that can co-ordinate with K^+ to form a ring shaped complex about the central cation.

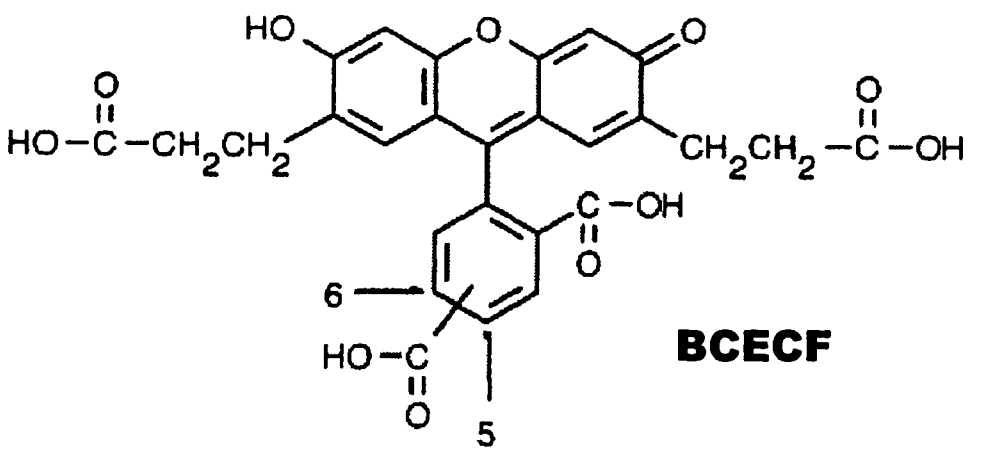


Figure 2.3. Chemical structure of BCECF (2',7'-bis-(2-carboxyethyl)-5-(and-6)-carboxyfluorescein). This dye is a mixture of two isomers with a carboxy group at C_5 and C_6, respectively.

2.5.2 pH-jump experiments

As an alternative way of imposing a pH gradient across the vesicle membrane, I used the pH jump method. All dye loading and washing steps were performed either in buffer containing 10 mM Mes-BTP at pH 7.4, pH 6.8, pH 6.2 and pH 5.5, respectively, to equilibrate the internal pH accordingly. For the Mes-BTP buffer, the Stern-Volmer quenching constant for lucigenin at each pH tested was determined and accounted for in the calculations. The experiments were started by adding the vesicles to assay buffer containing BTP-Tricine (pH 7.4). Thus, by pre-equilibrating the vesicles a pH jump between 0.6 and 1.9 units was imposed.

2.5.3 Energisation *via* the vacuolar H^+-ATPase

To generate a ΔpH using the vacuolar H^+-ATPase, vesicles were prepared and measurements conducted as in section 2.5.1. Vesicles (150 µg) loaded with 200 mM K_2SO_4 were added to 500 µl of K^+-free assay buffer containing 5 mM quinacrine. To activate the H^+-ATPase, 5 mM $MgSO_4$ and 3 mM ATP were added to the assay medium while measuring the quinacrine fluorescence. Further additions were made as specified.

2.5.4 Measuring the ΔpH using BCECF

To estimate the size of the pH gradient formed by the K^+/nigericin clamp, an internal calibration was conducted using the ratiometric fluorescent dye BCECF (2',7'-bis-(2-carboxyethyl) -5-(and-6)-carboxyfluorescein: Figure 2.3). While the free acid form of BCECF is highly membrane impermeant (4 to 5 negative charges at pH 7.0), a recent report suggests that plant vacuoles can show MgATP dependent uptake of BCECF (Swanson *et al.*, 1998). Therefore, vesicles were incubated for 60 min at 25°C

in loading buffer containing 1.25 µg ml^{-1} BCECF, 5 mM ATP, 20 mM $MgSO_4$, 100 mM K_2SO_4, 2.5 mM BTP-Tricine (pH 7.4) and mannitol to adjust the osmolality to 500 mosmol kg^{-1}. Subsequently, the vesicles were washed twice to remove external dye and MgATP by pelleting them at 100 000 *g* for 15 min and re-suspending in 100 mM K_2SO_4, 2.5 mM BTP-Tricine (pH 7.4) and mannitol to adjust the osmolality to 500 mosmol kg^{-1}.

To start an experiment, 50 µg of vesicles (10 mg ml^{-1}) were added to a cuvette containing 2 ml of K^+ free assay medium (5 µM nigericin, 25 mM BTP-Tricine (pH 7.4) and mannitol to adjust osmolality). After a ΔpH was established, an excitation wavelength scan from 400 to 550 nm was performed (emission wavelength 535, both slits at 10 nm).

Then, 200 mM KCl (final concentration) was added to abolish the K^+ gradient, and therefore also the pH gradient. Furthermore, nigericin equilibrates the internal and external pH in the absence of a K^+ gradient (Chao *et al.*, 1990). Hence, the external pH should also predominate in the vesicular lumen. So the pH in the medium measured using a Φ50 pH meter (Beckman, Fullerton, CA., USA), can be directly correlated with the ratioed fluorescence signal (i.e. pH-sensitive excitation wavelength at 505 nm divided by insensitive excitation wavelength at 439 nm; emission 535 nm) as obtained from the excitation scan. Then the pH was changed by adding an aliquot of 1 M HCl to the cuvette and again the pH was measured, and a wavelength scan performed. This was repeated several times to obtain an internal calibration curve for the intravesicular pH.

2.6 Inhibitor studies

The assay buffer for the study of inhibitors was composed of 10 mM BTP-Tricine (pH 7.4), 25 mM K_2SO_4 and enough mannitol to keep total osmolality at 500 mosmol kg^{-1}. Vesicles were loaded with lucigenin as described in section 2.3.1, with the exception that no DTT was used since it might have interfered with some of the substances tested. Since DMSO quenches lucigenin fluorescence at high concentrations (see section 4.2.3), 10 mM fresh stock solutions of DIDS and SITS, and 25 mM stocks of *p*CMBS where made up in assay buffer prior to the experiments. Flufenamic acid, niflumic acid and 9-AC were prepared as a 20 mM stock solution in 100% ethanol, so the controls also contained 0.5% ethanol.

Vesicles were pre-incubated in the inhibitor-containing assay buffer 4 min prior to adding Cl^-.

2.7 Patch-clamp studies

2.7.1 Isolation of mesophyll protoplasts

Mesophyll protoplasts and vacuoles were isolated from 6- to 9-week-old leaves from *M. crystallinum* using an enzymatic digest of the cell wall. Using fine forceps, the lower epidermis was peeled off one or two leaves and major veins were removed. The leaves were then washed in medium A (Table 2.1) for 15 min on ice. The mesophyll tissue was left floating on medium B for 60 min at 25 to 30°C. After the incubation, the remaining leaf tissue was removed and the released protoplasts were left to settle at the bottom of a Falcon tube for 15 to 20 min on ice. The supernatant was subsequently taken off and the protoplasts resuspended in medium C

Table 2.1. Solutions for the isolation of protoplasts and vacuoles. Concentrations are given in mM, percentages as w/v

Solution	Mannitol	Glycerol	$MgSO_4$	K_2SO_4	Cellulase Onozuka RS[a]	Pectyolase Y-23[b]	PVP-40	EGTA	DTT[c]	BSA[c]	Mes	pH
A	475	-	-	-	-	-	-	-	-	-	25[d]	5.7
B	-	264	5	67	0.45%	0.025%	0.2%	-	1	0.5%	25[d]	5.7
C	-	465	5	-	-	-	0.2%	-	1	0.05%	25[d]	5.7
D	-	175	5	-	-	-	0.2%	2	-	-	25[e]	7.4

[a] obtained from Yakult Honsha Co., Tokyo, Japan
[b] obtained from Seishin Pharmaceutical Co., Tokyo, Japan
[c] added fresh
[d] pH adjusted with NaOH
[e] pH adjusted with Tris

and left to settle again. This washing was repeated twice and the protoplasts were kept in medium C on ice until further use. Intact protoplasts could be kept for more than 24 h this way, but were usually used within 8 hours of isolation.

To release vacuoles from the protoplasts, an aliquot of protoplasts was transferred to the recording chamber filled with the hypotonic medium D. After the protoplasts settled to the bottom of the chamber (within 2 min), excess bath solution was taken off. As soon as the rupture of the protoplasts was observed and the first vacuoles were released, the bath was perfused with an appropriate isotonic recording solution to stabilise the vacuoles. After perfusion with at least eight times the chamber volume, the patch-clamping process was started.

Vacuoles could remain intact for more than 3 h after isolation, but were usually used within 1 to 2 h after release.

2.7.2 Electrophysiological recordings

The amplifier used for patch-clamping vacuoles was an L/M-EPC-7 (List-electronic, Darmstadt, Germany). The signal was low-pass filtered with an 8-pole Bessel filter (FD 902, Frequency Devices Inc., Haverhill, MA, USA) at a cut-off frequency between 200 Hz and 4 kHz and fed to a PC *via* the TL-1 DMA interface (Axon Instruments). For the online data acquisition and command-voltage protocols, the electrophysiological software suit pClamp 6 (Axon Instruments) was used. The sampling rate was between 0.5 and 10 kHz and was always at least 2.5 fold higher than the filter cut-off frequency, according to the sampling theorem of Nyquist (Heinemann, 1995), to avoid aliasing of the data.

According to the convention proposed by Bertl *et al.* (1992), all voltages refer to the cytosolic potentials with respect to the vacuolar lumen. Furthermore, positive currents are by definition positive charges moving from the cytosolic side into the vacuole, while negative currents reflect the movement of positive charges from the vacuolar side to the cytosolic side of the membrane. To conform to this convention, all signals were inverted during recording in the whole vacuole (wv) and cytosolic-side-out modes (co, meaning the cytosolic side faces the bath solution, equivalent to the 'inside-out' configuration). In the vacuolar-side-out mode (vacuolar-side-out, vacuolar side faces the bath, equivalent to an 'outside-out' patch), the signal did not have to be inverted.

Electrodes were pulled on an L/M-3P-A (List-electronic) electrode puller from thin-walled borosilicate microcapillaries (Sigma; outer diameter 1.72 mm, inner diameter 1.36 mm) in two stages. The electrode tips were subsequently dipped into inlay casting wax (Kerr UK Ltd., Peterborough, UK), which was kept at 72°C. Just prior to use, the pipettes were polished on a CPZ-101 pipette forge (List-electronic) and filled with filtered pipette solution using a syringe.

The perfusion system was designed as a dual chamber system (Figure 2.4) manufactured by the workshop. The actual recording chamber had a volume of about 250 µl and was connected *via* a short canal to the reference chamber. The height-adjustable outlet and the reference electrode were placed into the reference chamber, while the inlet was at the opposite end of the recording chamber. The height of the water level and hence the volume of the bath medium was adjusted by the position of the outlet. The inlet was connected to eight separate reservoirs and the flow rate could effectively be adjusted by a pinch valve. Flow rates varied between 0.5 to 1 ml min^{-1} and were adjusted so as not to wash out the vacuoles sticking on the glass bottom of the chamber. This set-up enabled an efficient, controlled and gentle perfusion of the

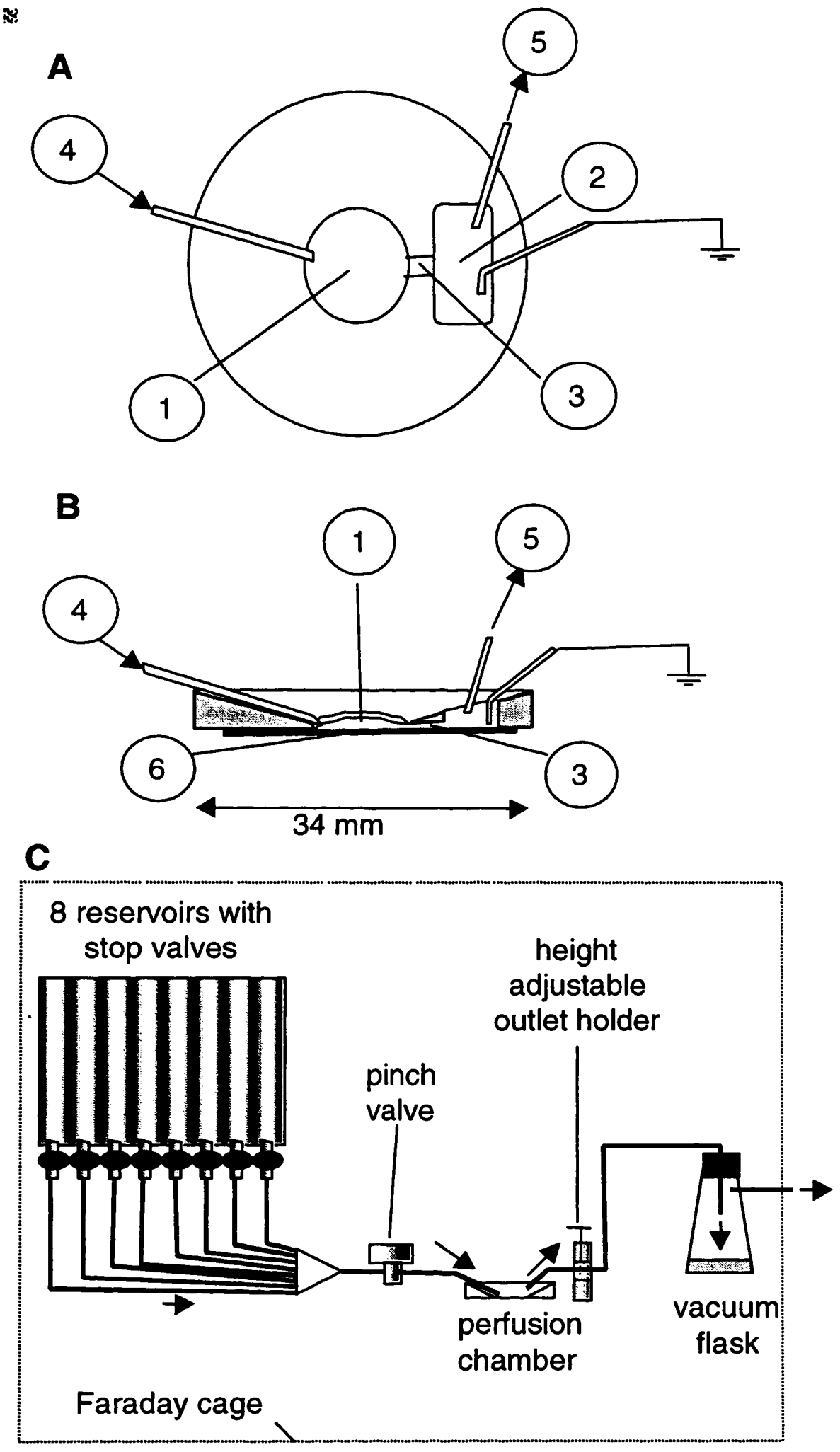


Figure 2.4. Perfusion system for patch-clamping whole vacuoles. View from top (**A**) and middle section (**B**) of the recording chamber. (**C**) The complete perfusion system. Labels: (1) Recording chamber; (2) outlet chamber for reference electrode and solution outlet; (3) connection between outlet and bath chamber; (4) solution inlet tube; (5) outlet tube (6) glass cover slip

vacuoles. At least eight to ten chamber volumes were exchanged when the recording solution was changed.

In order to obtain low-resistance electrodes (300 to 800 kΩ) to record from large membrane patches, pipettes with openings of up to 15 µm tip diameter and a short taper were fabricated according to the method described by Hilgemann (1995). A bead of soft glass (i.e. with a high lead content) was heated on a platinum wire of a micro-forge, and then a pipette was pushed into the molten glass (Figure 2.5). The pipette was fabricated from thin-walled borosilicate microcapillaries as described above.

For the analysis of voltage-ramps leak-currents obtained from "silent" recordings were subtracted from recordings with single-channel activity to obtain the single channel currents. Only those traces were analysed where single-channel activity could be seen just before or during the voltage ramp so that the single-channel amplitude and background levels were well defined. The recordings were analysed using the pClamp 6 software-suit and Microsoft Excel. Excel was also used for curve fitting using the solver function to iterate a least squares algorithm.

2.7.3 Recording solutions

All recording solutions were adjusted to either pH 7.4 for cytosolic solutions or pH 5.5 for vacuolar solutions. The osmolality of the solutions was determined cryoscopically (Osmomat 030, Gonotec, Berlin, Germany) and was adjusted to 500 ± 5 mosmol kg^{-1} with glycerol. Free Ca^{2+} concentrations were estimated using the programme GEOCHEM-PC 2.0 (Parker *et al.*, 1995). This programme was also used to calculate ionic activities for determining Nernst potentials. A summary of solutions used is listed in Table 2.2.

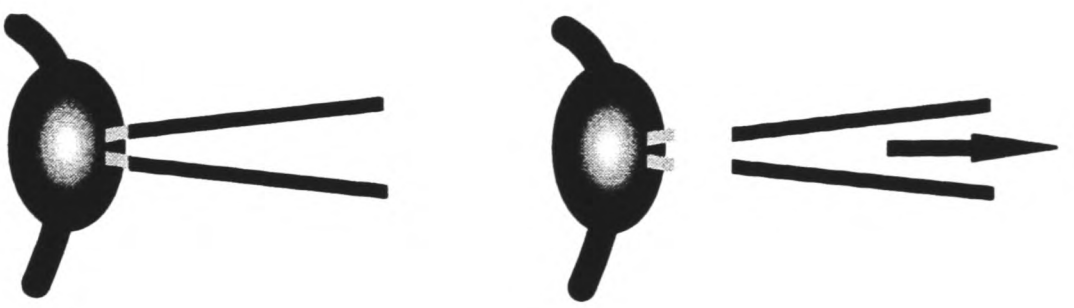


Figure 2.5. Breaking pipette tips for macropatch recordings. A soft-glass bead is melted on a platinum wire on the microforge. A pipette tip is then pushed into the glass bead and after a few seconds retracted swiftly to give a clean break

Table 2.2. Recording solutions. An appropriate amount of glycerol was added to each solution to give a total osmolality of 500 mosmol kg^{-1}. Concentrations are in mM, except for Ca^{2+} (in M)

Solution	KCl	NMDG-Cl	K-gluconate	$MgCl_2$	$CaCl_2$	Na_2EGTA	Tricine/Tris, pH 7.4 [a] Mes/Tris, pH 5.5 [a]	~ Free Ca^{2+} [b]
E	100	-	-	2	1	-	10	10^{-3}
F	4	-	-	2	1	-	10	10^{-3}
G	200	-	-	2	1	-	10	10^{-3}
H	-	100	-	2	1	-	10	10^{-3}
I	4	-	96	2	1	-	10	10^{-3}
J	100	-	-	2	1	1.07	10	10^{-6}
K	4	-	-	2	1	1.06	10	10^{-6}
L	200	-	-	2	1	1.09	10	10^{-6}
M	-	100	-	2	1	1.07	10	10^{-6}
N	4	-	96	2	1	1.07	10	10^{-6}
O	100	-	-	2	1	1.94	10	10^{-9}
P	4	-	-	2	1	1.70	10	10^{-9}
Q	200	-	-	2	1	2.08	10	10^{-9}
R	-	100	-	2	1	1.94	10	10^{-9}
S	4	-	96	2	1	1.94	10	10^{-9}

[a] Tricine/Tris, pH 7.4, was used for solutions on the cytoplasmic side
Mes/Tris, pH 5.5, was used for solutions on the vacuolar side

[b] The estimated free Ca^{2+} concentration is given as M

Chapter 3

Properties of the Cl^- indicators and tonoplast vesicles

3.1 Introduction

Initially, SPQ (6-methoxy-*N*-(3-sulphopropyl)quinolinium) was used to measure Cl^- transport into tonoplast vesicles. However, a recent report suggested an alternative Cl^--sensitive fluorescent dye, lucigenin, with improved properties (Biwersi *et al.*, 1994). Since lucigenin has not been previously used in plants to measure Cl^- transport, it was necessary to characterise the dye in more detail. In particular its sensitivity and specificity towards Cl^- needed to be determined under typical experimental conditions. Further characteristics, such as the pH sensitivity and the ability to load lucigenin into vesicles, had to be studied to evaluate its usefulness as well as its possible limitations for studying Cl^- transport in tonoplast vesicles.

Also, this chapter describes some properties of *Mesembryanthemum crystallinum* tonoplast vesicles that are needed to quantify Cl^- transport activity.

3.2 Results

3.2.1 Properties of SPQ

SPQ (6-methoxy-*N*-(3-sulphopropyl)quinolinium) is a pale, water-soluble yellow powder with a molecular weight of 281. Figure 3.1 shows the spectral properties of 20 mM SPQ loaded into tonoplast vesicles. It has two excitation peaks at 320 and 350 nm, respectively. The emission spectrum showed a broad peak between

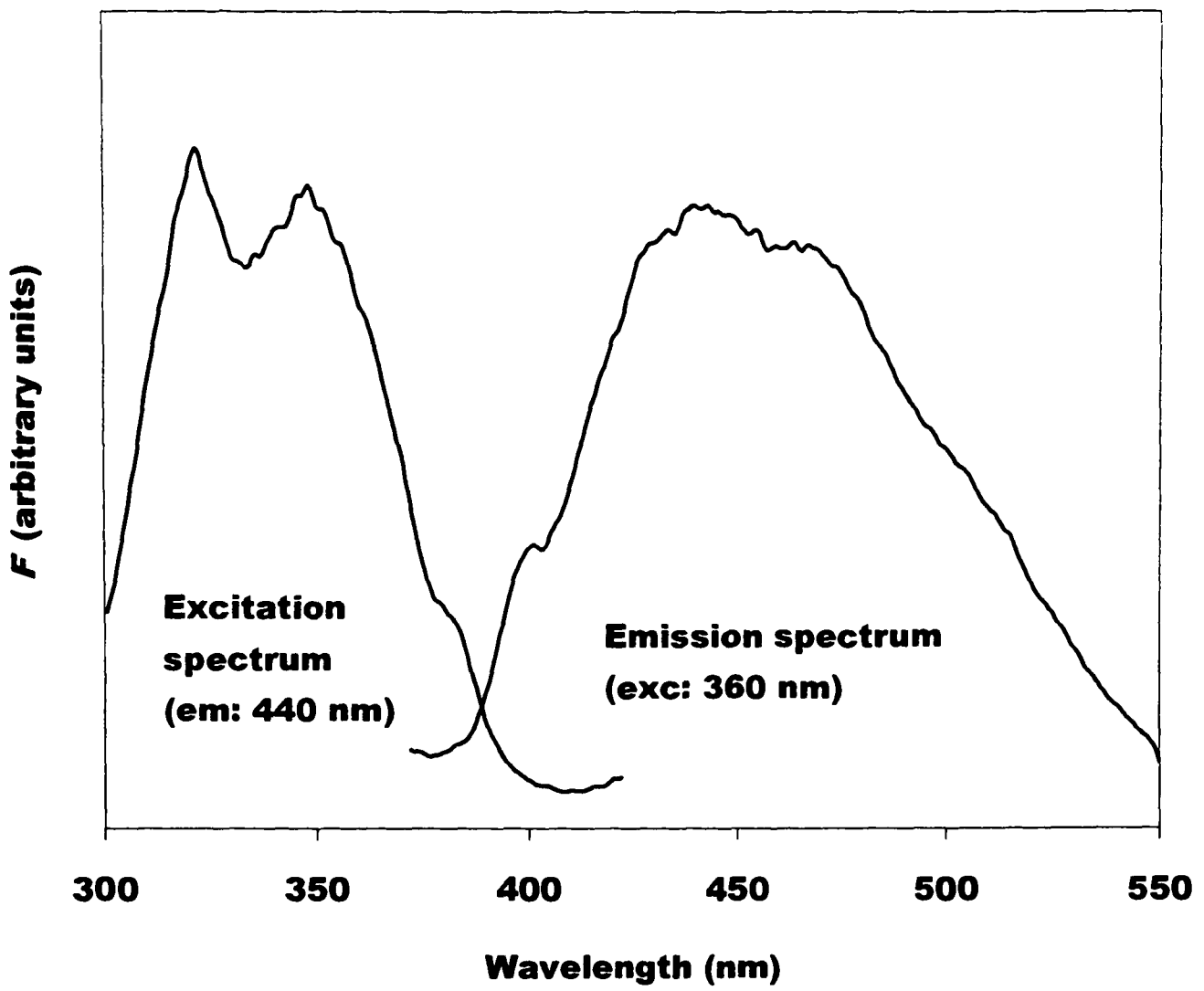


Figure 3.1. Excitation and emission spectra of SPQ loaded vesicles. Vesicles were loaded with 20 mM SPQ. For the excitation scan an emission wavelength (em.) of 440 nm was used and for the emission scan an excitation wavelength (exc.) of 360 nm. Both slits were set at 10 nm

430 and 470 nm. The short excitation wavelength made it more susceptible to signal noise due to small particles in solution. This led to fluorescence traces obscured by noisy spikes size (see Figure 4.2), which made it difficult to analyse the data, even though all solutions had been filtered through a 0.2 μm filter.

As also described by other reports, SPQ is very sensitive to millimolar concentrations of halides (Table 3.1), and has a Stern-Volmer quenching constant for Cl^- of 0.081 mM^{-1} in 10 mM Tricine-BTP, pH 8.0 at 25°C. It is insensitive to potassium, nitrate, sulphate, and only slightly sensitive to citrate (K_{sv} = 0.014 mM^{-1}).

The dye could be easily loaded into the vesicles by incubating them at 38°C for 30 min, essentially following the method of Pope and Leigh (1988). At lower temperatures (25°C) its retention in the vesicles is sufficiently high to allow even prolonged recordings over up to 30 min (discussed further in Chapter 4).

Adding Triton X-100 to the vesicles to disrupt the membrane actually enhanced the fluorescence intensity at lower Cl^- concentrations (< 15 mM Cl^-), similar to the Pope and Leigh (1988) observation made for beet-root storage-tissue. This effect might be attributable to an endogenous quencher, as assumed in that report.

3.2.2 Characterisation of the fluorescent dye lucigenin

The susceptibility of the SPQ recordings towards signal noise at shorter wavelengths made them difficult to analyse, so another Cl^--sensitive fluorescent indicator lucigenin (*N,N'*-dimethyl-9,9'-bisacridinium dinitrate) was tested.

Lucigenin is a bright yellow, water-soluble powder with a molecular weight of 511. It is somewhat less water soluble than SPQ, and saturated between 15 and 20 mM in the buffer solutions used. Therefore, vesicles were usually loaded with 10 mM lucigenin. As with SPQ, lucigenin could be loaded easily into the vesicles at 38°C for

Table 3.1. Effect of various solutes on the fluorescence of 0.1 mM SPQ. Measurements were made in assay medium, pH 8.0, at room temperature using a well-plate reader. The slope of the F_0/F plots gives the Stern-Volmer quench constant

Addition	**Stern-Volmer quench constant (10^{-3} mM^{-1})**	**Solute concentration (mM) giving 50% fluorescence quench**
KCl [a]	80.6	12
KCl	66.8	15
KBr	113.8	9
KI	149.2	7
KNO_3	0.2	5000
K_2SO_4	0.7	1429
$(NH_4)_2SO_4$	0.6	1667
K-acetate	6.7	149
Na_3-citrate	14.3	70

[a] Measurements were performed at 25°C in a 500 µl cell

30 min, and showed good retention at lower temperatures (discussed further in Chapter 4).

3.2.2.1 Spectral properties

Figure 3.2 shows the spectral properties of lucigenin. The spectra are similar for lucigenin in free solution and loaded into vesicles. It has a maximum excitation peak around 370 nm, and two smaller peaks at 433 and 455 nm. This broad excitation spectrum means that it can be used at much longer wavelengths, and the signal consequently contains much less noise.

The emission spectrum shows a broad peak between 473 and 506 nm. For most subsequent experiments, an excitation wavelength of 433 nm and an emission wavelength of 506 nm were used. The excitation wavelength of 433 nm was used instead of 455 nm because it gave slightly more intensive fluorescence signal without much increasing the signal noise.

3.2.2.2 Sensitivity and specificity

To determine the sensitivity of lucigenin to Cl^-, different concentrations of lucigenin were added to assay medium with increasing amounts of KCl. Figure 3.3 shows the hyperbolic decrease of lucigenin fluorescence with increasing Cl^- concentration. The relative changes in fluorescence were the same for all lucigenin concentrations tested. Higher concentrations than 0.2 mM lucigenin could not be tested because of the high fluorescence intensity, which saturated the detector. The hyperbolic relationship can also be expressed as a Stern-Volmer plot (maximum fluorescence F_0 divided by the decreased fluorescence F, Figure 3.3). This showed a nearly linear increase with increasing Cl- concentration, following the Stern-Volmer

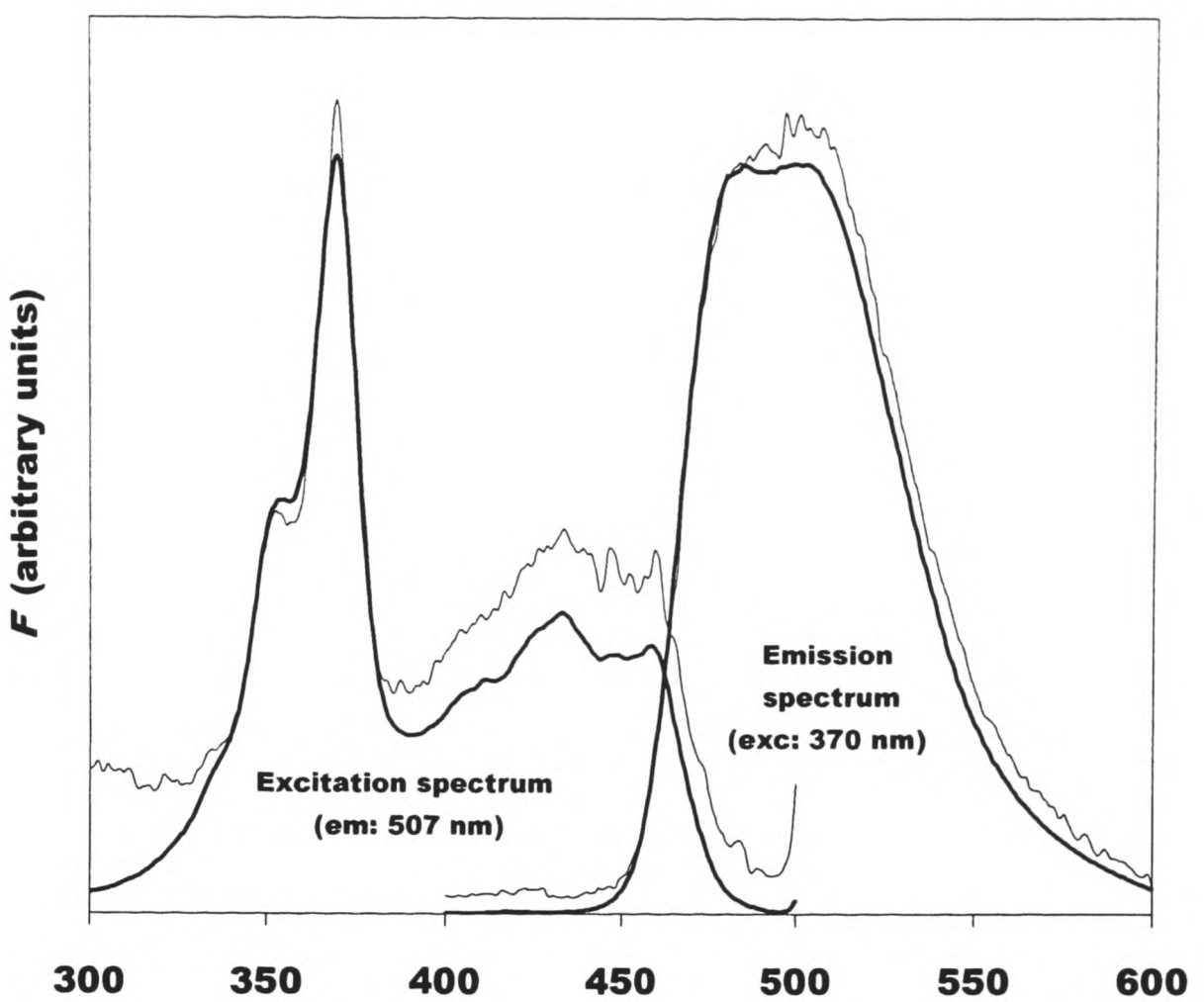


Figure 3.2. Excitation and emission wavelength of lucigenin. Excitation wavelength (exc.) for the emission scan was 370 nm, and the emission wavelength (em.) for the excitation scan 507 nm. The thick lines show scans of a 0.05 mM solution of lucigenin, while the thin lines represent similar scans of vesicles loaded with 10 mol m^{-3} lucigenin

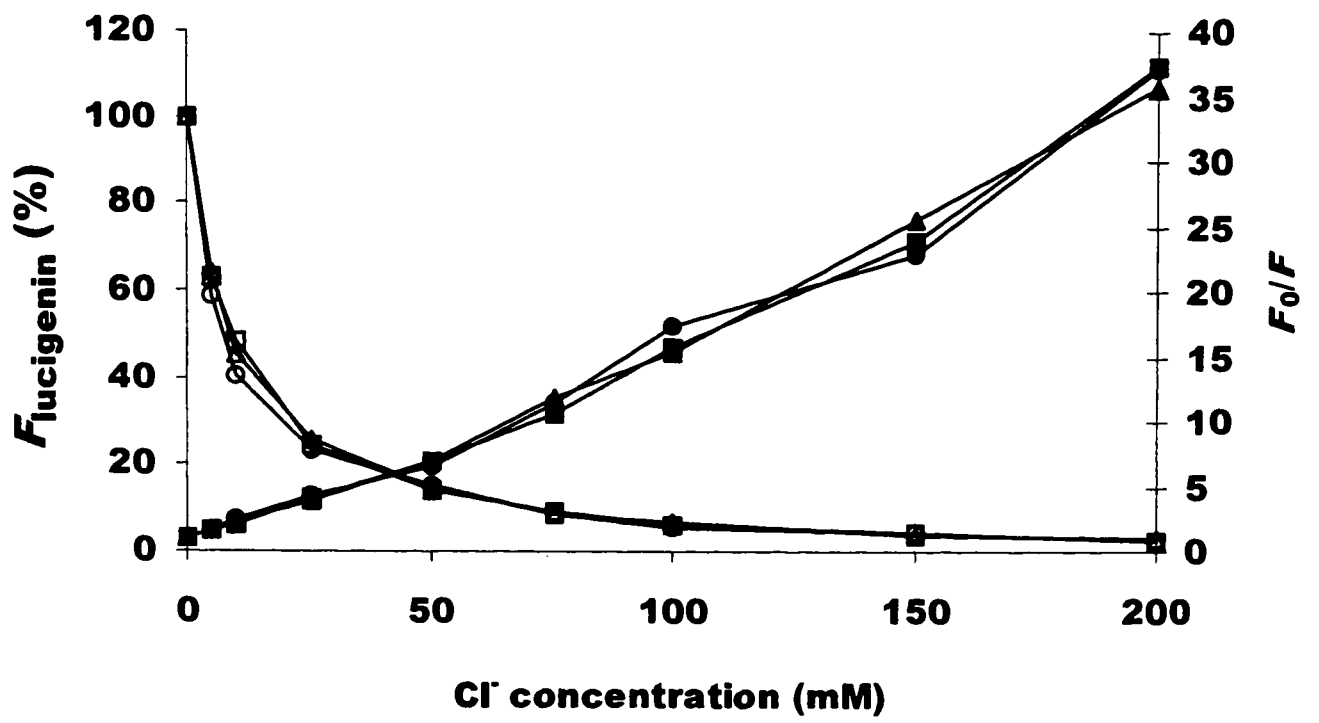
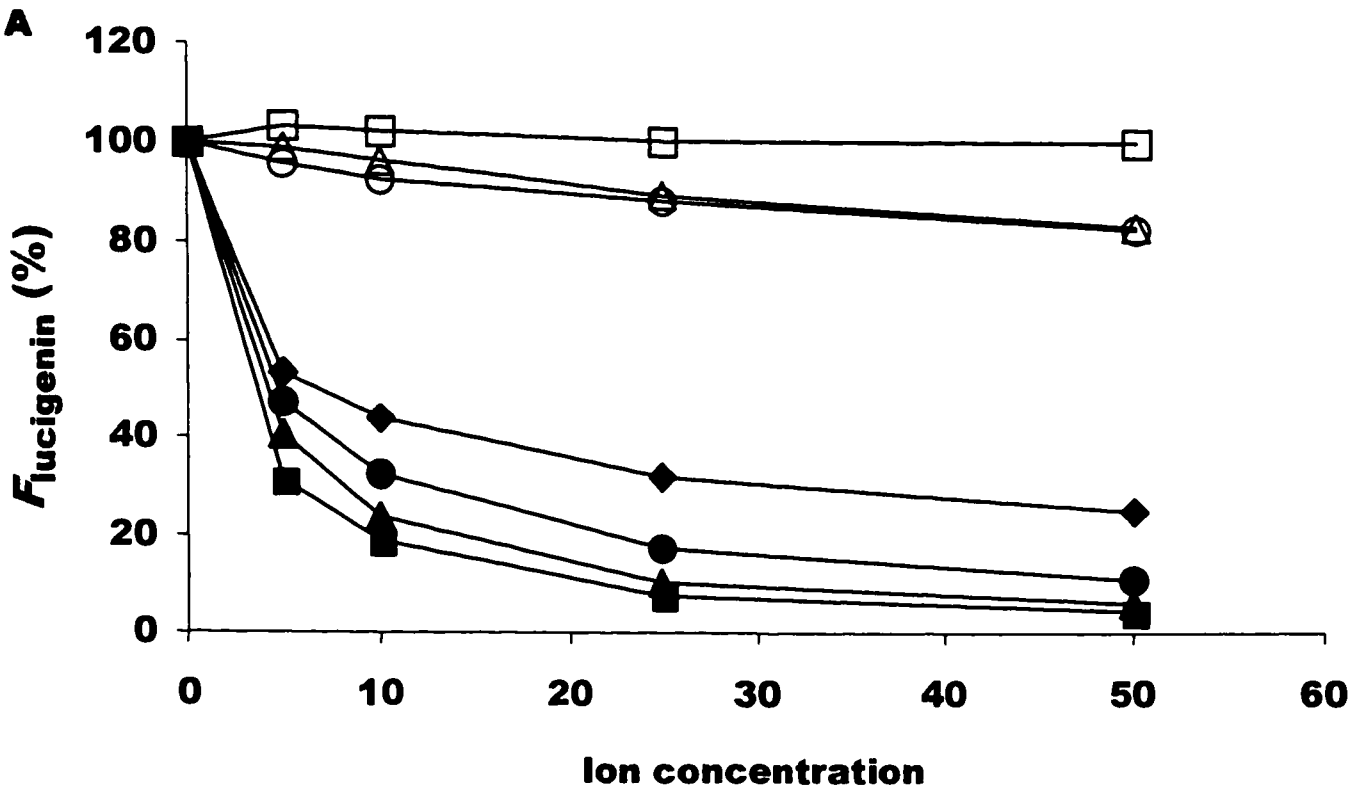


Figure 3.3. Fluorescence quenching of lucigenin by Cl^-. The fluorescence intensity (exc. 433 nm; em. 506 nm) of three different lucigenin concentrations of 0.2 mM (❑), 0.1 mM (Δ) and 0.01 mM (○) was measured at various Cl^- concentrations. The closed symbols represent the equivalent Stern-Volmer plots (F_0/F). All measurements were performed in assay medium at pH 7.4 in a stirred 2 ml cell at 25°C. Data points are the means of duplicate measurements

relationship $F_0/F = 1+K_{sv}[Q]$ (K_{sv} = Stern-Volmer constant; [Q] = concentration of quenching ion). With higher Cl^- concentration, the increase became slightly steeper. The average Stern-Volmer constant for Cl^--dependent lucigenin fluorescence quenching was 0.173 mM^{-1} (25°C, 10 mM Tricine-BTP, pH 7.4).

To determine the specificity of the lucigenin fluorescence quenching for Cl^-, various solutes were tested for their ability to reduce the fluorescence intensity. Figure 3.4 shows the fluorescence in response to increasing solute concentration, and the corresponding Stern-Volmer plots, for some of the solutes tested. It showed that while citrate, Cl^-, Br^- and I^- with increasing concentrations quenched lucigenin fluorescence, other ions, such as nitrate, sulphate and malate had no effect on the fluorescence.

Table 3.2 summarises the results for all solutes tested. Besides chloride, lucigenin is even more sensitive towards the other halides bromide and iodide. The Stern-Volmer constant for the Cl^--dependent fluorescence quenching was 0.192 mM^{-1}, as obtained in measurements using the well-plate reader, which was higher than the value obtained with a temperature controlled cell (0.173 mM^{-1}), due to the strong temperature dependence of the collisional quenching. BTP-Cl (pH 7.4) showed a higher Stern-Volmer constant (0.217 mM^{-1}) than KCl, indicating additional quenching by BTP. Citrate, DTT and BTP showed a significant amount of fluorescence quenching, while nitrate, sulphate and many of the organic anions showed only a very limited quenching of lucigenin fluorescence. Mannitol and sorbitol did not show any quenching at all. These results thus demonstrate a very high degree of specificity of the lucigenin fluorescence quenching for halides.



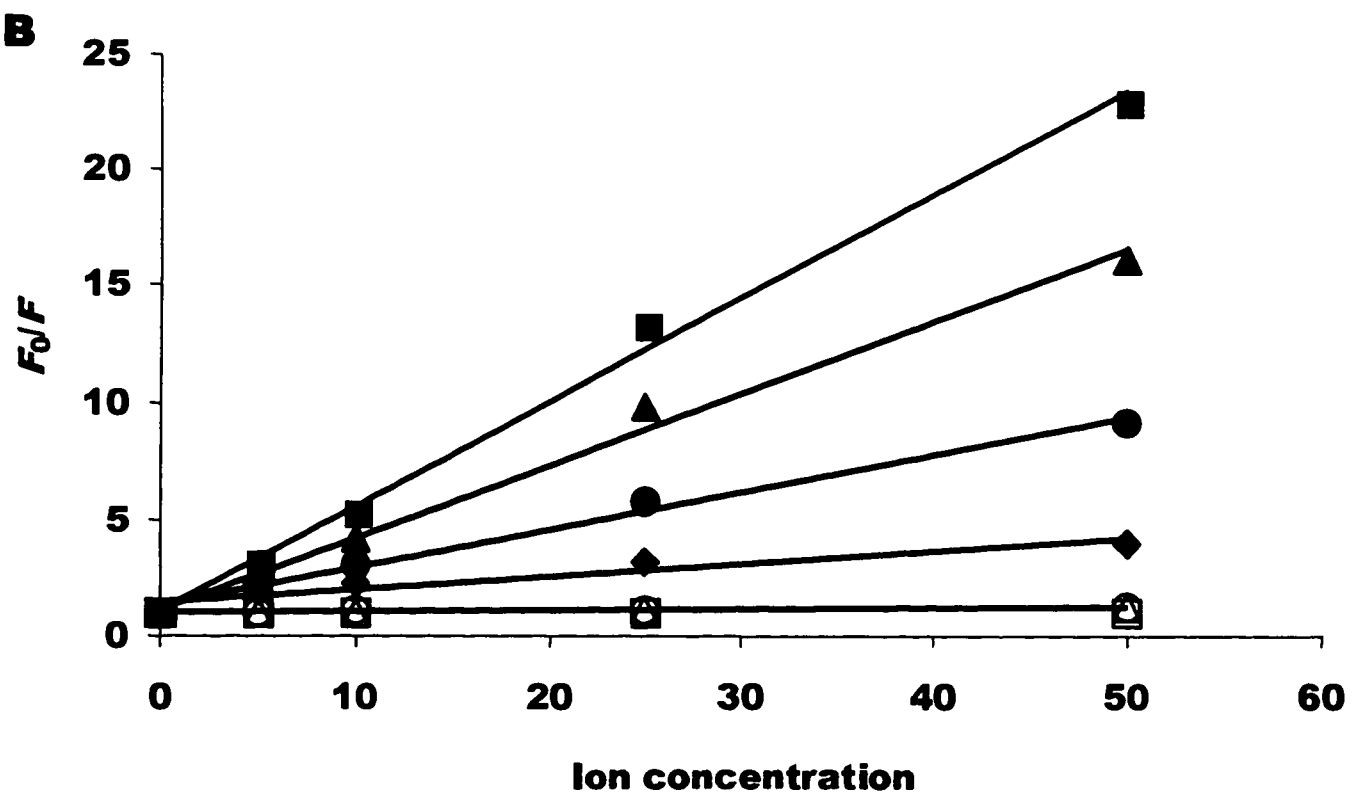


Figure 3.4. Fluorescence quenching of lucigenin by various substances. The fluorescence quenching of 0.1 mM lucigenin is shown in **A**), with the corresponding Stern-Volmer plots in **B**), fitted with linear regression. Symbols: (■) potassium iodide; (▲) potassium bromide; (●) potassium chloride; (♦) sodium citrate; (○) potassium sulphate; (Δ) malic acid; (❑) potassium nitrate. All measurements were performed in assay medium (see Materials and Methods) at room temperature using a well plate reader. Total assay volume was 300 µl. All points are the means of duplicate measurements

Table 3.2. Effect of various solutes on the fluorescence of lucigenin. Unless indicated, measurements were made in assay medium (see Materials and Methods) at room temperature using a well-plate reader. The slope of the F_0/F plots gives the Stern-Volmer quench constant

Addition	**Stern-Volmer quench constant (10^{-3} mM^{-1})**	**Solute concentration giving 50% fluorescence quench (mM)**
KCl [a]	173.0	6
KCl	191.9	5
KBr	357.0	3
KI	495.9	2
K_2SO_4	5.2	192
$(NH_4)_2SO_4$	4.7	213
KNO_3	0.5	2000
Malic acid	4.5	222
Malic acid [b]	6.3	159
Maleic acid	22.5	44
Oxalic acid	21.1	47
K-aspartate	11.7	85
Succinic acid	0.3	3333
Iminodiacetic acid	3.0	333
K-acetate	31.0	32
K-gluconate	22.6	44
Tricine [b]	4.4	227
Tricine-BTP (pH 7.4)	18.2	55
Cl-BTP (pH 7.4) [a]	216.5	5
DTT [b]	91.5	11
BTP [b]	51.6	19
DMSO	19.1	52
Na_3-citrate	79.4	13
Sorbitol [b]	0.0	-
Mannitol [b]	0.0	-

[a] Measurements were performed at 25° C in a 500 µl cell
[b] Measurements were performed in water

3.2.2.3 Effect of pH

While lucigenin has been reported to be insensitive to pH (Biwersi *et al.*, 1994), it has been found that the related dye SPQ shows pH dependent changes in fluorescence, depending on the buffering ion used (Vasseur *et al.*, 1993). Therefore, a series of experiments was performed to establish the effect of the buffering ion on the pH dependence of lucigenin.

As is apparent in Figure 3.5.A, in Tricine-BTP buffer above pH 7 the fluorescence showed a steady decrease and above pH 11 fell below 30% of the maximum intensity. In the presence of 45 mM Cl^- the fluorescence signal was generally much lower due to the Cl^- quenching, and the pH dependent decrease was much less pronounced. Hence, the Stern-Volmer constant K_{SV} for Cl^--dependent quenching, as obtained from the ratio of F_0/F, also showed a non-linear pH dependence above pH 7.0 (Figure 3.5.B). This decrease is steepest around the pK_a for Tricine of 8.1.

Other buffer pairs were tested as well (Figure 3.6), and apart from the phosphate buffer all other buffers showed a significant effect on the K_{SV} for Cl^-. Hepes also showed a pH-independent reduction of the Stern-Volmer constant, reducing it to a maximum value of about 0.120 mM^{-1} at low pH.

Depending on the pK_a value of the buffer, the range for pH sensitivity was shifted accordingly, for example in Mes-BTP buffer the steepest decline in K_{SV} was around pH 6.2, and for Mops-BTP around pH 7.4.

Using Tris instead of BTP as the basic buffering ion did not change these effects, but led to a slight overall reduction in K_{SV} when used with Tricine.

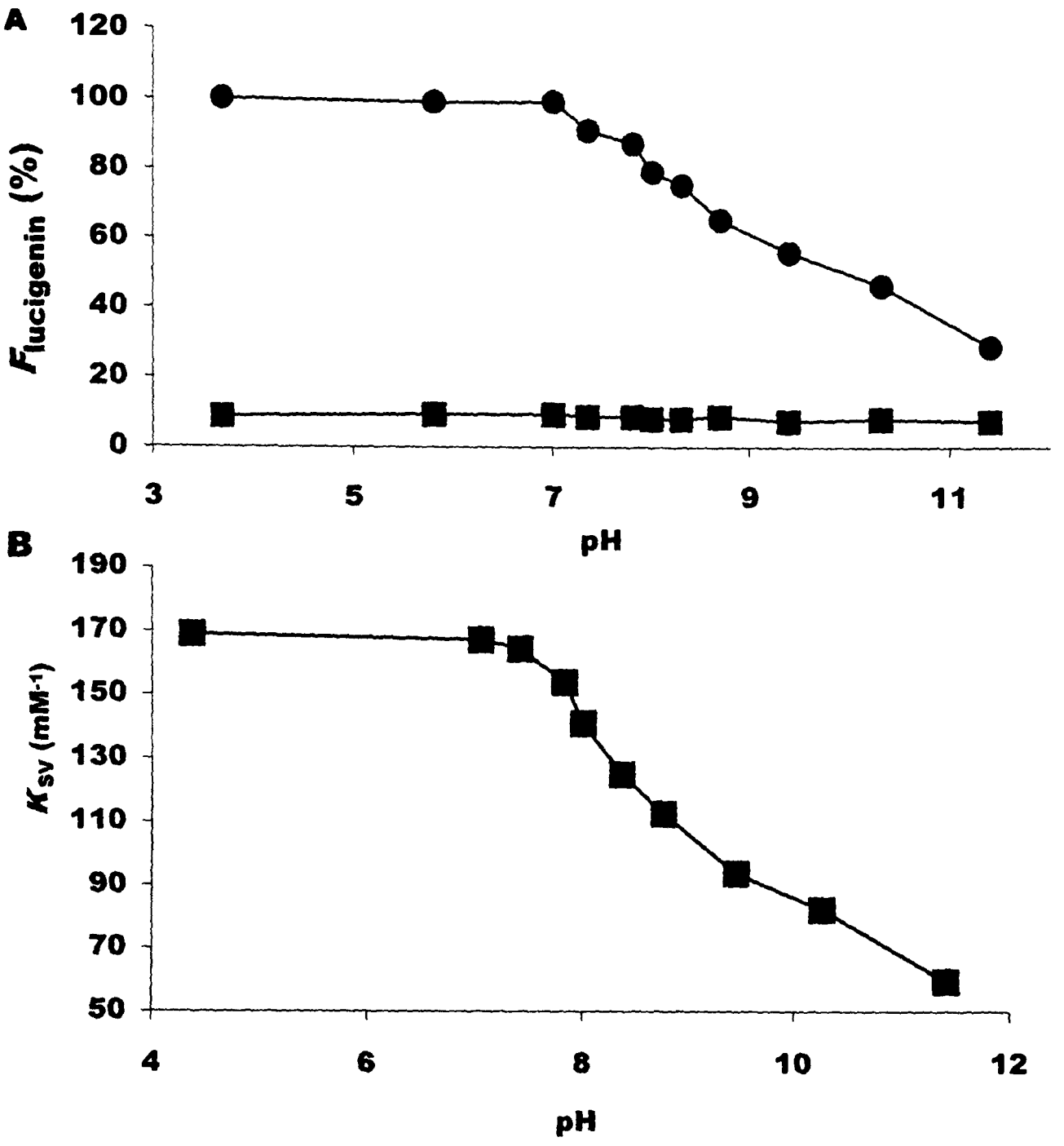


Figure 3.5. Effect of pH on lucigenin fluorescence. **A**) The fluorescence intensity of 0.05 mM lucigenin was measured in dependence on pH. The assay medium contained 10 mM Tricine, which was initially adjusted to pH 8.0 with BTP. Subsequently the pH was varied using sulphuric acid and KOH. The measurements were performed either in the absence (●) or presence of 45 mM Cl^- (■), using a well-plate reader (exc. 433 nm; em. 506 nm). **B**) Stern-Volmer constants (K_{SV}) for Cl^--dependent quenching of lucigenin fluorescence calculated from similar measurements to those in (A)

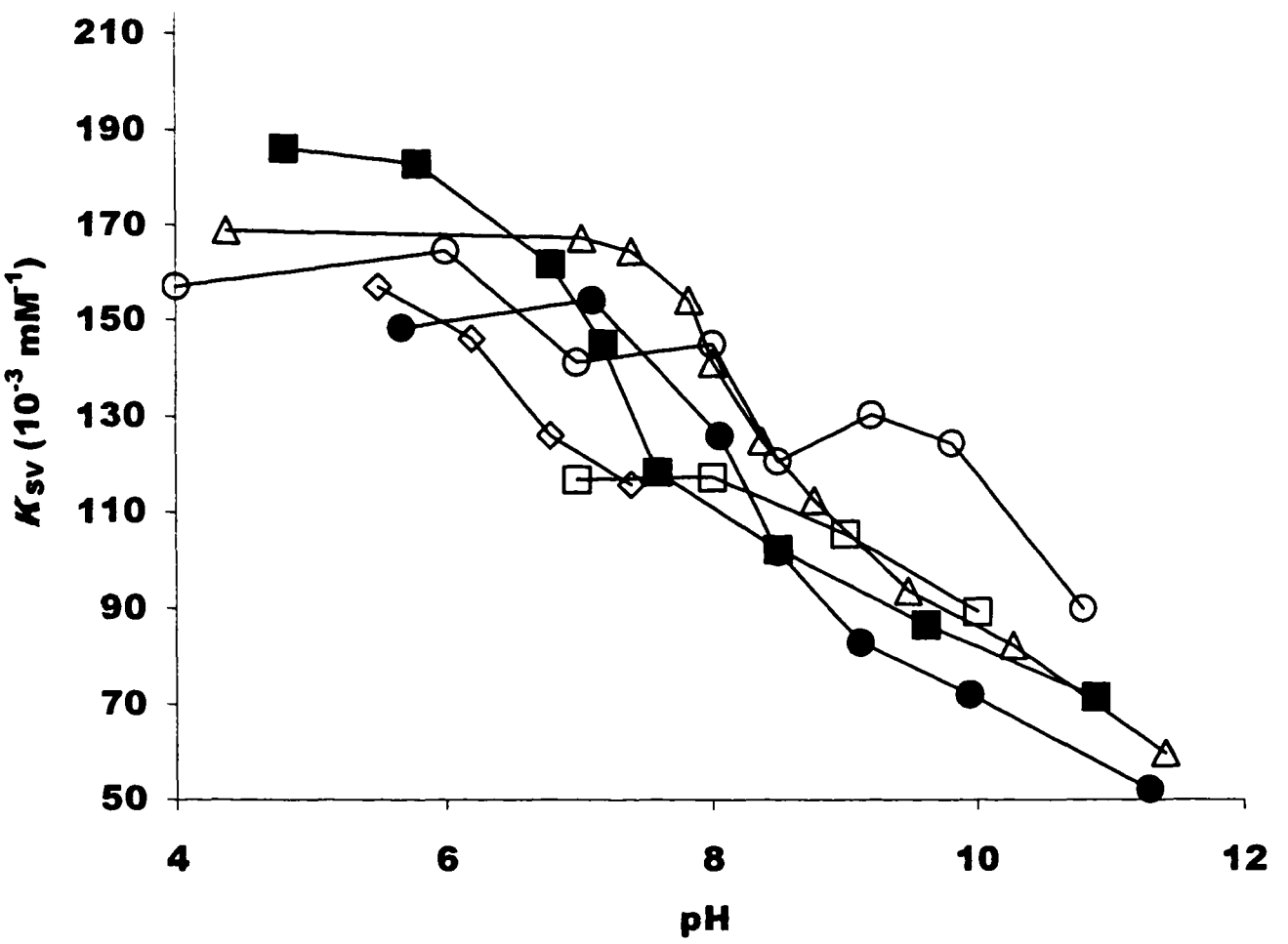


Figure 3.6. Effect of pH and buffering ion on the Stern-Volmer constant K_{SV}. The Stern-Volmer constants for Cl^--dependent quenching of lucigenin fluorescence were measured the following buffer systems (with initial pH): Tricine-BTP, pH 8.0 (Δ); Hepes-Tris, pH 8.0 (❑); Tricine-Tris, pH 8.0 (●); Mops-BTP, pH 8.0 (■); Mes-BTP, pH 6.2 (◊); phosphate buffer, pH 8.0 (○). The pH was first adjusted to a defined pH and then varied using sulphuric acid or KOH. Measurements were performed using a well-plate reader at room temperature with an emission wavelength of 506 nm and an excitation wavelength of 433 nm (all points are means of duplicate measurements)

In the light of these results, most of the subsequent experiments were performed with Tricine-BTP buffering the pH at 7.4. This is still within the recommended buffering range for Tricine and is close to the optimum pH for the Stern-Volmer constant for Cl^- quenching, allowing maximal Cl^- sensitivity.

3.2.3 General properties of tonoplast vesicles of *M. crystallinum*

To be able to quantify the Cl^- fluxes, some further characterisation had to be undertaken to determine the purity of the vesicle preparation and also the average size of the vesicles.

3.2.3.1 Hydrolytic H^+-ATPase activity as a marker for tonoplast membrane

Initially, these measurements were performed at 38°C for 30 min, according to Struve and Lüttge (1987) and Müller *et al.* (1996), but it subsequently became apparent, that this temperature was higher than the optimum for these preparations (Figure 3.7). For example, the total hydrolytic activity of the membrane preparation from salt-treated plants (200 mM for 2 weeks) was 45 µmol P_i h^{-1} mg^{-1} protein at 33°C, while at 38°C it was only 32.8 µmol P_i h^{-1} mg^{-1} protein, a 27% decrease in activity. Furthermore, the difference in hydrolytic activity of the H^+-ATPase between salt-treated and control plants was less pronounced at 38°C (16% difference) than at 33°C (27% difference). Later measurements were therefore conducted at 30°C to allow comparisons with other studies using this temperature (Bremberger *et al.*, 1988; Barkla *et al.*, 1995; Ratajczak *et al.*, 1995).

To determine the purity of the vesicle preparation, the hydrolytic activity of the V-type H^+-ATPase was measured. The nitrate-sensitive V-ATPase is predominantly localised in the vacuolar membrane, while mitochondrial (azide-sensitive) and

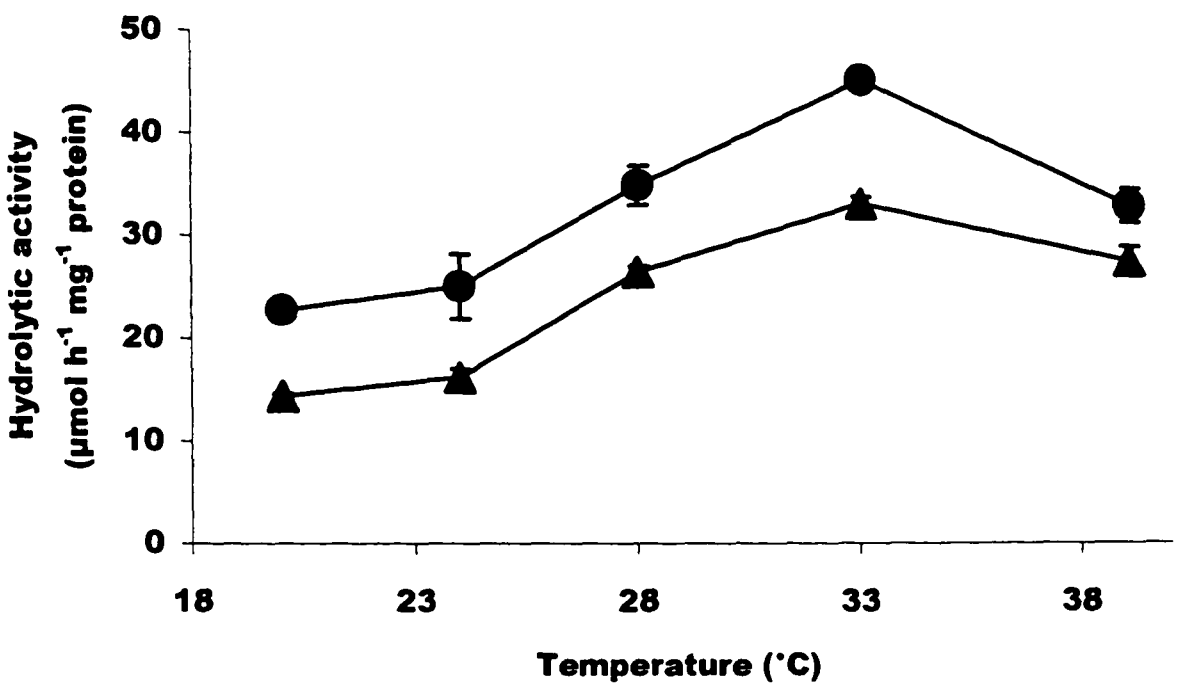


Figure 3.7. Temperature dependency of the ATPase. The total hydrolytic ATPase activities of vesicle preparations from salt treated (●; 200 mM NaCl for 2 weeks) and control plants (▲) were measured at various temperatures. Each datapoint is the average of three measurements from one preparation; error bars indicate s.e.m.

plasma-membrane H^+-ATPase activity (vanadate-sensitive) show less nitrate sensitivity, as do molybdate-sensitive nonspecific phosphatases (Smith *et al.*, 1984; Barkla and Pantoja, 1996; Lüttge and Ratajczak, 1997).

The total hydrolytic activity of vesicle preparations from 8-week-old control plants was 33.7 ± 2.2 μmol P_i h^{-1} mg^{-1} protein (mean ± sem, n = 8). In the presence of 0.2 mM azide, 0.1 mM vanadate and 0.1 mM molybdate the hydrolytic activity was reduced by 7.5% to 31.1 ± 2.0 μmol P_i h^{-1} mg^{-1} protein. Only 9.0 ± 1.0 μmol P_i h^{-1} mg^{-1} protein remained when 50 mM nitrate was added together with the inhibitors. This is only 26.8% of the total and 29.0% of the azide-resistant hydrolytic H^+-ATPase activity, respectively. Hence, the azide-resistant, nitrate-sensitive hydrolytic activity was 65.6% of the total activity.

When plants were grown under controlled conditions in a growth room and harvested at the end of the light period the preparations became more pure, with 78.3 ± 1.5% of the total hydrolytic ATPase activity being azide-resistant and nitrate-sensitive for the control plants (n = 3). Similarly, 6-week-old control plants showed 78.3 ± 1.7%, and 8 to 9-week-old salt-treated plants (400 to 500 mM for 2 to 3 weeks) 75.7 ± 3.5% of the total hydrolytic ATPase activity being azide-resistant and nitrate-sensitive. The effect of salt treatment on the hydrolytic activity of the V-type H^+-ATPase will be discussed in further detail in Chapter 4 (see also Table 4.3 for a summary).

To determine the orientation of the vesicles, the asymmetric vacuolar (V) -type ATPase was used as a marker enzyme to determine the ratio of "right-side out" (i.e. cytosolic side exposed) to "inside out" (vacuolar side exposed) vesicles. As long as the membrane integrity is intact, only the right-side out vesicles will have their

catalytic side exposed, so only their hydrolytic H^+-activity can be measured, as the membrane is effectively impermeable to ATP. To estimate the amount of latent V-ATPase activity of inside-out vesicles, the mild detergent Brij-58 was used. As has been shown recently, Brij-58 does not impair the function or structure of the V-ATPase, but can severely disrupt membrane integrity (Palmgren *et al.*, 1990; Ratajczak, 1994).

Without Brij-58 in the assay medium, the total hydrolytic activity was 17.7 ± 0.6 µmol P_i h^{-1} mg^{-1} protein (n = 3). In the presence of 0.15 mg ml^{-1} Brij-58 the total activity was 32.3 ± 0.5 µmol P_i h^{-1} mg^{-1} protein (n = 3). Therefore, the latent activity (i.e. ratio of sealed right-side out vesicles to inside-out vesicles) of the vacuolar vesicle fraction could calculated as 100 : 82, indicating an almost random tissue homogenisation.

3.2.3.2 Vesicle size

The size of the vesicles was determined using transmission electron microscopy. Figure 3.8 shows a fairly homogeneous population of uni-lamellar membrane vesicles. From these electron micrographs, the diameter of 86 vesicles was measured. Since for each individual a micrograph is a geometric section through a random plane, the measured diameter had to be corrected according to the following calculation (Elias *et al.*, 1971): actual diameter = observed diameter × $4/\pi$.

Figure 3.9 shows the frequency distribution of the corrected vesicle diameters. The distribution was skewed towards the larger diameters, with a mode between 250 and 300 nm, probably due to the smaller vesicles escaping detection. The average vesicle size was 0.336 ± 0.019 µm, with the largest being over 0.860 µm in diameter.

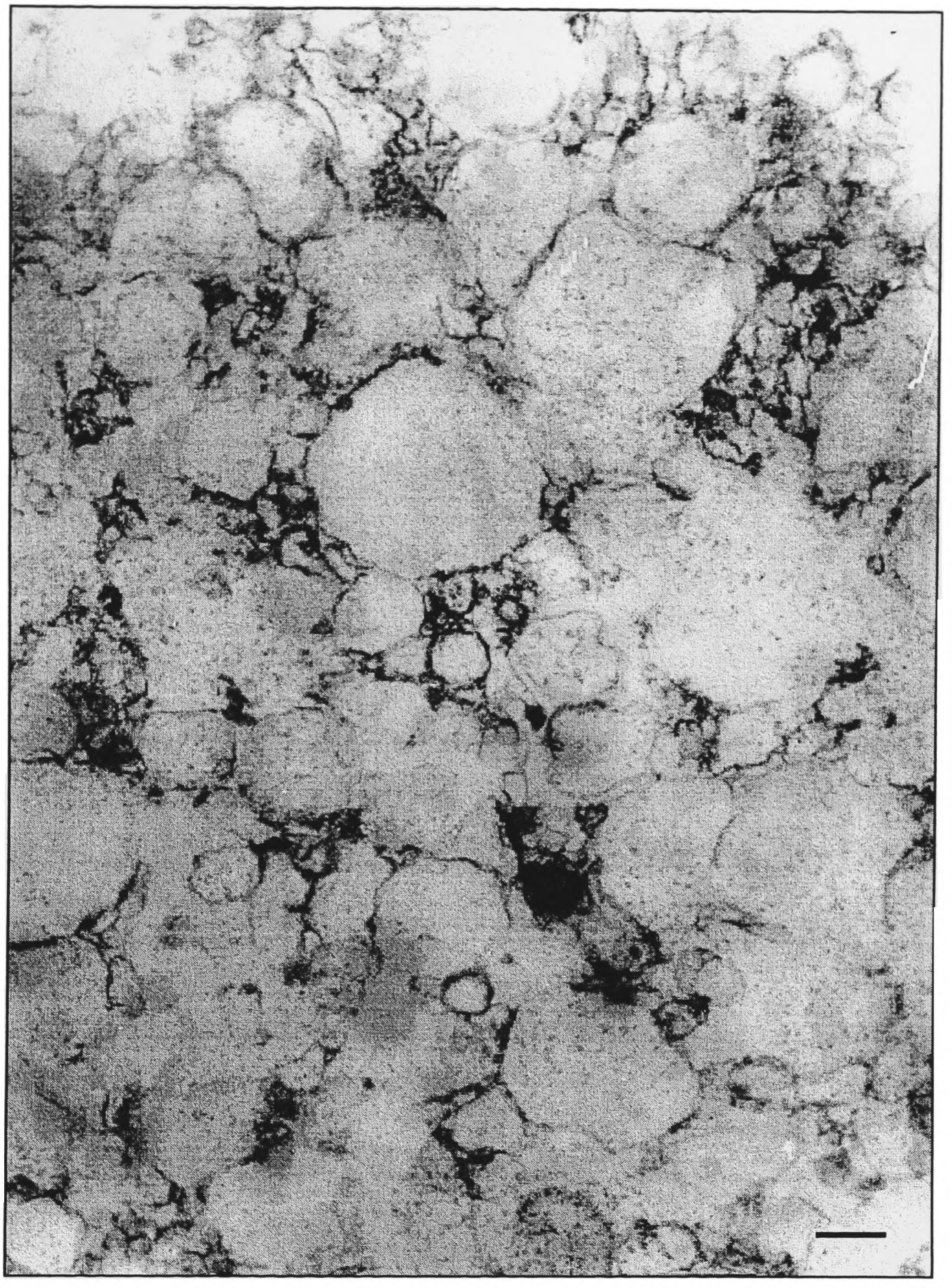


Figure 3.8. Electron micrograph of tonoplast vesicles isolated from *Mesembryanthemum crystallinum*. The bar equals 200 nm

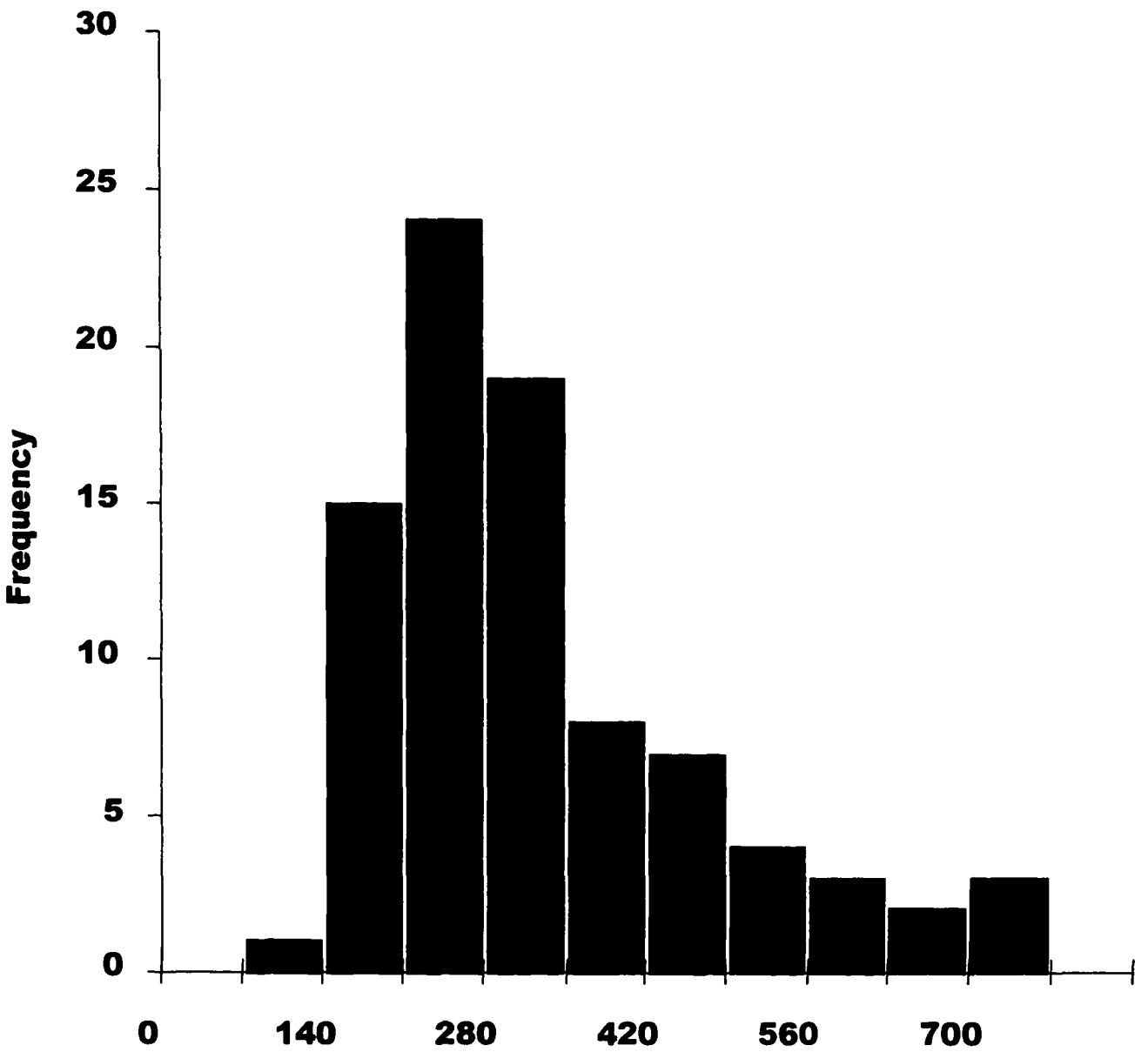


Figure 3.9. Frequency distribution of vesicle diameters. Vesicle diameters were obtained from electron micrographs and the average was corrected for geometric underestimation. The average corrected vesicle size was 0.336 ± 0.019 μm (s.e.m.). A class width of 70 nm and a total number of 86 vesicles was used

The total area of 86 measured vesicles was 3.92×10^{-11} m^2 and the total volume 3.46×10^{-18} m^3. The corresponding average area to volume ratio was 1.13×10^7 m^{-1}.

3.3 Discussion

3.3.1 Lucigenin as a Cl^- indicator

Lucigenin proved to be a useful tool for detecting changes in Cl^- concentration, showing a high fluorescence intensity and a very high sensitivity to halides. Similar studies had been performed previously by other researchers using the Cl^--sensitive dye SPQ (Illsley and Verkman, 1987; Pope and Leigh, 1988; Pope and Leigh, 1990; Chao *et al.*, 1990; Pope *et al.*, 1990), but lucigenin showed superior optical properties. It gives a much greater emission intensity when excited with UV light than SPQ (Biwersi *et al.*, 1994), which means that a small amount of dye-loaded vesicles is sufficient to give a detectable signal. Lucigenin was also much more sensitive to Cl^-, with a Stern-Volmer constant almost twice as high SPQ under similar conditions. Biwersi *et al.* (1994) reported a Stern-Volmer constant of 0.390 mM^{-1} for the quenching of lucigenin fluorescence by Cl^- in aqueous solution, while under the conditions used in this study the constant was 0.173 mM^{-1} for KCl. This was caused by the presence of other fluorescence-quenching compounds, such as DTT and BTP, in the assay media. Nevertheless, this value is much higher than the equivalent Stern-Volmer constant measured for SPQ (0.081 mM^{-1}). Hence, even small changes in Cl^- concentration led to an easily detectable change in lucigenin fluorescence. Since lucigenin showed a considerable sensitivity towards citrate, with a Stern-Volmer

constant of 0.079 mM^{-1}, it might be also potentially be useful in studying citrate transport in a similar fashion to this study with Cl^-.

Because lucigenin can be used with much longer excitation and emission wavelengths, the assay system is also less susceptible to signal noise caused by the diffraction of short-wavelength light.

As with SPQ (Vasseur *et al.*, 1993), the fluorescence intensity and Cl^--dependent quenching of lucigenin fluorescence was affected by pH. While lucigenin fluorescence is pH-independent in aqueous solution (Biwersi *et al.*, 1994), it is presumably the buffer-ion which interferes with the fluorescence. As shown in Table 3.2, unbuffered Tricine in aqueous solution (pH ~5.3) did not quench lucigenin fluorescence at all. However, the effect of pH on the quenching of lucigenin fluorescence closely followed the titration curves for the buffers tested. This indicates that the protonation of the buffer ion might play a role, as has been suggested for SPQ (Vasseur *et al.*, 1993). That means the more the ion becomes de-protonated with increasing pH, the more it quenches lucigenin fluorescence. Hence, care needs to be taken to perform Cl^- transport studies using lucigenin in a pH range where the fluorescence remains constant. Furthermore, all calibration experiments and the determination of the Stern-Volmer constant had to be performed under the same conditions as the transport experiments. On the other hand, the pH-dependent fluorescence quenching by the buffer-ion might be a useful tool to study proton transport into vesicles, as changes in fluorescence can reflect changes in protonation of the buffer ion (Garlid *et al.*, 1996). Thus, by carefully choosing buffering ions with different pK_a values, the pH range of the detection system can be easily adjusted according to demand.

Lucigenin showed a similar behaviour to SPQ in terms of water solubility and vesicle loading properties, so the experimental design of transport studies was almost identical to the experiments performed by Pope and Leigh (1990). As with SPQ, there seems to be an endogenous quencher present inside the vesicles, which was released and diluted by disrupting the vesicle membrane. This means that the volume of the vesicle had to be kept constant by maintaining iso-osmotic conditions. Any shrinkage of the vesicles would lead to an increase in the endogenous quencher concentration and hence to a decrease in fluorescence (Pope and Leigh, 1988).

As Biwersi *et al.* (1994) have pointed out in their study, a major drawback of lucigenin is that it is not stable in the cell cytoplasm. While it is stable for a long period in cytoplasm-free vesicles and liposomes, it becomes hydroxylated in the presence of nucleophiles, a feature common to most acridinium-based compounds. Therefore, where cytosolic Cl^- concentrations need to be determined, quinolinium-based compounds such as SPQ should be used instead. Since only cytoplasm-free vesicles were used in this study, no problems with dye instability were encountered.

In conclusion, lucigenin is a sensitive and selective Cl^- fluorescent indicator that has superior qualities over conventional Cl^--sensitive dyes such as SPQ. However, lucigenin shares with SPQ the property of buffering-ion-dependent pH-sensitivity, which has to be taken care of in the experimental design and the data analysis. While lucigenin cannot be used for cytosolic Cl^- measurements due to its chemical instability, it should be given preference over quinolinium-based compounds when measuring changes in Cl^- concentrations in vesicles or free solution.

3.3.2 The vesicle preparation

The hydrolytic H^+-ATPase activity assays have clearly shown that the membrane fraction taken from the 0/23% sucrose gradient is highly tonoplast enriched. This is in good agreement with various other studies of *Mesembryanthemum crystallinum* (Bremberger *et al.*, 1988; Klink *et al.*, 1990; Bremberger and Lüttge, 1992; Ratajczak, 1994; Barkla *et al.*, 1995), which also indicate that azide-resistant, nitrate-sensitive V-type ATPase activity represented 65 to 71% of the total ATPase activity (between 65 to 78% in this study). Furthermore, the amount of azide-sensitive mitochondrial and vanadate-sensitive P-type ATPase activity was less then 8% of the total ATPase activity, further indicating the high purity of the preparation.

The absolute figures for hydrolytic H^+-ATPase activities vary considerably in the literature. For example, Tsiantis *et al.* (1996) gave a value of only 2.9 µmol P_i h^{-1} mg^{-1} protein V-type ATPase activity of 9-week-old plants, Barkla *et al.* (1995) measured 5.7 µmol P_i h^{-1} mg^{-1} protein, while Ratajczak (1994) reports a value of 43 µmol P_i h^{-1} mg^{-1} protein. These huge differences can be due to differences in plant cultivation, vesicle preparation and assay conditions. Furthermore, some of the authors do not clearly state the amount of Brij-58 used, and also the temperatures under which these experiments where performed. The value of 33.7 µmol P_i h^{-1} mg^{-1} protein is in a comparable range with the value from Ratajczak *et al.* (1994), who used a very similar assay with 0.002% (w/v) Brij-58. However, they used plants that were only between 6 to 7 weeks old, i.e. 1 to 2 weeks younger than the plants used in this study.

Latency studies on the V-type H^+-ATPase using Brij-58 have been used successfully to determine vesicle-membrane orientation (Evetts, 1998). Brij-58 is a

very mild detergent, and as previous studies have shown, it conserves the structure and the function of the V-type H^+-ATPase even at high concentrations, while disrupting the membrane diffusion barrier at relatively low concentrations (Palmgren *et al.*, 1990; Ibarz *et al.*, 1994; Ratajczak, 1994). Similar values for the more or less random orientation of the vesicle membrane have been reported for vacuolar vesicle preparations from *Kalanchoë daigramontiana* and *M. crystallinum* on a sucrose-step density gradient in those studies. The random orientation of the vesicles during the preparation has to be kept in mind when studying transport processes in tonoplast vesicle preparations. The only method described so far to selectively separate inside-out and outside-out tonoplast vesicles, respectively, involves additional free-flow electrophoresis after a step-gradient preparation (Canut *et al.*, 1990). This greatly increases the length of the preparation while drastically reducing the enzyme activity of the fractions obtained. Thus, for bulk preparations of sealed tonoplast vesicles with high enzyme activities this method is only of limited use.

The average vesicle diameter of 336 nm reported in this study is similar to the sizes measured by Ratajczak *et al.* (1995) for *M. crystallinum.* Their reported values for the vesicle membrane-area correspond to a calculated diameter of 336 nm. Furthermore, similar electron microscopy measurements performed with *Kalanchoë daigramontiana* tonoplast vesicles also gave an average diameter of 330 nm (Evetts, 1998). This good agreement of vesicle sizes from different studies and plant material indicates that tonoplast vesicle preparations generally give a typical vesicle diameter of around 330 nm.

The large volume to surface ratio of 1.13×10^7 m^{-1}, taking into account the skewed distribution of vesicle sizes with diameters ranging from 70 nm to over 800

nm, is considerably higher than for intact vacuoles. Whole *M. crystallinum* mesophyll vacuoles, which have a diameter of 60 to 200 µm, have a surface to volume ratio of only around 0.08×10^6 m^{-1}, 140-fold smaller than for vesicles. This difference in surface to volume-ratio has to be taken into account when considering the time course of the transport processes studied, especially when comparing data obtained from whole vacuoles and vesicle preparations.

Chapter 4

Chloride transport into tonoplast vesicles studied using lucigenin

4.1 Introduction

The previous chapter has shown lucigenin to be a sensitive tool to measure changes in Cl^- concentrations in the millimolar range. This chapter describes experiments using tonoplast vesicles loaded with lucigenin to measure Cl^- fluxes across the membrane into the vesicles. A similar approach, using SPQ, was used previously to study vacuolar transport in vesicles from red-beet storage tissue (Pope and Leigh, 1988, 1990). For both probes, the time course of the change in fluorescence intensity is proportional to the change in luminal Cl^- concentration. Using the Stern-Volmer relationship $F = F_{external}+F_0/(1+K_{SV}[Cl^-])$, where $F_{external}$ is the time-independent external fluorescence, F_0 is the fluorescence in the absence of Cl^-, and K_{SV} is the Stern-Volmer quenching constant, the fluorescence signal can be converted into the initial rate of Cl^- transport ($d[Cl^-]/dt_{t=0}$) by differentiation with respect to time (Illsley and Verkman, 1987). This chapter characterises the initial Cl^--transport rate in terms of its kinetics, specificity, inhibitor sensitivity and the effect of the membrane potential and salt stress on vacuolar Cl^- transport.

4.2 Results

4.2.1 Cl^- transport shows saturation kinetics

To determine the initial Cl^--transport rate, the time course of the change in fluorescence intensity was recorded. Figure 4.1 shows a recording of Cl^--free vesicles loaded with 10 mM lucigenin that were added at $t = 0$ to a medium containing 100 mM Cl^-. Over 1800 s, the time course could be best fitted with a double exponential function with time constants $\tau_1 = 57$ s and $\tau_2 = 403$ s. However, as the inset shows, the initial change in fluorescence over the first 20 s could not be properly described by this double exponential function. Also, using higher order exponentials did not improve the fitting. Since the initial part is the most relevant of the recording, measuring under defined initial transport conditions, the protocol was standardised by fitting the first 30 s with a single exponential function to allow the calculation of the initial Cl^--transport rate.

To determine the kinetics of the initial Cl^--transport rate, Cl^- transport was measured under various external Cl^- concentrations, both using SPQ (Figure 4.2) and lucigenin (Figure 4.3). The fluorescence recordings in the absence of Cl^- showed hardly any time-dependent decrease in intensity (see also Figure 4.20). This indicated that no loss of fluorescent dye occurred during the measurement. Increasing concentrations of Cl^- in the external medium led to an immediate drop of the intensity, followed by a time-dependent decrease of the fluorescence signal, which became steeper with increasing Cl^- concentrations.

Addition of 0.03% Triton X-100 (v/v, final concentration) disrupted the vesicles and released the dye into the external medium. At lower external Cl^-

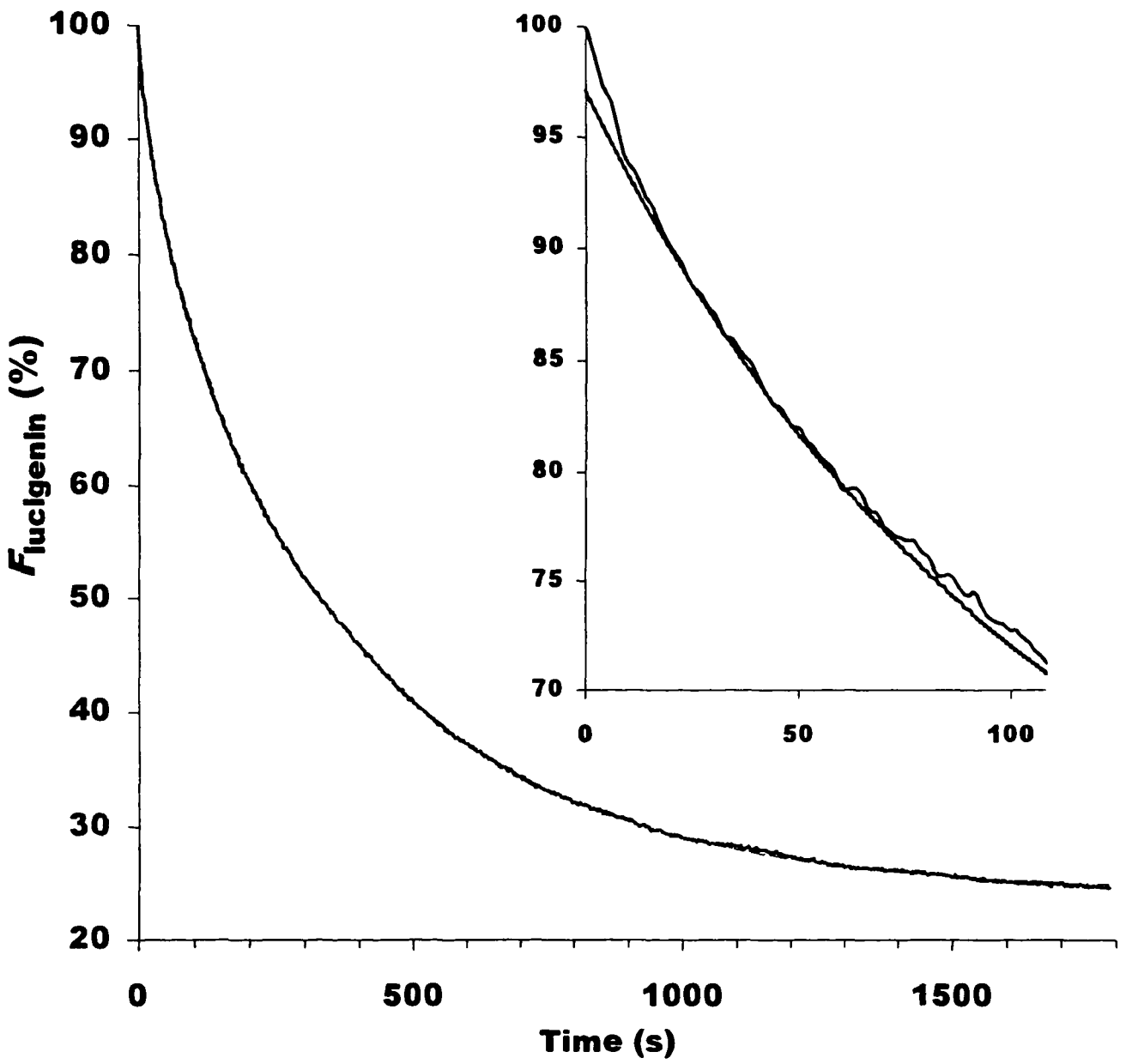


Figure 4.1. Time course of lucigenin fluorescence of vesicles in 100 mM Cl^-. Thirty μg of vesicles loaded with 10 mM lucigenin were added to assay medium containing 100 mM Cl^- and the time course of fluorescence was recorded for 30 min (exc. 433 nm, em. 506 nm, slits 5 nm). The time course over 30 min could be best fitted with a double exponential function with time constants of 57 s and 403 s. The inset shows that the initial part of the time course was not adequately described by this fitting procedure (even with higher order exponentials, data not shown)

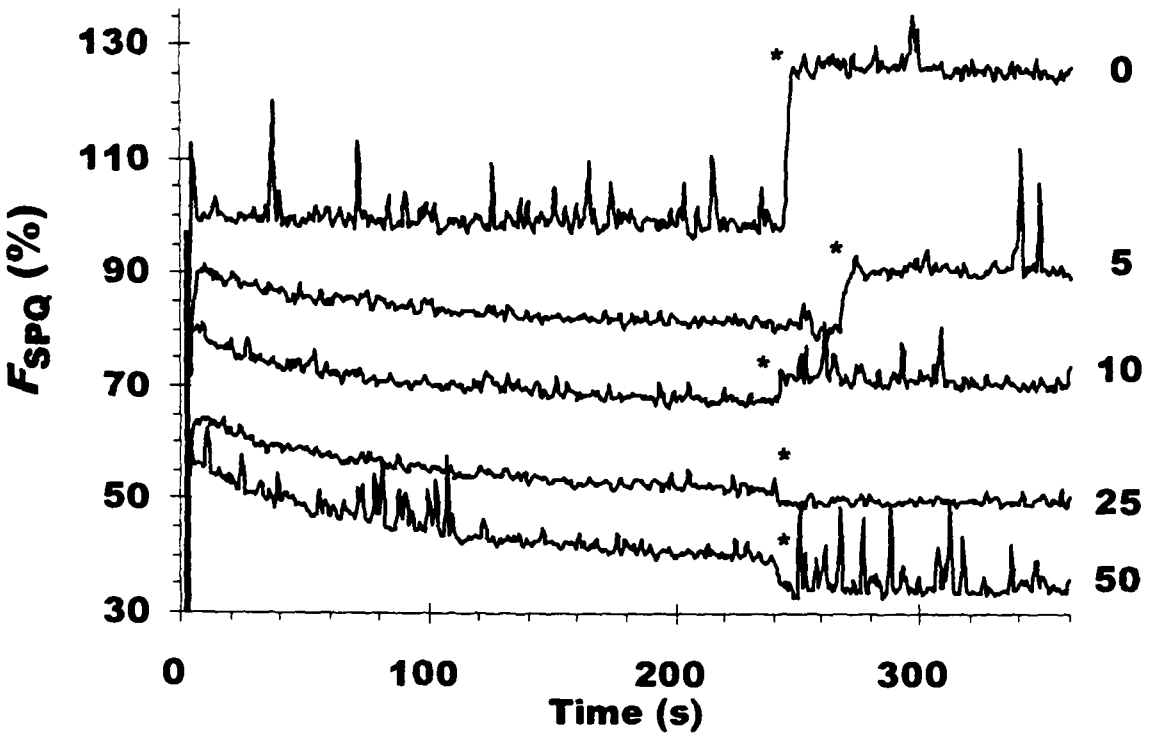


Figure 4.2. Measuring the initial Cl^- transport rate using SPQ. Thirty μg of vesicles loaded with 20 mM SPQ and 100 mM K_2SO_4 were added to assay medium containing various amounts of KCl (as indicated in mM) and sufficient K_2SO_4 to give a total K^+ concentration of 200 mM (5 μM valinomycin was present as well). The asterisks mark the addition of 0.03% (v/v) Triton X-100 to disrupt the vesicles. Note the increase in fluorescence intensity at lower external Cl^- concentrations. Excitation: 360 nm; emission 440 nm; both slits at 10 nm

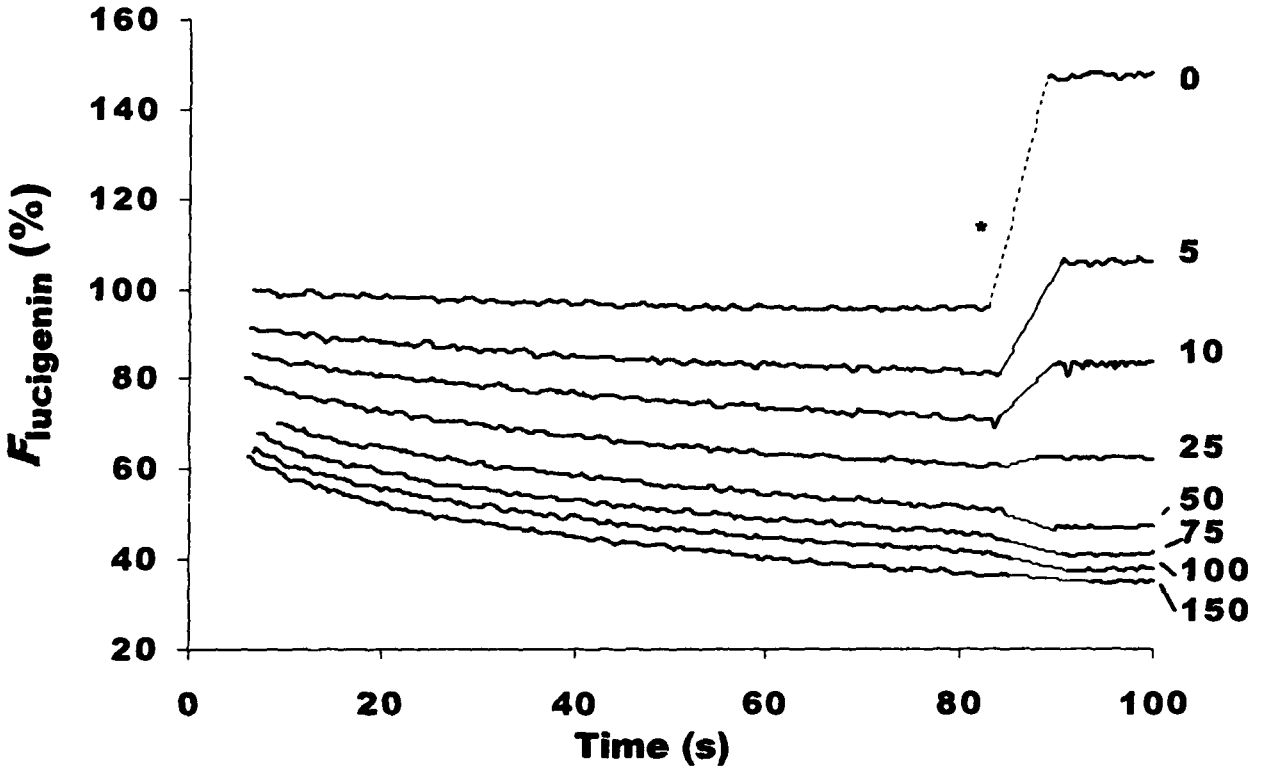


Figure 4.3. Time course of the Cl^--dependent lucigenin fluorescence quenching. Twenty μg of vesicles loaded with lucigenin were added at $t = 0$ to media with increasing Cl^- concentrations as indicated. The asterisk marks the addition of Triton X-100 to a final concentration of 0.03% (v/v). The dashed lines replace the traces during stirring. Excitation: 433 nm; emission 506 nm; both slits at 5 nm

concentrations (between 10 to 25 mM Cl^- for SPQ, around 25 mM Cl^- for lucigenin) the actual signal increased, indicating that the internal fluorescence was partly quenched by an endogenous quencher (Pope and Leigh, 1988). Only at higher Cl^- concentrations did the fluorescence signal decrease after addition of Triton X-100.

The traces in Figure 4.2 show that SPQ was much more susceptible to noise with its lower excitation and emission wavelengths when compared with lucigenin (Figure 4.3), resulting in more "spiky" recordings. Such recordings were more difficult to analyse, and often rendered the data fitting impossible.

Figure 4.4 shows a set of traces recording vesicular lucigenin fluorescence. The first 30 s of each trace were fitted with a single exponential to calculate the initial Cl^--transport rate. This clearly shows that at higher Cl^- concentrations a single exponential was not adequate to describe the recordings over the whole recording period. However, they were adequate to extrapolate the signal back to $t = 0$, where the initial transport conditions prevail. Figure 4.4.B shows the internal fluorescence signal derived from the fitting results as described in section 2.3.3, as a function of the external Cl^- concentration. It shows that during storage of vesicles on ice the internal fluorescence signal decreased, probably due to leakage of lucigenin. Since for each recording the internal fluorescence was calculated separately, the leakage could be accounted for in the analysis.

Figure 4.4.B also shows that the initial internal fluorescence decreased slightly with increasing external Cl^- concentrations, with a linear slope around -0.13% mM^{-1}. That means that at external 100 mM Cl^- the internal fluorescence is reduced by about 13% with respect to 0 mM external Cl^-. Since the reciprocal of the internal fluorescence was used as a factor to calculate the initial Cl^--transport rate, this might

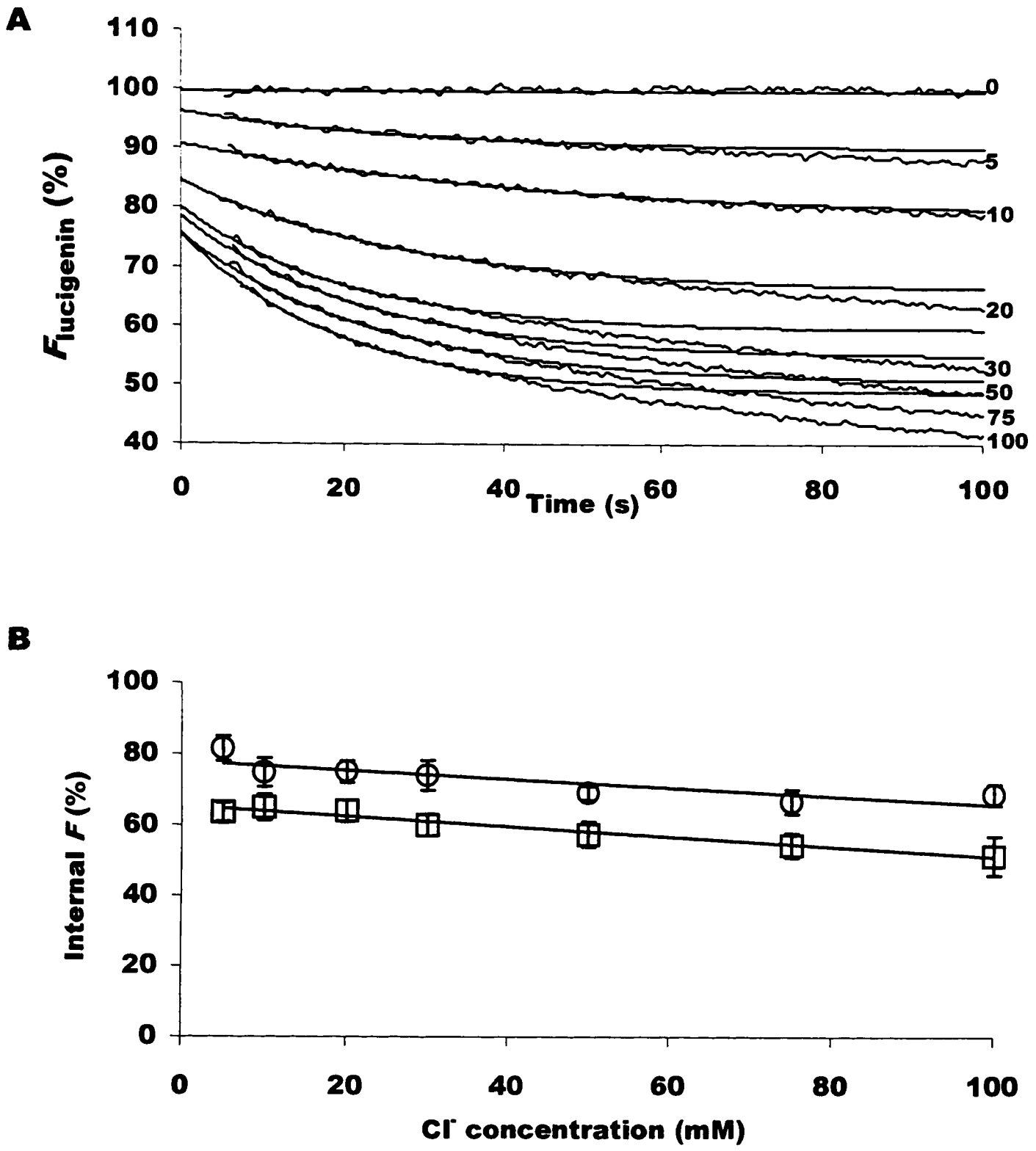


Figure 4.4. Describing the initial time course of lucigenin fluorescence quenching with a single exponential function. **A)** The first 30 s of traces were fitted with a single exponential to obtain the initial change of fluorescence at time point $t = 0$ ($dF/dt_{t=0}$). While the initial change of fluorescence is described adequately, the remainder of the trace is not. The different Cl^- concentrations were as indicated in mM. **B)** The initial internal lucigenin fluorescence F_{in} as calculated from the fit results (according to the formula given in section 2.3.3) from vesicles immediately after finishing the washing (○) and *ca.* 45 min later after being stored on ice (❑). Lines show linear regressions with slopes of -0.12% mM^{-1} for fresh vesicles and -0.14% mM^{-1} for stored vesicles. Values are means from three different preparations

lead to a slight overestimation of the transport rate at high external Cl^- concentrations. However, since it is not known what causes this effect and in which way it affects the initial change in lucigenin fluorescence $dF/dt_{t=0}$ it was not compensated for, especially since it would only make a small quantitative difference to the results obtained.

Analysing the kinetics of the initial Cl^--transport rate obtained from measurements using SPQ-loaded vesicles revealed saturating Michaelis-Menten type kinetics with an apparent K_m of 10.2 mM and a V_{max} of 5.9 mM min^{-1} (Figure 4.5.A). Very similar kinetics were obtained using lucigenin-loaded vesicles (Figure 4.5.B): in this case, the apparent K_m was 15.5 ± 1.6 mM and the V_{max} was 4.82 ± 0.70 mM min^{-1}.

These results show that lucigenin Cl^--sensitive fluorescence indicator gives comparable Cl^- transport rates to those obtained using SPQ. Hence, the results of this study can be directly compared with previous studies in which SPQ was used (Illsley and Verkman, 1987; Pope and Leigh, 1988, 1990; Pope *et al.*, 1990).

4.2.2 Voltage dependence of vacuolar Cl^- transport

An important tool to study the effect of the membrane potential on Cl^--transport into tonoplast vesicles was the K^+/valinomycin clamp. The peptide antibiotic valinomycin acts as a highly K^+-selective carrier in membranes (Stein, 1990; Duax *et al.*, 1996). Thus, by defining the internal and external K^+ concentrations, the membrane potential established in the presence of valinomycin can be calculated according to the Nernst-equation ($\Delta\psi = RT/zF \times \ln([K^+]_{out}/[K^+]_{in})$; R, universal gas constant; T, absolute temperature; z, valence, of +1 for K^+; F, Faraday constant).

In most experiments, the ratio of external to internal K^+-concentration was kept at unity to clamp the membrane potential for initial transport conditions at zero.

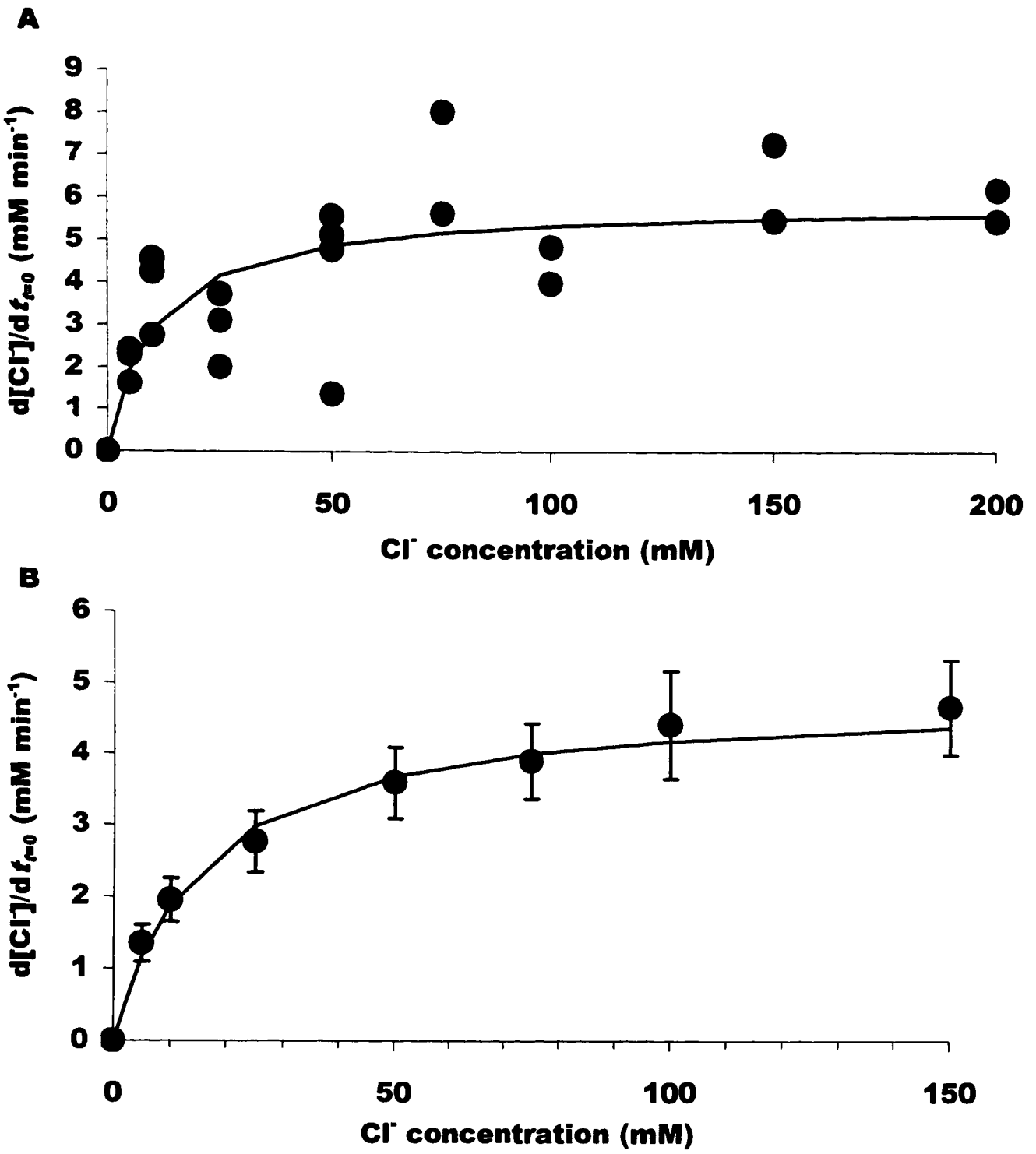


Figure 4.5. The concentration dependence of the initial Cl^--transport rate. **A)** Measurements using SPQ. Experiments were performed at pH 8.0 with vesicles from two separate preparations loaded with 20 mM SPQ. The curve indicates a best fit for Michaels-Menten kinetics with an apparent K_m = 10.2 mM and V_{max} of 5.9 mM min^{-1}. **B)** Measurements using lucigenin. Vesicles from three separate preparations were loaded with 10 mM lucigenin and added to media with increasing Cl^- concentrations at pH 7.4. The curve represents a best fit Michaelis-Menten kinetics (apparent K_m 15.5 ± 1.6 mM, V_{max} 4.82 ± 0.70 mM min^{-1}, $n = 6$)

To impose inside positive membrane potentials the ratio of external to internal K^+ was >1. For example, a ratio of 10 would impose a $\Delta\psi$ of +59 mV.

4.2.2.1 Validity of the K^+/valinomycin clamp

To test the validity of the K^+/valinomycin clamp, the potentiometric membrane dye oxonol-V was used. Oxonol-V has been used in many studies to measure formation of inside-positive membrane potentials (Kaestner and Sze, 1987; White and Smith, 1989; Faraday and Spanswick, 1995). However, the exact mechanism by which the negatively charged Oxonol-V senses the membrane potential is still uncertain. It appears to be both membrane binding as well as partitioning and "stacking" of dye molecules in compartments that decreases its fluorescence (Scherman and Henry, 1980; Loew, 1993; Plasek and Sigler, 1996). Both processes are dependent on the membrane potential, so with inside-positive membrane potentials enhancing both the binding and accumulation of the anionic dye oxonol-V the fluorescence signal decreases.

Figure 4.6 shows recordings from oxonol-V fluorescence recordings with various K^+ gradients in the absence or presence of valinomycin. Only a small drop in fluorescence could be observed after imposing inwardly directed K^+ gradients in the absence of 5 μM valinomycin, indicating that the membrane is not depolarised. In the presence of 5 μM valinomycin, an exponential decrease in oxonol-V fluorescence could be observed over time. This indicated that oxonol-V binding and partitioning was enhanced, due to the formation of inside-positive membrane potentials.

As Figure 4.7.A shows, the difference in the fluorescence signal showed a linear relationship with the calculated Nernst potential over the range from 0 to +100 mV. At 100 mV, the fluorescence signal was reduced by about 50% compared with 0

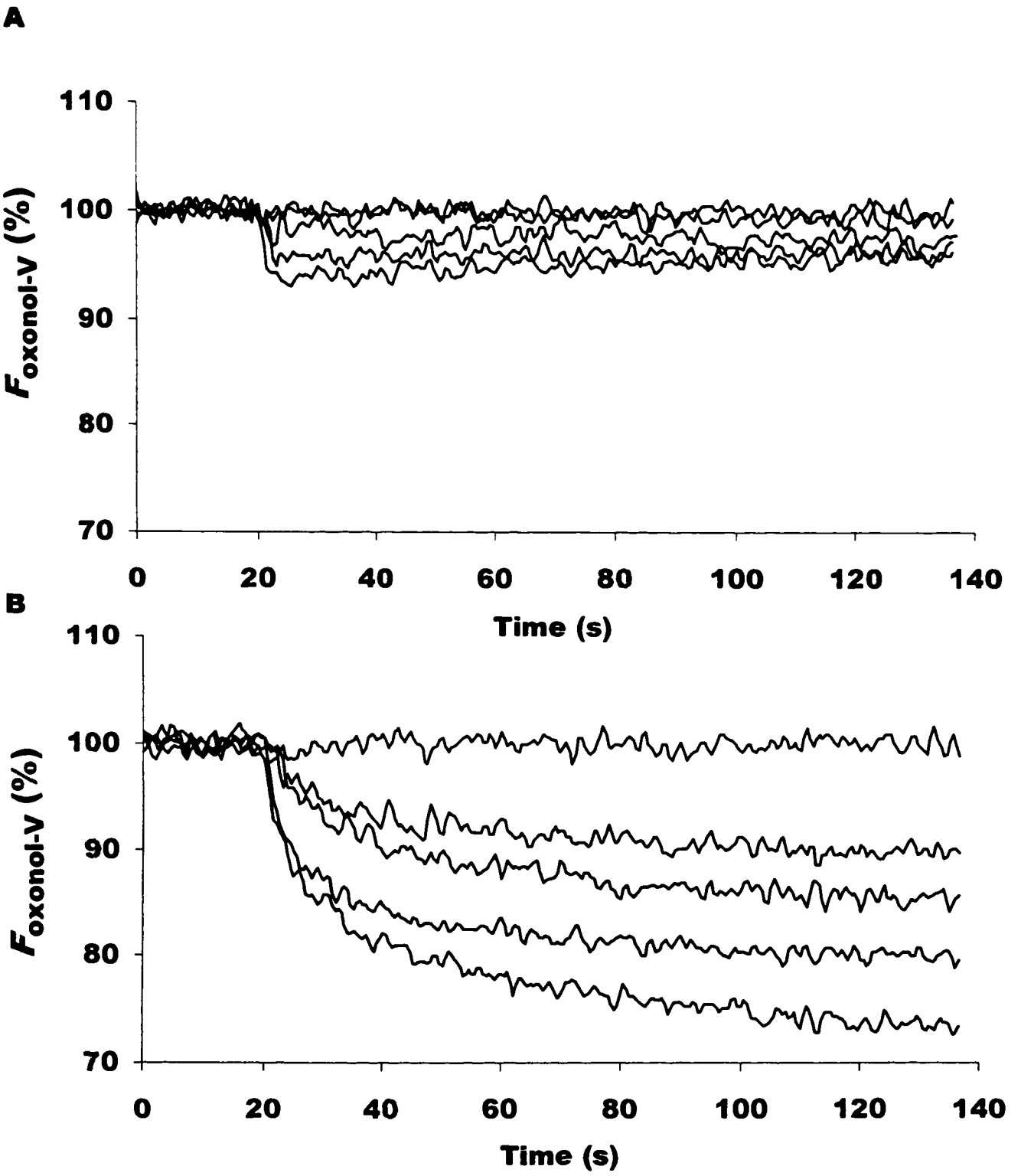


Figure 4.6. Testing the K^+/valinomycin clamp using the potentiometric dye oxonol-V. The time course of the fluorescence of vesicles incubated with 8 μM oxonol-V and with either no valinomycin (**A**) or 5 μM valinomycin (**B**) were recorded. Various membrane potentials of (from top to bottom) 0, 18, 28, 46 and 59 mV, respectively, were imposed by adding an aliquot of 500 mM K_2SO_4 stock solution (at t = 20 s), as calculated by the Nernst equation. Excitation and emission wavelengths were 610 nm and 639 nm, respectively, and the slits were set to 5 nm

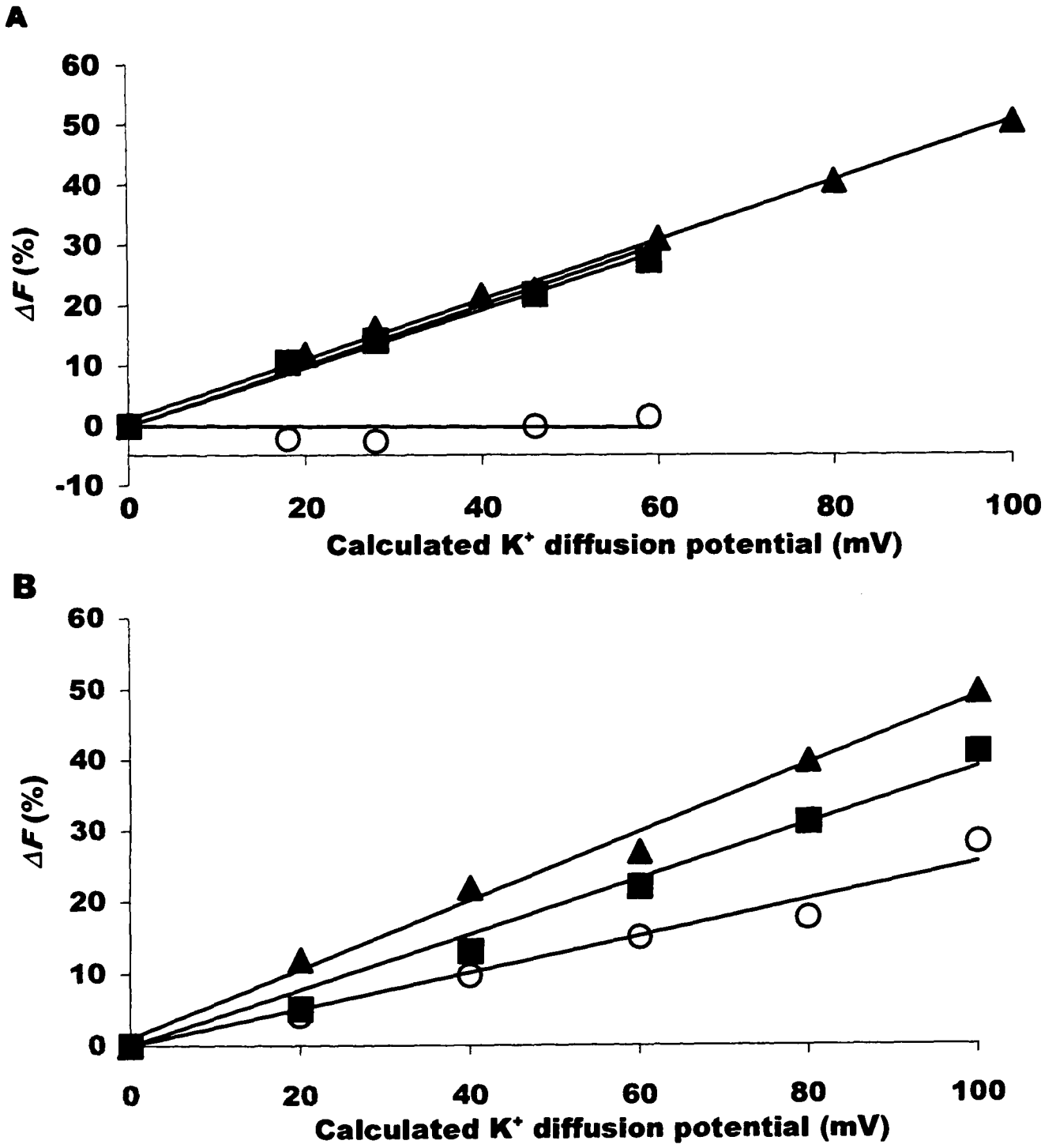


Figure 4.7. Change of oxonol-V fluorescence plotted against the predicted membrane potential. **A**) Measurements in the absence of Cl^-. Symbols: (●,▲) 5 μM valinomycin; (■) 10 μM valinomycin; (○) no valinomycin. **B**) Measurements in the presence of 50 mM BTP-Cl. Symbols: (▲) 5 μM valinomycin, vesicles pre-incubated in 50 mM BTP-Cl; (■) 5 μM valinomycin, 50 mM Cl-BTP outside only; (○) no valinomycin, vesicles pre-incubated with 50 mM Cl-BTP. Each value represents the average of duplicate measurements; lines show linear regressions of data

mV. Furthermore, this relationship remained the same when the valinomycin concentration was increased from 5 to 10 μM. Incubating the vesicles with 50 mM Cl^- several minutes before imposing the K^+ gradients did not alter the oxonol-V response (Figure 4.7.B). However, adding Cl^- at the same time as imposing the K^+ gradient, hence creating an inwardly directed Cl^- gradient, did reduce the oxonol-V response. The maximum decrease in oxonol-V fluorescence at 100 mV under these conditions about was 40%, or 20% smaller than in the absence of Cl^-. However, the relationship still remained linear over the whole voltage range tested. This effect of Cl^- on the K^+/valinomycin clamp was further explored as shown in Figure 4.8. At external Cl^- concentrations above 5 mM the voltage dependent decrease in oxonol-V fluorescence became slightly reduced by about 2.5% to 3%. Above 25 mM Cl^- no further reduction could be observed. However, this saturating Cl^- dependence did not show simple Michaelis-Menten type kinetics but had a sigmoidal response.

4.2.2.2 Cl^- transport under varying membrane potentials

As Figure 4.9 shows, at both 50 mM and 150 mM Cl^- concentrations the presence of 5 μM valinomycin increased the initial Cl^--transport rate by about 50%. Since the K^+ concentration was 100 mM on both sides of the membrane, the membrane potential was effectively clamped to zero. Imposing a $[K^+]_o/[K^+]_i$ of 10 in the presence of 5 μM valinomycin, thereby generating a K^+-diffusion potential of +59 mV inside the vesicles, increased the initial Cl^- transport rate at all Cl^- concentrations (Figure 4.10). Fitting the data with a Michaelis-Menten relationship revealed that the apparent K_m was lowered from 22.1 ± 7.2 mM at 0 mV to 6.4 ± 1.4 mM at 59 mM, while the V_{max} increased by almost 50% from 4.1 ± 0.4 mM min^{-1} to 6.0 ± 0.9 mM min^{-1}, respectively.

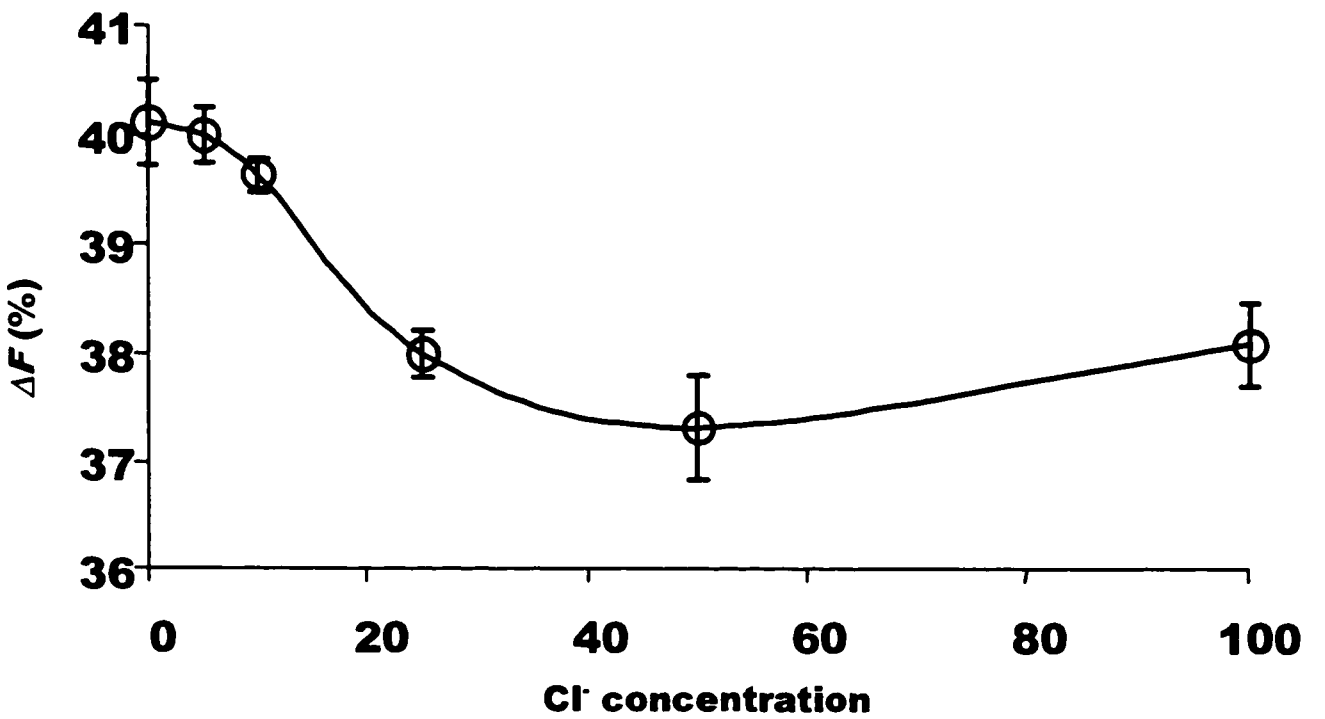


Figure 4.8. Effect of increasing Cl^--concentrations on the K^+/valinomycin clamp. Thirty µg of vesicles were loaded with 2.5 mM K_2SO_4 and added to assay buffer containing 2.5 mM K_2SO_4, 5 µM valinomycin, 8 µM oxonol-V and BTP-Cl varying from 0 to 100 mM. After the oxonol-V fluorescence had stabilised, K_2SO_4 was added to a total final concentration of 50 mM, thereby imposing a 10-fold inward-directed concentration difference. The difference in oxonol-V fluorescence, ΔF, was calculated as the fluorescence intensity before adding 50 mM K_2SO_4 minus the intensity 100 s after addition (n = 3)

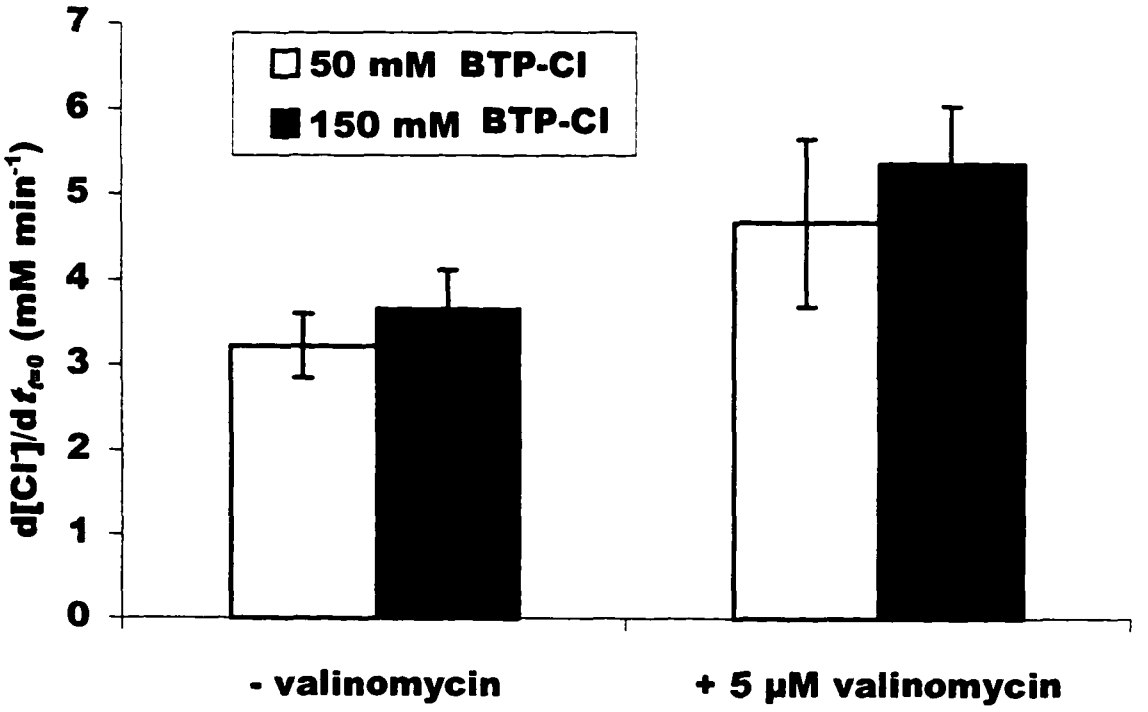


Figure 4.9. Effect of valinomycin on initial Cl^--transport rate. Transport rates were measured at 50 mM K_2SO_4 inside and outside, and either 50 mM and 150 mM BTP-Cl outside. The buffer contained either no valinomycin (with 0.5% ethanol) or 5 µM valinomycin ($n = 3$)

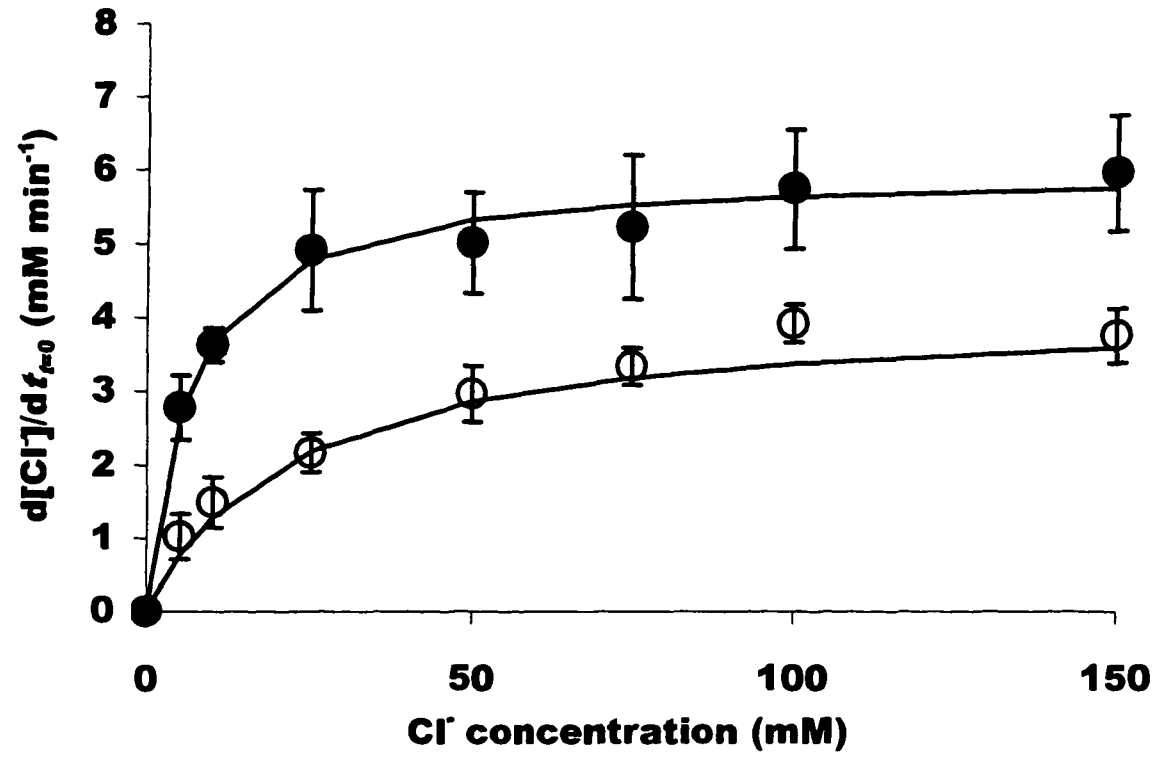


Figure 4.10. Effect of the membrane potential on the kinetics of initial Cl^--transport rate. Tonoplast vesicles were loaded with 10 mM K_2SO_4 and 10 mM lucigenin. Vesicles were added to buffer containing 5 µM valinomycin and either 10 mM K_2SO_4 (○) or 100 mM K_2SO_4 (●). The lines indicate best fits of Michaelis-Menten kinetics for the data. Parameters for $K^+_{out}/K^+_{in} = 1$ (i.e. 0 mV) are $K_m = 22.1 \pm 7.2$ mM, $V_{max} = 4.1 \pm 0.4$ mM min^{-1}, $n \geq 4$. Parameters for $K^+_{out}/K^+_{in} = 10$ (i.e. 59 mV, inside-positive) are $K_m = 6.4 \pm 1.4$ mM, $V_{max} = 6.0 \pm 0.9$ mM min^{-1}, $n \geq 3$

Figure 4.11 shows the effect of various electrical potentials across the vesicle membrane on the initial Cl^- transport rate at 20 mM and 50 mM Cl^-. At 50 mM, Cl^- uptake showed a sigmoidal increase in transport rate with increasing membrane potential, the steepest being between 20 to 40 mV (vesicle lumen positive). The Cl^--transport rate did not increase any further above 50 mV, and remained constant at around 3.8 mM min^{-1}, about 75% higher than the transport rate at 0 mV. At 20 mM Cl^-, the transport rate observed in a single experiment showed only a linear increase with increasing membrane potential. While at 0 mV the transport rate was 1.1 mM min^{-1}, it increased by 75% to 1.96 mM min^{-1} at 80 mV.

4.2.3 Inhibition of the vacuolar Cl^- transport

Before the sensitivity of the initial Cl^--transport rate towards various inhibitors could be tested, the potential interference of these inhibitors with the lucigenin-based assay system had to be determined. The fluorescence characteristics of the inhibitors were thus tested, along with their ability to quench lucigenin fluorescence.

Most of the known anion-transport inhibitors tested initially were maintained as stock solutions in 100% DMSO (dimethylsulphoxide). It was found, however, that DMSO quenched lucigenin fluorescence. Furthermore, it also seemed to act as a potent inhibitor of the initial Cl^--transport rate itself at concentrations above 0.1% (v/v). It was therefore necessary to dissolve the inhibitors in other solvents. The inhibitors tested here were dissolved in either 0.2 M KOH, 100%, ethanol or water.

Figure 4.12 shows the decrease of the fluorescence intensity of lucigenin with increasing concentrations of DMSO, DIOA, DIDS, SITS and NPPB. This clearly shows that at 0.5% (v/v) DMSO, equivalent to about 70 mM, the lucigenin

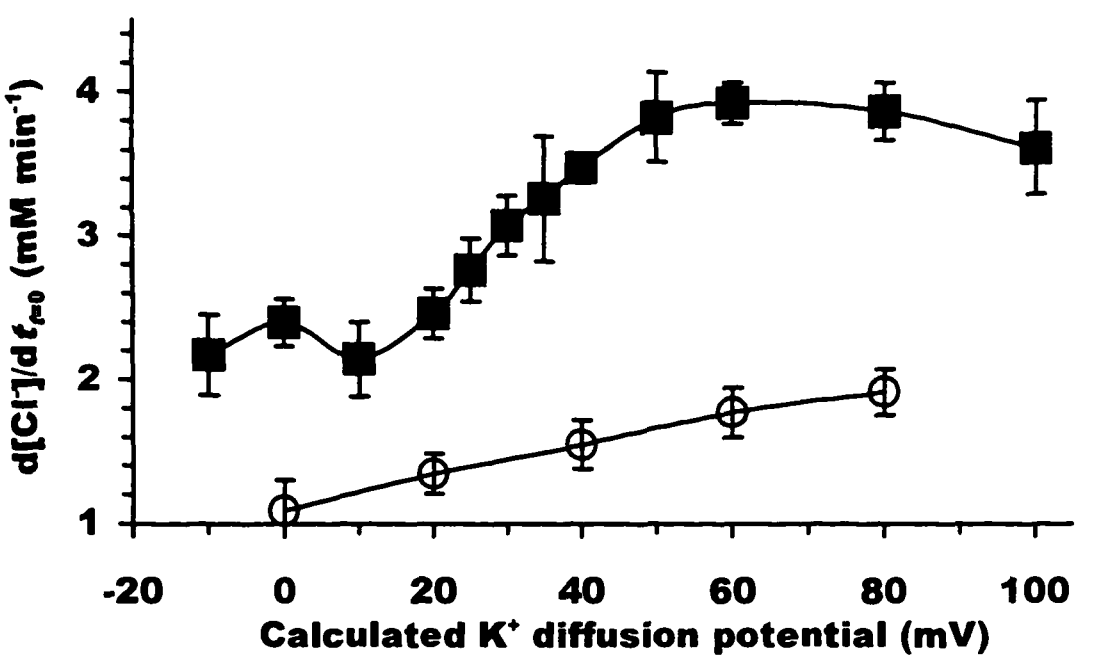


Figure 4.11. Effect of membrane potential on the initial Cl^--transport rate. Tonoplast vesicles, loaded with 10 mM lucigenin and 2.5 mM K_2SO_4, were added to assay media containing either 20 mM BTP-Cl (○; $n = 4$; one preparation) or 50 mM BTP-Cl (■; $n \geq 5$; three preparations), plus different amounts of K_2SO_4 to increase the imposed K^+ diffusion potential according to the Nernst equation

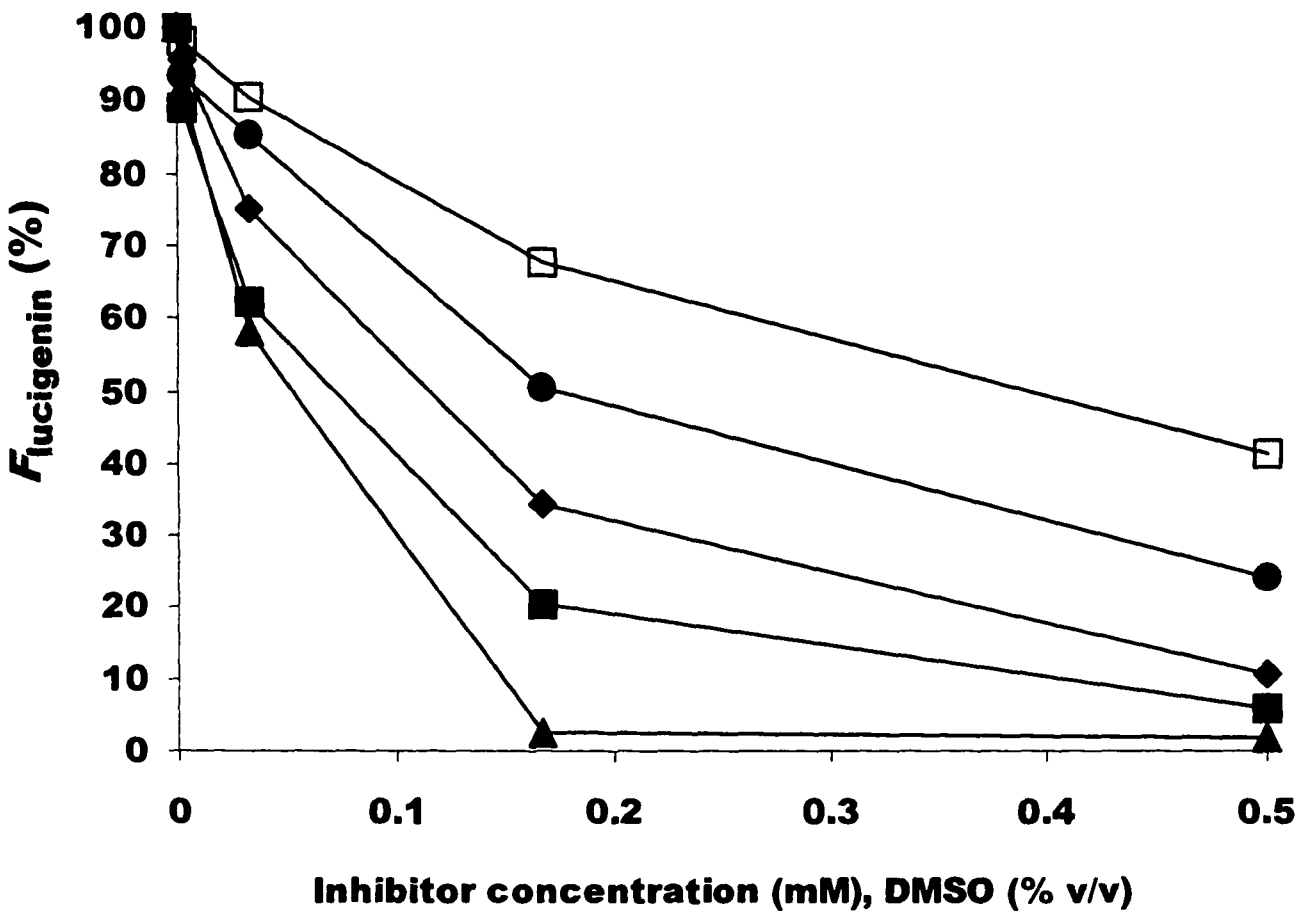


Figure 4.12. Quenching of lucigenin fluorescence by various inhibitors. Aliquots of stock solutions were added to assay medium (pH 7.4). Inhibitors: (❑) DMSO, 100% (v/v) stock; (•) DIOA, 100 mM stock in 100 % ethanol; (♦) DIDS, 100 mM stock in 0.2 M KOH; (■) SITS, 100 mM stock in water; (▲) NPPB, 100 mM stock in 0.2 M KOH

fluorescence intensity was reduced by 50% from its maximum value (with K_{SV} = 0.019 mM^{-1}). Less than 200 µM of NPPB, the most potent quencher tested, abolished the fluorescence signal completely. Table 4.1 summarises the data obtained for lucigenin quenching caused by the tested inhibitors and the fluorescence intensity at the wavelength pair 433 nm/506 nm.

Only a few inhibitors showed a detectable fluorescence signal at an excitation wavelength of 433 nm and emission at 506 nm, measured at 1 mM concentration. And although DIDS fluorescence was fairly prominent at 1 mM, at 100 µM it was less then 3% of the fluorescence intensity of lucigenin-loaded vesicles. Almost all of the inhibitors had a very high Stern-Volmer quenching constant, even higher than for Cl^-. The highest was NPPB, with a quenching constant of more than 11 mM^{-1} for lucigenin, 64-fold higher than Cl^-. This means that even at 100 µM NPPB the lucigenin fluorescence would already be quenched by more than 50%. Others, such as DIDS and SITS, still caused a 20% reduction of the lucigenin fluorescence intensity at 100 µM.

As mentioned above, DMSO not only quenched lucigenin fluorescence, but also directly inhibited Cl^- uptake into tonoplast vesicles. As Figure 4.13 shows, with increasing DMSO concentrations from 0 to 0.8% (v/v, equivalent to 113 mM DMSO), the initial Cl^- transport rate showed a sigmoidal decrease, a characteristic dose response-curve. Half-maximal inhibition was reached at 30.8 mM [approx. 0.2% (v/v)]. Even at higher DMSO concentrations the rate of fluorescence change was not completely abolished: a residual of about 30% of the maximum rate was still measurable. This sigmoidal dose-response curve is very different to the hyperbolic quenching characteristics, suggesting a genuine inhibition rather than an interference

Table 4.1. Effect of inhibitors on lucigenin fluorescence intensity. Aliquots of inhibitor stock solutions in 0.2 M KOH were added to assay medium, pH 7.4. Since most inhibitors were used at 100 µM final concentration, the fluorescence of lucigenin at that inhibitor concentration is given. To determine the fluorescence signal of the inhibitors, wavelength scans for emission (exc. 433 nm) and excitation (em. 506 nm) were performed (both slits at 5 nm)

Inhibitor	Quenching constant for lucigenin (10^{-3} mM^{-1})	Lucigenin fluorescence at 100 µM inhibitor concentration (%)	Fluorescence (exc. 433 nm; em. 506 nm)
9-AC[a]	140	99	-
bumetamide	260	98	+
DMSO	19	100	-
DIDS	2 200	82	++
DIOA[a]	1 240	89	-
DNDS	206	98	+
flufenamic acid	390	96	-
furosemide	208	98	-
N-EM	10	100	-
niflumic acid	470	96	-
NPPB[c]	11 400	47	-
*p*CMBS[b]	156	99	-
SITS[b]	2 500	80	+

[a] stock solution in 100% ethanol

[b] stock solution in assay buffer, pH 7.4

[c] stock solution in 20% DMSO, 50% ethanol

with the assay. However, both effects occur over a similar concentration range, and it cannot be ruled out that DMSO is affecting the internal lucigenin fluorescence. This would also lead to a reduction in the initial Cl^--transport rate and be difficult to distinguish from an actual inhibition of Cl^- transport.

A number of inhibitors were tested for their effect on the initial Cl^- transport rate of *M. crystallinum* tonoplast vesicles. Since some of the inhibitors tested caused significant quenching of lucigenin fluorescence, the assay had to be designed accordingly. At the start of every recording, dye-loaded vesicles were added to Cl^--free media. Then the inhibitor was added and the vesicles incubated for 4 min, during which lucigenin fluorescence was measured. After this pre-incubation period, 50 mM BTP-Cl (final concentration) was added and the change in internal lucigenin fluorescence observed. All traces were normalised with respect to the fluorescence intensity before inhibitor addition. As long as only the external fluorescence was quenched by the inhibitor, the amplitude of the internal fluorescence should remain unchanged, albeit having different offsets. Any interference with the internal fluorescence should be easy to observe. A fluorescence decrease during the pre-incubation indicated that the internal fluorescence became quenched due to inhibitor influx. In contrast, any increase in lucigenin fluorescence should indicate rupturing of vesicles or increased leakage of solutes (see section 4.2.1). If the signal remained constant during the incubation, no unspecific interference of the test substance with the assay had taken place. Under these conditions, the initial rate of change in lucigenin fluorescence, which is directly proportional to the initial Cl^- transport rates, could be directly compared between the different treatments.

Figure 4.14.A shows representative recordings for experiments with 100 µM DIDS (4,4'-diisothiocyanato-stilbene-2-2'disulphonic acid), SITS (4-acetamido-4'-isothiocyanato-stilbene-2-2'-disulphonic acid) and flufenamic acid. All three substances caused an instant drop in lucigenin fluorescence after they were added to the vesicles. This indicates that they partially quenched the external lucigenin fluorescence. During pre-incubation with SITS, the fluorescence of the dye remained constant and the change rate of change of lucigenin fluorescence after the addition of Cl^- remained the same as for the control (101 ± 9%).

In contrast, when the vesicles were pre-incubated with 100 µM DIDS the fluorescence signal slowly decreased with time. This was not observed when lucigenin was incubated in a vesicle-free system with 100 µM DIDS or 1 mM DIDS (data not shown). The observed fluorescence decrease might therefore indicate that DIDS crossed the membrane during the pre-incubation period and quenched internal lucigenin fluorescence. Subsequent addition of Cl^- after the incubation showed that the rate of change in lucigenin fluorescence intensity was drastically reduced (by 61 ± 3% as compared with the control).

The presence of flufenamic acid caused a small but steady increase in lucigenin fluorescence during the pre-incubation period. This indicated that the vesicles might have become leaky or disrupted, and were thereby releasing dye, which shows brighter fluorescence outside the vesicles (see section 4.2.1). Incubation of vesicles for more than 30 min with flufenamic acid led to the complete loss of internal lucigenin fluorescence (addition of these vesicles to Cl^--containing medium led to an instantaneous drop of most of the fluorescence intensity), and a similar effect was observed for NPPB (data not shown). The Cl^--induced rate of fluorescence change

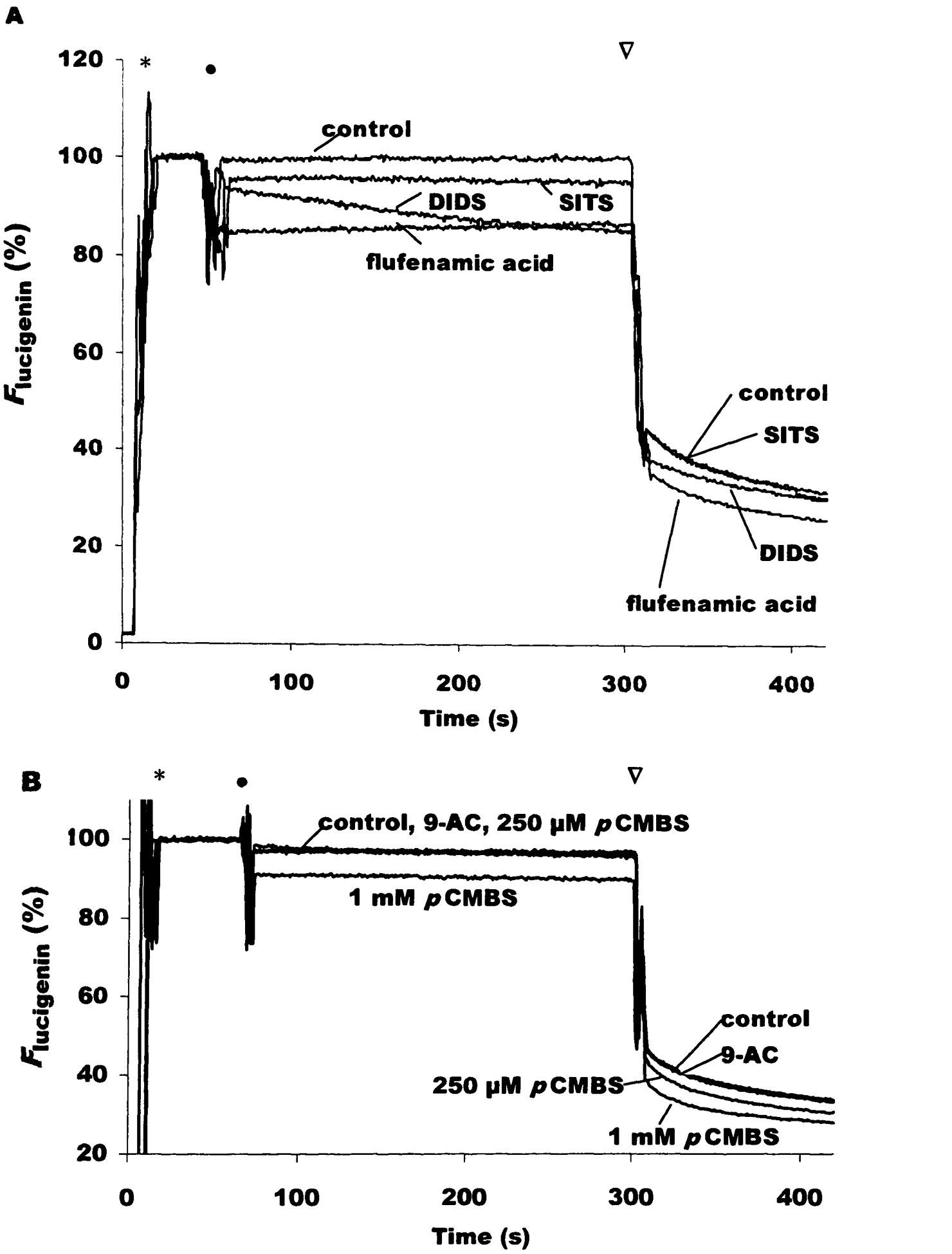


Figure 4.14. Time course of lucigenin fluorescence with various inhibitors. **A,B**) Tonoplast vesicles loaded with 10 mM lucigenin were added to Cl^--free assay medium (*). Subsequently, the inhibitor (100 µM, unless otherwise stated), was added (●), and the fluorescence during the incubation recorded. After 220 s incubation, 50 mM BTP-Cl was added to measure the initial change of fluorescence (∇)

was also reduced by 32 ± 6% with 100 µM flufenamic acid compared with the control. 100 µM niflumic acid and 9-AC did not show any effect on the initial Cl^- transport rate (Figure 4.14.B).

Interestingly, incubating the vesicles with 250 µM *p*CMBS (*p*-chloro-mercuribenzene sulphonate) for 4 min resulted in a significant increase in the initial Cl^- transport rate by more than 20%, whereas 1 mM *p*CMBS seemed to have no effect (Figure 4.14.B). During the pre-incubation period, no effect of *p*CMBS on the dye could be observed directly. Table 4.2 and Figure 4.15 summarise the results found for all the inhibitors tested, giving the rate in the presence of inhibitors as compared with the control rates.

4.2.4 Selectivity of the vacuolar Cl^--transport system

In order to determine the selectivity of this Cl^--transport system, measurements were also performed in the presence of 50 mM malate-BTP and 50 mM $NaNO_3$. As shown in Figure 4.16.C, there was no change in Cl^- transport activity in the presence of malate. Nitrate, however, seemed to reduce the measured Cl^- transport rate at all Cl^- concentrations by about the same amount. However, as the traces in 4.16.B show, this was due to an unspecific effect. It was observed even in the absence of Cl^-, causing the lucigenin fluorescence to increase with time after addition of vesicles. This nitrate-dependent increase in fluorescence intensity overlaid the Cl^--dependent fluorescence quenching of lucigenin and hence caused an offset when calculating the initial Cl^- transport rate. After subtraction of this constant offset of -1.29 mM min^{-1}, the initial Cl^--transport rate in the presence or absence of nitrate did not differ (Figure 4.17), and the linearisation in the Hanes plot in Figure 4.17.B did not reveal any difference between the measurements.

Table 4.2. Effect of inhibitors on initial rate of Cl^--dependent lucigenin fluorescence quenching ($dF/dt_{t=0}$).

Inhibitor	Concentration	$dF/dt_{t=0}$ relative to control (%)	*n*
DIDS*	100 µM	39 ± 3[c]	4
flufenamic acid*	100 µM	68 ± 6	4
niflumic acid	100 µM	93 ± 8	4
9-AC	100 µM	96 ± 6	4
SITS	100 µM	102 ± 7	8
*p*CMBS	250 µM	124 ± 7[b]	8
	1 mM	102 ± 7	4
DMSO	7 mM	97 ± 5	4
	28 mM	69 ± 7[c]	4
	70 mM	34 ± 2[a]	3
	112 mM	31 ± 2[a]	4

* the actual amount of inhibition might be less due quenching of internal fluorescence by the inhibitor or vesicle rupture (see text)

[a,b,c] Significantly different from control at $P < 0.001$, $P < 0.01$; $P < 0.05$, respectively

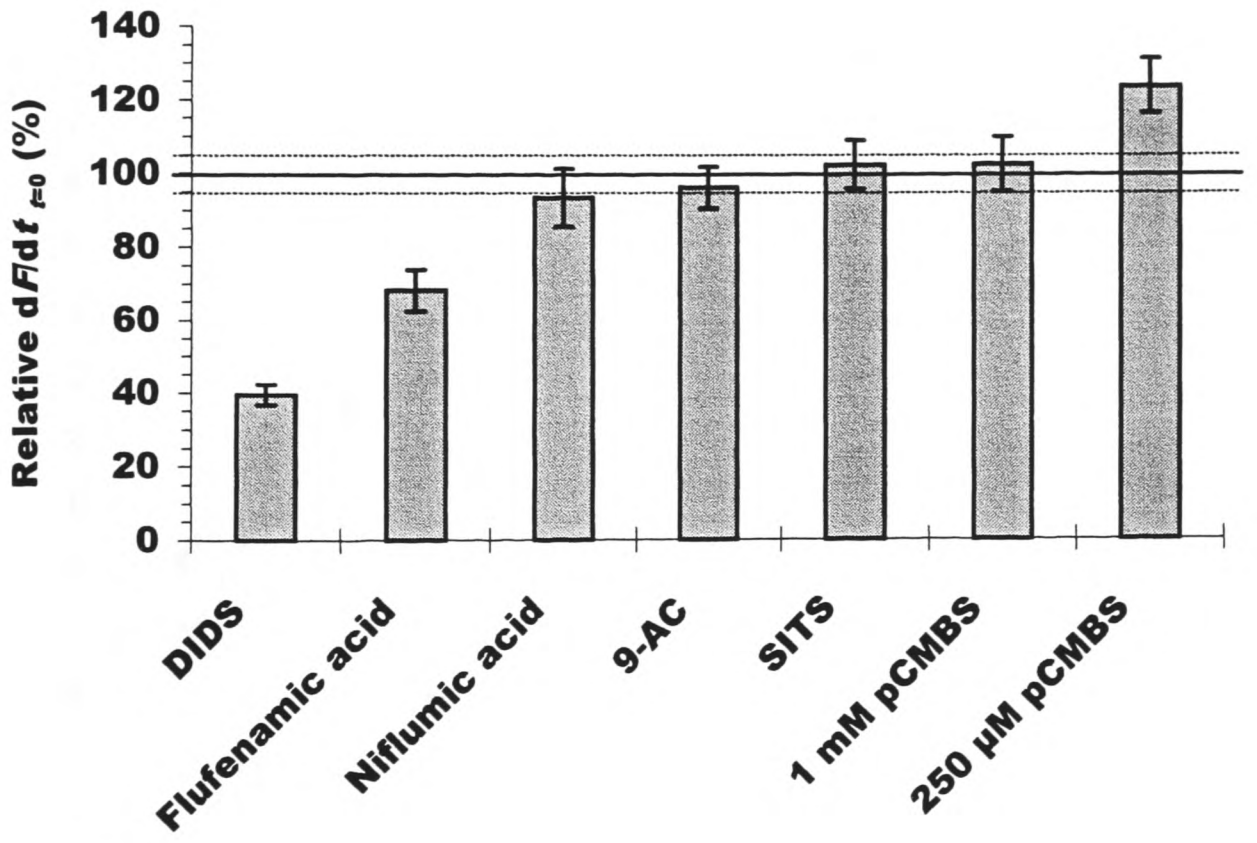


Figure 4.15. Inhibition of the initial rate of Cl^--dependent fluorescence quenching ($dF/dt_{t=0}$). Bars show the change of lucigenin fluorescence in the presence of 100 µM inhibitor (or 250 µM and 1 mM *p*CMBS) relative to the control. The control (100%) is marked by the solid line, the dotted lines indicate the standard error of the mean for the control. See Figure 4.14 for further details

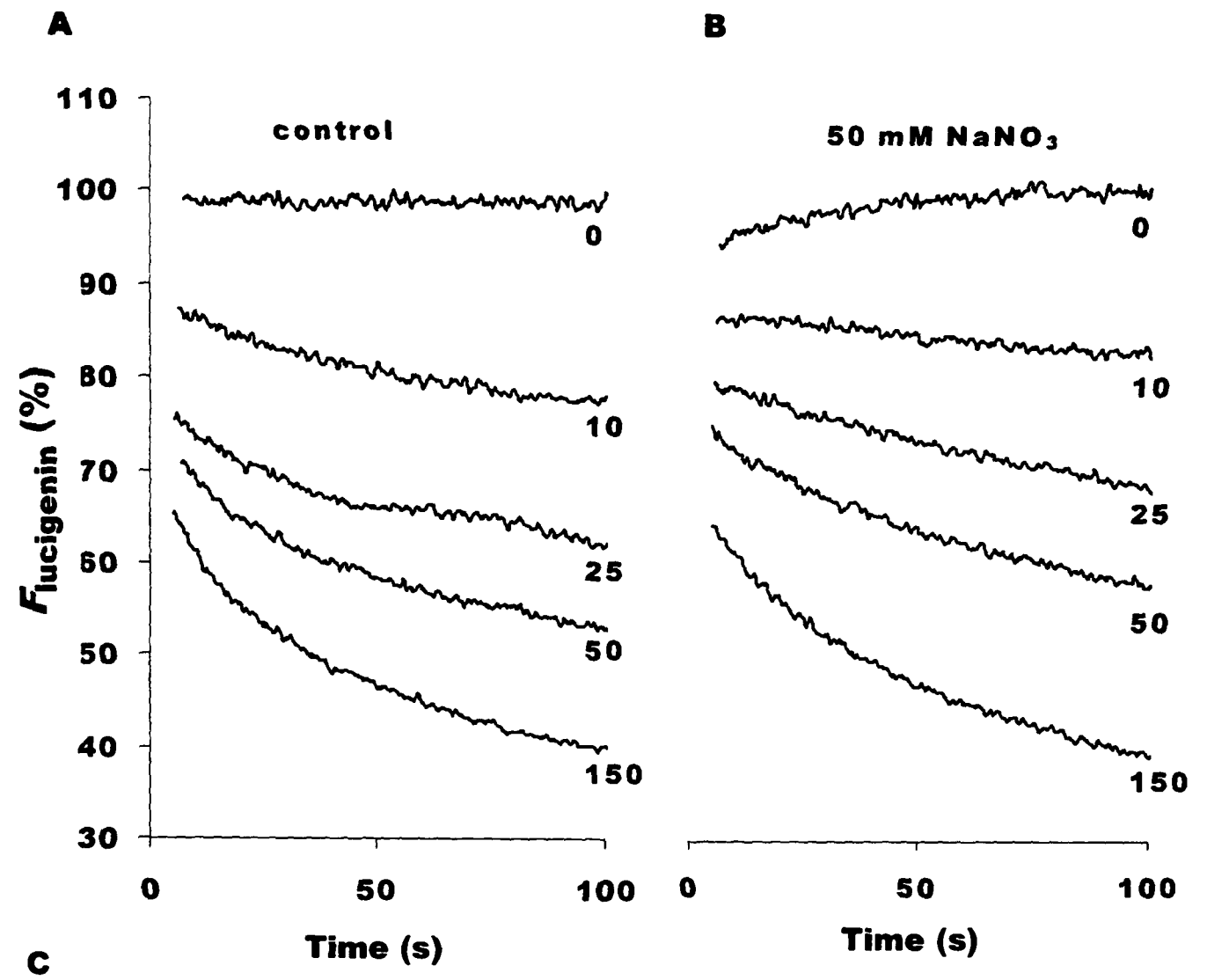
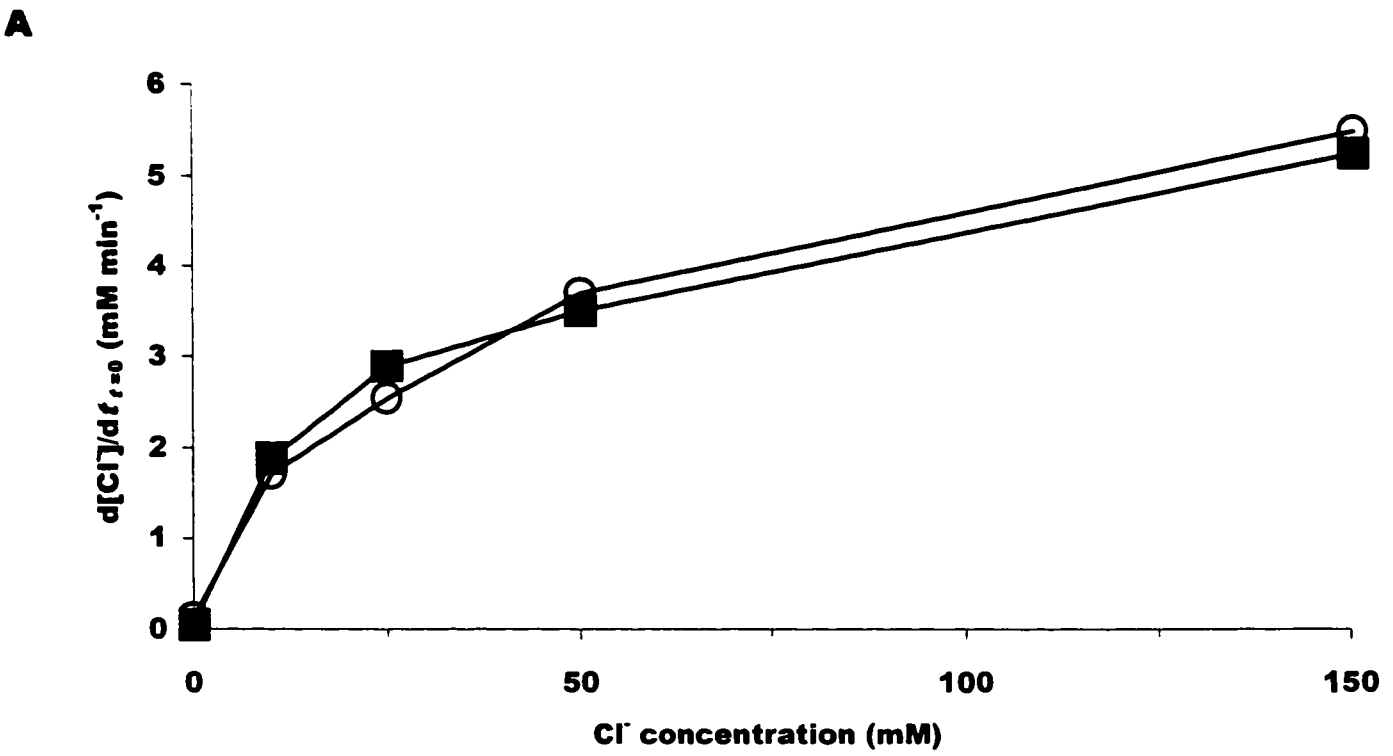


Figure 4.16. Cl^- transport in the presence of nitrate and malate. **A,B**) Original recordings of Cl^- transport in tonoplast vesicles in the absence (A) and presence (B) of 50 mM $NaNO_3^-$. Note the time-dependent increase in fluorescence in (B) in the absence of Cl^-. **C**) Kinetics of Cl^- transport in the absence (○) or presence of 50 mM $NaNO_3^-$ (■) or 50 mM malate-BTP (▲), respectively (n = 6, two separate preparations)



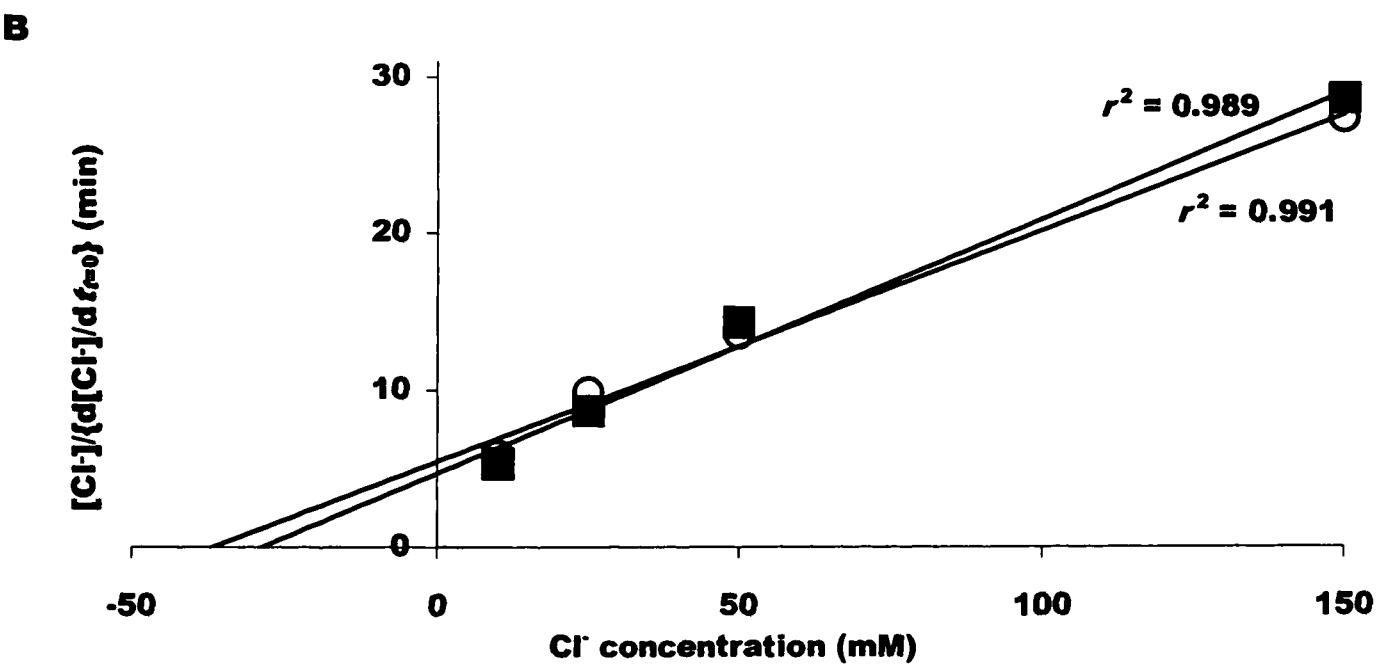


Figure 4.17. Kinetics of initial Cl^--transport rate after subtracting the offset observed in the presence of nitrate. A constant offset of -1.29 mM min^{-1} was subtracted from the data in Figure 4.16.C. **A**) Kinetics in the absence (○) and presence of 50 mM $NaNO_3^-$ (●) after subtraction. **B**) Plotting the data as a Hanes plot reveals a linear relationship. The linear regressions of the Hanes plots were not significantly different

To test whether the different K_2SO_4 concentrations in the various experiments might have any impact on the initial Cl^--transport rate, measurements were performed with either 100 mM or 200 mM K^+ in the vesicles and in the assay medium. The addition of KCl was compensated for by adding an appropriate amount of K_2SO_4 to keep the total K^+ concentration constant. Figure 4.18 shows that there was no difference in the initial Cl^--transport rate at 10 mM or 50 mM Cl^- when measured with different K_2SO_4 background concentrations.

4.2.5 Vacuolar Cl^- transport under salt stress

The accumulation of Cl^- in the vacuole of mesophyll cells of *M. crystallinum* is a major physiological response when these plants are challenged with high soil salinity. Hence, a series of experiments was performed to study the effect of salt stress on the initial Cl^--transport rate. Initially, a number of experiments were conducted according to a protocol by Barkla *et al.* (1995), treating 6-week-old plants with 200 mM NaCl for 2 weeks. Figure 4.19 shows the averaged initial Cl^--transport rates from three independent experiments with increasing Cl^- concentrations in the assay medium. Both data sets could be described by Michaelis-Menten kinetics, whereby neither the apparent K_m, nor the V_{max} values for the initial Cl^--transport rates of the two treatments were different (control: K_m = 15.5 ± 1.6 mM, V_{max} = 4.82 ± 0.70 mM min^{-1}; salt-treated: K_m = 13.3 ± 2.8 mM, V_{max} = 3.99 ± 0.45 mM min^{-1}). Furthermore, with these treatments no increase in hydrolytic V-ATPase activity could be observed: salt-treated plants showed 91 ± 10% of the hydrolytic V-ATPase activity of the control plants of the same age (n = 5). Only in one experiment out of a total of 8 did

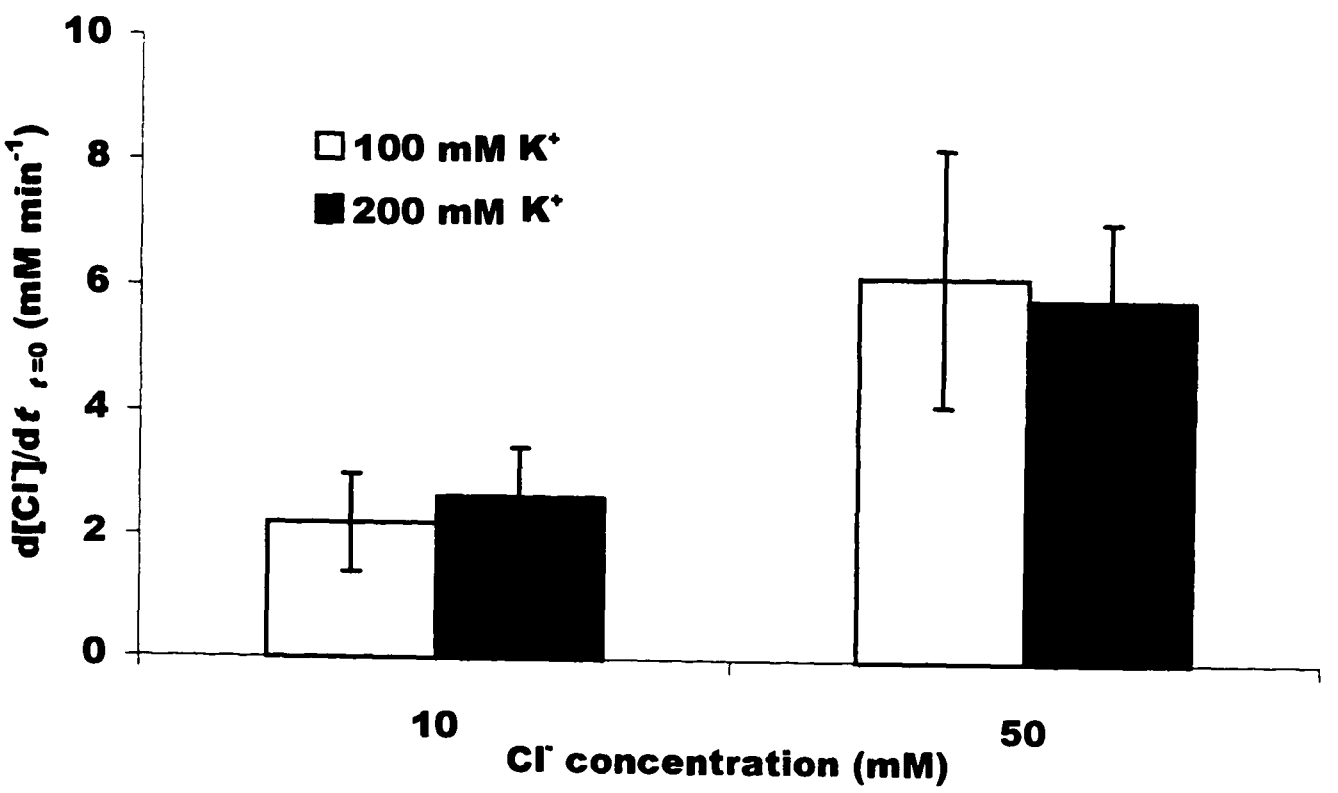


Figure 4.18. Effect of the K_2SO_4 background concentration on the initial Cl^--transport rate. Measurements of the initial Cl^--transport rate were performed with constant K^+ concentrations of either 100 mM or 200 mM on both sides of the membrane. KCl and K_2SO_4 were added to give the appropriate K^+ and Cl^- concentrations, e. g. at 10 mM Cl^-, 10 mM KCl and 45 mM K_2SO_4 were added to give 100 mM K^+, or 10 mM Cl^- and 95 mM K_2SO_4 to give 200 mM K^+. Transport rates were measured for 10 mM and 50 mM external Cl^- ($n = 3$)

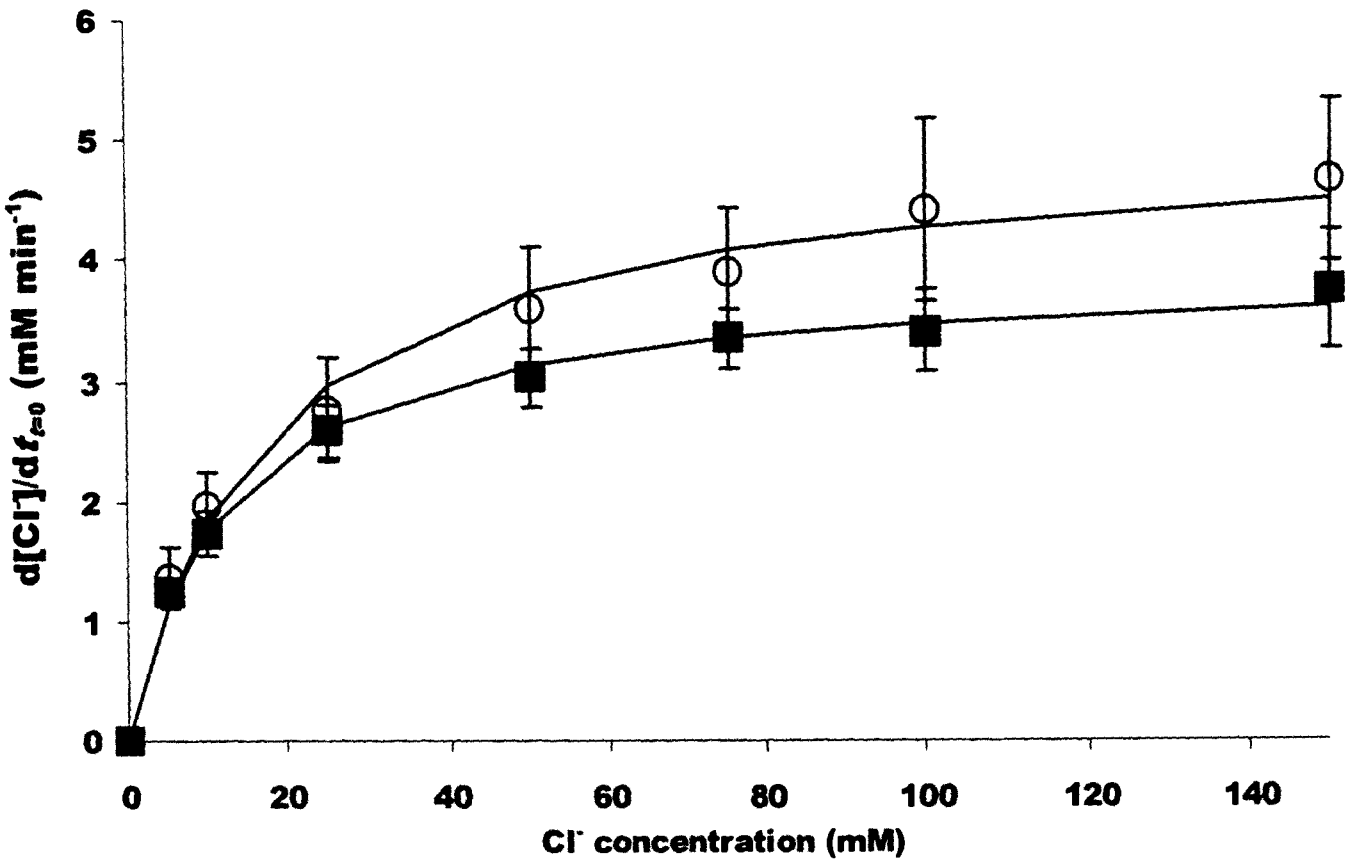


Figure 4.19. Effect of 200 mM NaCl treatment of *M. crystallinum* plants on the initial Cl^--transport rate of tonoplast vesicles. Plants were treated with 200 mM NaCl for 2 weeks from age 6 weeks onwards (■) or with water only (○). The lines are best fits for Michaelis-Menten kinetics with the following parameters: control K_m = 15.5 ± 1.6 mM, V_{max} = 4.82 ± 0.70 mM min^{-1}; salt-treated K_m = 13.3 ± 2.8 mM, V_{max} = 3.99 ± 0.45 mM min^{-1} (three preparations, n = 6)

plants treated with 200 mM NaCl for 2 weeks actually show an increased H^+-ATPase activity (as shown in Figure 3.7).

A subsequent experiment was then conducted according to Struve *et al.* (1985), with 400 mM NaCl for 2 weeks (Experiment 1) and plants growing under controlled conditions from week 3 onwards in a growth cabinet. Subsequently, two further experiments were conducted according to the protocol of Adams *et al.* (1998), with 500 mM NaCl for 3 weeks (Experiments 2 and 3). Both control and salt-treated plants were harvested when 9 weeks old. Younger plants were grown in parallel under similar conditions and harvested when 6 weeks old. All plants were grown in a growth cabinet from 3 weeks onwards and harvested at the end of the light period.

Table 4.3 summarises the values for the hydrolytic ATPase activities and the apparent K_m and V_{max} values of the initial Cl^--transport rate for all preparations from the three experiments. This reveals some degree of variability in the ATPase activities within and also between the different experiments. For example, the hydrolytic V-ATPase activity of the 6-week-old plants in Experiment 3 was only 18.4 µmol P_i h^{-1} mg^{-1} protein, whereas it was 35.1 µmol P_i h^{-1} mg^{-1} protein for the 9-week-old salt-treated plants of the same experiment. A similarly high activity was measured in the 6-week-old plants in Experiment 1 (37.4 µmol P_i h^{-1} mg^{-1} protein), while the salt-treated plants in that experiment showed a slightly lower activity with 33.1 µmol P_i h^{-1} mg^{-1} protein.

However, within each experiment the salt-treated plants consistently showed an increase in ATPase activity, and in the apparent K_m and the V_{max} of the initial Cl^--transport rate when compared to the control plants of the same age. Figure 4.20.A shows the initial Cl^--transport rates for the three preparations in Experiment 3. At

Table 4.3. Summary of hydrolytic ATPase activities and kinetic parameters of the initial Cl^--transport rate of the salt-stress experiments. Salt treatment was initiated at 6 weeks, with the Cl^- concentration increased daily by 50 mM to the final value as indicated. The treatment was continued until the plants were harvested for vesicle preparations (age as indicated). The nitrate-sensitive/azide-resistant V-type ATPase activity was calculated as described in section 3.2.3.1. Standard error of mean is given when there were more than two replicates per experiment

Experiment	Age at harvest (weeks)	Treatment (mM NaCl)	Duration of treatment (weeks)	Hydrolytic ATPase activity					Initial Cl^- transport rate	
				Total ATPase activity (µmol P_i/h /mg protein)	+ Inhibitors (µmol P_i/h /mg protein)	+ Inhibitors + Nitrate (µmol P_i /h /mg protein)	Nitrate sensitive azide resistant (µmol /h /mg protein)	% of total	K_m (mM)	V_{max} (mM min^{-1})
1	6	-	-	47.0 ± 0.9	41.0 ± 0.8	9.6 ± 1.0	37.4	80	16.1 ± 4.3	2.1 ± 0.1
	8	-	-	39.6 ± 1.6	39.6 ± 2.4	9.4 ± 1.1	30.2	76	24.2 ± 2.7	3.2 ± 0.3
	8	400	2	47.4 ± 2.1	48.8 ± 2.7	14.3 ± 2.1	33.1	70	45.0 ± 4.4	4.7 ± 0.3
2	6	-	-	25.6 ± 0.5	24.9 ± 0.8	5.1 ± 1.6	20.5	80	22.1	2.9
	9	-	-	36.4 ± 1.2	33.5 ± 0.4	7.0 ± 0.1	29.4	81	25.0	2.9
	9	500	3	43.6 ± 0.5	40.4 ± 0.2	7.9 ± 0.1	35.7	82	39.5	4.5
3	6	-	-	25.3 ± 0.5	22.5 ± 1.4	4.1 ± 0.6	18.4	75	36.0	6.5
	9	-	-	27.5 ± 0.8	26.0 ± 1.0	4.7 ± 0.2	21.4	78	31.6	5.2
	9	500	3	46.6 ± 0.9	44.3 ± 1.3	9.2 ± 0.2	35.1	75	45.5	8.2

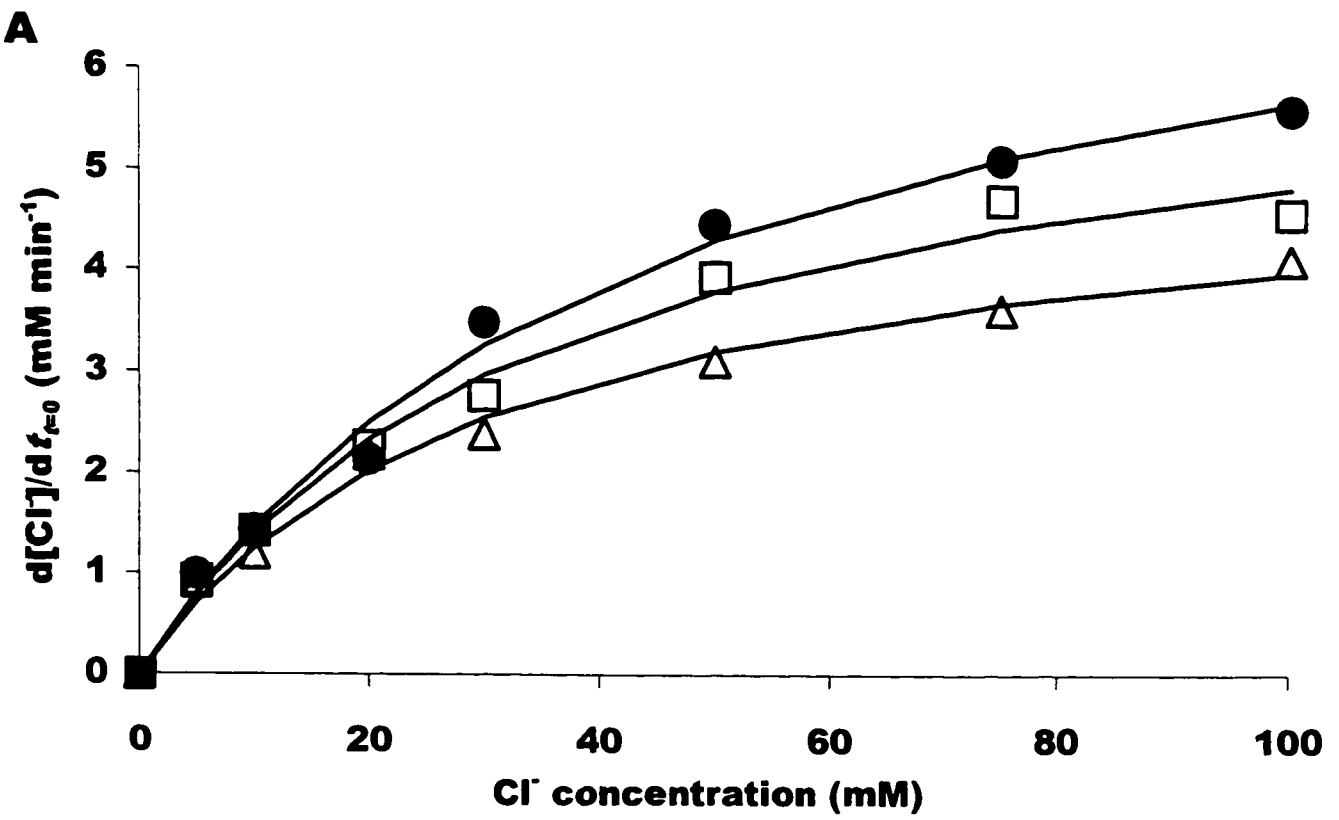


Figure 4.20. Experiment 3: Effect of treating *M. crystallinum* plants with 500 mM NaCl for 3 weeks on the initial Cl^--transport rate. The treatments were conducted in the same way to Experiment 3. **A)** The initial Cl^--transport rate with increasing Cl^- concentrations of plants that were harvested when 6 weeks old (❑), 9 weeks old (Δ) and 9 weeks old after 3 weeks of 500 mM NaCl treatment (●), respectively (n = 2). The curves are best fits for Michaelis-Menten kinetics with the parameters given in Table 4.3. **B)** Time course of lucigenin fluorescence over 20 min for the 9-week-old controls and the salt treated plants. Twenty µg of lucigenin-loaded vesicles were added to medium without Cl^- or with 100 mM Cl^-. The asterisks mark the addition of 0.03% Triton X-100 (v/v, final concentration)

higher Cl^- concentrations, the difference between the transport rates of the salt-treated plants and the control plants becomes more apparent. At 100 mM external Cl^- in the assay medium, the initial Cl^--transport rate was about 50% higher under the salt treatment. Fitting the data with Michaelis-Menten kinetics revealed an apparent K_m and V_{max} for the 9-week-old control plants of 31.6 mM and 5.2 mM min^{-1}, respectively. Under salt stress the apparent K_m was increased to 45.5 mM and the V_{max} increased to 8.2 mM min^{-1}. This was a 58% increase compared to the V_{max} of the control. This difference was also apparent in the original recording of the time course of lucigenin fluorescence for the two preparations at 100 mM Cl^- (Figure 4.20.B). The vesicles from salt-treated plants show a much steeper initial decrease in lucigenin fluorescence than the controls, as was quantified previously.

The V_{max} of the initial Cl^--transport rate varied quite substantially between the three experiments. For example, all three preparations in Experiment 3 showed about double the rate of initial Cl^- transport compared to the corresponding values in Experiment 2 (see also Figure 4.21). To allow comparisons between the different experiments, all data sets from one experiment were normalised with respect to the values of the 9-week-old control plants. Figure 4.22 shows the normalised values for the different parameters of each preparation. The relative differences between the different treatments were compared using a paired *t*-test. The hydrolytic V-ATPase activity showed an average increase of only 6% from 6-week-old to 8/9-week-old plants, which was not statistically significant. However, within each experiment salt-treated plants consistently showed an increased hydrolytic ATPase activity, but the average increase by 32% was not significant at $P < 0.2$ only. The low significance was mainly due to Experiment 1, were only a small increase in ATPase activity was

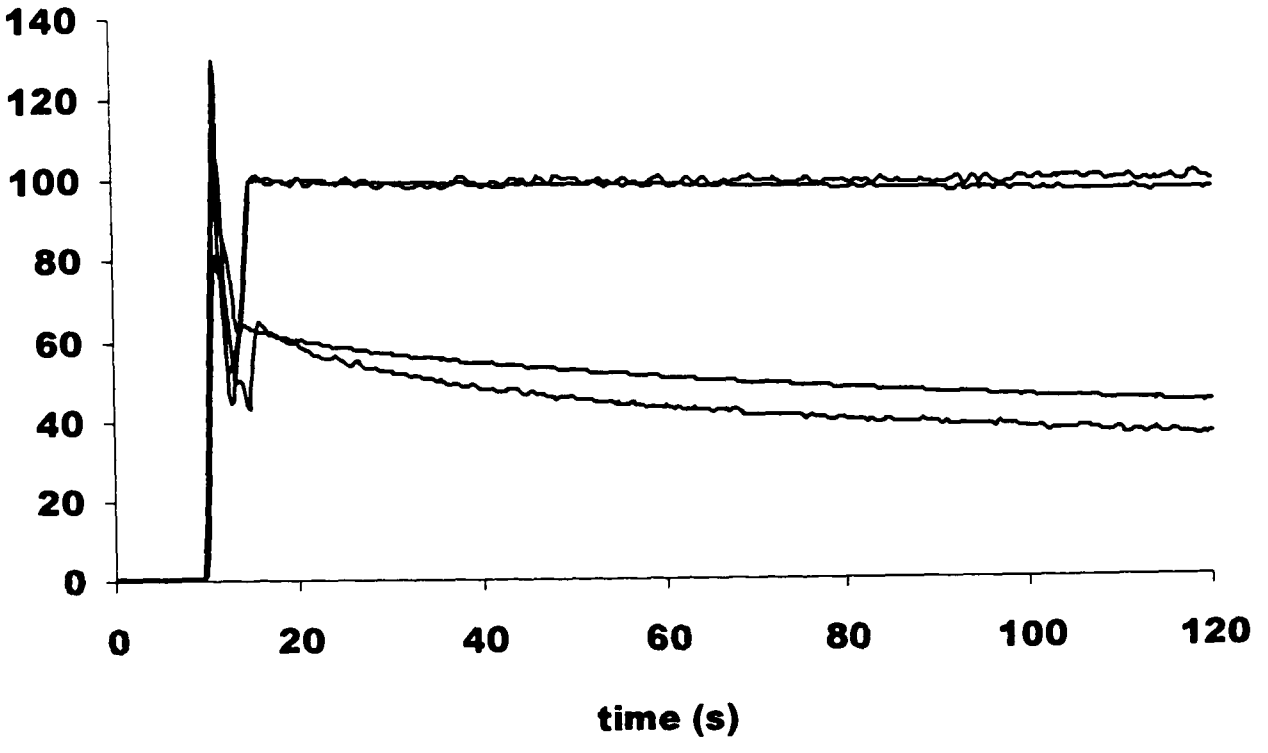


Figure 4.21. Time course of lucigenin fluorescence of 9-week-old salt-treated plants from Experiment 2 and 3. Twenty μg of lucigenin loaded vesicles from different preparations were added to assay media containing 0 mM or 100 mM Cl^-

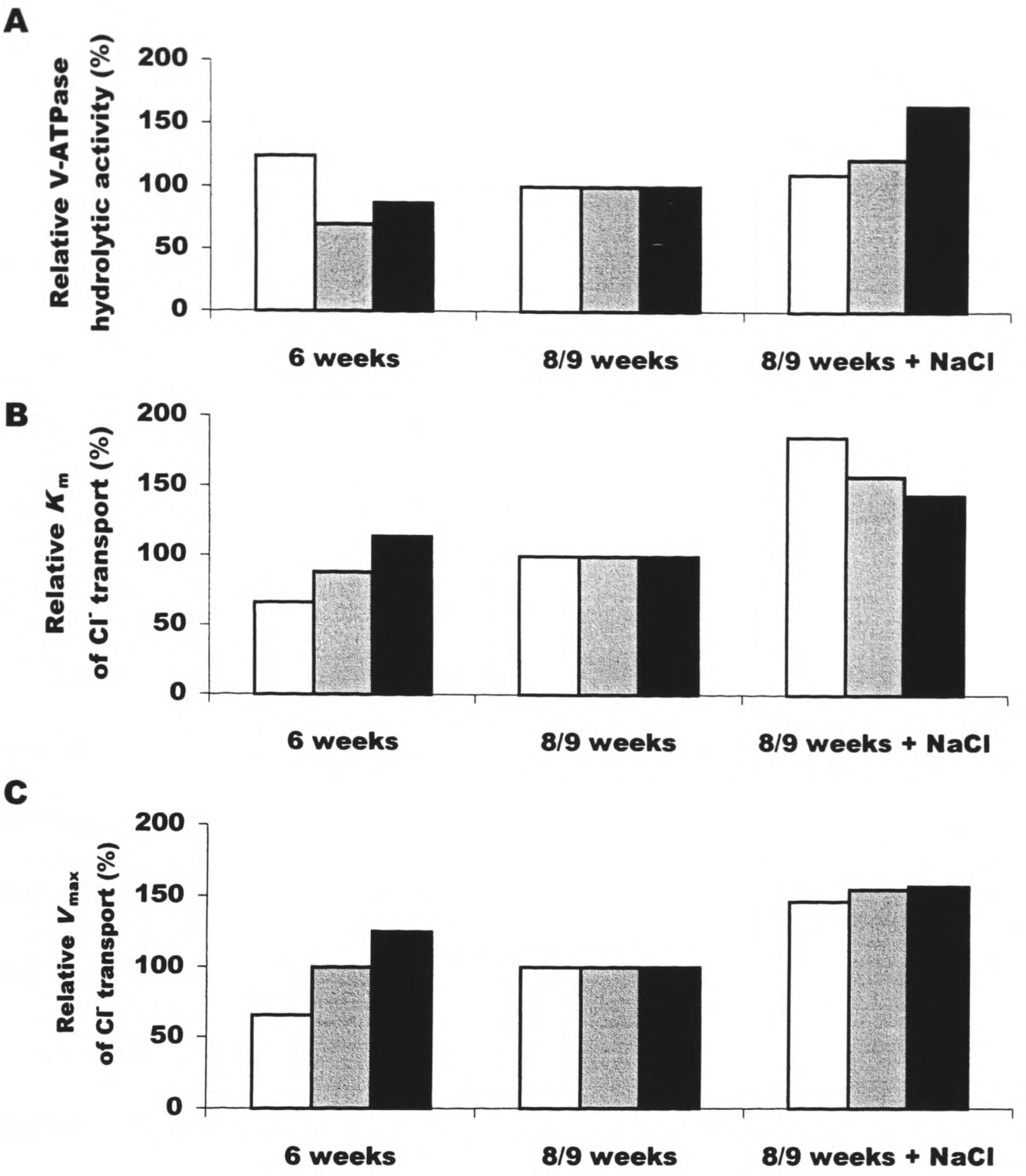


Figure 4.22. Effect of salt stress on the V-ATPase hydrolytic activity and the initial Cl^--transport rate of *M. crystallinum* tonoplast vesicles. All values are expressed as percentages of the 9-week-old controls for each experiment and are taken from Table 4.3. **A)** Relative hydrolytic activity of the nitrate-sensitive/azide-resistant V-type ATPase for each preparation. In Experiment 1 (white bars) salt treatment was 400 mM NaCl for 2 weeks (plants were therefore 8 weeks old at vesicle preparation). In Experiment 2 (grey bars) and 3 (black bars) the salt treatment of 500 mM NaCl lasted for 3 weeks (plants were 9 weeks old at harvest). A younger set of plants was grown in parallel with each experiment to be harvested at age 6 weeks. **B,C)** The equivalent values for the relative K_m and V_{max} of the initial Cl^--transport rate, respectively. Bars represent the same preparations as in part A

observed. This might be due to the shorter treatment (2 weeks) and lower NaCl concentrations (400 mM) used. In Experiment 2 and 3 higher NaCl concentrations (500 mM) for 3 weeks led to a higher average increase in ATPase activity with 21% and 65%, respectively.

Comparing the differences in the apparent K_m values of Cl^- uptake for the different treatments revealed no significant difference between 6 and 8/9-week-old plants. However, the salt-treated plants showed an average increase of 63% when compared with control plants of the same age, which was significant at $P < 0.05$. This increase corresponded to an absolute increase in the apparent K_m value from 26.9 ± 2.3 mM to 43.4 ± 1.9 mM under salt stress. Similarly, the V_{max} of the initial Cl^--transport rate was not significantly increased when comparing 6-week-old plants with the older control plants. But as with the apparent K_m value, under salt stress an average increase of the V_{max} of 53.2% was observed, which was significant with $P < 0.01$. This corresponded to an increase in the maximum initial Cl^--transport rate from 3.8 ± 0.7 mM min^{-1} in the control plants to 5.8 ± 1.2 mM min^{-1} under salt stress.

These experiments have shown that treating plants with 200 mM NaCl is not sufficient to elicit increases in the apparent K_m and V_{max} of initial Cl^- transport rate. More severe treatments with 400 and 500 mM NaCl led to a significant increase in the apparent K_m value and also in the maximum initial Cl^--transport rate of tonoplast vesicles. Any age-related effects between 6- and 8 to 9-week-old plants could not be demonstrated with statistical significance.

4.3 Discussion

These experiments have shown that lucigenin can be successfully used to study Cl^- transport into tonoplast vesicles. In *M. crystallinum*, this gave comparable results to those obtained using SPQ. It can therefore be concluded that the results observed in this study can also be compared with other studies in which SPQ was used to investigate Cl^- transport (Pope and Leigh, 1988, 1990; Pope *et al.*, 1990). The cause for the slight apparent reduction in the internal lucigenin fluorescence with increasing Cl^- concentrations is not known. A likely explanation is that the curve fitting and extrapolation slightly underestimated the initial drop in fluorescence, since the traces were not ideal single exponential functions. The internal fluorescence is used as a reciprocal when calculating the initial Cl^--transport rate, thereby leading to a slight overestimation of the transport rate at higher Cl^- concentrations. On the other hand, the same process also slightly reduces the initial change in lucigenin fluorescence, thereby compensating for a smaller apparent internal fluorescence.

Alternatively, the apparent decrease in the internal concentration could be caused by a sub-population of vesicles with very high Cl^--permeability (e.g. containing high-conductance Cl^- channels of lower abundance). These vesicles would rapidly equilibrate with the external Cl^- within the first few seconds of stirring before the fluorescence signal can reliably be recorded. This would lead to an apparent decrease in the initial intravesicular lucigenin fluorescence. However, this effect would show a hyperbolic Cl^- concentration dependence according to the Stern-Volmer relationship, while the observed effect was linear. The non-hyperbolic apparent decrease in the initial internal fluorescence therefore indicates that there was no sub-population of vesicles with high Cl^- permeability.

The saturating concentration dependence of the initial Cl^--transport rate indicates that Cl^- transport is protein-mediated, and probably catalysed by a single transport system only. The apparent K_m for Cl^--transport in *M. crystallinum* tonoplast vesicles under control conditions at 0 mV, based on the extrapolated initial rates of lucigenin fluorescence quenching, was slightly variable between experiments, varying between 10 mM to 36 mM Cl^-. However, this is considerably higher than the values reported for vacuolar Cl^- transport systems in other plants, which vary between 2.3 mM in barley mesophyll vacuoles (Martinoia *et al.*, 1986), 5 mM in corn root vesicles (Bennett and Spanswick, 1983), 6.5 mM in red beet storage tissue (Pope and Leigh, 1988, 1990) and between 5 to 10 mM in oat root vesicles (Schumaker and Sze, 1987). However, a later study of Pope *et al.* (1990) reported a higher apparent K_m for red beet storage tissue at 0 mV trans-tonoplast membrane potential of 22 mM. While this value is similar to the apparent K_m obtained for mesophyll tonoplast vesicles from *M. crystallinum*, the studies from all other species suggest saturation of Cl^- uptake at much lower Cl^- concentrations. This might reflect an adaptation to higher cytosolic Cl^- concentrations in *M. crystallinum*, which is a halophyte. Furthermore, in salt-treated *M. crystallinum* plants the apparent K_m increased to values around 46 mM Cl^-. Interestingly, this is similar to the apparent K_m values obtained for the H^+-dependent Na^+ uptake by tonoplast vesicles of *M. crystallinum*, which was 44 mM in control and 51 mM in salt-treated plants, respectively (Barkla *et al.*, 1995).

The absolute initial Cl^--transport rates obtained for *M. crystallinum* were also about three to four times higher than those in red beet and barley root (Pope and Leigh, 1988, 1990). Again, this might reflect an adaptation to the higher rates of Cl^- transport required across the tonoplast in this halophytic plant. The fact that a modest

salt treatment of 200 mM did not increase the initial Cl^--transport rate suggested that this baseline transport capacity may be sufficient to allow adequate rates of Cl^- transport into the vacuole under these conditions. Furthermore, 200 mM NaCl in the soil does not actually impose salt stress on *M. crystallinum*, since this is in fact the concentration required for optimal growth (Adams *et al.*, 1998). More severe salt treatment significantly increased the Cl^- transport rates by about 50%, indicating an upregulation of vacuolar Cl^- transport activity under these conditions.

While some studies of vacuolar transport have suggested no changes in ATPase activities or ionic currents under salt stress (Maathuis *et al.*, 1992), others have reported differences in channel open probabilities, rectification, or Na^+/H^+ transport activities in vacuoles of various plants (Pantoja *et al.*, 1989; Ayala *et al.*, 1996; Ballesteros *et al.*, 1997). The Na^+/H^+-antiport activity in *M. crystallinum*, along with vacuolar H^+-ATPase activity, has been shown to increase under salt stress by more than 100% (Barkla *et al.*, 1995). However, using the conditions employed in that study (200 mM NaCl treatment for 2 weeks), I failed to detect a significant increase in V-ATPase and Cl^- transport activities in the present work. Only a more severe treatment of 500 mM NaCl for 3 weeks led to an increase in the Cl^- transport rate and in hydrolytic V-ATPase activity. The evidence from other studies on the effect of similarly high salt treatments on the V-type ATPase activity is also rather confusing. A study by Ratajczak *et al.* (1994) failed to detect any salt induced increases in the V-ATPase activity where previously significant salt-induction was reported from the same group (Struve and Lüttge, 1987; Bremberger and Lüttge, 1992). As Ratajczak *et al.* (1994) pointed out, the previous studies apparently did not take into account the age-related increase in hydrolytic ATPase activity that occurs during ageing when

using control plants of a significantly younger age than the salt treated plants. While these studies measure ATPase activity on a total protein basis, other studies have shown that the expression levels of several subunits increase (Tsiantis *et al.*, 1996; Rockel *et al.*, 1998). But so far it remains uncertain whether any increase in hydrolytic ATPase activity is due to an increase in specific activity per unit of V-type ATPase protein, or merely reflects an increase in amount of V-type ATPase protein relative to the total tonoplast protein.

For the Cl^--transport rates in tonoplast vesicles from *M. crystallinum*, there seems to be on average no significant change with increasing plant age. This is in stark contrast to the V-ATPase activity in *M. crystallinum*, which shows an increase of activity during development, while the vacuolar PPase activity shows a strong decrease (Bremberger and Lüttge, 1992; Ratajczak *et al.*, 1994). This suggests that the basic Cl^- transport activity of *M. crystallinum* vacuoles is sufficient to maintain Cl^- homeostasis during ageing and mild salt stress. Only at higher soil salinity is an increase in Cl^- transport apparently required at the vacuolar level in mesophyll cells.

The values for the initial Cl^--transport rates obtained in this study, and also those using SPQ (Pope and Leigh, 1988, 1990; Pope *et al.*, 1990), only reflect changes in intravesicular Cl^- concentrations. To express Cl^- flux on the basis of membrane area or mg protein, the total vesicle volume and the corresponding area were taken into account, as calculated from the electron micrographs. On an area basis, a concentration change of 4.8 mM min^{-1} therefore corresponds to 7.1 nmol m^{-2} s^{-1}. Using the data published by Ratajczak *et al.* (1995), giving a protein to surface area ratio between 7.4 and 8.8 mg m^{-2} for *M. crystallinum* tonoplast vesicles, the Cl^- transport rate per g protein is 0.81 to 0.96 µmol g^{-1} s^{-1}.

Recalculating the data from Martinoia *et al.* (1986) on $^{36}Cl^-$ uptake into barley mesophyll vacuoles gives a value of 33 nmol m^{-2} s^{-1} at 50 mM Cl^-. This is about 4.6-fold higher than the Cl^- transport rate obtained for *M. crystallinum* tonoplast vesicles. However, the initial Cl^--transport rates measured using lucigenin most probably underestimates the true Cl^- transport rate. This is due to the fact that the Stern-Volmer constant for Cl^- is much lower in the vesicles than in the assay medium. This is indicated by the measurements in Figure 4.20.B The amount of external fluorescence could be calculated to be 58% before and to be about 3% just after the addition of 100 mM Cl^-, according to the Stern-Volmer equation $F = F_0/(1+K_{SV}[Cl^-])$, with the external K_{SV} being 0.173 mM^{-1}. The drop of the internal fluorescence could therefore be calculated to be from initially 42% down to 8% after about 20 min of Cl^- transport. Assuming that the internal Cl^- concentration is almost identical with the external Cl^- concentration of 100 mM after that time, this drop would be equivalent to an internal apparent K_{SV} for Cl^- of only 0.040 mM^{-1} for both traces. This is about 4.4-fold lower than the K_{SV} measured in assay buffer and suggests that lucigenin is less sensitive in the vesicles than in the external medium, most likely due to partial quenching of the dye by other quenchers. Since the reciprocal of the Stern-Volmer constant was used to calculate the initial Cl^--transport rate, the actual rate is accordingly 4.4-fold higher than the one calculated here. An initial Cl^--transport rate of around 4.8 mM min^{-1} measured using lucigenin should therefore reflect an actual transport rate of 21 mM min^{-1}, or 31 nmol m^{-2} s^{-1}.

Although this correction provides only a rough estimate of the actual Cl^- transport activity of *M. crystallinum* tonoplast vesicles, it certainly puts it into the same range of the Cl^- uptake rates measured in barley mesophyll vacuoles. For

comparison, in vesicles derived from human placenta and loaded with SPQ, a similarly high transport rate of 0.61 μmol g^{-1} s^{-1} has been determined (Illsley and Verkman, 1987). However, the type of Cl^- transporter involved is still unknown.

It should be noted that the lucigenin based method has practical limits, in that it is not possible to measure very rapid Cl^- uptake. For example, an initial Cl^--transport rate of 4000 mM min^{-1} at 100 mM Cl^- outside - about a thousand times what was been measured here - would completely equilibrate an average vesicle in less than 10 s. This is a transport rate one could expect if each vesicle contained on average a small single Cl^- channel with a conductance of 0.4 pS and an open probability of one (assuming 100 mM external Cl^-, 0.001 mM Cl^- inside the vesicle and the membrane potential clamped to 0 mV). Since the first 5 to 8 s of a recording are usually lost due to mixing and stirring, these fast processes could not be resolved in the time course of fluorescence. To measure faster transport systems, a stopped-flow apparatus would need to be used. However, if the majority of vesicles exhibited such a high transport rate, this would lead to almost complete quenching of lucigenin fluorescence within 10 s at higher Cl^- concentrations, which was not observed in the present experiments.

A concentration of 5 μM valinomycin combined with varied potassium concentrations inside and outside the vesicles was sufficient to establish a defined membrane potential in the tonoplast vesicles, which could be calculated by the Nernst equation. However, the experiments using the potentiometric dye oxonol-V were not able to give clear results about the speed of generation of the membrane potential. This is due to the "slow" response of the dye following the imposed membrane potential with time constants between 0.3 s and 20 s (Scherman and Henry, 1980), which seems to be rate-limiting the speed of this assay. Given that the amount of

valinomycin is in excess, it can be assumed that the establishment of the membrane potential (within less than a second) is much faster than the kinetics of Cl^- influx (Loew, 1993; Plasek and Sigler, 1996). That there was still a linear increase, albeit smaller, in oxonol-V fluorescence in the absence of valinomycin but with Cl^- present might reflect the existence of a significant membrane permeability for K^+. Increased cytosolic Cl^- concentrations have been shown to increase the activity of vacuolar K^+ channels, leading to an increased K^+ permeability (Pantoja *et al.*, 1992a).

In the presence of Cl^- the K^+/valinomycin induced oxonol-V response was less than in the absence of Cl^-. This might reflect the ability of Cl^- to counter-balance part of the K^+-imposed membrane potential, suggesting electrogenic Cl^- uptake. This was supported by the concentration dependence of this effect, which showed saturation in a similar range as the initial Cl^--transport rate. However, under initial transport conditions at $t = 0$, the valinomycin-induced K^+ permeability is much greater than the endogenous Cl^- transport capacity, and should therefore dominate the $\Delta\psi$. This was indicated by a maximum Cl^- induced reduction of the ΔF by less than 3%. While the Cl^- induced effect on the K^+/valinomycin clamp in this case was small, it shows that in the presence of considerable permeabilities other than for K^+ the Nernst equation might not be adequate and the Goldman-Hodgkin-Katz voltage equation would be more appropriate to calculate the imposed diffusion potential.

Similar to vacuolar Cl^- transport in red beet (Pope *et al.*, 1990), the initial Cl^- transport rate in tonoplast vesicles of *M. crystallinum* showed a sigmoidal increase with increasing inside-positive membrane potentials at 50 mM Cl^-. The steepest response was around 30 mV, inside positive, with saturation at membrane potentials above 50 mV. This saturation does not seem to be due to a limit in detection of fast

Cl^- uptake, since theoretical calculations have shown that even a 10-fold increase in initial Cl^--transport rate can still be measured using this method. A saturating response might therefore reflect a saturation of the transport system, due to the steep concentration and voltage gradient. However, this voltage response is linear at 20 mM Cl^-, which is in contrast to the measurements on red beet vesicles, which show the strongest sigmoidal response at lower concentrations (Pope *et al.*, 1990). In red beet, elevated Cl^- concentrations lead to a linearisation of the voltage response. Also, as with red beet vacuoles, the apparent K_m is substantially reduced at higher inside-positive membrane potentials, indicating saturation at lower Cl^- concentrations. By fitting several transport models to their data, Pope *et al.* (1990) found a three-state model based on a Cl^--uniport mechanism to be sufficient to describe their data. But the results presented in the present work on vacuolar Cl^--transport in *M. crystallinum* are not sufficient to pursue a similarly detailed modelling approach. However, the fact that with an imposed membrane potential the concentration-dependence of the initial Cl^--transport rate still showed a single saturating response is consistent with the interpretation that the increase in Cl^- uptake is based on the regulation of a single transport system.

Recently, a CDPK (Ca^{2+}-dependent protein kinase) activated Cl^- channel has been characterised in *Vicia faba* guard cells and red beet storage vacuoles (Pei *et al.*, 1996) that was activated at negative membrane potentials (equivalent to a positive membrane potential in cytosolic-side-out vesicles). Whether this is the same transport system as that investigated here is unlikely, since it is seen only in the presence of Ca^{2+}, ATP and CDPK together, indicating that the channel is strongly regulated.

The use of various known inhibitors of anion transport was not very conclusive due to a number of technical problems. The fact that DMSO not only interferes with lucigenin fluorescence, but also inhibits Cl^- transport directly, complicated the use of certain inhibitors, since many stock solutions were originally made up with DMSO. A similar inhibition by DMSO has been seen for vacuolar malate currents; concentrations as low as 0.001% (v/v) were sufficient to inhibit these currents in *Kalanchoë daigramontana* (O. Pantoja and J. A. C. Smith, unpublished results). Even in the absence of DMSO, it was still difficult to separate the effects of vesicle lysis and quenching of lucigenin fluorescence by flufenamic acid and DIDS from genuine inhibition of initial Cl^- transport. Both substances are known to affect Cl^- transport in the micromolar range (Hedrich and Kurkdjian, 1988; Chao and Mochizuki, 1992; Meyer *et al.*, 1996), although DIDS can act both as activator or inhibitor, depending on the transport system studied (Weber *et al.*, 1995).

In oat root tonoplast vesicles, the reported effect of DIDS varied according the assay employed. While the Cl^--dependent dissipation of a K^+/nigericin-generated ΔpH showed sensitivity towards DIDS, the Cl^--dependent dissipation of a PPase-generated $\Delta\psi$ was shown to be DIDS-insensitive (Kaestner and Sze, 1987; Schumaker and Sze, 1987). The authors have taken this as an argument for the existence of two separate Cl^--transport mechanisms within the same system. However, it has to be kept in mind that a major difference between energisation of vesicles *via* K^+/nigericin and PPase-mediated proton pumping is that the first energises all vesicles and is electroneutral, whereas the latter energises cytosolic-side-out vesicles only. That means that any effect of DIDS on PPase-activated, randomly orientated vesicles can only be seen if the inhibitor binding side is also at the cytosolic side. In contrast, if DIDS affects Cl^-

transport at the vacuolar side of the membrane, Cl^--dependent dissipation of a PPase-generated $\Delta\psi$ should not be inhibited, whereas the randomly oriented vesicles energised *via* K^+/nigericin will be at least partly affected. One has therefore to be cautious when comparing inhibition of membrane transport processes measured using different assay systems.

Whether vacuolar Cl^- transport studied in tonoplast vesicles of *M. crystallinum* is affected by these substances remains uncertain. Furthermore, the apparent transport of DIDS into the vesicles, as suggested by the quenching of intravesicular lucigenin fluorescence during incubation with DIDS, could indicate that inhibition by DIDS might be due to a competitive rather than an allosteric effect on some transport systems. Although the doubly charged anion DIDS is generally regarded as relatively membrane impermeant, uptake of sulphonated compounds has been shown in vacuoles from barley mesophyll (Klein *et al.*, 1997), although only in the presence of MgATP. Also, an earlier study on the human bile-acid transporter has shown that DIDS could be translocated by this transporter (Eleno *et al.*, 1992). This is particularly interesting in light of the findings by Blake-Kalff and Coleman (1996), where DIDS was shown to inhibit the MgATP-dependent uptake of taurocholate into barley vacuoles. Since taurocholate is a also a substrate of human bile-acid transporters, the inhibitory effect should be reassessed under the light of possible DIDS transport, leading to competitive inhibition of taurocholate uptake. SITS, niflumic acid and 9-AC, although all known to be anion transport inhibitors ((Hedrich and Kurkdjian 1988); Lambert *et al.*, 1991; Marten *et al.*, 1993; Meyer *et al.*, 1996), did not show any effect on the initial Cl^- transport rate at the concentration tested (100 µM) in the present work.

The significant increase in initial Cl^- transport rate observed with 250 µM *p*CMBS (*p*-chloromercuribenzene sulphonate) is very interesting, since Martinoia *et al.* (1986) reported a similar increase in Cl^- efflux rates of barley vacuoles after incubation with *p*CMBS, although the effect on the influx of Cl^- was not studied. Furthermore, *p*CMB (*p*-chloromercuribenzoic acid), a homologue to *p*CMBS has been shown to activate Cl^-/OH^- exchange activity in mammalian cells (Karniski, 1989). In contrast, vacuolar malate transport in *Kalanchoë daigremontiana* has been shown to be inhibited by *p*CMBS (Evetts, 1998). Finding the optimum concentration range for the activation of vacuolar Cl^- transport might therefore give a useful tool to dissect vacuolar anion transport mechanisms in plants.

Given the strong interference of some of the tested transport inhibitors with the assay system, further experiments are needed using other techniques, such as patch-clamping vacuoles of *M. crystallinum*, to allow for a more reliable pharmacological characterisation of vacuolar Cl^- transport in this plant. The fact that many of the known anion inhibitors show a direct effect on lucigenin fluorescence might indicate their ability to mimic Cl^-, allowing them to interact not only with potential Cl^--binding sites of transporters, but also with this Cl^--sensitive dye.

The observation that the presence of SO_4^{2-}, NO_3^- or malate did not reduce the initial Cl^--transport rate underlines the specificity of this transport system. In contrast, in the study by Pope and Leigh (1990) on tonoplast red-beet storage root, an apparent competitive inhibition by NO_3^- of the Cl^- transport was shown. At low Cl^- concentrations, nitrate significantly decreased Cl^- transport, whereas at higher Cl^- concentrations the degree of inhibition was reduced. A similar apparent reduction in the initial Cl^--transport rate by NO_3^- was seen in this study, but is more likely to have

been due to an unspecific effect, causing an increase in lucigenin fluorescence itself. This effect is proportional, so leading to lower relative inhibition at higher Cl^- concentrations. Since Pope and Leigh (1990) also used a fluorescence-based approach with SPQ to detect changes in Cl^--transport rate, it would be useful to compare original recordings to rule out the possibility of an artefact. What causes this time-dependent increase in fluorescence in the presence of NO_3^- has not been determined. In a vesicle-free medium, NO_3^- showed no effect on lucigenin fluorescence. A possible mechanism might be the transport of NO_3^- into the vesicle, charge balanced by parallel net influx of K^+ *via* the K^+/valinomycin clamp, thereby increasing the osmolality in the vesicles and leading to vesicle swelling. This should lead to an increase in fluorescence intensity, since the concentration of the endogenous quencher decreases with increasing vesicle volume. Other studies have shown similar effects of NO_3^- and Cl^- on dissipation of ΔpH or $\Delta\psi$ gradients, but it has remained unresolved whether a single transport system, or two separate systems, are involved (Kaestner and Sze, 1987; Pope and Leigh, 1987; Schumaker and Sze, 1987). However, it is generally thought that NO_3^- can easily cross the tonoplast. Similarly, it has not yet been established whether vacuolar malate uptake and Cl^- uptake are mediated by the same transport system. Several studies have shown the existence of a transport system highly selective for malate over Cl^-, making separate uptake mechanisms for Cl^- and malate likely (Cerana *et al.*, 1995; Pei *et al.*, 1996; Cheffings *et al.*, 1997).

This chapter has provided a general characterisation of Cl^- uptake into tonoplast vesicles from *M. crystallinum*. This Cl^- transport saturated with an apparent K_m around 20 mM, was Cl^--specific and voltage dependent. Only severe salt treatment with 500 mM NaCl for 3 weeks had a stimulating effect on vacuolar Cl^- uptake, when

it showed an increased V_{max} and lower affinity for Cl^-. Based on the results in this chapter, it could not be distinguished between passive or active vacuolar Cl^- uptake. This question will therefore be explored in more detail in the following chapter.

Chapter 5

Testing for active Cl^- transport in tonoplast vesicles

5.1 Introduction

The previous chapter presented the evidence for protein-mediated Cl^--transport in tonoplast vesicles of *Mesembryanthemum crystallinum* and characterised certain kinetic properties of this transport process. However, the main driving force present in most of those experiments was a transmembrane Cl^--concentration difference, with zero Cl^- in the vesicles and various Cl^- concentrations in the assay media. Although the Cl^--concentration gradient was sufficient to drive Cl^- uptake into vesicles, uptake was enhanced by the presence of an inside-positive electrical potential difference. Since both effects could be a function of either passive or active Cl^--uptake, further experiments were conducted to test for ATP-dependent Cl^--pumping or for H^+-coupled secondary active Cl^--transport. H^+-linked Cl^--transport would be indicated by dissipation of an inside acidic ΔpH. Also, Cl^- uptake should be stimulated by the presence of such a ΔpH in case of a H^+/Cl^--antiporter. Three different methods to energise vesicles with an internal acidic ΔpH were tested: pH-jumps, the K^+/nigericin pH-clamp, and the endogenous vacuolar H^+-ATPase pump activity. While the first two methods energise both cytosolic-side-in and cytosolic-side-out vesicles, the H^+-ATPase pump energises only the latter.

5.2 Results

The aim of the experiments described in this section was to find evidence for direct Cl^--pump activity or H^+-linked Cl^- transport in tonoplast vesicles of *Mesembryanthemum crystallinum*. Direct Cl^--pumping would putatively be energised by ATP-hydrolysis, so the initial experiments determined the effect of ATP on Cl^- transport. Further experiments were performed to test for the dissipation of a ΔpH by Cl^- and whether an imposed ΔpH has an effect on Cl^- transport in tonoplast vesicles.

5.2.1 Effect of ATP on Cl^- uptake in tonoplast vesicles

To test for primary, ATP-energised active uptake of Cl^- into tonoplast vesicles from *M. crystallinum*, the initial Cl^--transport rate was measured in the presence or absence of 5 mM Mg/ATP. Figure 5.1 shows that at 50 mM Cl^- the initial Cl^--transport rate was slightly increased when 5 mM Mg/ATP were present (by 12.5% over the control). This increase had only a weak statistical significance when compared by a paired *t*-test (P = 0.083). To test for possible involvement of the V-type H^+-ATPase, which is active under these conditions, the effect of ATP on the initial Cl^--transport rate was also tested in the presence of the V-ATPase inhibitor bafilomycin-A (Bowman *et al.*, 1988) at 500 nM. In this case the activity was 100% of the control, and not significantly different from the rate observed in the absence of bafilomycin-A. It can therefore be concluded that the presence of MgATP had no direct effect on the initial Cl^--transport rate.

5.2.2 pH-jump experiments

To directly measure Cl^--uptake under ΔpH conditions, pH-jump experiments were conducted. Vesicles were incubated for 30 min at 38°C in loading buffer

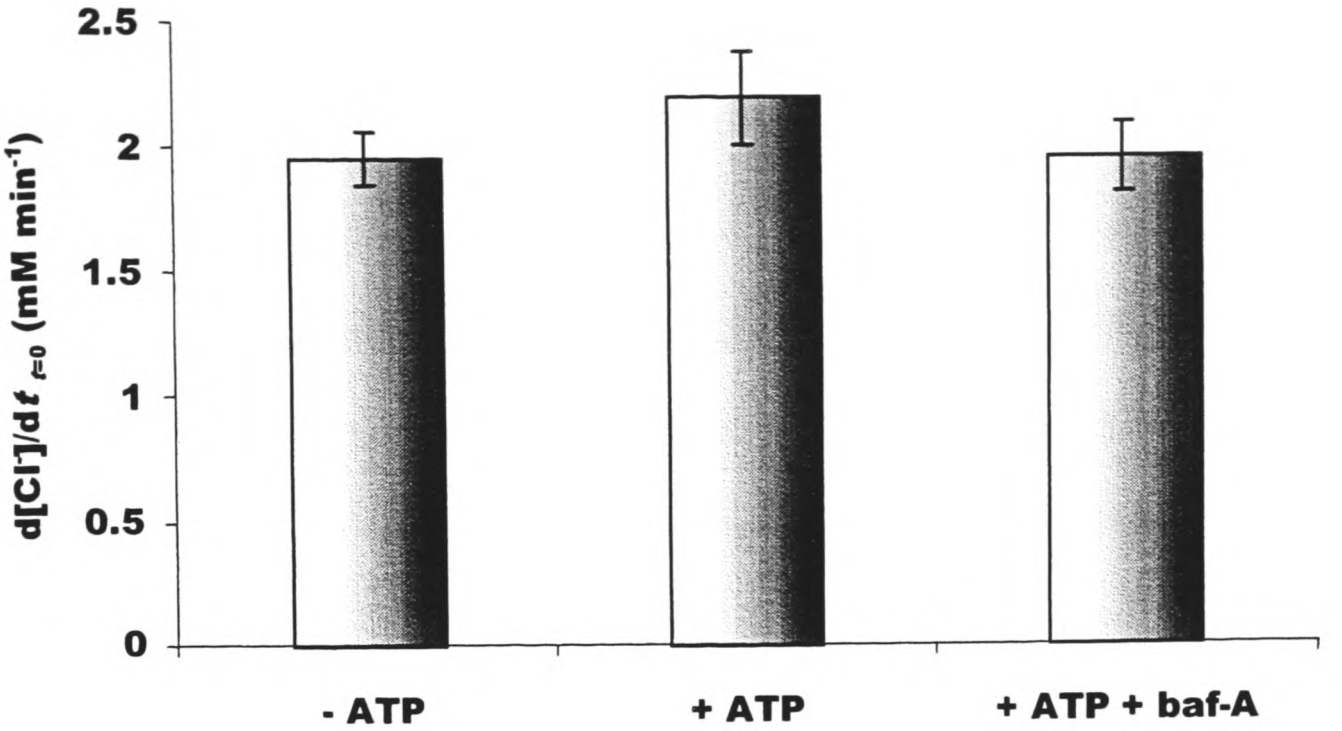
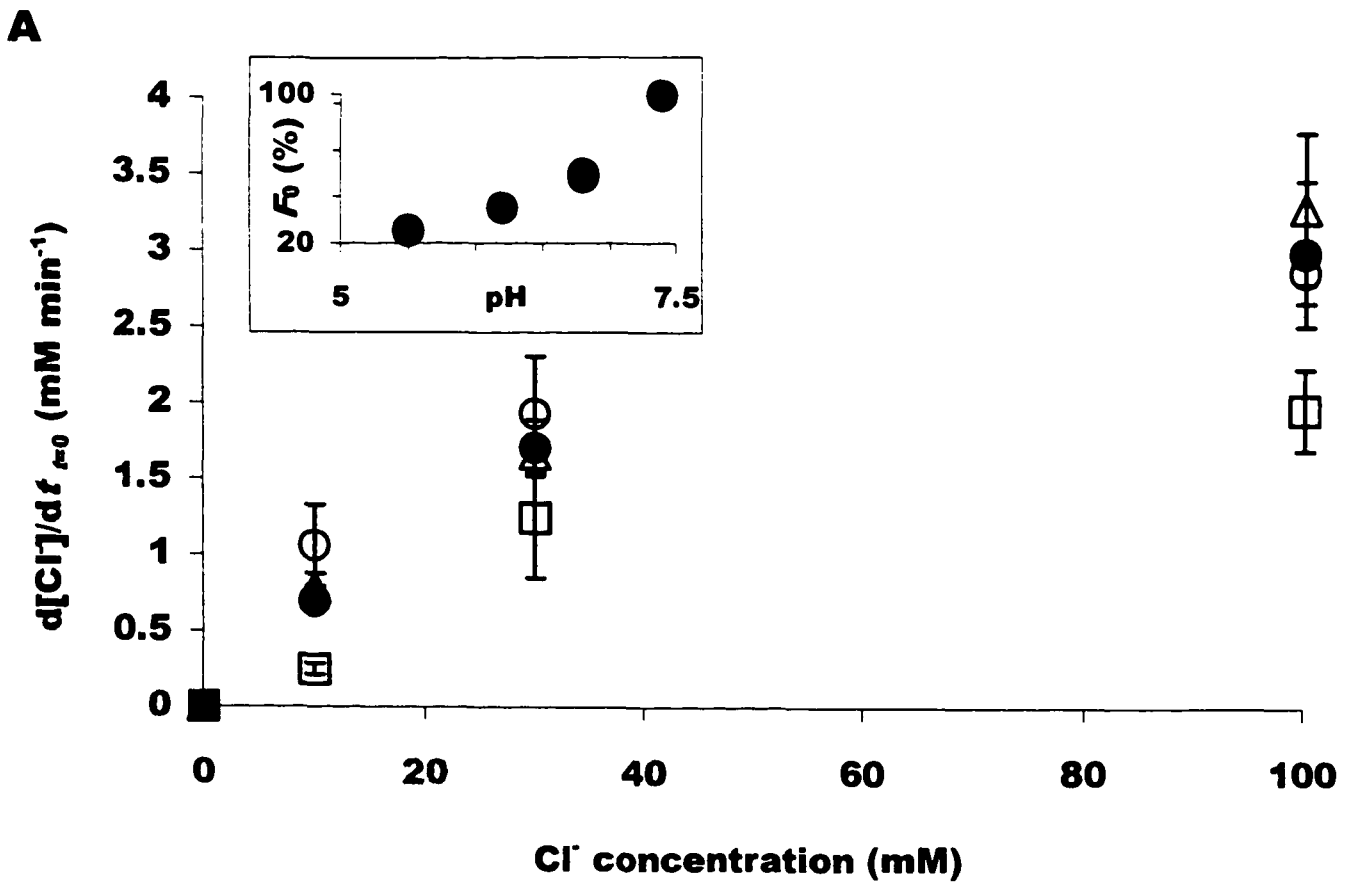


Figure 5.1. Effect of 5 mM ATP on the initial Cl^--transport rate. Lucigenin-loaded vesicles were added to assay buffer (pH 7.4) containing 50 mM Cl-BTP, 5 mM $MgSO_4$, 10 mM K_2SO_4, 5 μM valinomycin and either 5 mM Na_2SO_4, 5 mM Na_2ATP, or 5 mM Na_2ATP + 500 nM bafilomycin-A (a V-type ATPase specific inhibitor). Values are means of five measurements from two preparations; error bars are s.e.m.

containing 10 mM lucigenin, 100 mM K_2SO_4 and 10 mM Mes-BTP buffer adjusted to pH 5.5, pH 6.2, pH 6.8, or pH 7.4. Twenty µl of vesicle suspension (1 mg ml^{-1}) pre-loaded at a certain pH were then added to 500 µl of assay medium at pH 7.4, thereby imposing an inside-acidic ΔpH of 1.9, 1.2, 0.6 and 0, respectively. The initial Cl^--transport rate was measured at various Cl^- concentrations under these conditions.

This protocol, however led to a number of complications. First, the loading of the dye seemed to be impaired at lower pH. The inset in Figure 5.2.A shows that at lower pH the amount of total fluorescence in the absence of Cl^- was greatly reduced. For vesicles loaded at pH 5.5, the fluorescence signal was only about 25% of that measured at pH 7.4. This could not be due to an interaction of the buffer with dye, since it was shown in section 3.2.2.3 that with increasing protonation of the buffering ion (i.e. at lower pH) the fluorescence signal increased. It seemed rather that the amount of un-protonated lucigenin, likely to be the membrane-permeant form, was reduced at lower pH. A second complication was due to the fact that for each pH tested the Stern-Volmer constant (K_{SV}) for Cl^--dependent quenching had to be determined. This was necessary because the pH range tested was around the pK_a of the Mes buffering ion (pK_a = 6.2), which was used to allow most effective pH buffering. But as was shown in section 3.2.2.3, the Stern-Volmer constant was highly dependent on the protonation of the buffering ion (see Figure 3.6). Hence, for calculating the initial Cl^--transport rate the appropiate K_{SV}-value was used at each pH, with an external K_{SV} of 0.173 mM^{-1} for the Tricine-based assay buffer.

Figure 5.2 shows the results obtained. No differences in the initial Cl^--transport rate were observed between pH 7.4, pH 6.8 and pH 5.5 for all Cl^- concentrations tested. However, at pH 6.2 the initial Cl^--transport rate was reduced between 36% to 73% at all Cl^- concentrations tested. Due to the limited number of



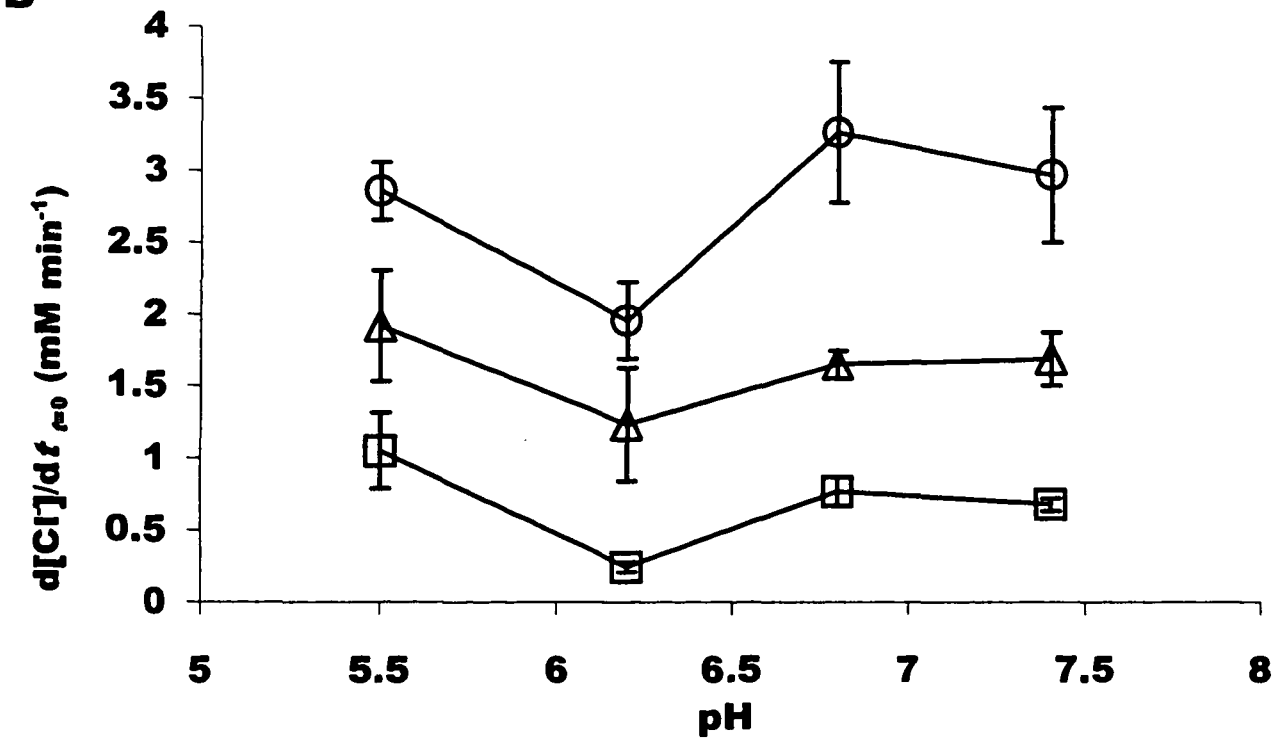


Figure 5.2. The initial Cl^--transport rate under pH-jump conditions. Vesicles were pre-incubated with 10 mM lucigenin, 50 mM K_2SO_4 and 10 Mes-BTP at pH 5.5, pH 6.2, pH 6.8, pH 7.4, for 30 min at 38°C. The initial Cl^--transport rate was then measured after adding 20 µl of the vesicle suspension (1 mg ml^{-1}) to assay buffer containing 50 mM K_2SO_4, 5 µM valinomycin and Tricine-BTP, pH 7.4. For each pH the Stern-Volmer constant for Cl^--dependent lucigenin-fluorescence quenching was determined and used to calculate the initial Cl^--transport rate accordingly ($n \geq 3$, two preparations). **A)** The initial Cl^--transport rate as a function of the external Cl^- concentration. Values for the internal pH: 7.4 (●), 6.8 (Δ), 6.2 (❑), 5.5 (○). The inset shows the fluorescence signal in the absence of Cl^- (F_0) as a function of the pH. **B)** The initial Cl^--transport rate as a function of the loading pH. Symbols for the external Cl^- concentrations: 10 mM (❑), 30 mM (Δ), 100 mM (○)

observations, this reduction was statistically significant only at 10 mM Cl^- ($P < 0.01$), while at higher Cl^- concentrations this decrease was either not, or was only weakly significant, ($P < 0.2$ at 100 mM Cl^-).

5.2.3 Forming a ΔpH using the K^+/nigericin clamp

Due to the uncertainties in the pH-jump experiments, an alternative and more reliable method of imposing a ΔpH across the vesicular membrane was employed. The K^+/H^+-exchanging ionophore nigericin was used to generate an inside-acidic pH difference. In order to establish a ΔpH, a large, opposed K^+-concentration difference was set up, i.e. high K^+ in the vesicles, low K^+ outside. In exchange for a K^+ ion exported from the vesicle, nigericin then transports a H^+ ion back into the vesicles, thereby generating an electroneutral net influx of protons.

To demonstrate the establishment of the ΔpH, the fluorescent dye quinacrine (6-chloro-9-[(4-diethylamino)-1-methylbutyl]amino-2-methoxyacridine dihydrochloride) was used. While the weak base quinacrine in its non-protonated form freely crosses the membrane, once it becomes protonated in the vesicles at lower pH its permeability is greatly reduced and it therefore accumulates in the vesicles. Self-quenching of quinacrine fluorescence upon accumulation then leads to a pH-dependent decrease in fluorescence intensity. In this way, a reduction in quinacrine fluorescence indicates the formation of an inside-acidic ΔpH. While this partitioning-based mechanism reports only pH-differences across the membrane, other dyes, such as the fluorescein-derivative BCECF (2',7'-bis-(2-carboxyethyl)-5-(6)-carboxyfluorescein) can report absolute pH values due to the fluorescence intensity being directly dependent on the protonation of the dye molecule. Since the pH dependence of quinacrine fluorescence can be reliably calibrated only for small

changes in pH (Bennett and Spanswick, 1983), BCECF to was used to estimate the magnitude of the ΔpH generated.

5.2.3.1 Validity and calibration of the K^+/nigericin clamp

Figure 5.3 shows the time course of quinacrine fluorescence during a typical experiment. The K^+-free assay buffer containing 5 µM quinacrine showed a stable fluorescence signal, which was slightly enhanced on the addition of K^+-loaded vesicles, but thereafter remained constant. The addition of 5 µM nigericin immediately started the K^+/nigericin clamp and within 50 s the fluorescence signal was reduced more than 60%. At this stage the signal stabilised again, indicating that the H^+ influx and efflux were almost equal, i.e. that the net H^+ flux was zero. Adding 20 mM K_2SO_4, which drastically reduced the K^+ gradient, immediately abolished the ΔpH.

In order to estimate the magnitude of the ΔpH the fluorescent dye BCECF was used. Unlike quinacrine, which partitions across the membrane in a pH-dependent manner, BCECF does not easily cross the membrane at pH 7.4. Various attempts to load BCECF into vesicles *via* freeze-thaw cycling and/or sonication failed to generate a detectable internal fluorescence signal. However, recent reports suggest the existence of MgATP-driven uptake of BCECF into plant vacuoles (Swanson *et al.*, 1998). Therefore, vesicles were incubated in buffer containing both BCECF and MgATP as described in Materials and Methods. After washing the vesicles twice, a considerable amount of internal BCECF fluorescence could be observed, indicating the successful loading of dye into the vesicles.

To estimate the ΔpH generated by the K^+/nigericin clamp, vesicles loaded with BCECF and 100 mM K_2SO_4 were added to K^+-free assay medium containing 5 µM

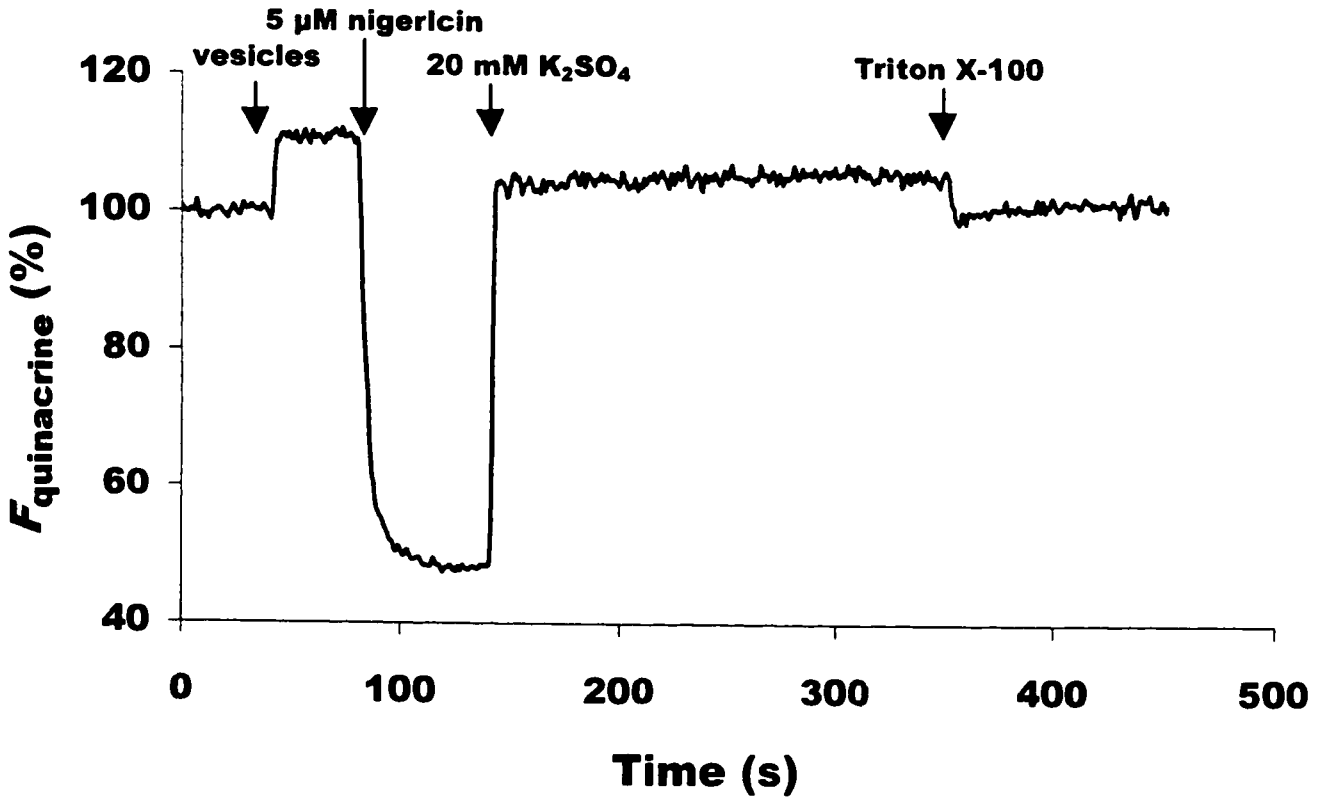


Figure 5.3. Generating an inside-acidic ΔpH using the K^+/nigericin clamp. Vesicles were pre-loaded with 100 mM K_2SO_4 and diluted 200-fold into a K^+-free assay medium containing 5 µM quinacrine to report the formation of a ΔpH (exc. 427 nm; em. 495; slits 5 nm). After addition of 5 µM nigericin (final concentration) a ΔpH was formed as indicated by the decrease in quinacrine fluorescence. The imposed gradient could be abolished by the addition of 20 mM K_2SO_4 to decrease the steep K^+ gradient. Triton X-100 was added to a final concentration of 0.03% (v/v)

nigericin (Figure 5.4). After the ΔpH was formed, the BCECF-excitation spectrum was scanned. Then KCl was added to give a final concentration of 200 mM to abolish the K^+ gradient. Under these conditions, nigericin equilibrates the external and the internal pH (Nett and Deitmer, 1996). The excitation was scanned again and the external pH measured using a pH-electrode. The pH was subsequently lowered by adding an aliquot of 1 M HCl, and the pH was measured together with another excitation scan. This step was repeated several times to obtain a calibration curve for several pH values. All scans were ratioed by dividing the fluorescence intensity by the intensity at 439 nm excitation wavelength, the pH-insensitive wavelength (Figure 5.5.A).

The values of the ratioed fluorescence intensity at the pH-sensitive excitation wavelength of 505 nm are plotted against the pH in Figure 5.5.B. The values could be fitted according to the Henderson-Hasselbalch equation, with a pK_a of 6.89 (James-Kracke, 1992; Nett and Deitmer, 1996). The pH-dependent response in the vesicles was slightly less sensitive in vesicles than in assay medium, indicating the need for an internal calibration. The internal pH generated by the K^+/nigericin clamp could be calculated using the parameters from the best fit of the calibration. In two experiments, the values for internal pH obtained were 6.24 and 6.15, with external pH values of 7.32 and 7.31, respectively. This would mean an average ΔpH of around 1.1 units. However, this is only a rough estimate, and the actual ΔpH is likely to be larger. As the trace in Figure 5.4.A shows, the BCECF fluorescence slowly increased as the ΔpH was imposed. This effect was not seen when quinacrine was used to indicate the formation of the ΔpH in a similar experiment. The increase is probably due to BCECF leaking out of the vesicles at low pH, with BCECF fluorescence increasing at the higher external pH. At low pH, the anionic groups of BCECF become increasingly

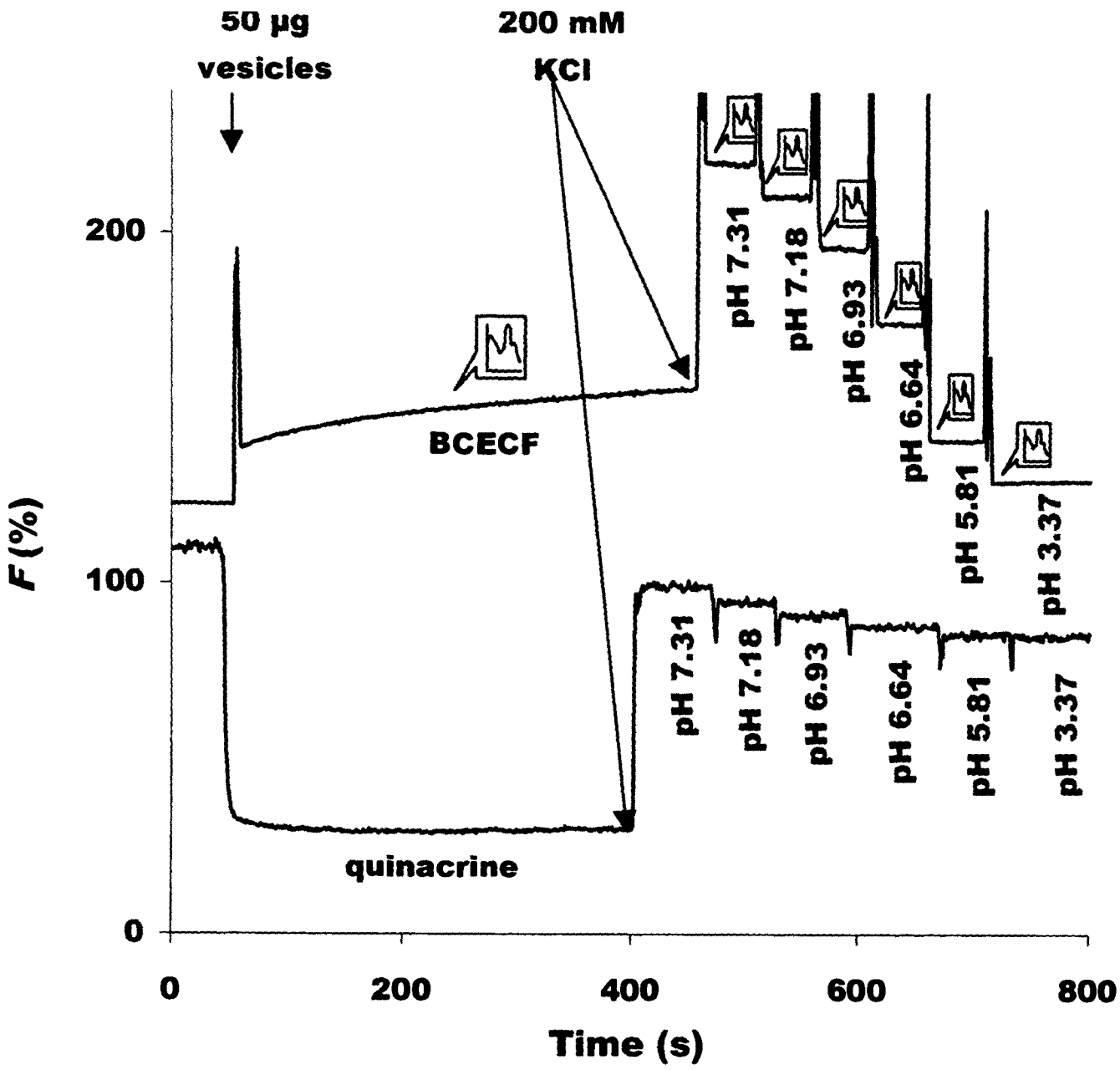
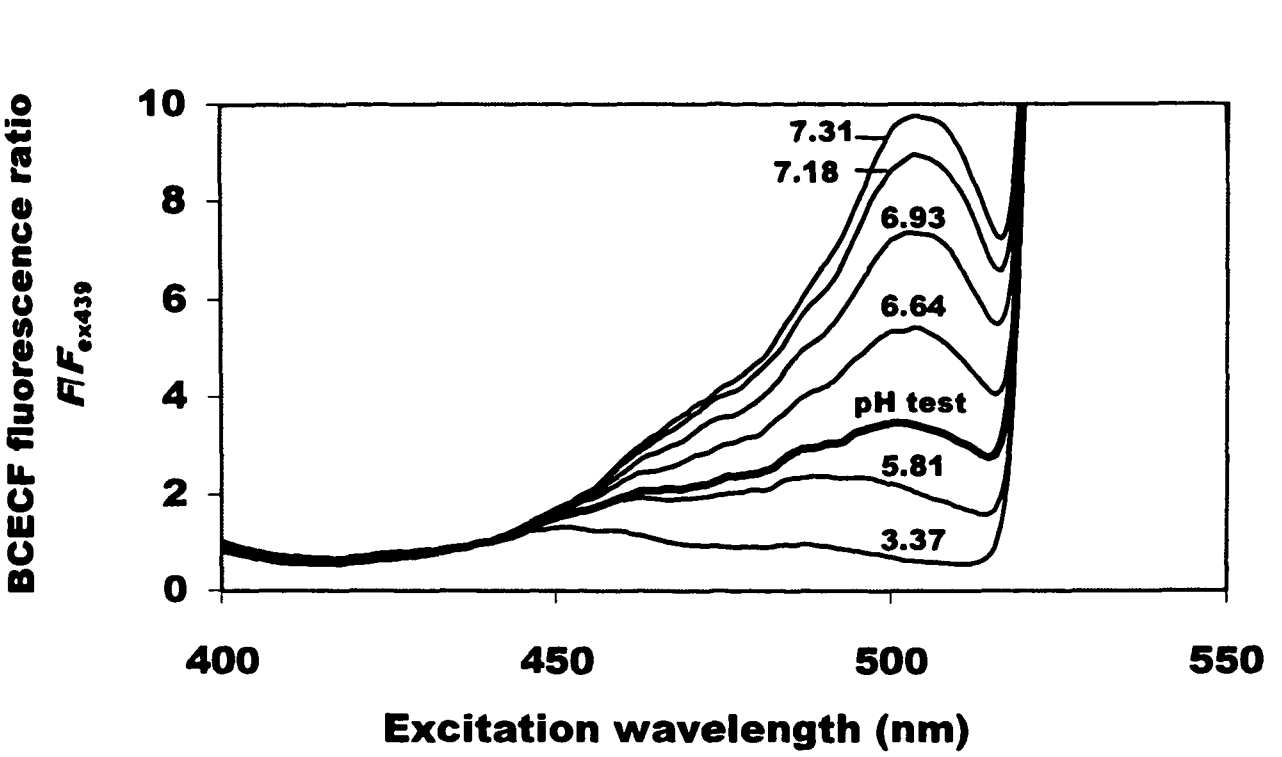


Figure 5.4. Calibrating the K^+/nigericin clamp. Vesicles loaded with BCECF and 200 mM K_2SO_4 were added to K^+-free assay medium, pH 7.4, and the BCECF fluorescence signal was recorded (exc. 505 nm, em. 535 nm, slits 10 nm). After about 400 s, 200 mM KCl (final concentration) was added to abolish the K^+ gradient. Under these conditions nigericin equilibrates the pH of the internal and the external lumen. By adding aliquots of 1N HCl the external pH was subsequently stepwise reduced. In a similar experiment using an identical protocol the BCECF excitation was scanned (em. 535 nm) at various time points shown by the symbol ( ). Immediately after each scan the pH values in the cuvette were measured with a pH-electrode. The pH values given in the figure are the means of two such experiments. The lower trace shows a similar experiment, using the vesicles from the same preparation but in buffer containing additionally 5 µM quinacrine in which the quinacrine fluorescence was recorded (exc. 427 nm, em. 495 nm, slits 5 nm). Both traces were normalised to 100%, but the upper trace was drawn with an offset for display purposes



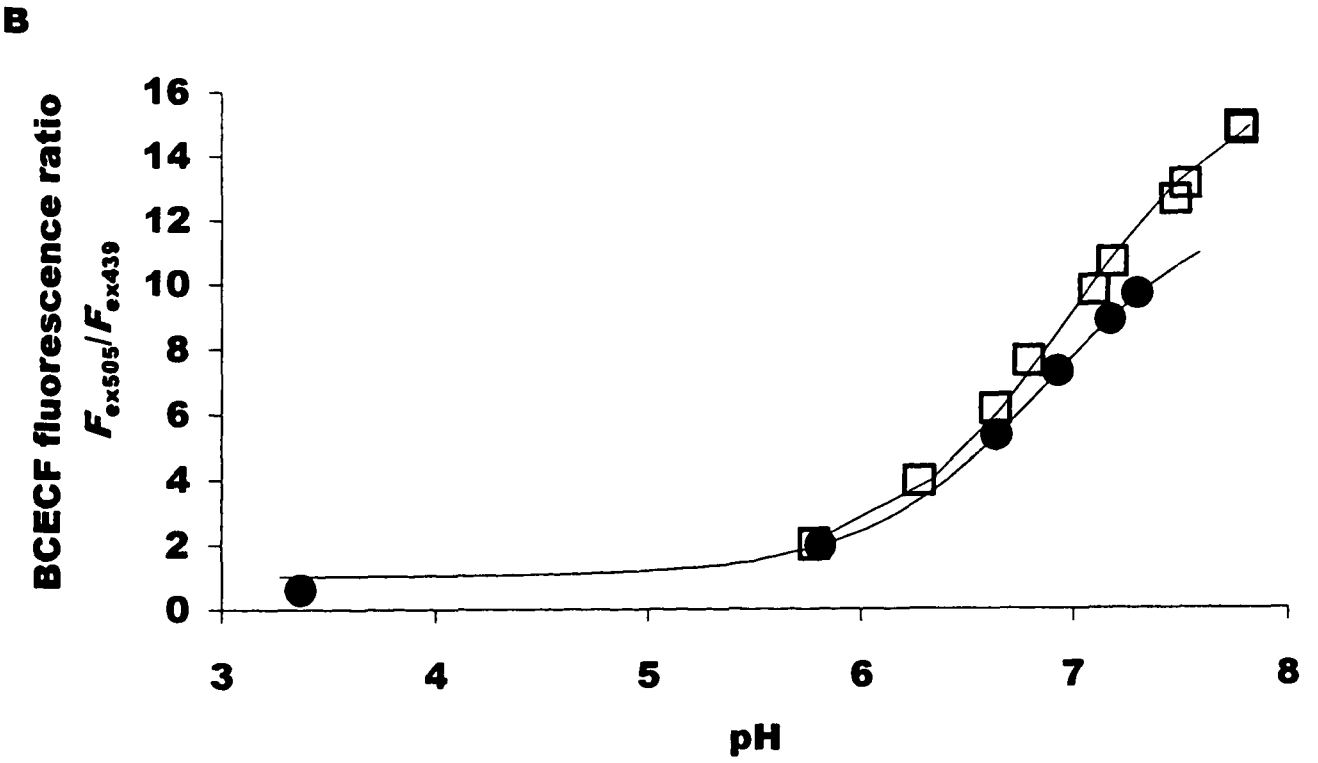


Figure 5.5. BCECF calibration curve for the K^+/nigericin clamp. **A)** Ratioed excitation scans of the BCECF fluorescence intensities (em. 535 nm). The fluorescence intensity was divided by the signal at the pH-insensitive excitation wavelength of 439 nm. Several scans were obtained as indicated in Figure 5.4, and the values indicate the pH of the external medium as determined by the pH-electrode. **B)** Plot of the ratioed BCECF-fluorescence intensity (R) at the pH-sensitive excitation wavelength 505 nm against the external pH (●). The line shows a best fit according to the function $pH = pK_a - \log((R_{max} - R)/(R - R_{min}))$, as derived from the Henderson-Hasselbalch equation, with $pK_a = 6.89$, a maximum ratio R_{max} of 12.9, and a minimum ratio R_{min} of 1.03. Also plotted is the pH response in vesicle free assay buffer only (❑; $pK_a = 6.99$, $R_{max} = 17.0$, $R_{min} = 1.13$)

protonated, thereby increasing the membrane permeability of the dye. Using the initial value of fluorescence intensity just after adding the dye gives an internal pH of 5.80, equivalent to a ΔpH of 1.5 units. With the inadequacy of BCECF to report accurately at pH values below 5.5, its increased membrane permeability below pH 6.0, and the fact that any background fluorescence contributed by external dye could not be taken into account, these experiments could only estimate minimum values for the generated ΔpH. However, they clearly demonstrated that the K^+/nigericin clamp was sufficient to generate a considerable, inside-acidic ΔpH across the vesicle membrane that was stable for several minutes at 25°C.

5.2.3.2 No dissipation of the ΔpH by Cl⁻

The ΔpH generated by the K^+/nigericin clamp was used to study the ability of externally applied Cl^- to dissipate this ΔpH. Figure 5.6.A shows several traces of quinacrine fluorescence where a ΔpH was generated (vesicles were also loaded with 20 mM SPQ). Adding 20 mM K_2SO_4 immediately abolished the imposed pH gradient, as the K^+-gradient was drastically reduced. Adding 20 mM Na-gluconate (the gluconate anion being impermeant) completely dissipated the ΔpH within less than 30 s with an exponential time course. However, adding 20 mM BTP-Cl (BTP as the impermeant cation) was not sufficient to dissipate the ΔpH. The slow increase in quinacrine fluorescence seen with time after adding Cl^- was identical when an aliquot of Cl^--free assay buffer was added as a control.

Figure 5.6 shows an identical experiment in which the fluorescence intensity of the Cl^--sensitive dye SPQ was recorded instead. SPQ was used in these experiments since its fluorescence characteristics did not overlap with those of quinacrine. The fluorescence signal remained unchanged over time after the addition of Na-gluconate.

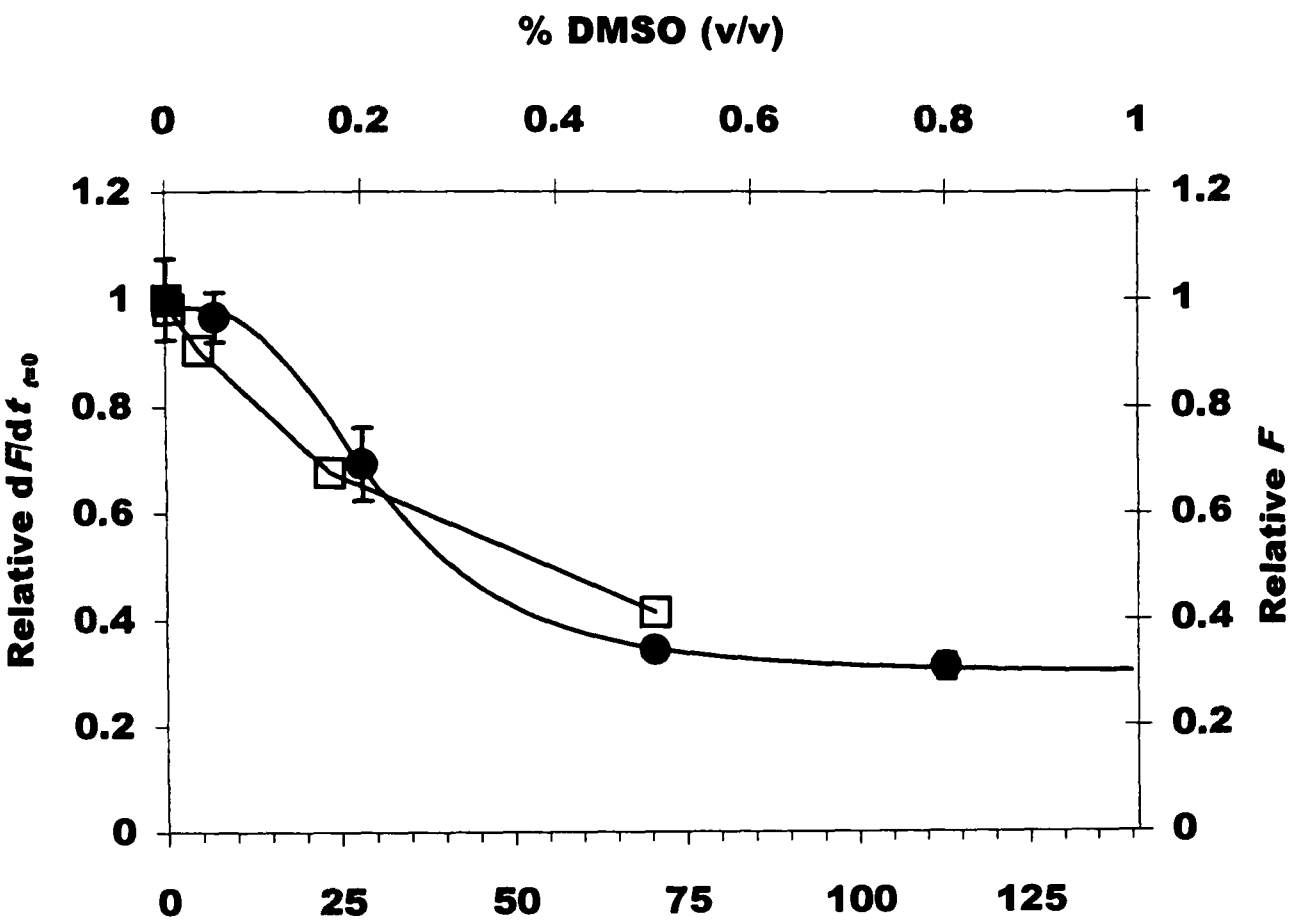
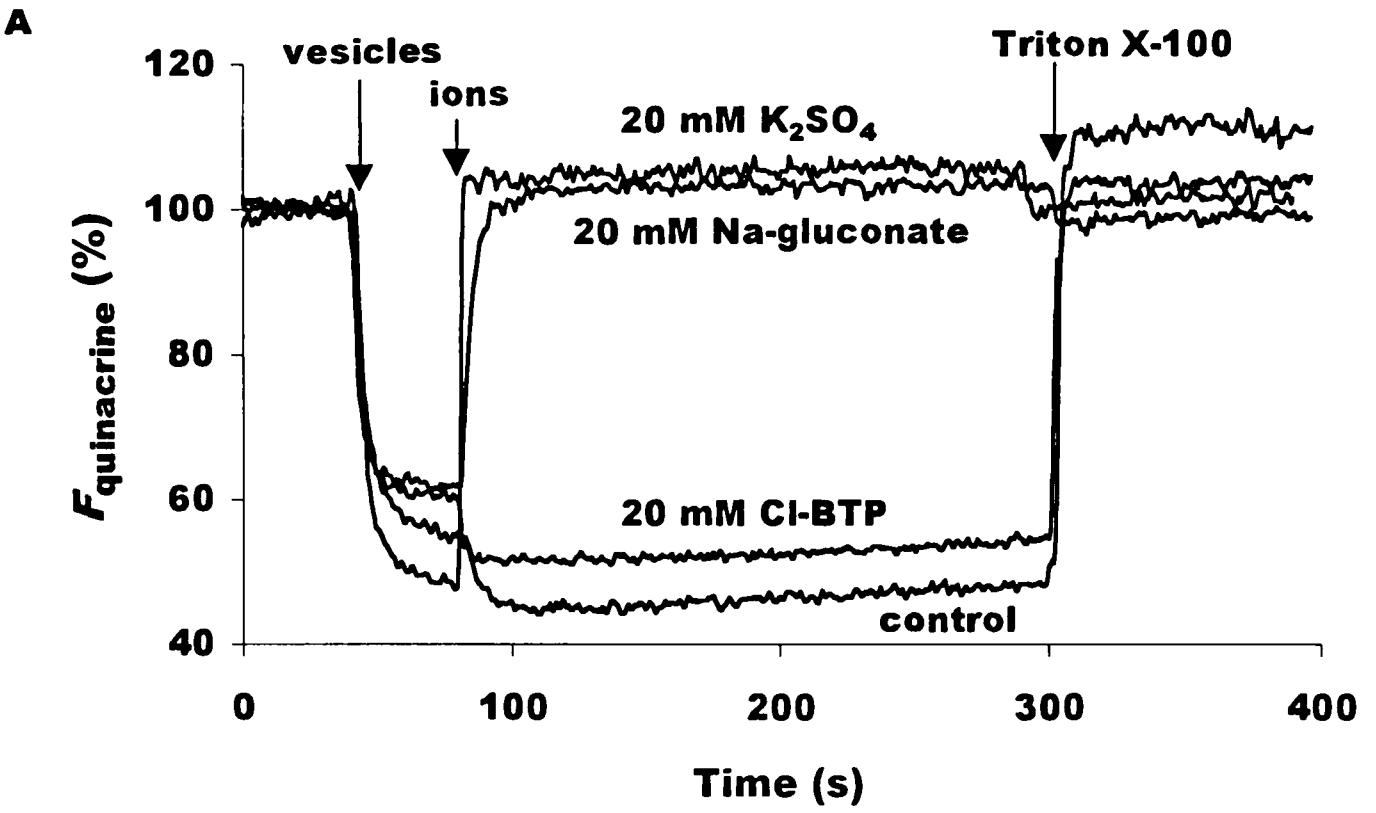


Figure 4.13. Inhibition of Cl^- influx by DMSO. The initial change in lucigenin fluorescence was measured at 50 mM Cl^- after incubating the vesicles with increasing concentrations of DMSO for 4 min (●), $n \geq 3$. The data points were fitted to the function:

$$f([DMSO]) = Min + (Max - Min) \times [DMSO]^n / ([DMSO]^n + [DMSO]_{50}{}^n),$$

with Min = 0.30; Max = 0.99; n = -3.0; $[DMSO]_{50}$ = 30.8 mM. For comparison, the quenching of lucigenin fluorescence by DMSO is plotted in the same graph (❑). Values are means of duplicate measurements



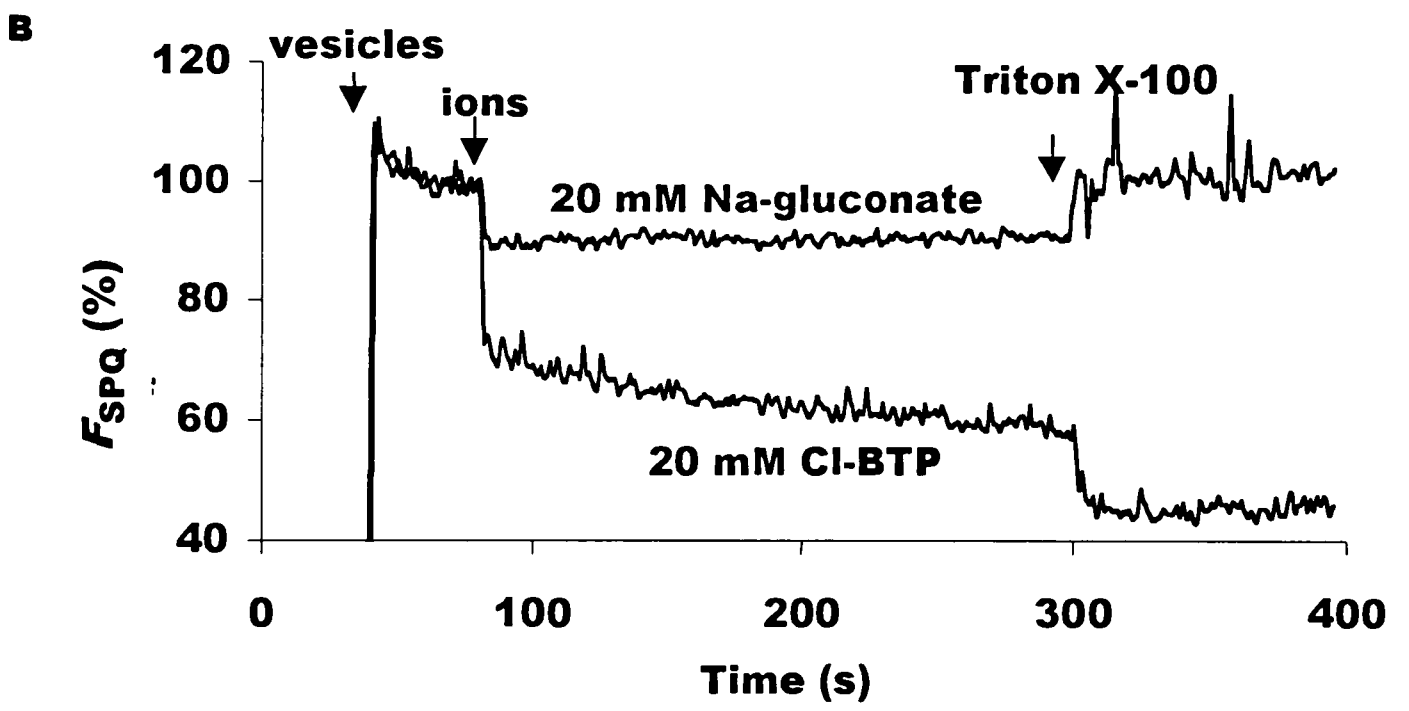
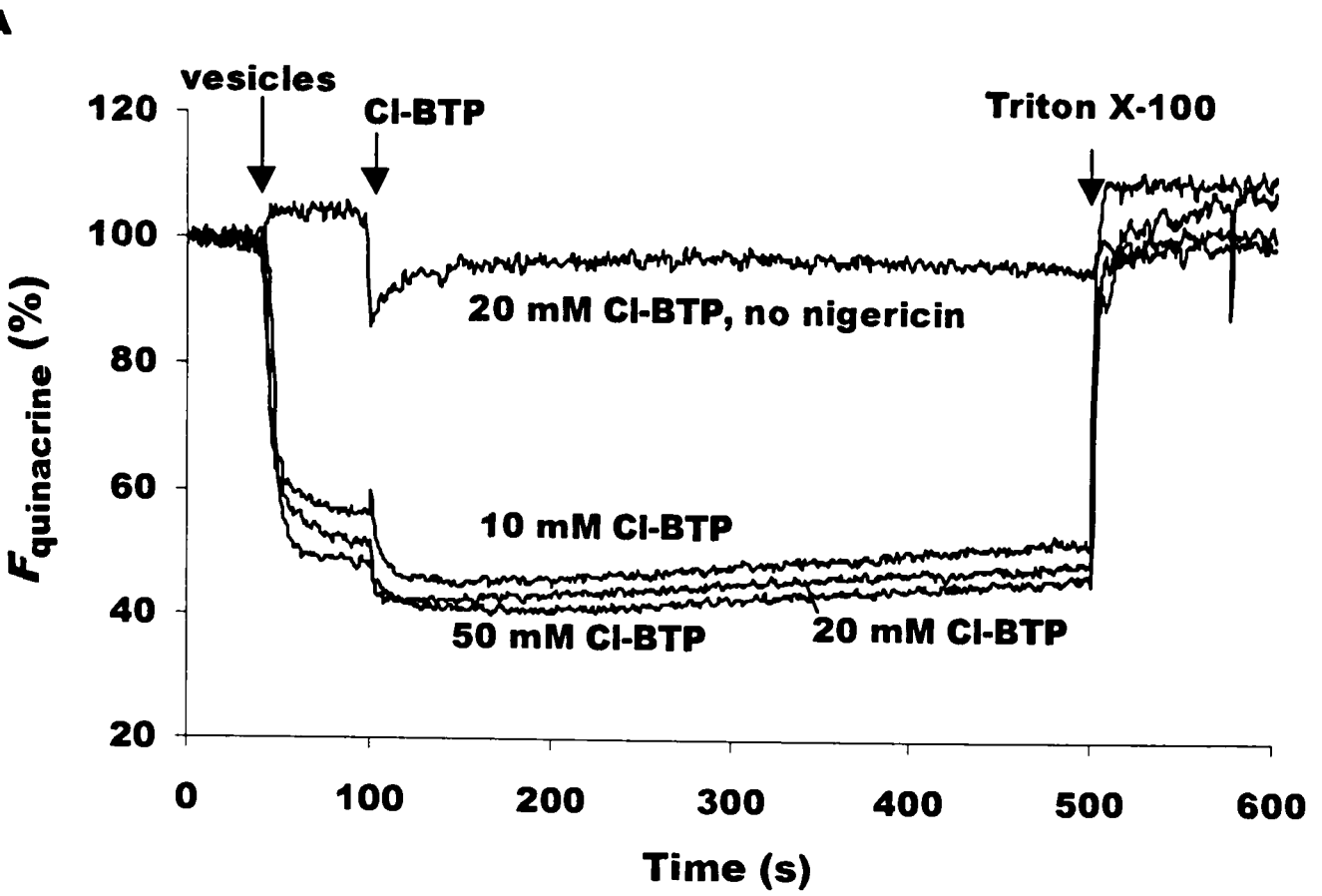


Figure 5.6. Dissipation of a ΔpH imposed by a K^+/nigericin clamp. **A)** Measuring quinacrine fluorescence to determine the formation of a ΔpH (exc. 427 nm, em. 495 nm). Vesicles (20 µg) loaded with 100 mM K_2SO_4 and 20 mM SPQ were added to assay buffer containing 5 µM nigericin, 5 µM quinacrine and no K^+. After a pH difference was established, either 20 mM BTP-Cl, 20 mM Na-gluconate, 20 mM K_2SO_4, or an aliquot of assay buffer (as a control) was added. At the end of each recording, 0.03% (v/v) Triton X-100 (final concentration) was added to disrupt the vesicles. **B)** Measuring SPQ fluorescence (exc. 350 nm, em. 440 nm) to determine Cl^- transport. Same experiment as in A), but assay buffer without quinacrine

Adding BTP-Cl instead led to a slow decrease in fluorescence intensity over time. This clearly indicated that Cl^- was still transported when a ΔpH was imposed. Figure 5.7.A shows that no dissipation of the ΔpH could be observed when adding 10 mM, 20 mM, or 50 mM BTP-Cl. This was in stark contrast to Na^+, which rapidly dissipated the ΔpH, albeit more slowly at 10 mM Na^+. Figure 5.8 shows that the dissipation of the ΔpH by Na^+ displayed saturating concentration dependence with an apparent K_m of 21 mM. At lower Na^+ concentrations the dissipation showed a bi-phasic behaviour. However, the data points varied too much to be fitted reliably. To give a rough estimate of the parameters for the kinetics at low Na^+, double Michaelis-Menten kinetics were fitted to the data, fixing one set of parameters to the values obtained above (K_m = 21 mM and V_{max} = 1.97 units). The parameters obtained for the second function indicated a apparent K_m in the order of magnitude around 0.1 mM.

5.2.3.3 Effect of ΔpH on Cl⁻ transport

To test whether the inside-acidic ΔpH had any effect on the initial Cl^--transport rate, vesicles were loaded with 100 mM K_2SO_4 and 10 mM lucigenin. The vesicles were then added to K^+-free medium containing 5 µM nigericin to impose a ΔpH and the lucigenin fluorescence was recorded. As a control experiment, buffer without nigericin was used. In the absence of Cl^-, the fluorescence did not show any time-dependent changes, neither with nor without nigericin (Figure 5.9.A). This indicated that the ΔpH did not have any direct effect on lucigenin fluorescence. With 50 mM Cl^- present in the assay medium the lucigenin fluorescence showed a time-dependent decrease in intensity, indicating uptake of Cl^-. Figure 5.9.A shows that the decrease was considerably steeper in the absence of nigericin than with 5 µM nigericin present



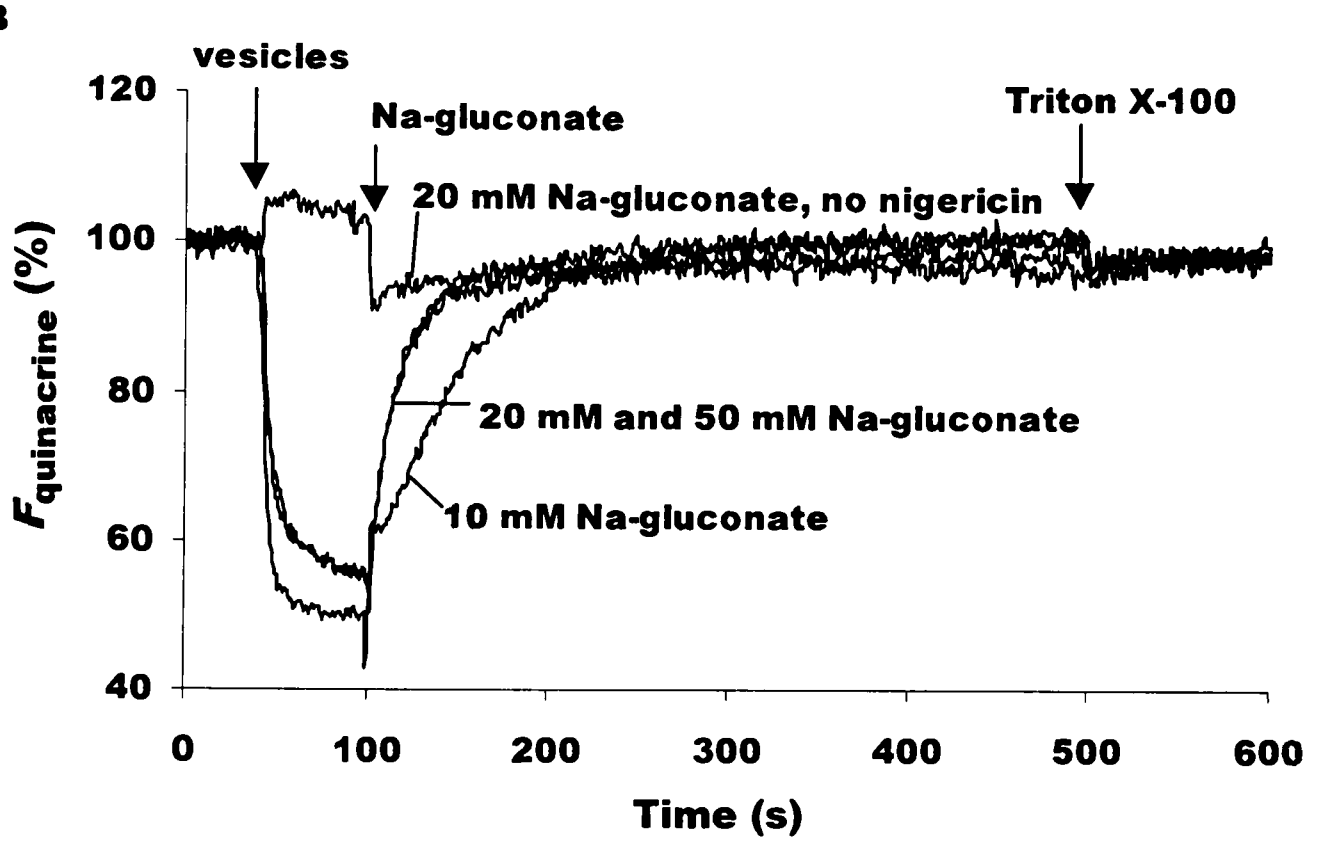


Figure 5.7. Dissipation of ΔpH by Cl^- and Na^+. Twenty μg of vesicles loaded with 100 mM K_2SO_4 were diluted 200-fold into K^+-free assay media containing 5 μM quinacrine and either zero or 5 μM nigericin, as indicated. After a ΔpH was established increasing amounts of BTP-Cl or Na-gluconate were added to test for dissipation of ΔpH. **A**) The time course of quinacrine fluorescence (exc. 427 nm, em. 495 nm) when adding BTP-Cl (pH 7.4), to final concentrations as indicated. **B**) Time course of quinacrine fluorescence when adding Na-gluconate (pH 7.4), to final concentrations as indicated

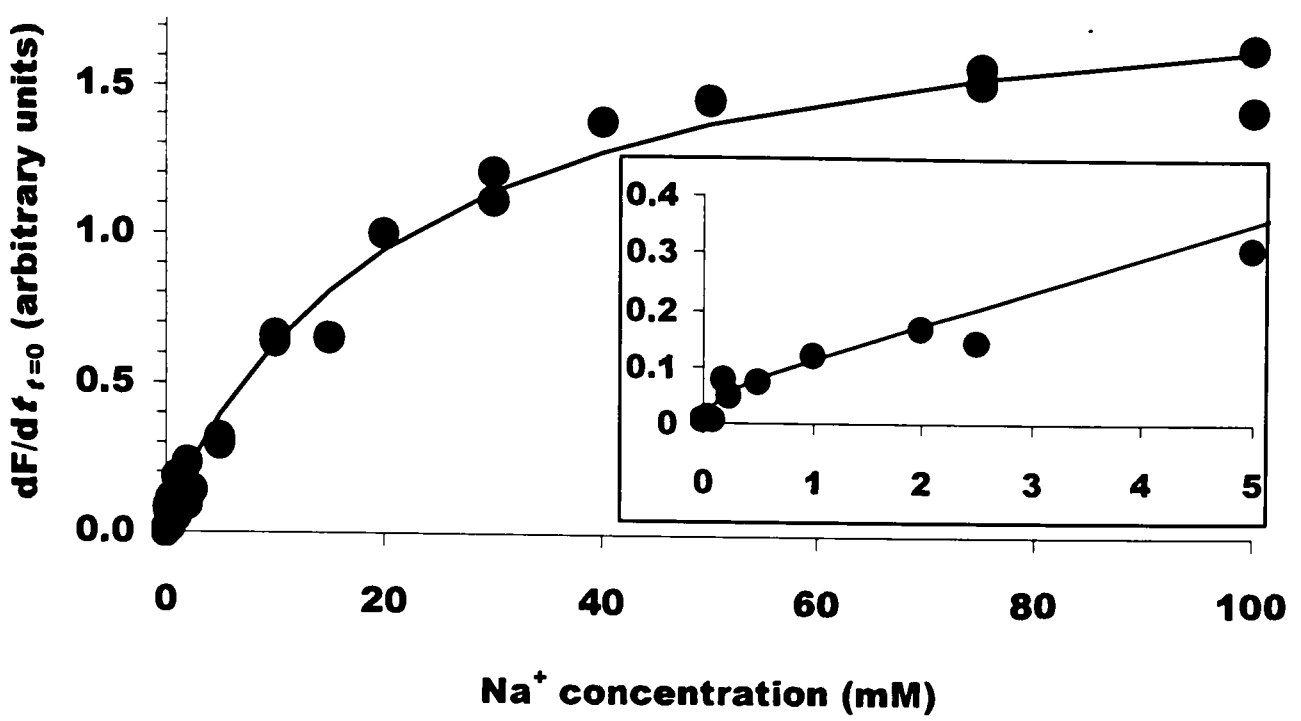
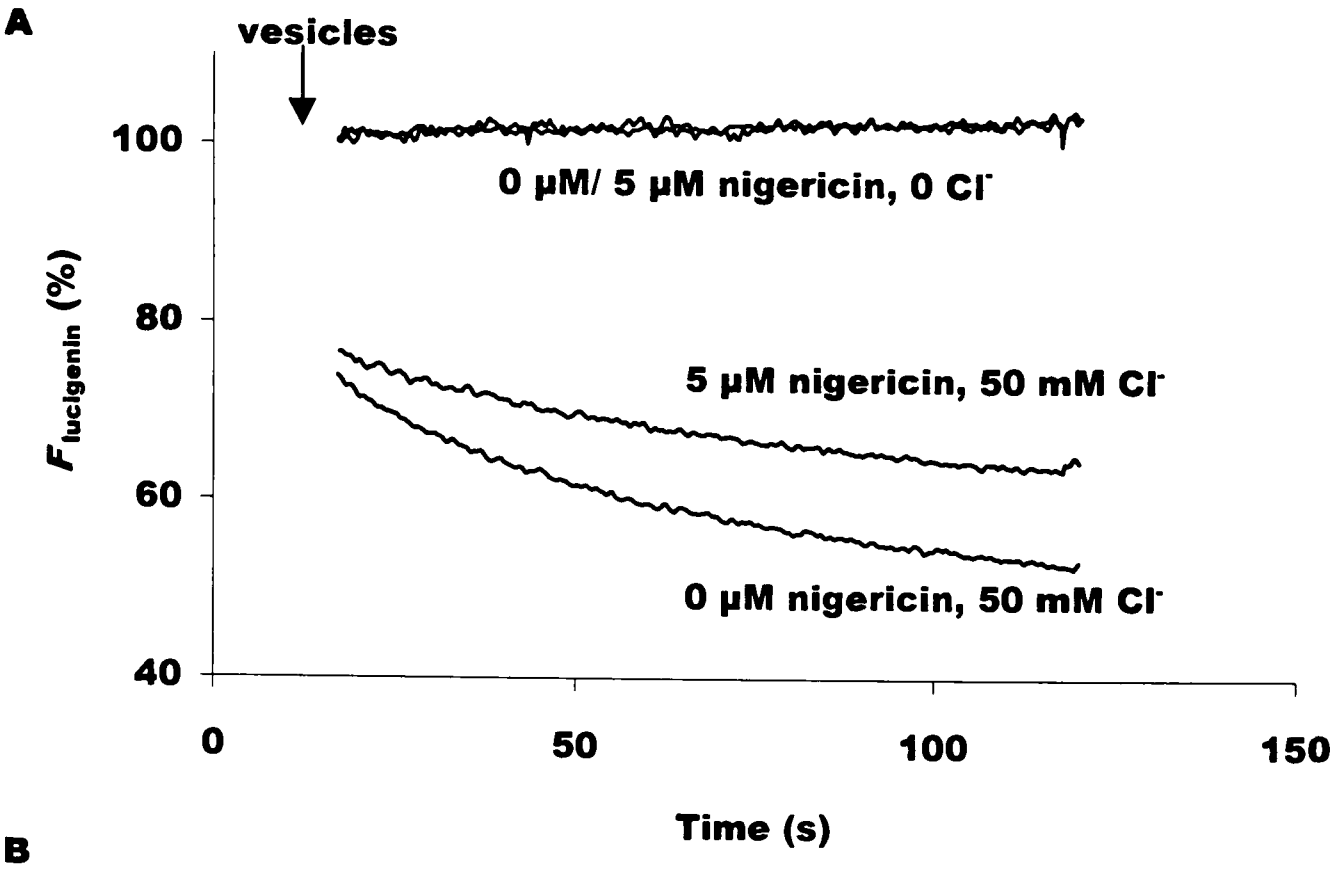


Figure 5.8. Concentration dependence of the ΔpH dissipation by Na^+. The initial change in quinacrine fluorescence $dF/dt_{t=0}$ was measured after addition of various amounts of Na-gluconate (see Figure 5.7.B). Data from three separate experiments, with change rates at 20 mM Na^+ set to unity. The line shows a best fit Michaelis-Menten curve for the combined data (K_m = 21 mM, V_{max} = 1.97 units).

The inset shows the mean values for the lower Na^+-concentration range on a larger scale. The lines indicate a best fit for double Michaelis-Menten kinetics, with the fixed parameters $K_{m,1}$ = 21 mM and $V_{max,1}$ = 1.97 units as obtained previously. The parameters obtained were $K_{m,2}$ = 0.093 mM and $V_{max,2}$ = 0.061 units. This values were only rough estimates since the fitting was unreliable due to the high variation of the data at lower Na^+ concentrations.



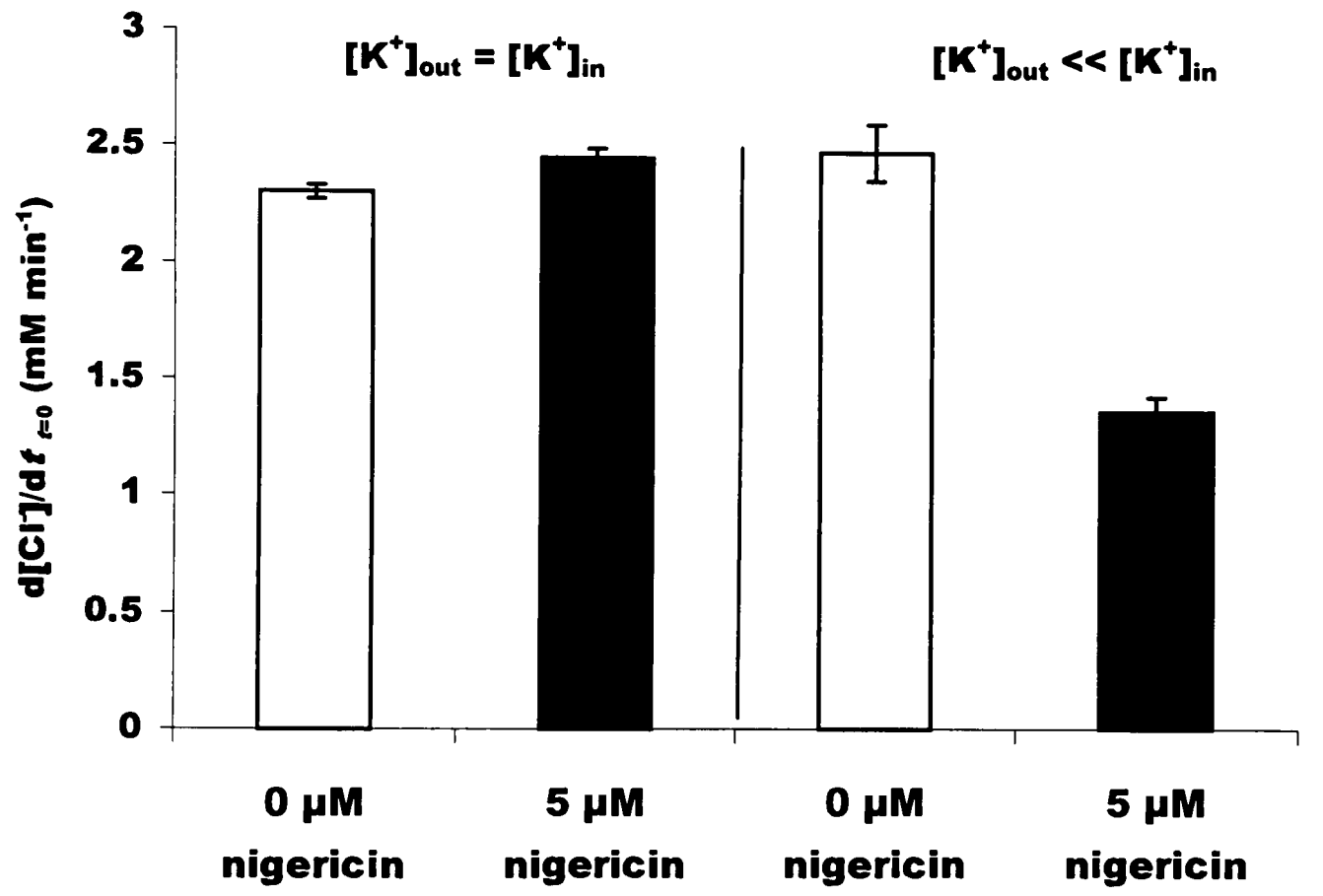


Figure 5.9. Effect of a K^+/nigericin imposed ΔpH on the initial Cl^--transport rate. **A)** Vesicles (20 µg) loaded with 10 mM lucigenin and 100 mM K_2SO_4 were diluted 200-fold into assay media containing 0 mM and 50 mM BTP-Cl, respectively, and either 0 µM or 5 µM nigericin. Time course of lucigenin fluorescence was recorded (exc. 433 nm, em. 506 nm). **B)** Data from several experiments, either in the absence of a K^+-gradient ($[K^+]_{in} = [K^+]_{out} = 200$ mM; $n = 6$) or with a K^+-gradient ($[K^+]_{in}/[K^+]_{out} = 200$; $n \geq 9$, 2 preparations). The initial Cl^--transport rate was determined at 50 mM Cl^- in all experiments

in the medium. Accordingly, the calculated initial Cl^--transport rate was significantly reduced by 45% ($P < 0.0001$) under the imposition of a ΔpH.

To test whether this decrease in initial Cl^--transport rate was due to a direct inhibition by nigericin, a similar experiment was conducted in the absence of a K^+-gradient, i.e. with 100 mM K_2SO_4 on both sides of the vesicle membrane (Figure 5.9.B). In this case, the initial Cl^--transport rate showed a slight increase of 6.5% in the presence of 5 µM nigericin ($P = 0.6$). This shows that nigericin itself has no inhibitory effect on Cl^- transport but that it is rather the inside-acidic ΔpH which reduces the initial Cl^--transport rate of the vesicles.

5.2.4 Energising vesicles using vacuolar H^+-ATPase pump activity

As a third way of energising vesicles with a ΔpH, the H^+-pump activity of the endogenous V-type ATPase was used to acidify the vesicle interior. This method had been successfully employed in an earlier study to characterise the Na^+/H^+ antiporter in tonoplast vesicles of *M. crystallinum* (Barkla *et al.*, 1995). In accordance with this earlier study, Figure 5.10 shows that 50 mM Na-gluconate could dissipate a ΔpH generated by the V-type ATPase due to the vacuolar Na^+/H^+ antiport activity found in *M. crystallinum*. However, the fact that the V-type H^+-ATPase activity is strongly dependent on the presence of cytosolic Cl^- complicates the use of the pump in this type of experiment studying Cl^- transport (Ratajczak *et al.*, 1994; Lüttge and Ratajczak, 1997). Alternative attempts to energise the vesicles with the vacuolar H^+-PPase (Kaestner and Sze, 1987; Pope and Leigh, 1987) failed since no PPase activity could be detected in the vesicle preparation (data not shown), which is in accordance with a previous study showing that H^+-PPase activity is drastically down regulated in older *M. crystallinum* plants (Bremberger and Lüttge, 1992).

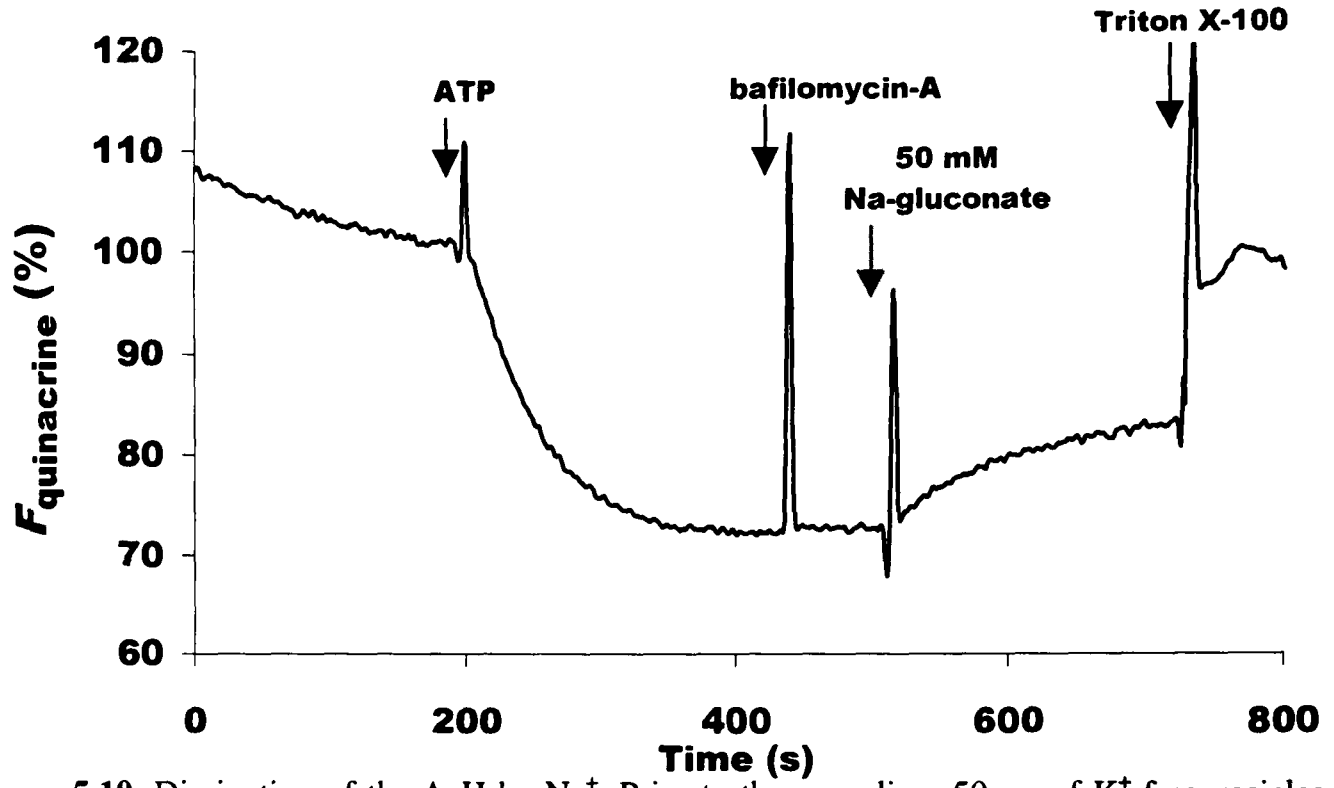


Figure 5.10. Dissipation of the ΔpH by Na^+. Prior to the recording, 50 µg of K^+-free vesicles were added to the assay medium containing 5 mM $MgSO_4$ and 5 µM quinacrine to record the formation of a ΔpH (exc. 427, em. 495 nm). Additions (final concentrations): 3 mM Na_2ATP to start H^+-pumping; 200 nM bafilomycin-A to specifically inhibit the V-type H^+-ATPase; 50 mM Na-gluconate (pH 7.4); 0.015% (v/v) Triton X-100 to disrupt the vesicle membrane

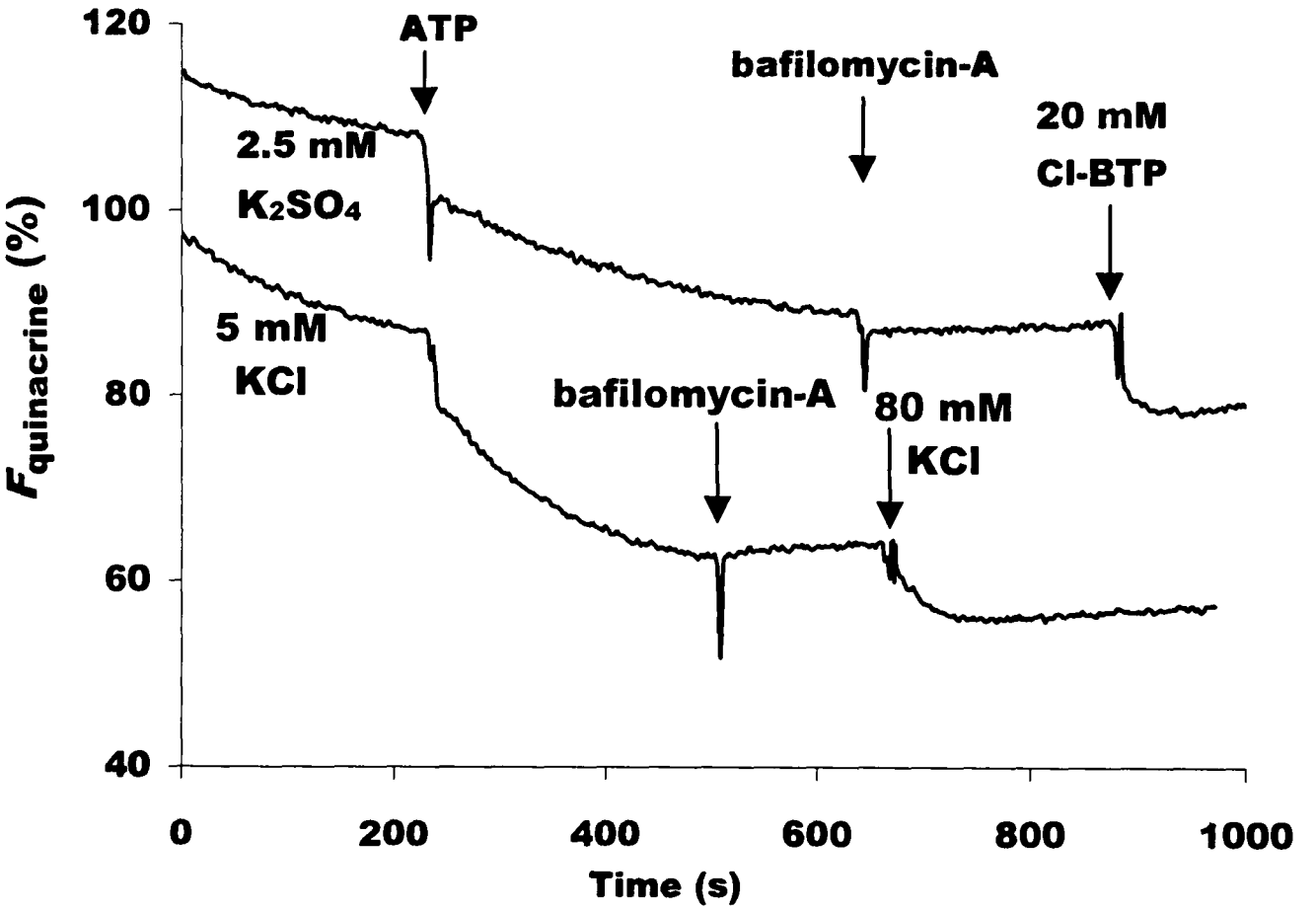
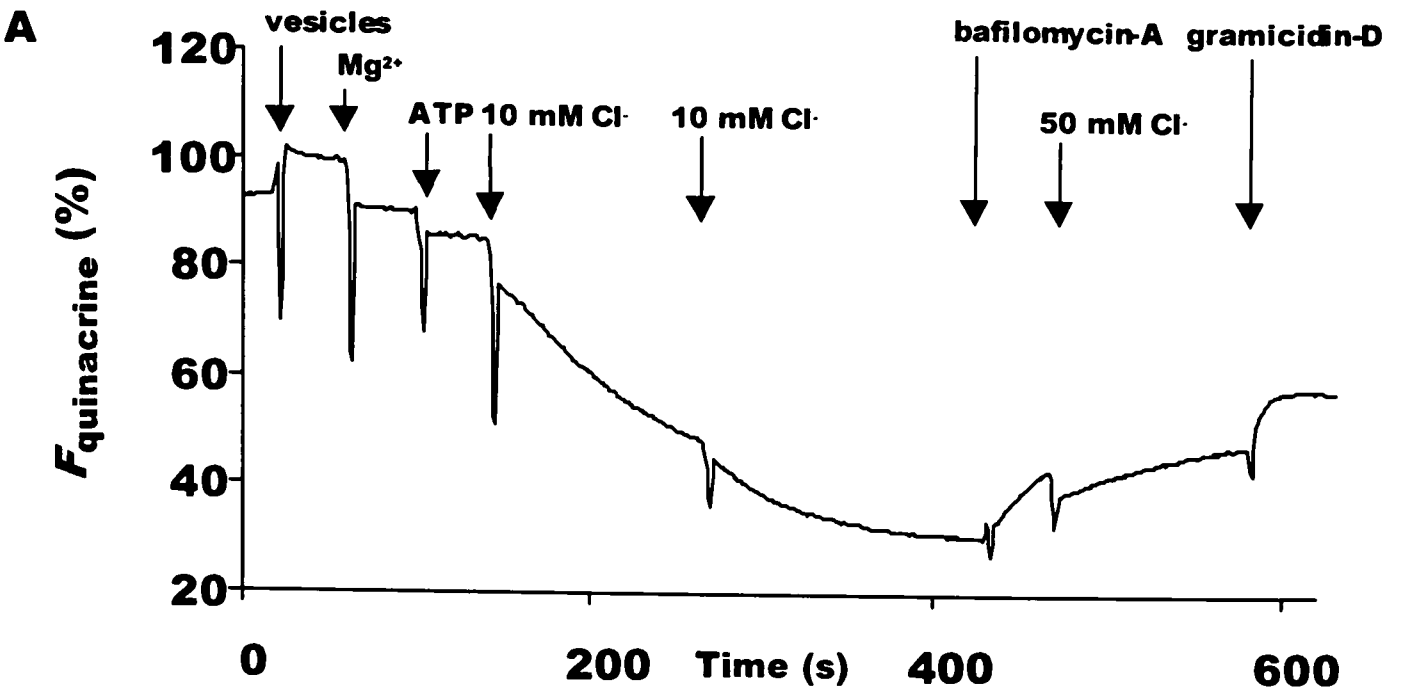


Figure 5.11. Generating a ΔpH using the vacuolar H^+-ATPase. 50 µg of vesicles loaded with 2.5 mM K_2SO_4 were added to assay medium with 5 µM quinacrine, 5 µM valinomycin, 5 mM $MgSO_4$ and either 2.5 mM K_2SO_4 or 5 mM KCl. After addition of vesicles, the time course of quinacrine fluorescence was recorded (exc. 427 nm, em. 495 nm). Additions during the recordings: 3 mM Na_2ATP to start H^+-pumping, 5 µM bafilomycin-A to specifically inhibit the V-type H^+-ATPase, and 20 mM BTP-Cl or 80 mM KCl to test for ΔpH dissipation (lower trace with -20 % offset for display purposes)

Figure 5.11 shows traces of quinacrine fluorescence during activation of the H^+-ATPase. The buffer and the vesicles both contained 5 mM K^+ and 5 µM valinomycin but no Cl^-. Addition of 3 mM ATP led only to a small decrease of quinacrine fluorescence with time, indicating only low (but measurable) H^+-pump activity. In buffer with 5 mM KCl, the H^+-pump activity was significantly enhanced, but was still not very high. The presence of the K^+/valinomycin clamp should prevent the build-up of an inside-positive membrane potential, which would reduce the H^+-pump capacity. In both cases, the addition of Cl^- did not lead to a recovery of quinacrine fluorescence after the V-type ATPase was specifically inhibited by bafilomycin-A.

Similarly, Figure 5.12.A shows that adding ATP to the vesicles in a K^+-free system did not lead to any quenching of quinacrine fluorescence. Only the addition of 10 mM BTP-Cl led to a steady decrease in quinacrine fluorescence, which could be slightly enhanced by adding a further 10 mM BTP-Cl. Bafilomycin-A led to the start of a recovery of quinacrine fluorescence, which was slowed down by adding a further 50 mM BTP-Cl. The remaining ΔpH could be abolished by finally adding 2 µg of the ionophore gramicidin-D. As Figure 5.12.B shows, only the addition of 50 mM BTP-Cl led to a steep quenching of quinacrine fluorescence after adding ATP. The recovery of quinacrine fluorescence after addition of bafilomycin-A was slightly reduced when further 50 mM Cl^- was added.

When vesicles were loaded with 25 mM K_2SO_4 and added to K^+-free medium, H^+-pump activity was observed already prior to the addition of valinomycin or Cl^- (Figure 5.13). But any ΔpH still present after adding bafilomycin-A could not be dissipated by Cl^-. This approach of using a steep outward-directed K^+-gradient was taken further by loading the vesicles with 100 mM K_2SO_4 and using a K^+-free assay



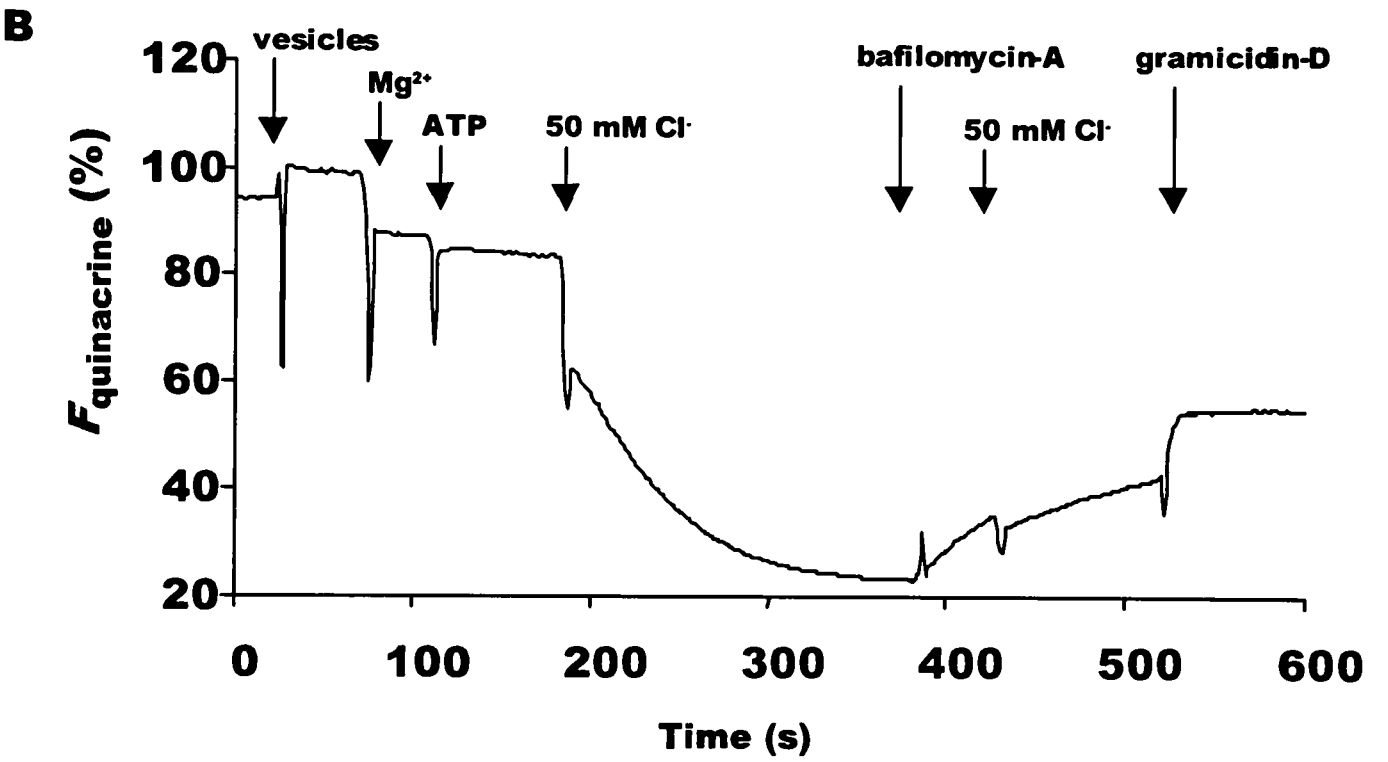


Figure 5.12. Cl^- dependence of the vacuolar ATPase H^+-pump activity in the absence of charge-balancing ions. Thirty µg of K^+-free vesicles were added to K^+-free assay buffer containing 5 µM quinacrine to record the formation of a ΔpH (exc. 427 nm, em. 495 nm). **A**) Stimulation by addition of two times 10 mM BTP-Cl, **B**) Stimulation by 50 mM BTP-Cl. Additions (final concentrations): 5 mM $MgSO_4$; 3 mM Na_2ATP to start H^+-pumping; Cl^- was added as BTP-Cl, pH 7.4, as indicated in part A) and B); 4 µM bafilomycin-A to specifically inhibit the V-type H^+-ATPase; 2 µg of gramicidin-D to abolish any remaining ΔpH

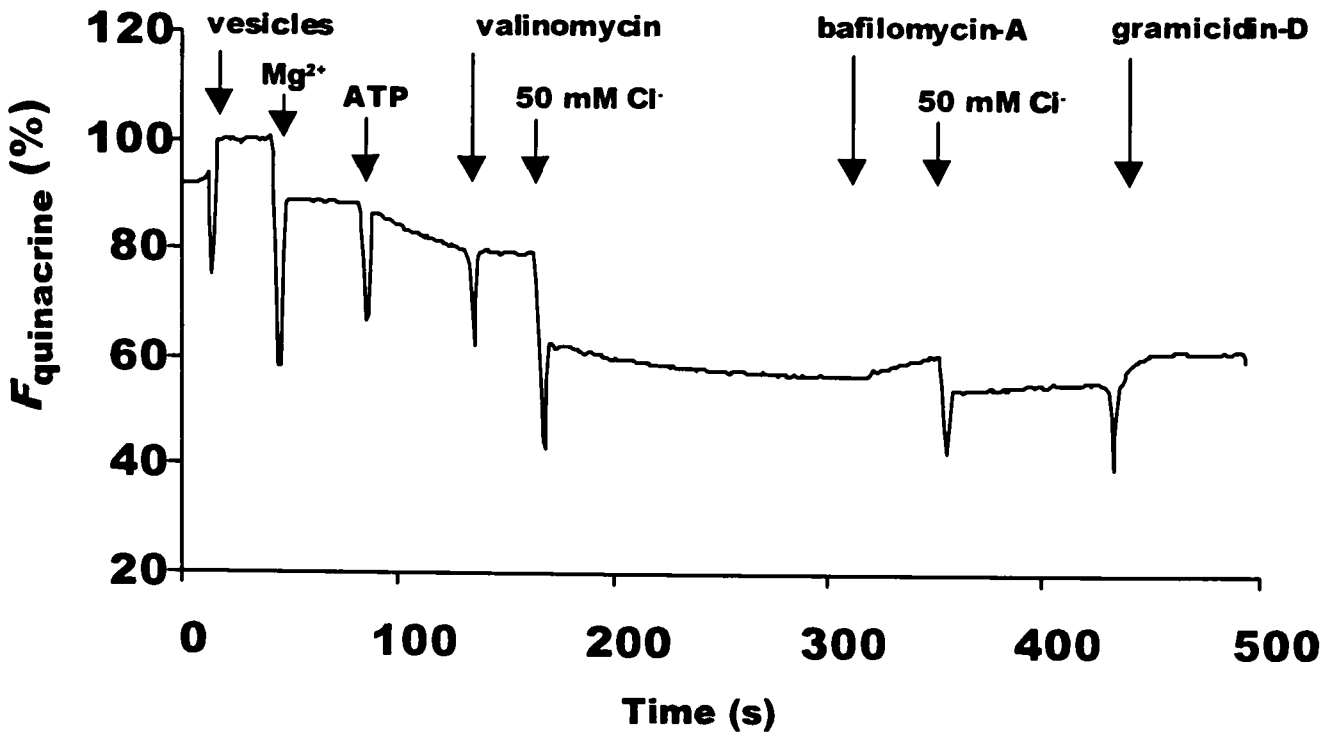


Figure 5.13. Cl^- dependence of the vacuolar ATPase H^+-pump in the presence of an inside-negative membrane potential. Fifty µg of 25 mM K_2SO_4-loaded vesicles were added to K^+-free assay buffer containing 5 µM quinacrine to record the formation of a ΔpH (exc. 427 nm, em. 495 nm). Additions (final concentrations): 10 mM $MgSO_4$; 3 mM Na_2ATP to start H^+-pumping; 5 µM valinomycin to increase K^+-specific permeability of the membrane; Cl^- was added as BTP-Cl, pH 7.4; 20 µM bafilomycin-A to specifically inhibit the V-type H^+-ATPase; 2 µg of gramicidin-D to abolish any remaining ΔpH

Figure 5.14. Stimulation of the ATPase H^+-pump activity in the absence of Cl^- by a steep outward-directed K^+-gradient. Initially, 150 µg of 100 mM K_2SO_4-loaded vesicles were added to K^+-free assay buffer containing 5 µM quinacrine to record the formation of a ΔpH (exc. 427 nm, em. 495 nm). Additions (final concentrations): 5 mM $MgSO_4$; 3 mM Na_2ATP to start H^+-pumping; 20 µM bafilomycin-A to specifically inhibit the V-type H^+-ATPase; 50 mM Cl^- was added as BTP-Cl, pH 7.4, to test for the dissipation of the ΔpH; 2 µg of gramicidin-D to abolish any remaining ΔpH

buffer (Figure 5.14). Under these conditions, a rapid quinacrine quenching was observed after the addition of $MgSO_4$ and ATP alone in the absence of any Cl^-. However, even under these conditions, no dissipation of the ΔpH by Cl^- could be observed; in fact, the rate of bafilomycin-A induced fluorescence recovery seemed to be slightly reduced after Cl^- was added. It is interesting that under these conditions the V-type H^+-ATPase shows maximum activity, since the addition of 15 mM KCl did not lead to any further stimulation of the activity (Figure 5.15).

The inside-acidic ΔpH that was generated in this way was estimated to be at least 0.82 units, using BCECF-loaded vesicles in a similar way to the method described in section 5.2.3.1 (Figure 5.15).

Despite the technical difficulties in using the V-type ATPase to energise the vesicles in this type of experiment, these results have shown that Cl^- could not dissipate the imposed ΔpH under any circumstances, under conditions where Na^+ mediated dissipation could be shown.

5.3 Discussion

As these experiments have clearly shown, there is no evidence for a direct energisation of the Cl^- uptake by ATP into tonoplast vesicles of *Mesembryanthemum crystallinum* . The slight stimulation of the initial Cl^--transport rate that was observed in the presence of ATP seemed rather be due to activity of the V-type ATPase, since no stimulation was observed in the presence of bafilomycin-A, a potent inhibitor of this enzyme (Lüttge and Ratajczak, 1997). The stimulatory effect might be due to the generation of a small inside-positive $\Delta\psi$ by the ATPase. Although the membrane potential was nominally clamped to 0 mV by the K^+/valinomycin clamp, the high activity of the V-type H^+-ATPase in the presence of Cl^- might be sufficient initially to

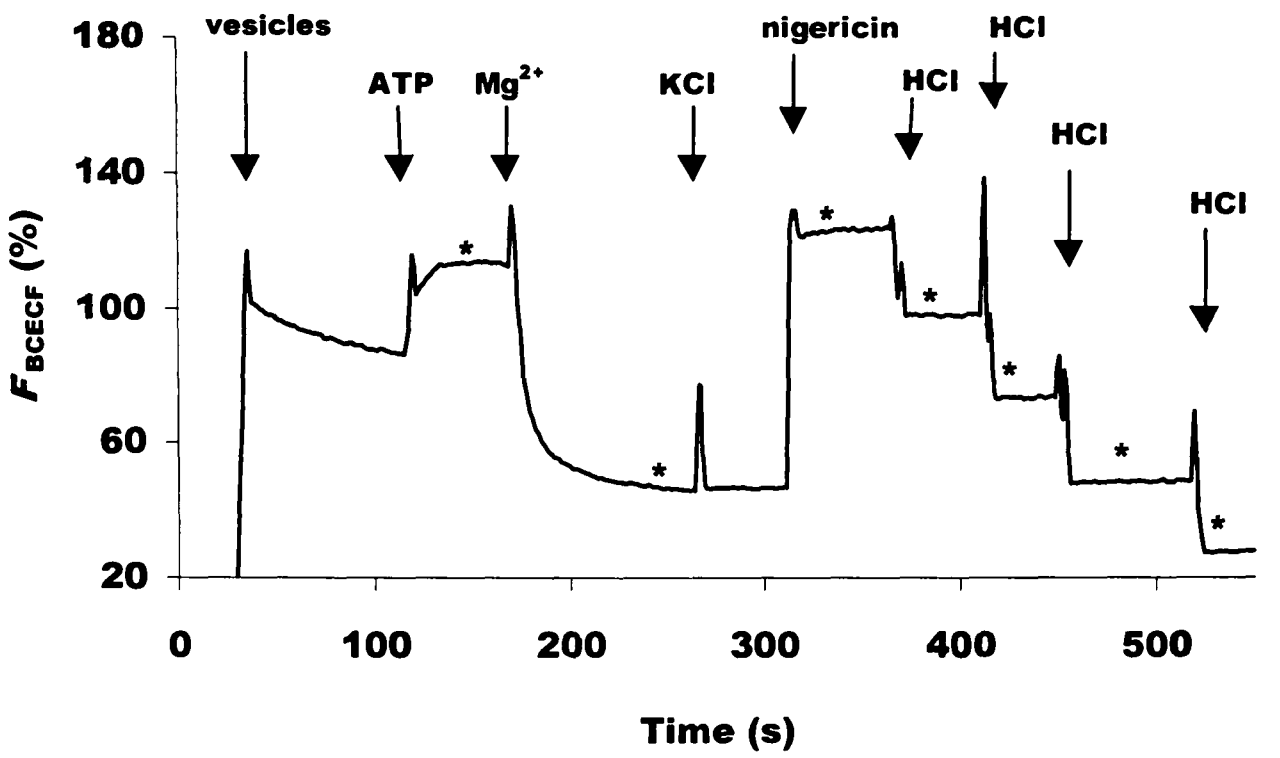


Figure 5.15. Estimating the ΔpH generated by the ATPase H^+-pump activity in the absence of Cl^- with a steep outward directed K^+-gradient using BCECF. Sixty µg of 100 mM K_2SO_4 and BCECF-loaded vesicles were added to K^+-free assay buffer (BCECF fluorescence recorded with exc. 427 nm, em. 495 nm). Additions (final concentrations): 5 mM $MgSO_4$; 3 mM Na_2ATP to start H^+-pumping; 15 mM KCl and 5 µM nigericin to equilibrate internal and external pH; 5 mM HCl was added repeatedly to decrease the pH. An identical experiment was performed and excitation scans taken at time points indicated by the asterisks to allow the internal calibration of the intravesicular pH

generate a small inside-positive membrane potential. While the K^+ permeability should by far exceed the membrane-permeabilities of the other ions, and thereby dominate the membrane potential, other ion fluxes can still lead to small shifts of the absolute membrane potential away from the Nernst potential for K^+ (as was seen in section 4.2.2.1).

Furthermore, no evidence was found in these experiments that external Cl^- can dissipate an inside-acidic ΔpH in *M. crystallinum* tonoplast vesicles, as would be expected if Cl^- uptake were coupled to H^+ efflux. This is in contrast with the uptake of Na^+ in *M. crystallinum* tonoplast vesicles (Figure 4.10) which could be shown to be energised by the inside-acidic ΔpH generated by the H^+-pump activity of the V-type H^+-ATPase (Barkla *et al.*, 1995). The existence of this Na^+/H^+-antiport could also be demonstrated by the dissipation of the K^+/nigericin generated ΔpH (Figure 5.8) which showed saturation-type kinetics similar to those observed by Barkla *et al.* (1995). It should be noted that the rates of quinacrine-fluorescence recovery observed in this study were generally much higher than those observed by Barkla *et al.* (1995). This might be due to the fact that Na^+ can also be transported by nigericin (Lutz *et al.*, 1970), thereby leading to a faster dissipation of the ΔpH. This was also indicated by the possible existence of biphasic kinetics at Na^+ concentrations below 1 mM Na^+, with an apperent K_m around 0.1 mM. This was close to the dissociation constant for the Na-nigericin complex around 0.150 mM and the formation of the Na-nigericin complex was shown to be the rate limiting step for the dissipation of ΔpH by Na^+ around pH 7.4 (Lutz *et al.*, 1970; Prabhananda and Ugrankar, 1991). The kinetics observed at higher Na^+ concentrations, with an apparent K_m bigger by two orders of magnitude, was therefore unlikely to be due to a direct dissipation of the ΔpH by Na^+/nigericin interaction. In fact, this value of 21 mM is in a similar range to that

reported by Barkla *et al.* (1995) for the Na^+/H^+-antiport in *M. crystallinum* tonoplast vesicles (between 44 and 51 mM).

The lack of evidence for H^+-coupled Cl^- transport in *M. crystallinum* tonoplast vesicles from leaf mesophyll is in stark contrast with a study on oat-root tonoplast vesicles, in which evidence for H^+-coupled Cl^--transport was found (Schumaker and Sze, 1987). In that study it was shown that both Cl^- and NO_3^- were able to dissipate a ΔpH imposed by the K^+/nigericin clamp, as well as in pH-jump experiments, in a saturating way with an apparent K_m of 5 to 10 mM. While this dissipation was independent of the $\Delta\psi$, other studies have shown dissipation of $\Delta\psi$ by Cl^- in the same system (Kaestner and Sze, 1987; Pope and Leigh, 1987). Also, the dissipation of the ΔpH was inhibited by DIDS, whereas the dissipation of a $\Delta\psi$ was DIDS insensitive in oat-root tonoplast vesicles (Kaestner and Sze, 1987; Schumaker and Sze, 1987). This suggests the presence of two Cl^--transport systems, one driven by $\Delta\psi$ and the other one by a ΔpH. When comparing these results with the findings in *M. crystallinum*, one has to keep in mind the different origin of the membranes, as they were not only from a different species, but also from a different tissue and developmental age [roots of 4-day-old oat seedlings in the study of Schumaker and Sze (1987)]. Another difference between tonoplast vesicle preparations of *M. crystallinum* and of oat roots seems to be the apparently high rates of H^+-leakage in the latter. While at 25°C the K^+/nigericin-induced ΔpH was maintained for several minutes in *M. crystallinum* tonoplast vesicles, only at temperatures well below 20°C could stable ΔpH formation be observed in oat-root vesicles, as determined by [^{14}C]methylamine accumulation (Schumaker and Sze, 1987).

While no dissipation of ΔpH by Cl^- could be observed in the present work, an inside-acidic pH clearly had an inhibitory effect on the initial Cl^--transport rate,

reducing it by around 50%. This was observed when the ΔpH was imposed by pH-jumps (Figure 5.2) as well as by the K^+/nigericin clamp (Figure 5.9). However, the pH-jump studies showed a reduction in the initial Cl^--transport rate at pH 6.2 inside (only), while at pH 5.5 showing normal Cl^- uptake again. The measurements using lucigenin were more difficult at low pH due to insufficient dye loading. The results at pH 5.5 might therefore best be treated with caution. Also, the K^+/nigericin generated internal ΔpH was estimated to be between 1.5 (this study) and 2.0 (Schumaker and Sze, 1986), therefore with an internal pH around 5.5. The K^+/nigericin method also caused a reduction in the rate of Cl^- transport of about 50% at 50 mM Cl^-. In the absence of nigericin or a K^+-diffusion gradient, no inhibition was observed, indicating that the effect on Cl^- transport was due to the ΔpH formed. Also, the stable fluorescence in the absence of Cl^- indicated that this effect was not due to a pH-dependent decrease in Cl^- sensitivity of lucigenin. However, it cannot be ruled out that an H^+-diffusion potential might be generated. While the K^+/H^+ exchange is electroneutral, leakage of H^+ out of the vesicles might lead to an inside-negative $\Delta\psi$, thereby decreasing Cl^- uptake. However, the pH-jump experiments, conducted in the presence of a K^+/valinomycin clamp, indicated that even in the absence of any $\Delta\psi$ the inside acidic pH can reduce the initial Cl^--transport rate. It therefore seems likely that the inside-acidic pH directly affects the initial Cl^--transport rate. The protonation of functional groups at low pH might directly regulate the Cl^- transporting protein. A regulation of activity by pH has been shown for many channels, such as the animal chloride channel ClC-2 (Begenisich and Melvin, 1998) or the vacuolar cation channels in plants (Davies and Sanders, 1995).

An alternative explanation for the reduced Cl^- transport might be that it would be mediated by a H^+/Cl^--symport mechanism. However, given a vacuolar acidic pH

around 5.0 and cytosolic pH around 7.1 under physiological conditions (Miller and Smith, 1992), such a symport could not drive vacuolar Cl^- uptake. Rather, it would cause Cl^- efflux from the vacuole into the cytoplasm. While Cl^-/H^+ symport can not be ruled out by these results, it certainly can not explain vacuolar Cl^- accumulation.

Initial attempts to load the pH-sensitive dyes pyranine (8-hydroxypyrene-1,3,6-trisulphonate) or the free acid form of BCECF (2',7'-bis(carboxyethyl)-5(6)-carboxyfluorescein)) into the vesicles *via* a freeze-thaw method, combined with sonication, failed to give sufficient internal fluorescence. The fact that BCECF is readily transported into *M. crystallinum* tonoplast vesicles in the presence of MgATP confirms the findings of Swanson *et al.* (1998). Their work suggests the presence of at least two ATP-dependent transporters for organic molecules in barley aleurone protein-storage vacuoles. Whereas one transports mainly glutathione-conjugates, the other transports non-conjugated organic molecules, such as free BCECF and has a different inhibitor profile (for a review see Rea *et al.*, 1998). However, in the present work the BCECF uptake was not further characterised, and it therefore cannot be ruled out that the uptake is H^+-coupled rather than directly driven by ATP. The V-type H^+-ATPase has to be assumed to be active during the BCECF incubation, thereby generating an inside-acidic ΔpH. One way to distinguish this would be to test for the vanadate sensitivity of BCECF-uptake, since the V-type ATPase is insensitive (Smith *et al.*, 1984), while vacuolar BCECF uptake in barley was shown to be sensitive to vanadate (Swanson *et al.*, 1998).

However, to actually measure absolute pH values below pH 6 BCECF is not the optimum choice. With its intracellular pK_a value between 6.7 and 7.3 (James-Kracke, 1992; Nett and Deitmer, 1996), it is close to the physiological pH of the cytosol and the linear range of its pH sensitivity lies between pH 6.0 and pH 8.0. But

the ability to load free BCECF into vesicles readily by means of ATP-dependent transport, together with the ability to perform an internal calibration, provides a sensitive tool to measure absolute pH changes around pH 7.0. This is particularly useful when studying H^+-coupled transport processes and the evoked changes in pH, if these are close to the cytosolic pH. Furthermore, this method has the considerable advantage that the fluorescence signal arises from cytosolic-side out vesicles only, thereby eliminating the uncertainty that exists when studying mixed vesicle populations. Furthermore, since ATP-dependent BCECF uptake seems specific for vacuoles, contamination by other membrane systems should therefore make no significant contribution to the measured fluorescence (Coleman *et al.*, 1997; Kearns *et al.*, 1998; Swanson *et al.*, 1998). However, a more detailed characterisation of vacuolar BCECF uptake in *M. crystallinum* tonoplast vesicles is needed, and this would also be interesting in the context of possible uptake of DIDS, which might be mediated by the same system (Eleno *et al.*, 1992; Hörtensteiner *et al.*, 1993).

In conclusion, despite extensive testing, no evidence for H^+-coupled Cl^- transport could be found in *M. crystallinum* tonoplast vesicles. If anything, the evidence suggests a reduced Cl^- uptake into tonoplast vesicles regulated by an inside-acidic ΔpH, which is in the opposite direction to that predicted for the operation of a putative H^+/Cl^- antiport system.

Chapter 6

Electrophysiological studies of vacuolar ion currents

6.1 Introduction

The studies of Cl^- transport in *Mesembryanthemum crystallinum* tonoplast vesicles described in the previous chapters have clearly shown the existence of a protein-mediated, voltage-dependent Cl^--uptake mechanism. To characterise further this vacuolar Cl^- transport process and to test for ion-channel mediated Cl^- transport, the patch-clamp technique (Hamill *et al.*, 1981) was employed both at the level of whole mesophyll vacuoles, as well as at the single-channel level using excised membrane patches. While studies based on Cl^--sensitive dyes specifically report changes in Cl^- concentrations, patch-clamp measurements are based on the movement of electrical charge across the membrane. For example, movement of Cl^- into the vacuole or K^+ out of the vacuole would generate negative (inward) currents. There is therefore no intrinsic specificity for Cl^- in the patch-clamp technique, movement of any ion is detected. However, this limitation can be overcome by using asymmetric ion concentrations on the two sides of the membrane. The contribution of the various ions towards the total current can thereby be quantified, based on the Nernst potential of each ionic species being of a different value. This powerful method provides a sensitive tool to study ion transport in intact vacuoles. Furthermore, it can provide high resolution of ion-channel activity down to the single-channel level.

Since there has been no detailed electrophysiological study on *M. crystallinum* mesophyll vacuoles to date, the present work was aimed at providing an overview of

the electrophysical properties of these vacuoles. First, some general aspects of patch-clamping the rather large vacuoles of *M. crystallinum* leaf mesophyll cells will be discussed. Then, using KCl-based solutions, a characterisation of macroscopic, as well as single-channel, currents will be presented, recorded at different cytosolic Ca^{2+} concentrations. Three cytosolic free Ca^{2+} ranges were selected (~100 nM, ~1 µM, and 0.1 to 1 mM), reflecting the important role of Ca^{2+} as a second messenger. Further experiments were conducted with NMDG-Cl (*N*-methyl-D-glucamine chloride) as the main charge carrier, as $NMDG^{+}$ is believed to be membrane impermeant (Cheffings *et al.*, 1997).

In general, the number of successful seals of *M. crystallinum* vacuoles was relatively low (about 1 or 2 out of every 10 attempts). Furthermore, due to the size of the vacuoles (50 to 200 µm diameter) it was generally difficult to perfuse the vacuoles over a longer period without losing the seal. The total number of replicates was therefore comparatively low, and under some conditions only single measurements could be completed. As an alternative to whole-vacuole measurements, large membrane patches similar to *Xenopus* oocyte macropatches were excised in some experiments. They were generally easier to obtain and more stable during the perfusion.

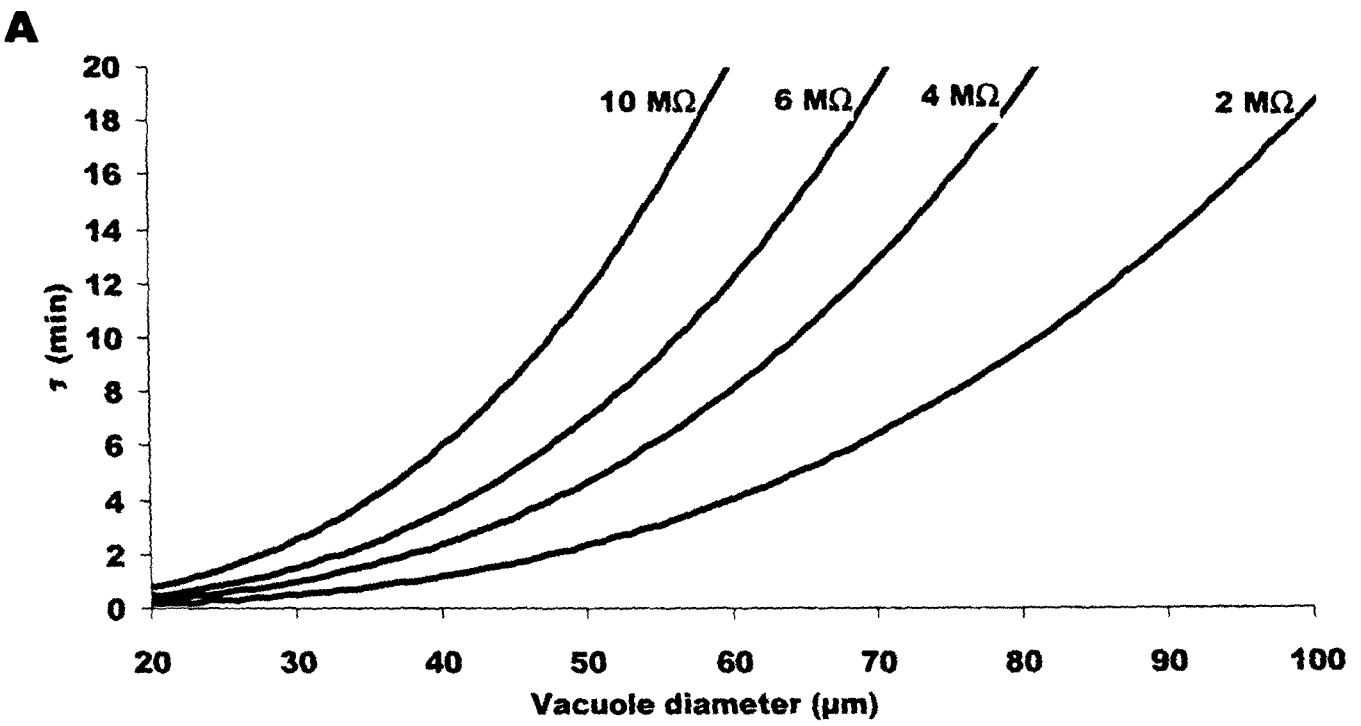
This work on isolated vacuoles of *Mesembryanthemum crystallinum* was initiated to determine possible Cl^{-} uptake mechanisms. By using a range of different recording conditions and by varying physiological regulatory factors, it was hoped to find optimum conditions for identifying Cl^{-} specific currents. The data presented will therefore provide not so much an in-depth analysis of the currents observed, but a

broad characterisation of the electrophysiological features of leaf mesophyll vacuoles of this extreme halophyte.

6.2 Results

6.2.1 Patch-clamping large vacuoles of *Mesembryanthemum crystallinum*

The diameters of intact vacuoles that were isolated from leaf mesophyll tissue of *M. crystallinum* varied considerably between 50 and 200 µm, due to the succulence of the leaves. The average diameter of vacuoles that were patched was 60 to 90 µm. The large size of the vacuoles raised some important questions when considering measurements in the whole-vacuole configuration. First, the time taken to equilibrate the vacuolar lumen with the pipette solution after breaking the seal had to be estimated. The time course is largely a function of the vacuolar size, described by the diameter (assuming a sphere), and of the pipette-tip geometry, which can as a first approximation be described by the access resistance R_a. Pusch and Neher (1988) gave an empirical description of the time course of equilibration, based on measurements on small spherical cells. Figure 6.1 contains examples calculated according to this relationship. Figure 6.1.A shows that for a typical vacuole of 80 µm diameter and a comparatively low access resistance of 2 MΩ the time constant is around 8 min. As Figure 6.1.B indicates, a time constant of 8 min means that it would take about 20 min to reach 90% of the final ion concentration. Although these estimates are extrapolations from measurements on cytosolic diffusion in small cells (Pusch and Neher, 1988), they nevertheless provide a useful estimate of the order of magnitude to be expected for diffusional exchange in larger vacuoles.



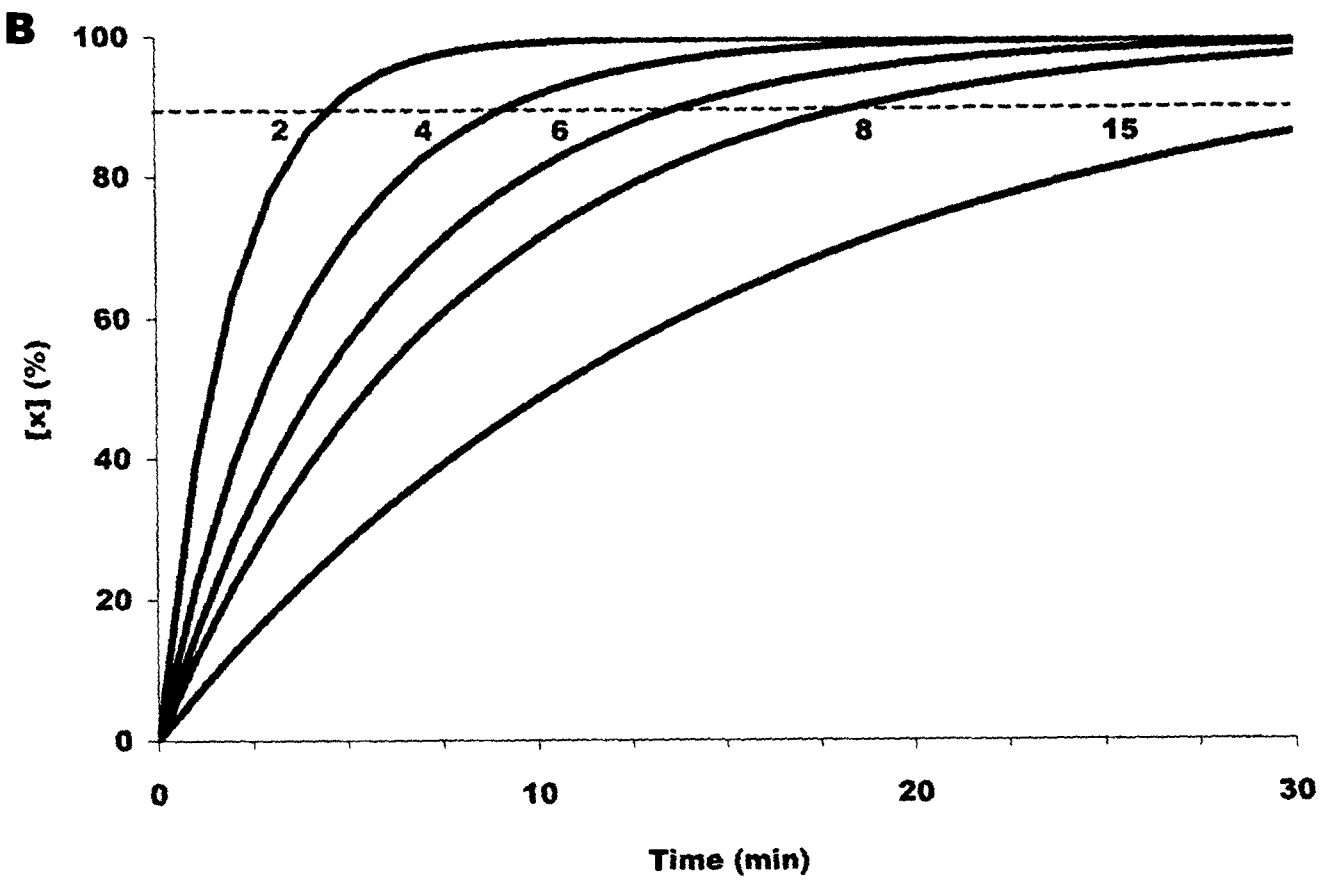


Figure 6.1. Relationship between the access resistance R_a, the vacuolar diameter and the time course of vacuolar perfusion with the patch pipette solution, calculated after Pusch and Neher (1988). **A**) The time constant τ of diffusion as a function of the vacuolar diameter and access resistance R_a, calculated for K^+. The time constants were calculated according to the empirical formula $\tau = 0.6 \times R_a \times M^{1/3} \times (d/15.38\ \mu m)^3$, with the access resistance R_a in MΩ, the molecular weight of the ion, M, in daltons, and the vacuolar diameter d in µm. **B**) Time course of equilibration of ion concentrations between the patch pipette and the vacuolar lumen, calculated for five time constants as indicated. The vacuolar ion concentration was calculated according to the formula $[X](t) = 100 - 100 \times \exp(-t/\tau)$, assuming no ions in the vacuole at $t = 0$ and a maximum concentration of 100%

To measure the actual time course of diffusional equilibration in large vacuoles, the membrane potential of whole vacuoles was measured in the current-clamp mode during the perfusion. Immediately after obtaining the whole-vacuole configuration, the access resistance R_a was estimated using the R_s-compensation circuit of the EPC-7 amplifier. Subsequently, the membrane potential of the vacuole was recorded in the current-clamp mode on a chart recorder. The holding current was 0 pA, with short -100 pA pulses every 30 s to monitor changes in R_a. Under symmetrical ion concentrations (100 mM on both sides on the membrane), the membrane potential should reach a steady state of 0 mV once the pipette solution has equilibrated with the vacuolar lumen. Any contributions of the Ca^{2+} or H^+ gradients might result in a deviation from the 0 mV asymptote, but the membrane potential should still reach a steady-state level once the concentrations have reached their final values.

Figure 6.2 shows a chart recording of the membrane potential of a vacuole of 70 µm diameter and 3.6 MΩ access resistance. This showed a steady increase in the membrane potential from around -30 mV to -10 mV in 24 min, with the access resistance remaining unchanged. Even after about 25 min of perfusion the membrane potential had not yet reached its steady-state level. The observed time course was actually considerably slower than predicted based on the model of Pusch and Neher (1988). Out of five similar measurements, only one was similar to the expected time course, the remaining measurements being considerably slower than the predicted.

The slow perfusion of the large vacuoles means that it was generally difficult to define the vacuolar ion concentrations precisely. Therefore, shifts in reversal

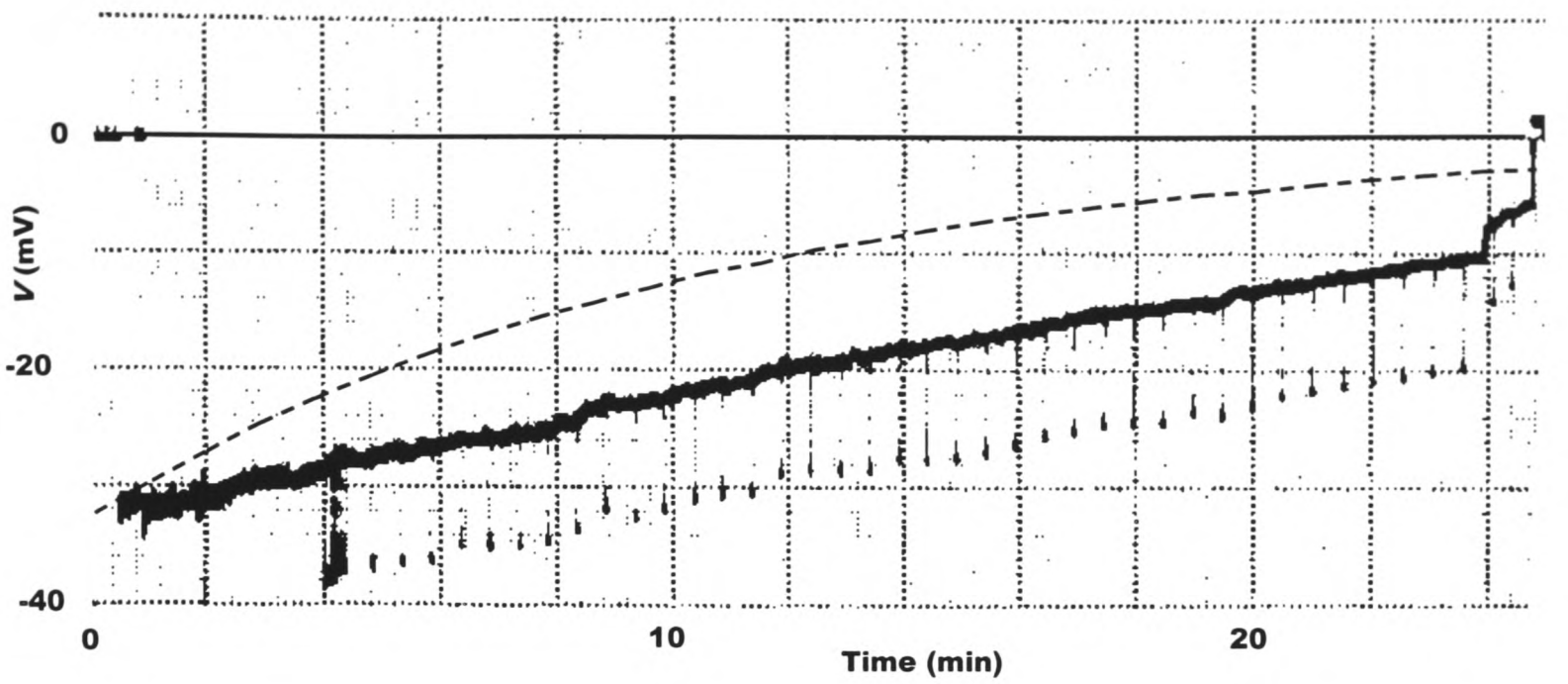


Figure 6.2. Time course of diffusion of the pipette solution into the vacuole. A vacuole of 70 µm diameter was perfused with 100 mM KCl (solution J) in the bath and 100 mM KCl (solution E) in the pipette. The pipette potential V_{pip} was continuously recorded on a chart recorder in the current-clamp mode. The holding current was 0 pA, with brief current pulses of -100 pA every 30 s. The series resistance R_s was estimated prior to the recording to be 3.6 MΩ, and the seal resistance was around 100 MΩ (> 1GΩ in the vacuole-attached configuration). The seal was lost and the recording stopped after 25 min of perfusion. The dotted line shows the estimated time course for diffusion of the pipette solution (for K^+) according to Pusch and Neher (1988)

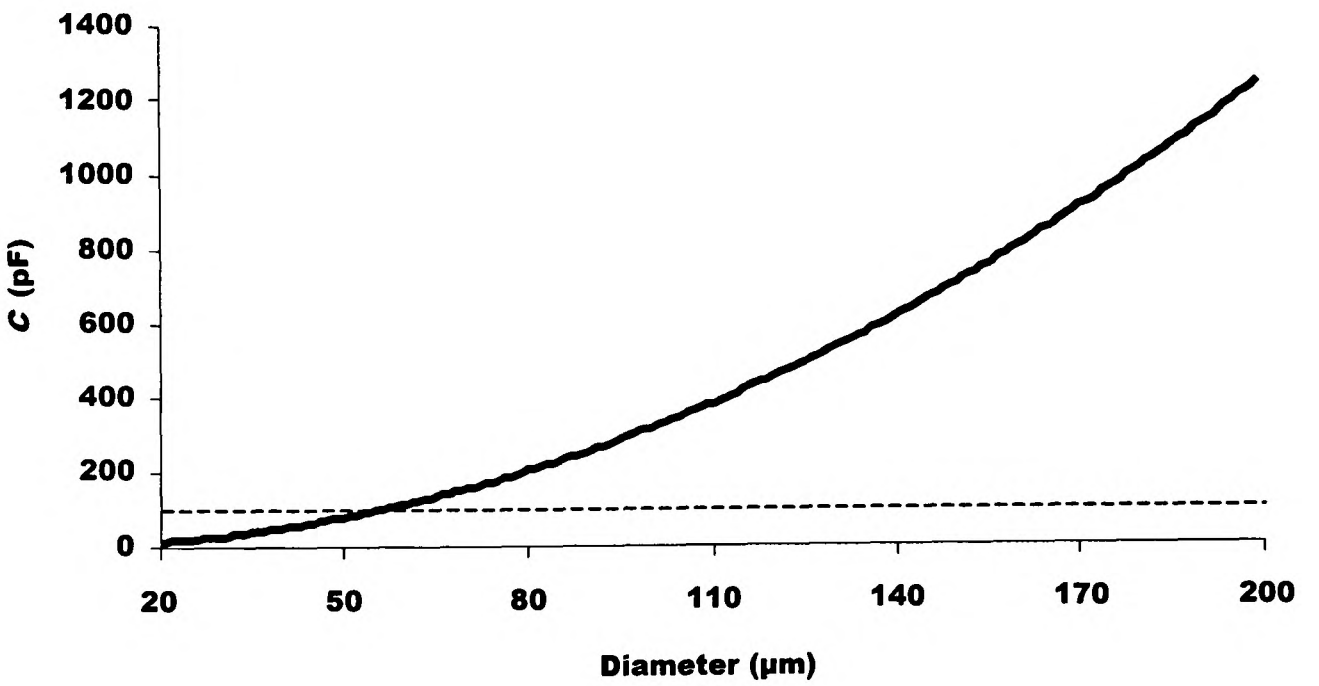


Figure 6.3. Relationship between vacuolar diameter and capacitance. The relationship was calculated assuming a membrane capacitance of 10 mF m^{-2} (Hille, 1992). The dotted line indicates the maximum of 100 pF that can be compensated by the EPC-7 amplifier

potentials measured in the whole-vacuole configuration by perfusing with different bath solutions could only give approximate results for these vacuoles.

Further limitations when working with large vacuoles arose from the fact that the large vacuolar capacitance, originating from the large surface area, could usually not be properly compensated for by the electronic circuit built into the EPC-7 amplifier. As Figure 6.3 shows, the maximum capacitance that can be compensated for is 100 pF, a value already attained with vacuoles around 60 µm in diameter. This could result in large transient capacitive spikes at the onset of voltage steps. Since the compensation of the membrane capacitance and the access resistance are electronically coupled, the R_s compensation for large vacuoles could only be performed approximately. Furthermore, the total resistance observed in whole-vacuole recordings was often very low, down to 100 MΩ, which was only one order of magnitude larger than the access resistance. Since the EPC-7 was originally designed for measurements on cells not larger than 50 µm, large vacuolar currents exceeding 20 nA would saturate the amplifier, thereby distorting the signal.

All these factors made it necessary to keep the access resistance R_a as low as possible. This would help not only to improve the speed of vacuolar perfusion, but should also guarantee that the imposed command voltage would drop mainly across the membrane resistance R_m and not across the R_a in series. This was especially crucial for the large currents observed. For example, a R_a of 5 MΩ and a current of 5 nA would lead to a voltage drop of 25 mV across the access resistance if left uncompensated, and with 50% R_s-compensation it would be 12.5 mV. If possible, R_s was compensated between 50 and 90%, with higher compensation made difficult by the insufficient compensation of the membrane capacitance C_m. Also, the speed of the

voltage-clamp depends on the access resistance according to $\tau = C_m \times R_a$, (Armstrong and Gilly, 1992; the resistance of the reference electrode, adding up to R_s, was not considered for simplicity). With the large capacitance C_m of the vacuoles, R_a had to be kept low to allow a fast response of the voltage clamp. The access resistance was therefore reduced by using pipettes with large opening diameters (between 1 to 2 µm) and resistances between 2 and 5 MΩ, resulting in access resistances below 10 MΩ in many cases, and after compensation below 2 to 5 MΩ. During the recordings, the compensation for the access resistance was checked regularly and readjusted.

These considerations meant that although whole-vacuolar recordings gave large current recordings, accurate quantification was difficult. Thus, as an alternative to recordings in the whole-vacuole configuration, the macropatch technique was used for some measurements to obtain macroscopic currents. Diffusion into the vacuole was not a limiting factor, and the smaller membrane area meant that the capacitance and R_s could be compensated for. Another method for obtaining smaller vacuoles is to break the vacuole into smaller vesicles (Pottosin *et al.*, 1997). However, this method did not work successfully with *M. crystallinum* vacuoles.

6.2.2 Recordings in KCl-based solutions

6.2.2.1 Macropatch recordings with high cytosolic Ca^{2+}

In order to obtain macroscopic currents with high cytosolic free Ca^{2+} (~0.1 to 1 mM), the macropatch technique was used. Electrodes with large tip openings of up to 15 µm were fabricated as described in Chapter 2, with resistances between 500 kΩ and 2 MΩ. After sealing of the pipette tip to the membrane, large macroscopic currents could be observed both in the vacuole-attached as well as the vacuolar-side-

out configuration after excision of macropatches. However, it was difficult to control reliably the size of the membrane area in the tip, which depended on how far the membrane moved up into the pipette when forming a Ω-shaped seal. Large macroscopic currents of several nA could usually be measured when an Ω-shaped vesicle was visible protruding up to 15 µm into the pipette tip. While the formation of such a seal often took several minutes to reach 1 GΩ or more, in some cases fast sealing occurred when no vesicle was visible in the pipette. These types of seals had relatively small current amplitudes of less than 100 pA and single-channel events could easily be resolved, equivalent to conventional single-channel recordings.

Figure 6.4.A shows typical macroscopic currents obtained with a macropatch in the vacuolar-attached configuration in symmetrical 100 mM KCl solutions. Large time-dependent outward currents of up to 3 nA could be observed, but only small inward currents. After excision of the macropatch to give the vacuolar-side-out (vo) configuration (Figure 6.4.B) the current amplitude of the outward current showed a six-fold decrease and had a maximum around 500 pA at +100 mV. The inward current did not show any decrease in amplitude and remained unchanged, but the higher amplification of the signal in the vo-configuration revealed some single-channel activity at negative membrane potentials (Figure 6.4.B). Subsequently, the vacuolar side of the patch was perfused with 4 mM KCl (Figure 6.4.C) or 200 mM KCl (Figure 6.4.D, note also the single channel activity at -100 mV), respectively. Figure 6.5.A. shows the current-voltage-plot of the instantaneous currents. They were linear over the whole voltage range from -100 mV to +100 mV. When the KCl concentration in the external medium (i.e. the vacuolar surface of the excised patch) was changed from 100 mM KCl to 4 mM KCl, the reversal potential E_{rev} was shifted negative by about

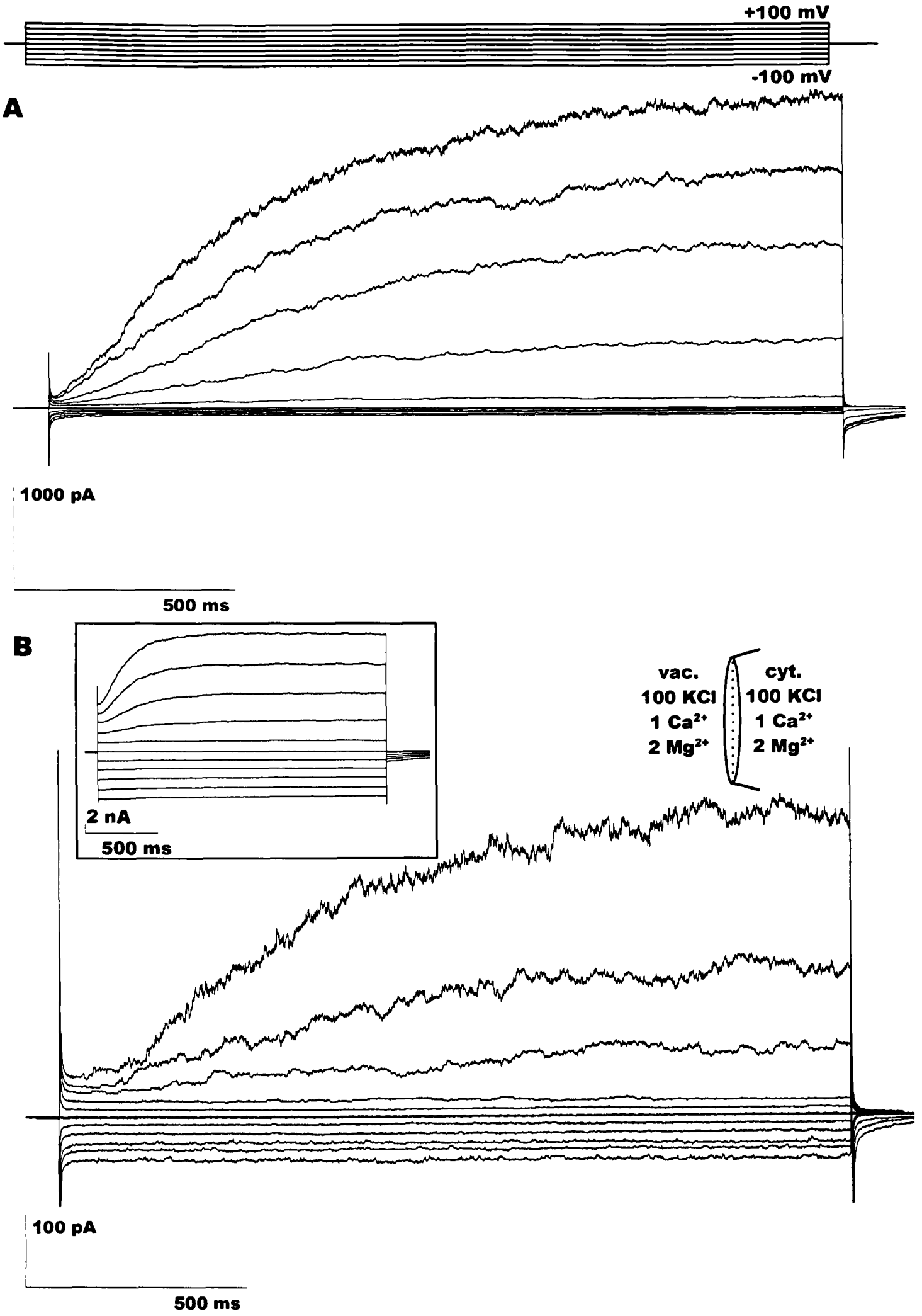
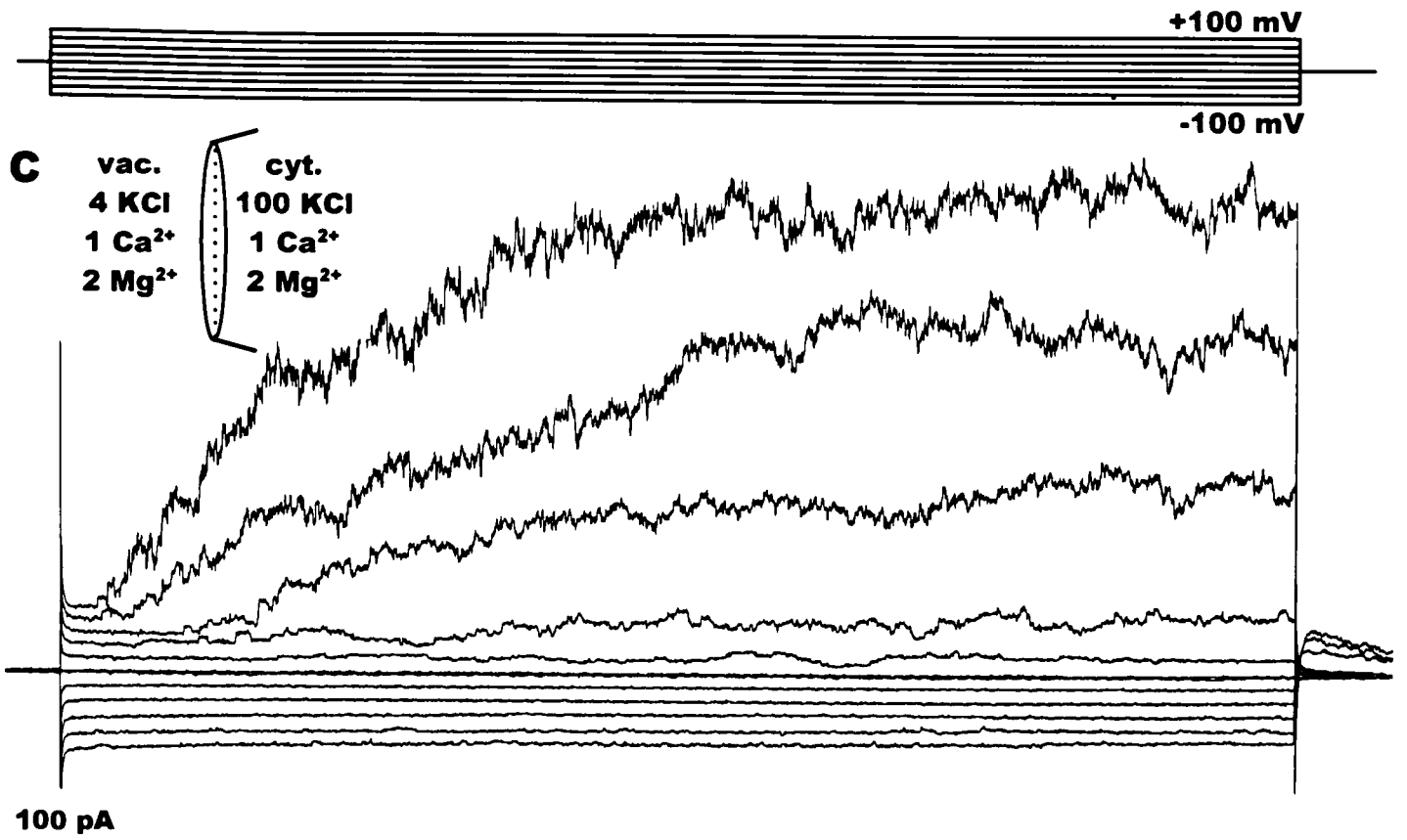


Figure 6.4. Macropatch recordings in symmetrical 100 mM KCl solutions with 1 mM cytoplasmic Ca^{2+} (solution E on both sides). **A**) Vacuole-attached recordings during voltage steps from -100 mV to +100 mV. **B**) Macropatch recordings after obtaining the vacuolar-side-out configuration. The inset shows typical whole-vacuole recordings under similar conditions (95 μm vacuole diameter). The cartoon indicates concentrations in mM. Figure continued on the next page



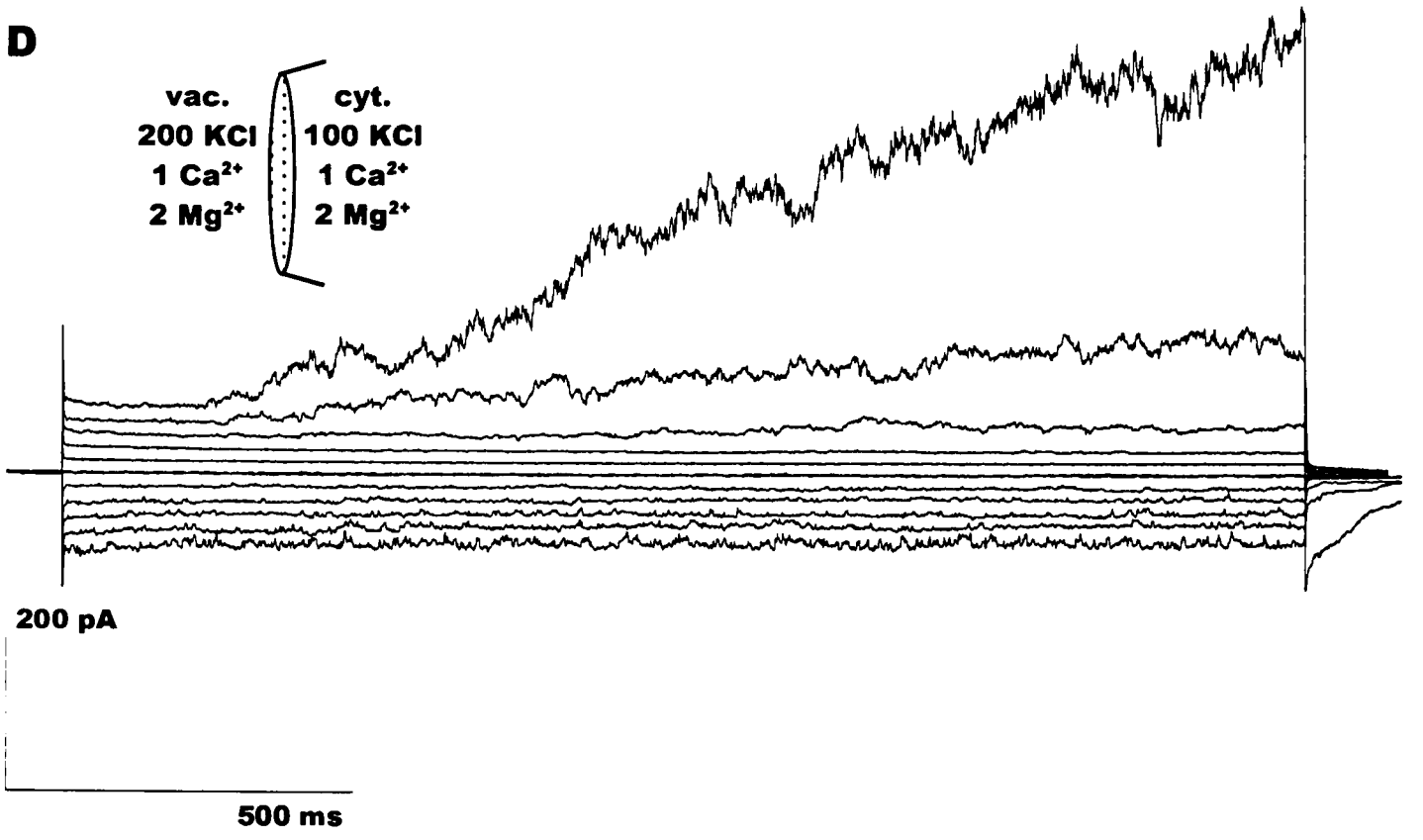


Figure 6.4. Continued from previous page. **C)** Macropatch recordings after perfusion of the vacuolar side with 4 mM KCl (solution F). **D)** Macropatch recordings after perfusion of the vacuolar side with 200 mM KCl (solution G). The cartoons indicate concentrations in mM

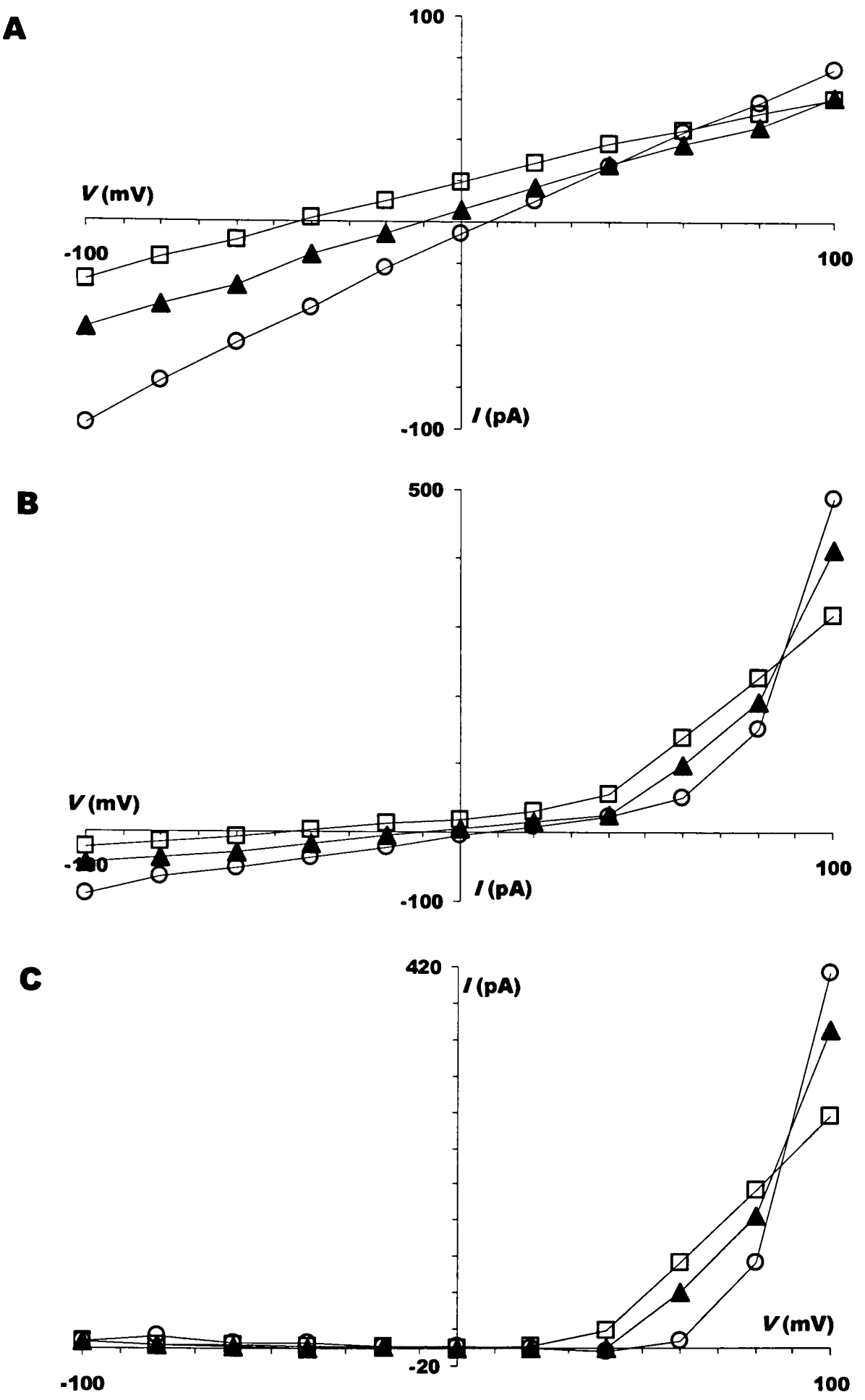


Figure 6.5. Current-voltage plots for the currents in Figure 6.4. The instantaneous currents (**A**), steady-state currents (**B**) and the difference between steady-state and instantaneous currents (**C**) were plotted against the membrane potential. Symbols: 100 mM KCl (▲), 4 mM KCl (❑), 200 mM KCl (○)

-35 mV, indicating a strong selectivity for K^+ over Cl^-. Similarly, changing the KCl concentration at the vacuolar-side to 200 mM led to a positive shift in E_{rev} to +18 mV, which was close to the value to be expected for K^+ being the major permeant ion, with a Nernst potential E_K of +16.4 mV. The steady-state currents (Figure 6.5.B) showed a strong outward rectification above +40 mV. The time-dependent component of the steady-state current was revealed by subtracting the instantaneous currents (Figure 6.5.C). In symmetrical 100 mM KCl solutions, this current was activated above +40 mV. When the vacuolar KCl concentration was reduced to 4 mM, activation could be seen already at lower membrane potentials (> +30 mV). However, the current amplitudes increased less steeply with voltage, resulting in about 25% less current at +100 mV than in 100 mM KCl, despite the steep outward gradient for K^+. Conversely, with 200 mM KCl at the vacuolar side the currents activated only at potentials above +55 mV but showed a steep voltage response; indeed the current amplitude was about 15% higher at +100 mV than in 100 mM KCl despite the inwardly directed K^+-gradient.

To determine the selectivity of the time-dependent current, a tail-current protocol was employed to measure the reversal potentials under asymmetric KCl concentrations (Figure 6.6). Figure 6.7 summarises the current-voltage plots obtained for the tail currents. This shows that by changing from 100 mM to 4 mM KCl the reversal potential shifted negative from +6 mV to -21 mV. Changing to 200 mM shifted the reversal potential positive by 15 mV to +20 mV with respect to the 100 mM KCl value, close to the E_K, of +16.4 mV. The tail-current amplitudes also show that with a steep outwardly directed K^+ gradient of 4 mM to 100 mM towards the vacuolar side the inward currents were reduced accordingly. With an inwardly

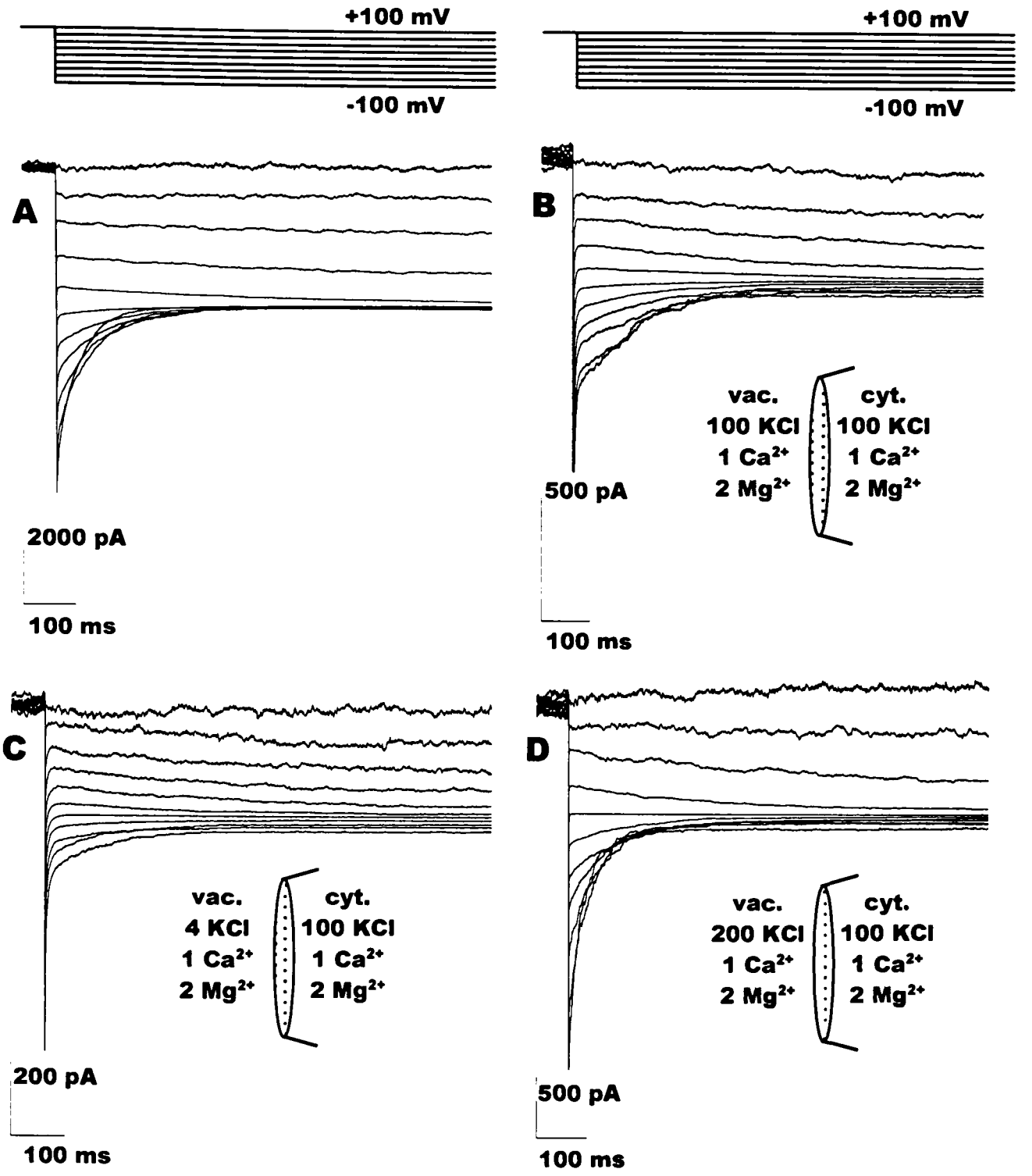


Figure 6.6. Tail currents of macropatch recordings at 1 mM cytoplasmic Ca^{2+}. After an activating pulse of +100 mV (5 s, from a holding potential of 0 mV), the membrane potential was stepped to values between -100 mV and +100 mV in 20 mV steps. **A**) vacuole attached (100 mM KCl in pipette and bath, solution E). **B**) Vacuolar-side-out with 100 mM KCl at the vacuolar side (solution E). **C**) Vacuolar-side-out with 4 mM KCl at the vacuolar side (solution F). **D**) Vacuolar-side-out with 200 mM KCl at the vacuolar side (solution E). The cartoons indicate concentrations in mM

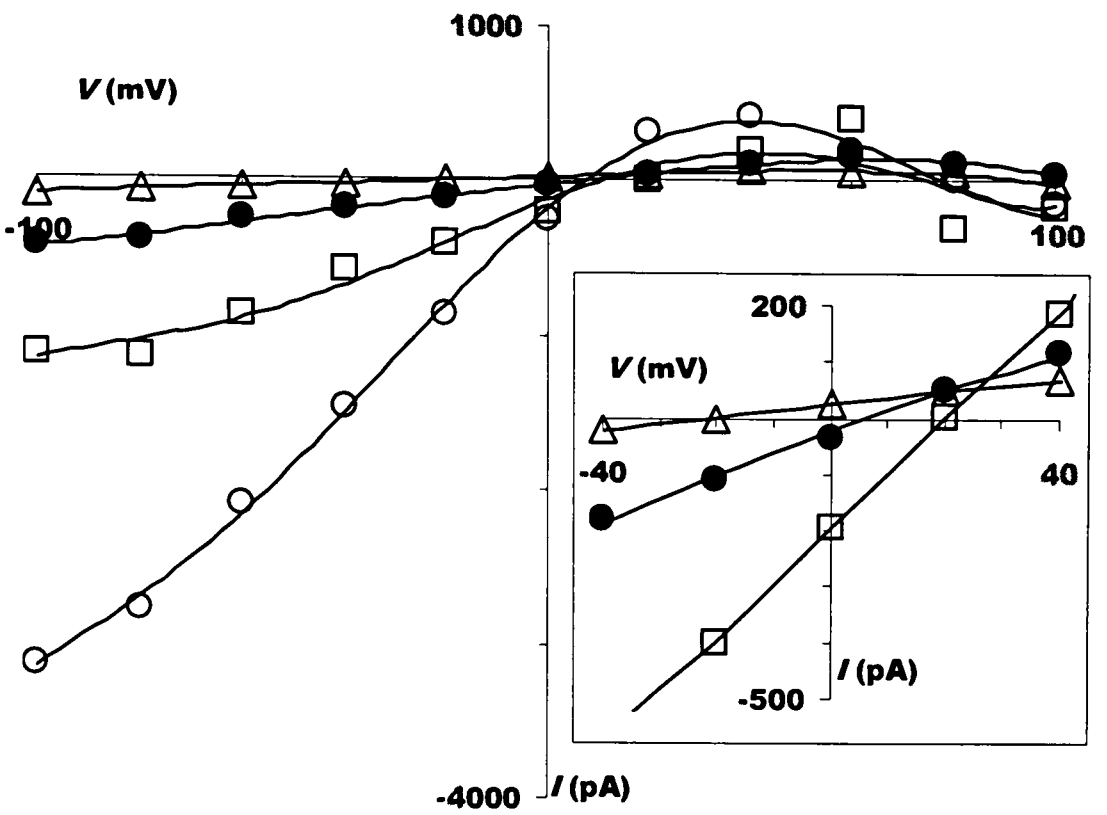


Figure 6.7. Current-voltage plot of the tail-currents (see Figure 6.6). The current amplitudes were obtained by fitting single exponentials to the tail currents, extrapolating back to the first 1 ms of the test pulse, and subtracting the steady-state currents. The inset shows the same plot on a larger scale, omitting the vacuole-attached data. Symbols: vacuole attached (○), 200 mM KCl (❑), 100 mM KCl (●), 4 mM KCl (Δ)

directed K^+ gradient of 200 to 100 mM the inward currents were increased correspondingly. Similar results were obtained in two further macropatch experiments.

6.2.2.2 Single channels with high cytosolic free Ca^{2+}

With high cytosolic free Ca^{2+} concentrations (0.1 to 1 mM), a number of different single-channel amplitudes could be observed in the patches. A total of 27 patches with GΩ seals were obtained under these conditions. Figure 6.8 shows a representative macropatch in the vacuole-attached and vacuolar-side-out configurations in symmetrical 100 mM KCl solutions. This illustrates both the presence of time-independent channels at negative membrane potentials, as well as a number of slowly activating channels at positive membrane potentials. Figure 6.9 shows a current-voltage plot of the single-channel amplitudes observed. At negative membrane potentials, only one amplitude level was seen at each potential, with a slope conductance of 36 pS. A similar conductance could be observed at positive membrane potentials with a slope conductance of 33 pS. Due to the large number of channels opening at membrane potentials above +60 mV, it was difficult to distinguish single-channel events, but a few could be detected with larger conductances of around 52 pS slope conductance. Both single-channel amplitudes could be detected in the vacuole-attached as well as the vacuolar-side-out configurations (Figure 6.9.A). As Figure 6.9.B shows, the reversal potential for the voltage-independent single-channel currents closely followed the Nernst potential for K^+ in 200 mM KCl, indicating a high K^+ selectivity. Similarly, voltage ramps in 4 mM KCl showed a shift E_{rev} to -28 mV (data not shown). This type of channel could be observed in five patches. Due to its selectivity for K^+, its voltage independence and

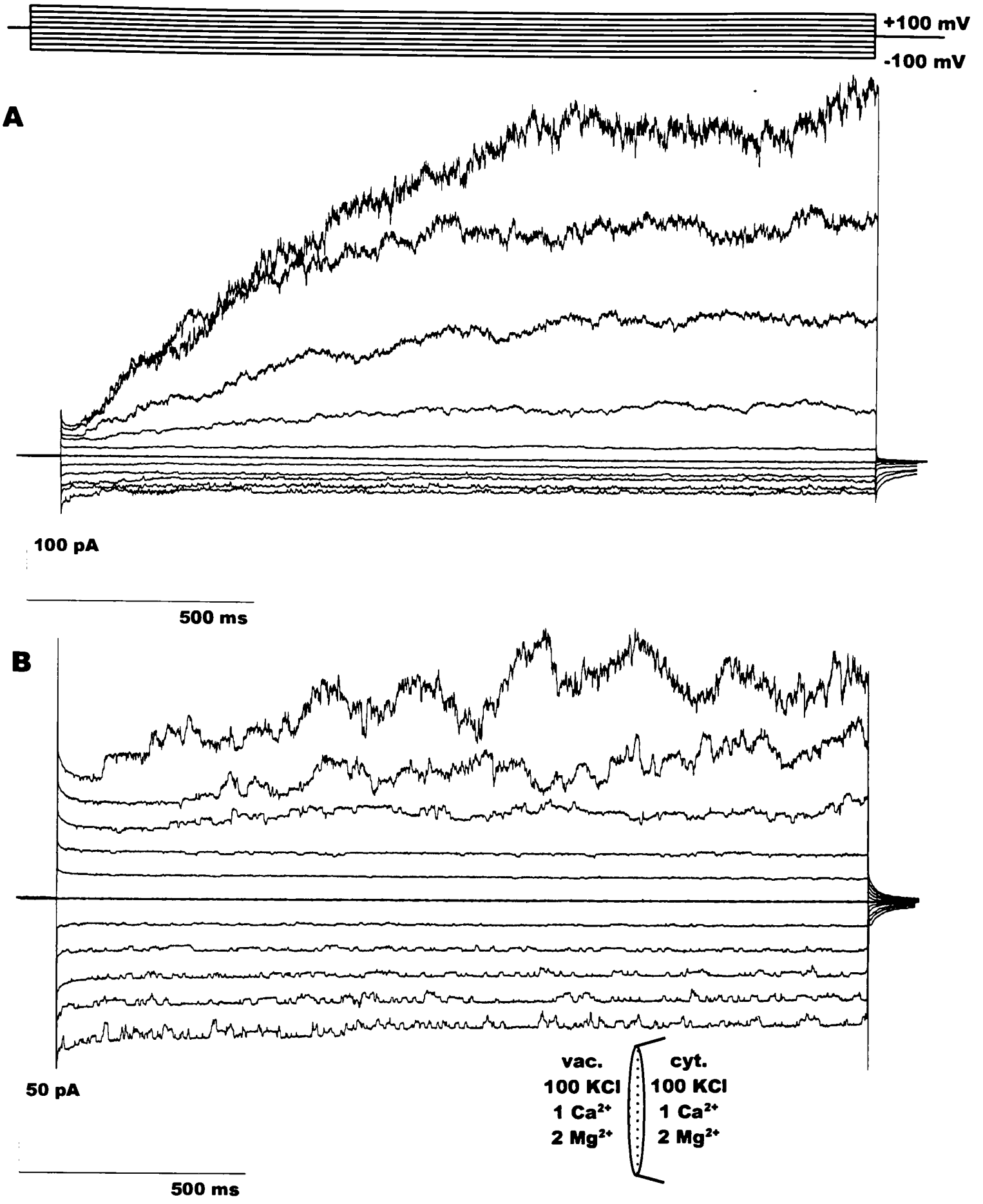
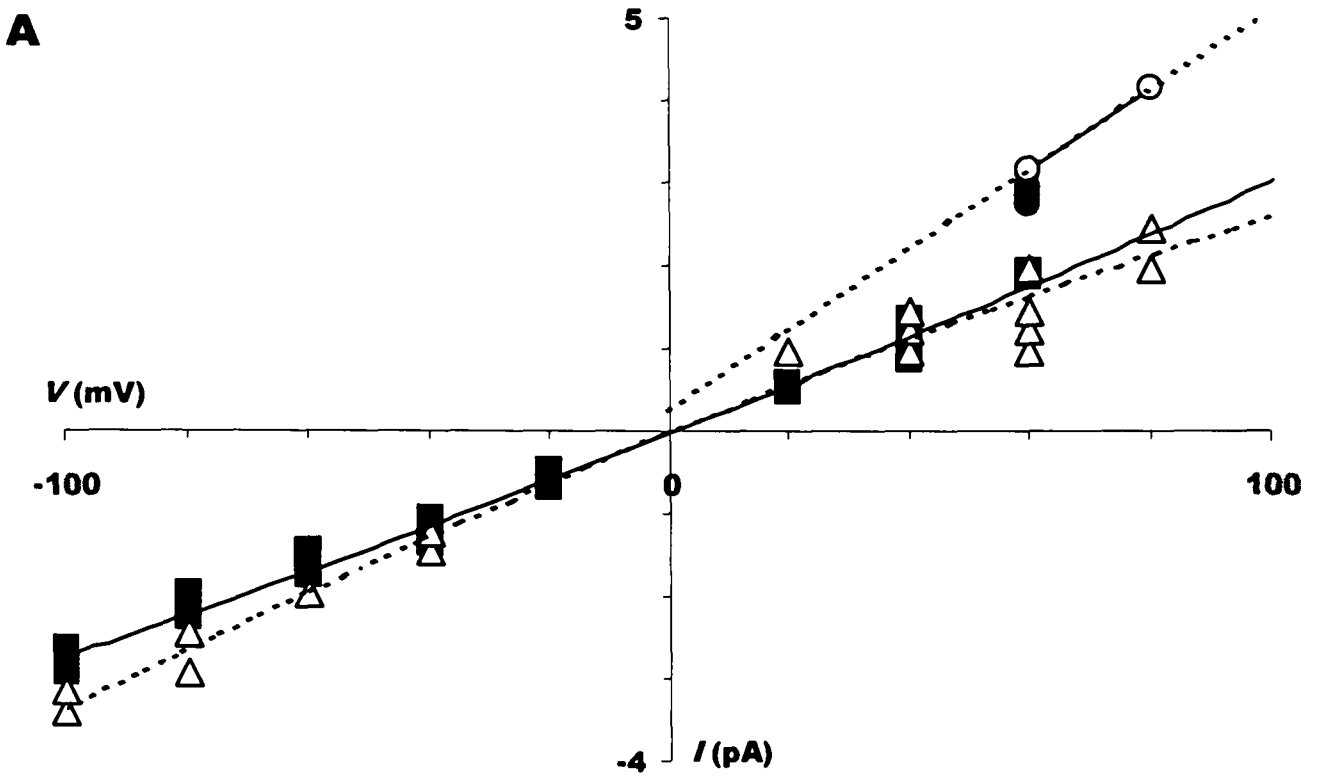


Figure 6.8. Single-channel currents at negative and positive membrane potentials. **A**) Macropatch recordings in the vacuole-attached configuration and **B**) in the vacuolar-side-out configuration. Symmetrical KCl concentrations with 100 mM KCl (solution E) on both sides. The cartoon indicates concentrations in mM



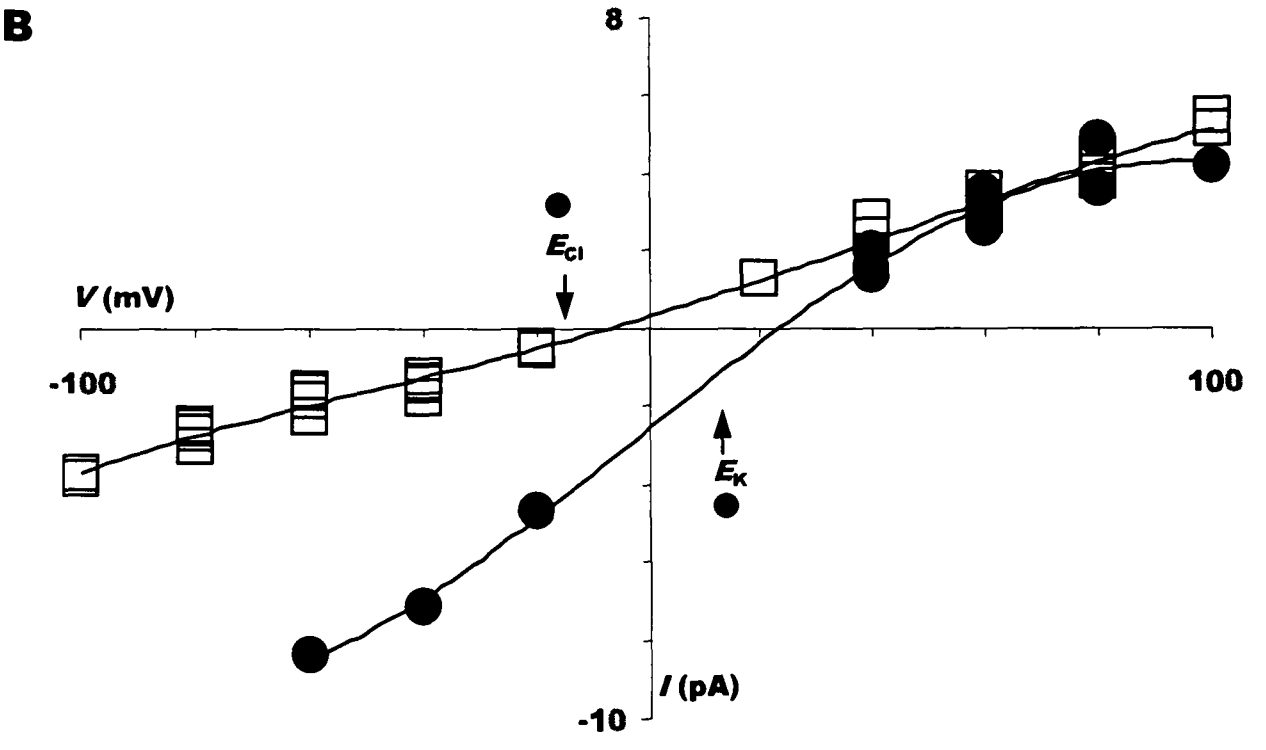


Figure 6.9. Current-voltage relationship and selectivity of KVIH1. **A**) Current-voltage plot of single-channel amplitudes as derived from Figure 6.8. The open symbols represent amplitudes obtained in the vacuole-attached configuration and the filled symbols are amplitudes measured in the vacuolar-side-out configuration. At positive membrane potentials above +40 mV, two distinct amplitude levels could be observed in both the vacuole-attached and the vacuolar-side-out configuration. The dotted lines are straight-line fits to the vacuole-attached data, and the solid line shows a straight-line fit to the vacuolar-side-out data. **B**) Current-voltage plots from similar single-channel recordings where the vacuolar KCl concentration was changed from 100 mM KCl (❑, solution E) to 200 mM KCl (●, solution G). The Nernst potential for K^+, E_K, in 200 mM KCl is indicated

its activity at high Ca^{2+} concentrations this type of channel will be referred to as KVIH1 (for K^+-selective, voltage independent, high Ca^{2+}).

Figure 6.10 shows a very similar type of channel that was observed in a single patch. Unfortunately, it was only recorded in asymmetric conditions, so it is not clear whether it is the same channel as described in Figure 6.8. With 200 mM KCl on the vacuolar side it was active over the whole voltage range and showed a slope conductance of about 50 pS between +60 and +80 mV, and of about 40 pS between -60 and -40 mV. This was much smaller than was observed for KIVH1, which had a slope conductance of around 98 pS between -20 and -60 mV in 200 mM KCl. The currents reversed at about +20 mV, close to E_K (+16.4 mV), thereby indicating high K^+ over Cl^- selectivity (Figure 6.10.B). Similarly, when the vacuolar KCl concentration was reduced to 4 mM KCl, the reversal potential was shifted negative towards -27 mV (Figure 6.10.C). This type of channel will be referred to as KVIH2.

Figure 6.11 and Figure 6.12 show recordings of single channels with a smaller conductance. In symmetrical 100 mM KCl, this channel had a slope conductance of about 10 pS between -80 and -100 mV. This single channel was active both at negative and positive membrane potentials. However, at positive membrane potentials above +60 mV the single-channel amplitude seemed to saturate and did not increase any further. When the vacuolar-side KCl concentration was changed to 4 mM KCl, the reversal potential was shifted negative, indicating selectivity of K^+ over Cl^- (Figure 6.11.C). A similar channel was also recorded under asymmetric 200 mM KCl concentrations (Figure 6.12) showing a reversal potential very close to E_K. This channel type was seen in three patches, and will be referred to as KVIH3.

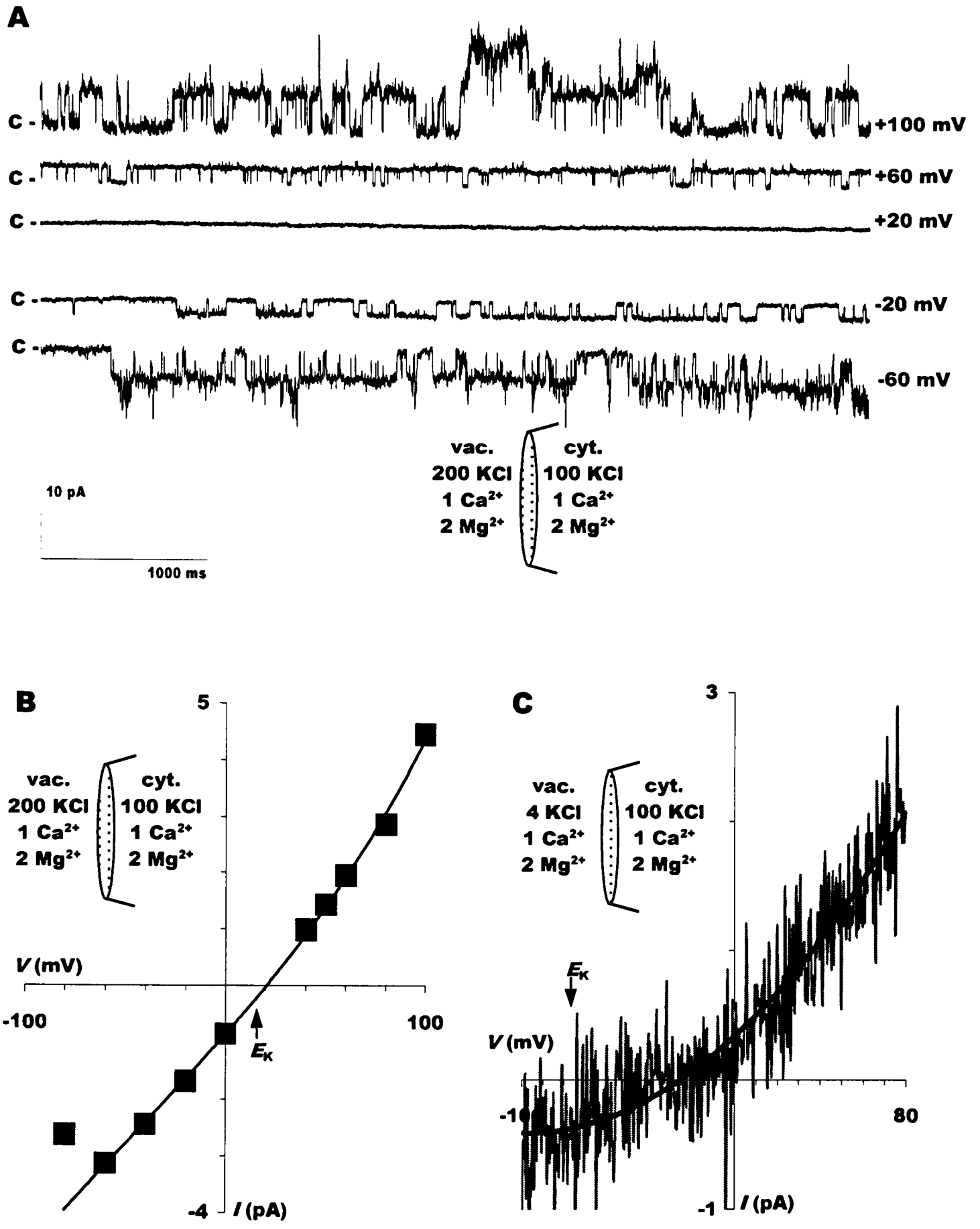


Figure 6.10. Single-channel activity of KVIH2 at negative and positive membrane potentials with asymmetric KCl concentrations. **A**) Single-channel recordings in the vacuolar-side-out configuration with 200 mM KCl (solution G) at the vacuolar side (cyt.: 100 mM KCl, solution E). The closed state is indicated by (c). **B**) Current-voltage plot of single-channel amplitudes derived from part A. **C**) Current-voltage plot constructed from a voltage ramp (from +100 mV to -100 mV in 25 ms) with 4 mM KCl (solution F) at the vacuolar side. The Nernst potential for K^+, E_K, is indicated. The cartoons indicate concentrations in mM

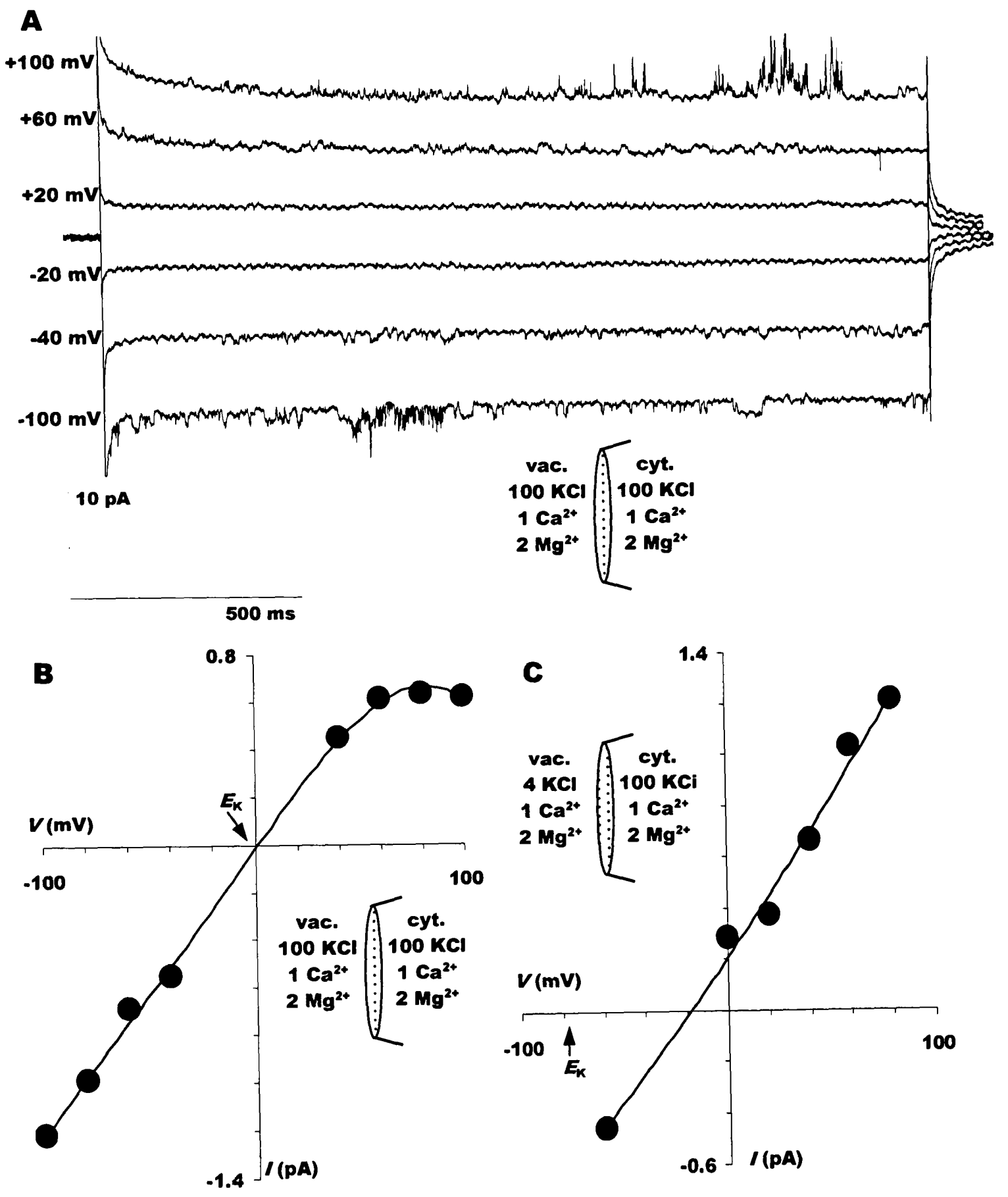


Figure 6.11. Small single-channel activity of KVIH3. **A)** Vacuolar-side-out recording with symmetrical 100 mM KCl concentrations (solution E). **B)** Current-voltage plot of the single-channel amplitudes in Figure A. **C)** Single channel current-voltage plot with 4 mM KCl on the vacuolar side (solution F). The Nernst potential for K^+, E_K, is indicated. The cartoons show concentrations in mM

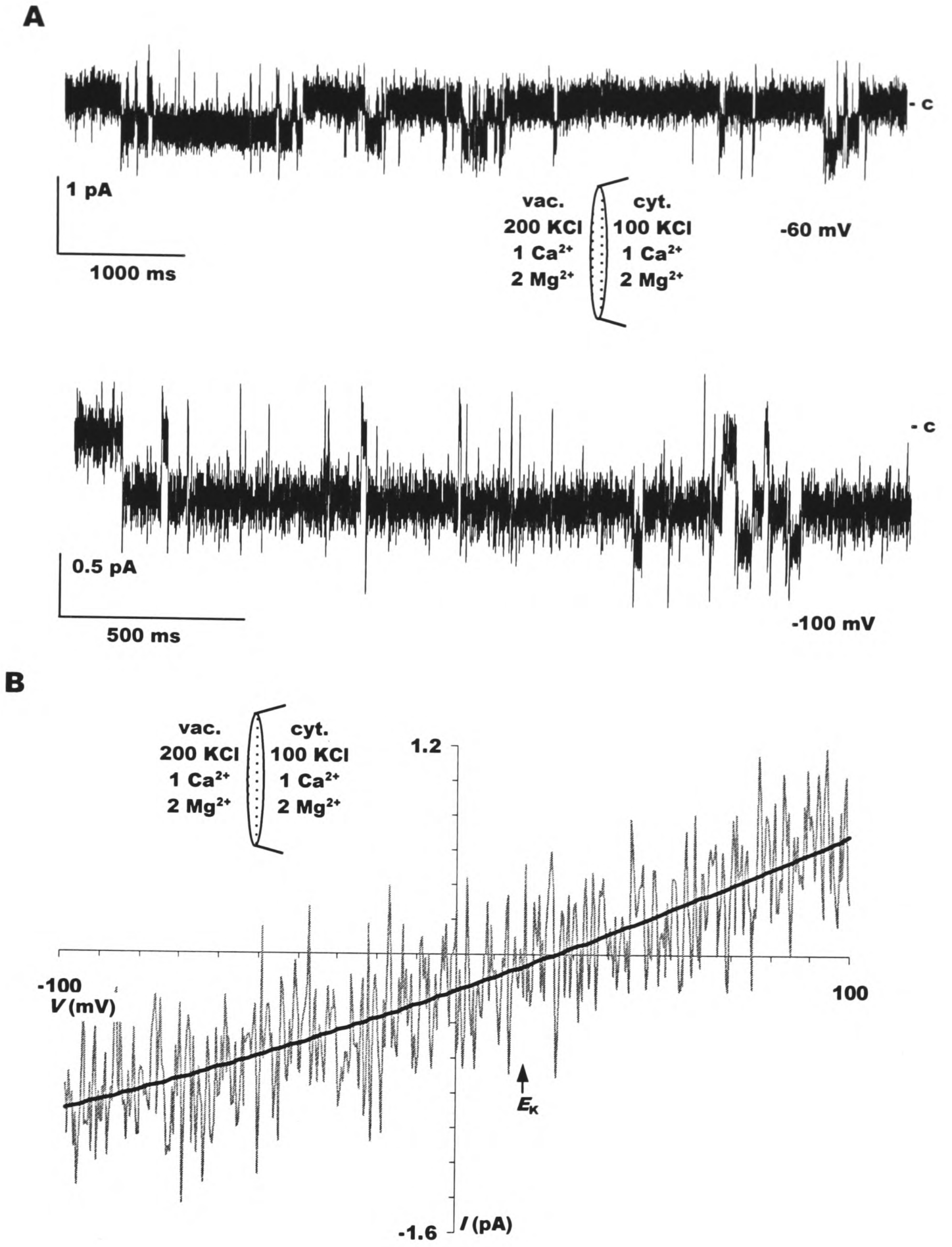


Figure 6.12. Single-channel activity of KVIH3 with asymmetric 200 mM KCl. **A**) Vacuolar-side-out recording with 200 mM KCl on the vacuolar side at -60 and -100 mV (solution G; cyt. 100 mM KCl, solution E). The closed state is indicated by (c). **B**) Current-voltage plot constructed from a voltage ramp (-100 mV to +100 mV in 25 ms). The Nernst potential for K^+, E_K, is indicated. The cartoons show concentrations in mM

A different channel type was observed in a single patch (Figure 6.13). It showed a flickering behaviour at very positive and negative membrane potentials. In asymmetric 200/100 mM KCl solutions, the reversal potential was again close to E_K (Figure 6.13.B). Similarly, without a K^+ gradient, but with a 10/100 mM Cl^- gradient, the reversal potential was close to 0 mV, indicating a very high K^+ over Cl^- selectivity (Figure 6.13.C). With steep outwardly directed K^+ gradients, the reversal potential was shifted negative accordingly (Figure 6.13.D, E). In 100 mM KCl, the channel had a slope conductance of about 130 pS between +30 and +50 mV. This channel will be referred to as KVIH4.

Another type of single channel showed strong outward rectification and slow activation. Figure 6.14 shows a typical recording. Single-channel activity could only be observed at positive membrane potentials and the number of open channels increased over a time course of 2 s from 0 to up to 5. The slope conductance was 61 pS (Figure 6.14.B). A multitude of this type of channel was usually seen in larger macropatches, making single-channel analysis difficult. However, this channel type was only observed in three small excised patches, and no measurements could be performed under asymmetric conditions. The larger conductance seen in Figure 6.8 might also be attributed to this type of channel, but was difficult to quantify due to high noise level. This type of channel will be referred to as ORH1 (for outward rectifying, high Ca^{2+}).

An indication of selectivity of ORH1 was obtained from a macropatch recording shown in Figure 6.15. A large cytosolic-side-out patch was initially perfused with 100 nM Ca^{2+}/ 4 mM KCl solution (with 100 mM KCl in the pipette). Apart from some current spikes at very negative potentials, no single-channel activity could be

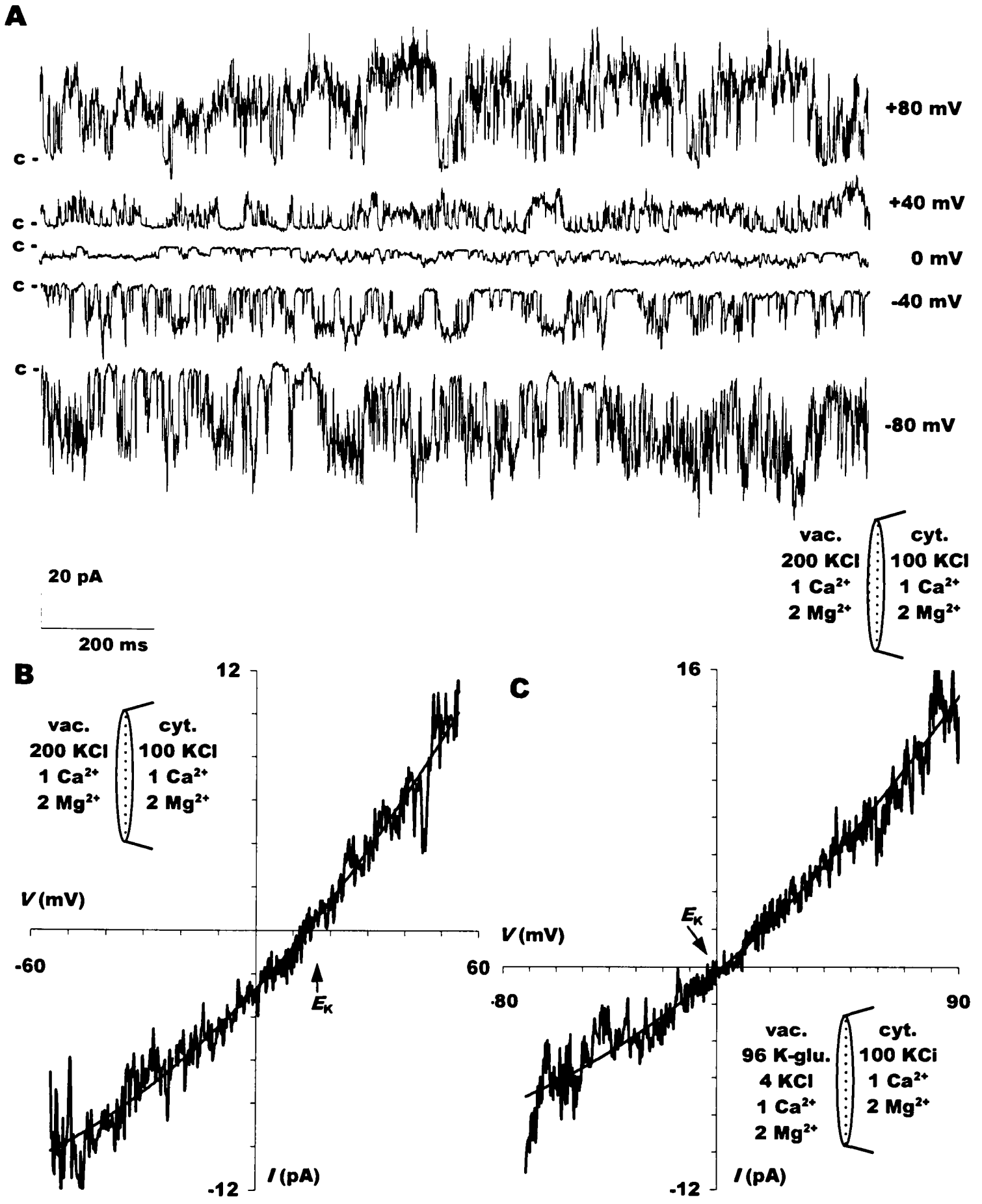


Figure 6.13. The large-conductance, voltage-independent channel KVIH4. **A**) Vacuolar-side-out recordings with asymmetric KCl concentrations (cyt.: 100 mM KCl, solution E; vac.: 200 mM KCl, solution G). The closed state is indicated by (c). **B,C**) Current-voltage plots constructed from voltage ramps (0 mV to +100 mV and 0 mV to -100 mV in 25 ms). **B**) 200 mM KCl on the vacuolar side (solution G). **C**) 100 mM K^+ / 10 mM Cl^- on the vacuolar side (solution I). The Nernst potential for K^+, E_K, is indicated. The cartoons show concentrations in mM. Figure continued on the following page

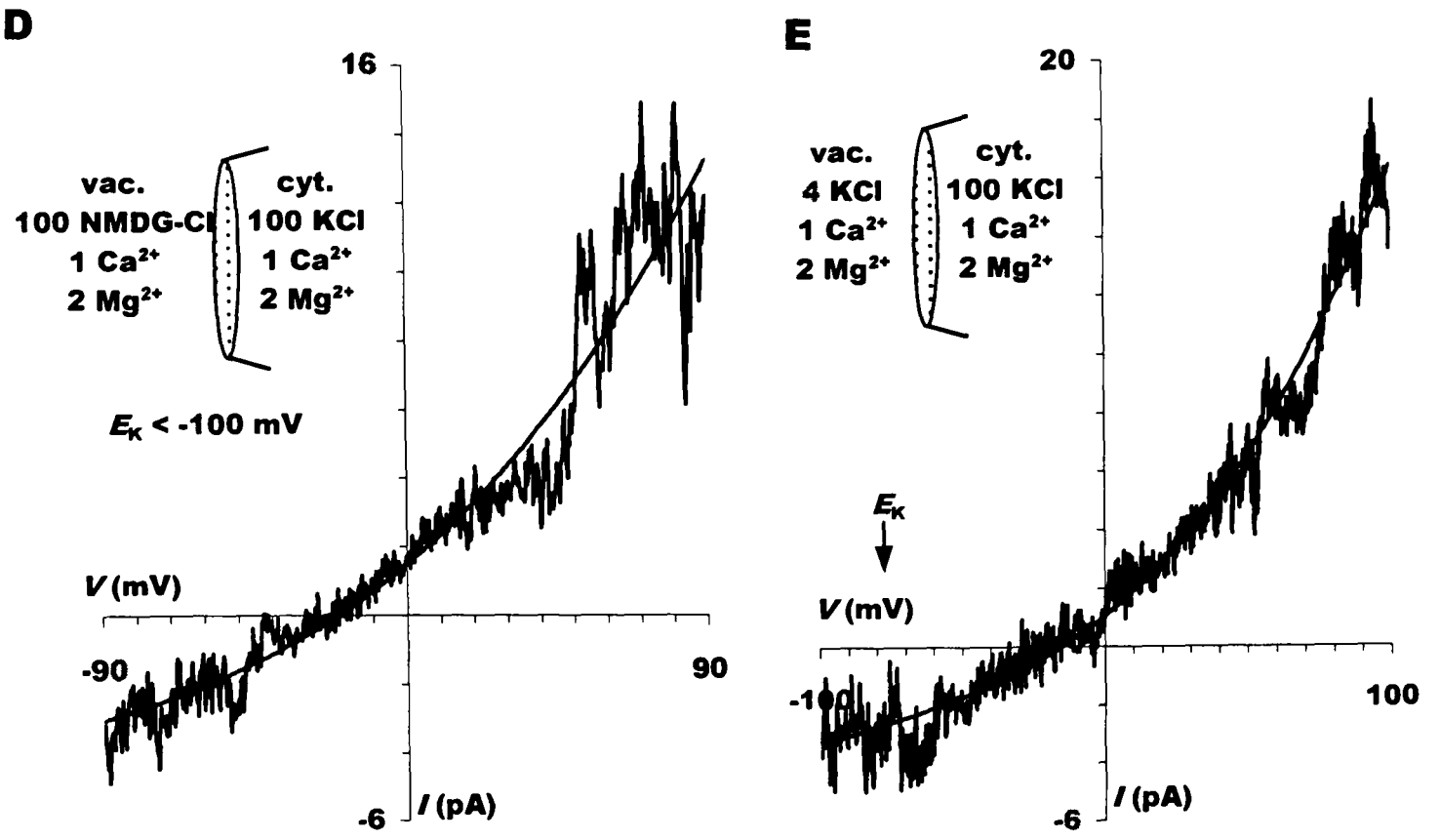


Figure 6.13. Continued from previous page. **D, E, F**) Current-voltage plots constructed from voltage ramps (0 mV to +100 mV and 0 mV to -100 mV in 25 ms). **D**) 100 mM NMDG-Cl on the vacuolar side (solution H). **E**) 4 mM KCl on the vacuolar side (solution F). **F**) 100 mM KCl on the vacuolar side (solution E). The Nernst potential for K^+, E_K, is indicated. The cartoons show concentrations in mM

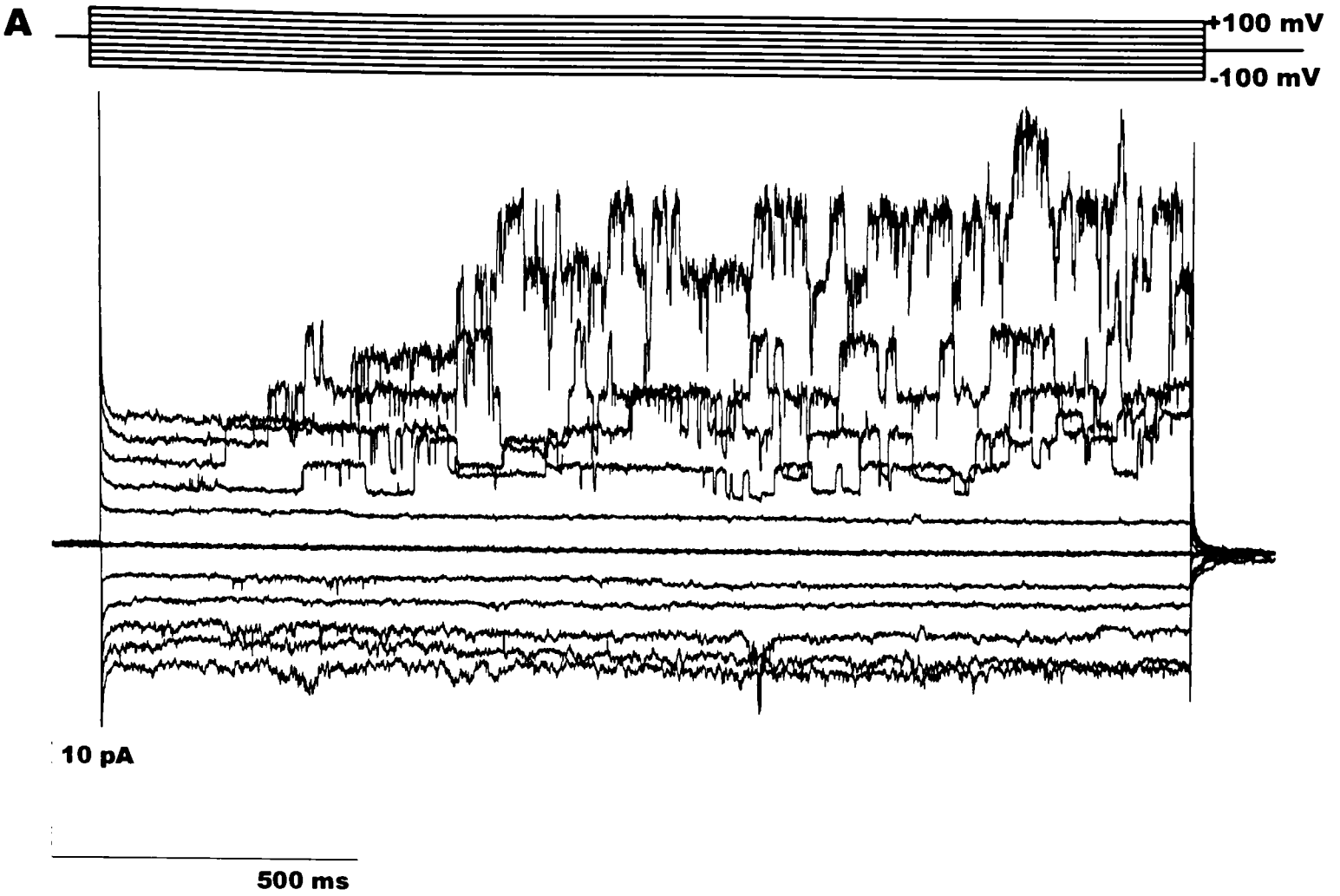


Figure 6.14. Single-channel recordings of the time-dependent outward rectifier ORH1. **A**) Vacuole-attached recording with 100 mM KCl (solution E) in pipette and bath. From a holding potential of 0 mV, the membrane potential was stepped to values between -100 mV and +100 mV with increments of 20 mV. **B**) Current-voltage plot of the current amplitudes in part A (○) and from similar recordings in the vacuolar-side-out configuration (❑). The line is a straight-line fit to the data

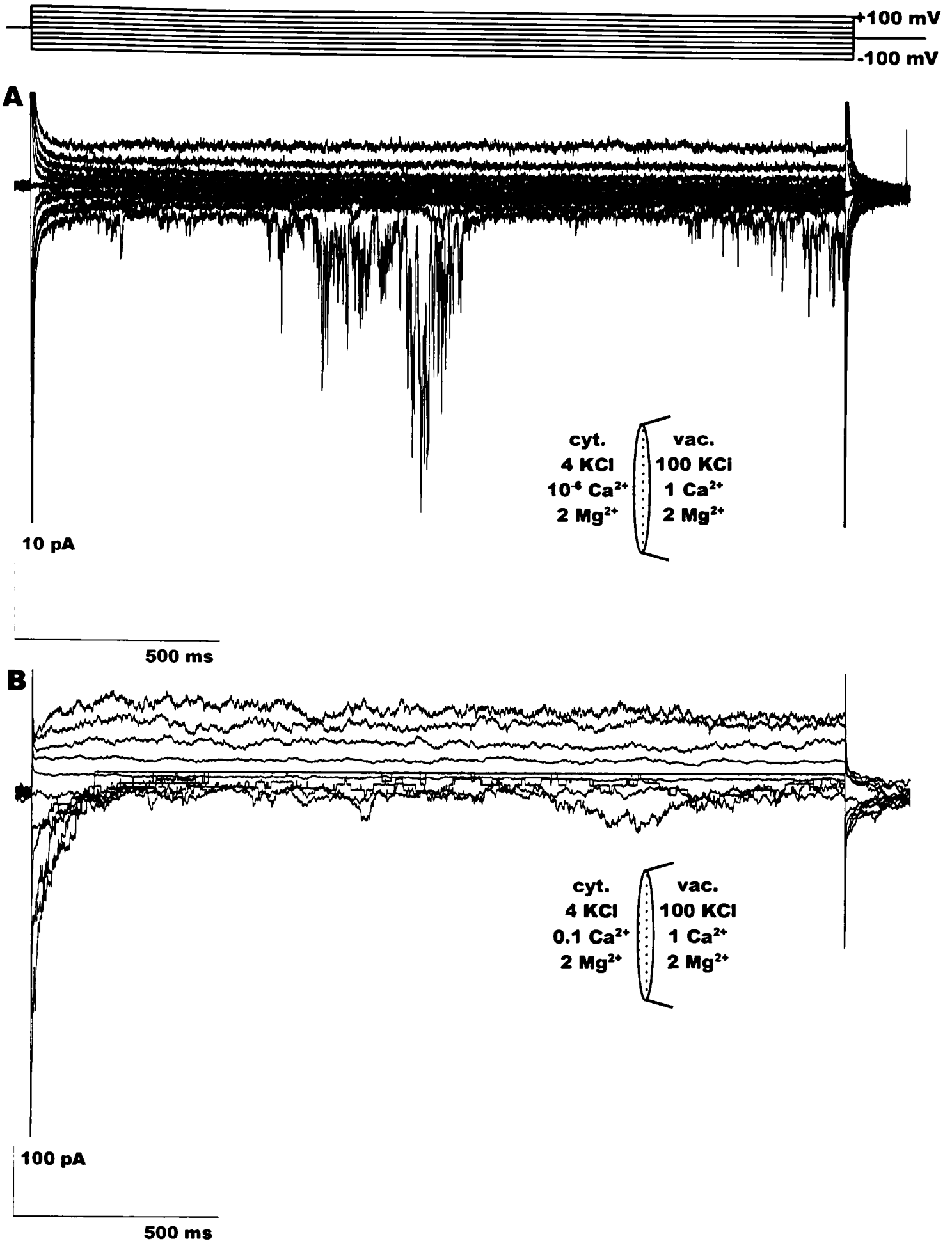


Figure 6.15. Cytoplasmic-Ca^{2+} dependence of single-channel activity. **A**) Macropatch in the cytoplasmic-side-out configuration perfused with 4 mM KCl and 100 nM Ca^{2+} (solution P), with 100 mM KCl (solution E) at the vacuolar side. **B**) The cytoplasmic side was perfused with 4 mM KCl and 0.1 mM Ca^{2+} (as solution F, but only 0.1 mM Ca^{2+} added). The cartoons indicate concentrations in mM. Note the differences in scale

observed. After increasing the cytosolic Ca^{2+} concentration to 0.1 mM, a large number of channels could be observed (Figure 6.15.B, Figure 6.16), which generated large, inactivating inward currents at negative membrane potentials and slowly activating outward currents at positive potentials. Voltage ramps under these conditions revealed two distinct conductances. The most prominent had a slope conductance around 199 pS under these conditions at potential more negative than -40 mV and could be seen in 22 out of 25 ramps (Figure 6.17.B). A similar conductance could also be extracted from the single-channel amplitudes of the currents in Figure 6.14. During three ramps, a smaller conductance could be observed with a slope conductance of 99 pS at negative membrane potentials (Figure 6.17.A). The reversal potentials could not be accurately determined, since at potentials positive of -20 mV a large number of channels opened. While the negative part of the ramp was linear, it had to be assumed that the current-voltage relationship becomes asymptotic at positive membrane potentials due to the highly asymmetric KCl gradient. However, it could be assumed that the macroscopic currents observed above -20 mV were mainly comprised of the large conductance channel, and to some extent by the smaller conductance, with the leak currents subtracted. Therefore, the macroscopic reversal potential of around +30 mV should be close to the single-channel reversal potential, indicating a high selectivity for K^+ over Cl^-. Which of the two conductances observed in these recordings could be attributed to ORH1 remains uncertain, but is likely to be the larger conductance of 199 pS given its high abundance. The 99 pS conductance will be referred to as ORH2.

Although a number of different channel types were thus observed in the patch-clamp recordings of the vacuolar membrane of *M. crystallinum*, no channel showing

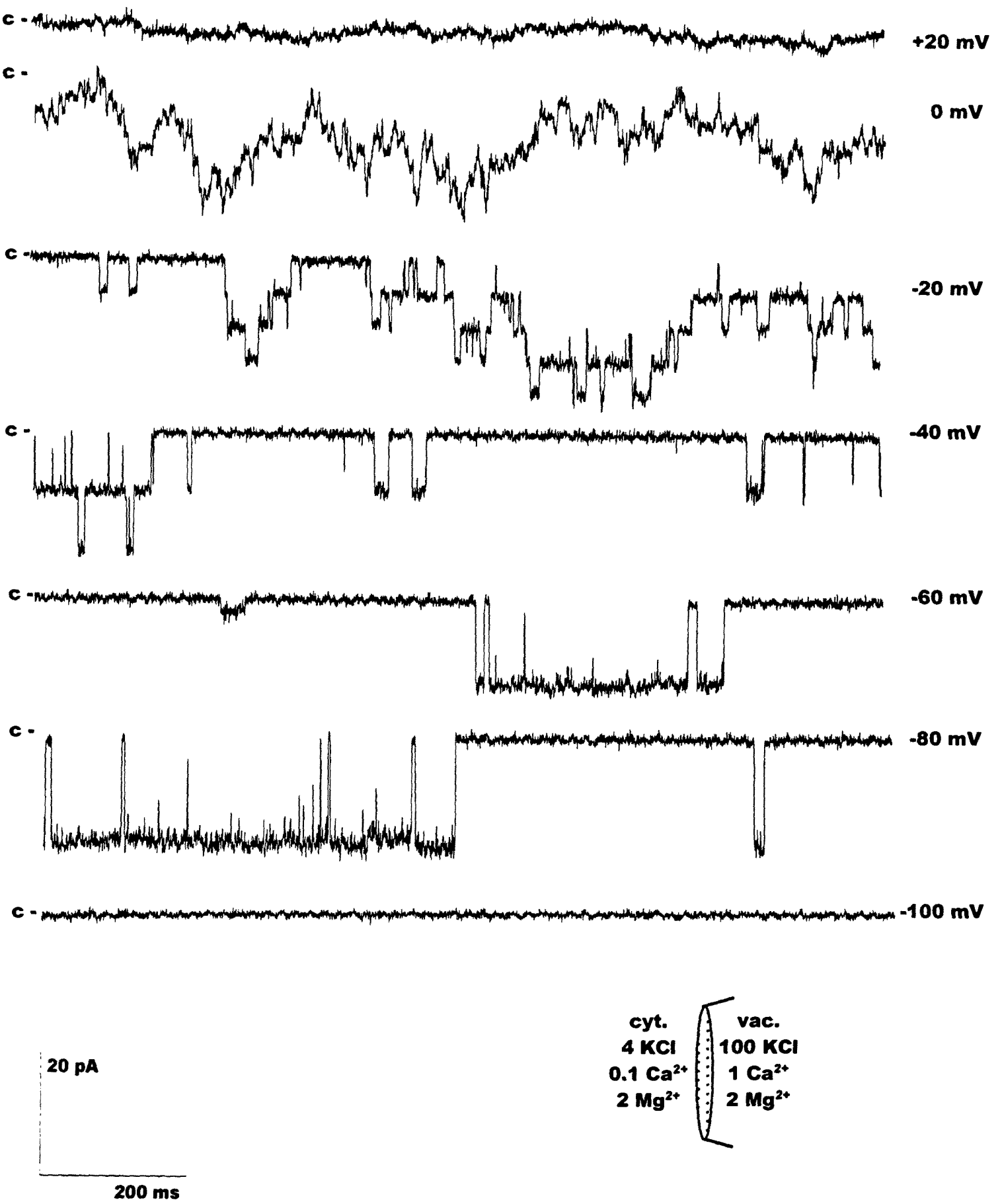


Figure 6.16. Single-channel recordings after changing from low (100 nM) to high (0.1 mM) cytoplasmic Ca^{2+} (see Figure 6.15). The currents were recorded in 4 mM KCl (co, solution F, but with 0.1 mM Ca^{2+}), with 100 mM KCl (solution E) on the vacuolar side. The membrane potential was stepped from a holding potential of -60 mV to the values indicated. The closed states are indicated by (c). The cartoon indicates concentrations in mM

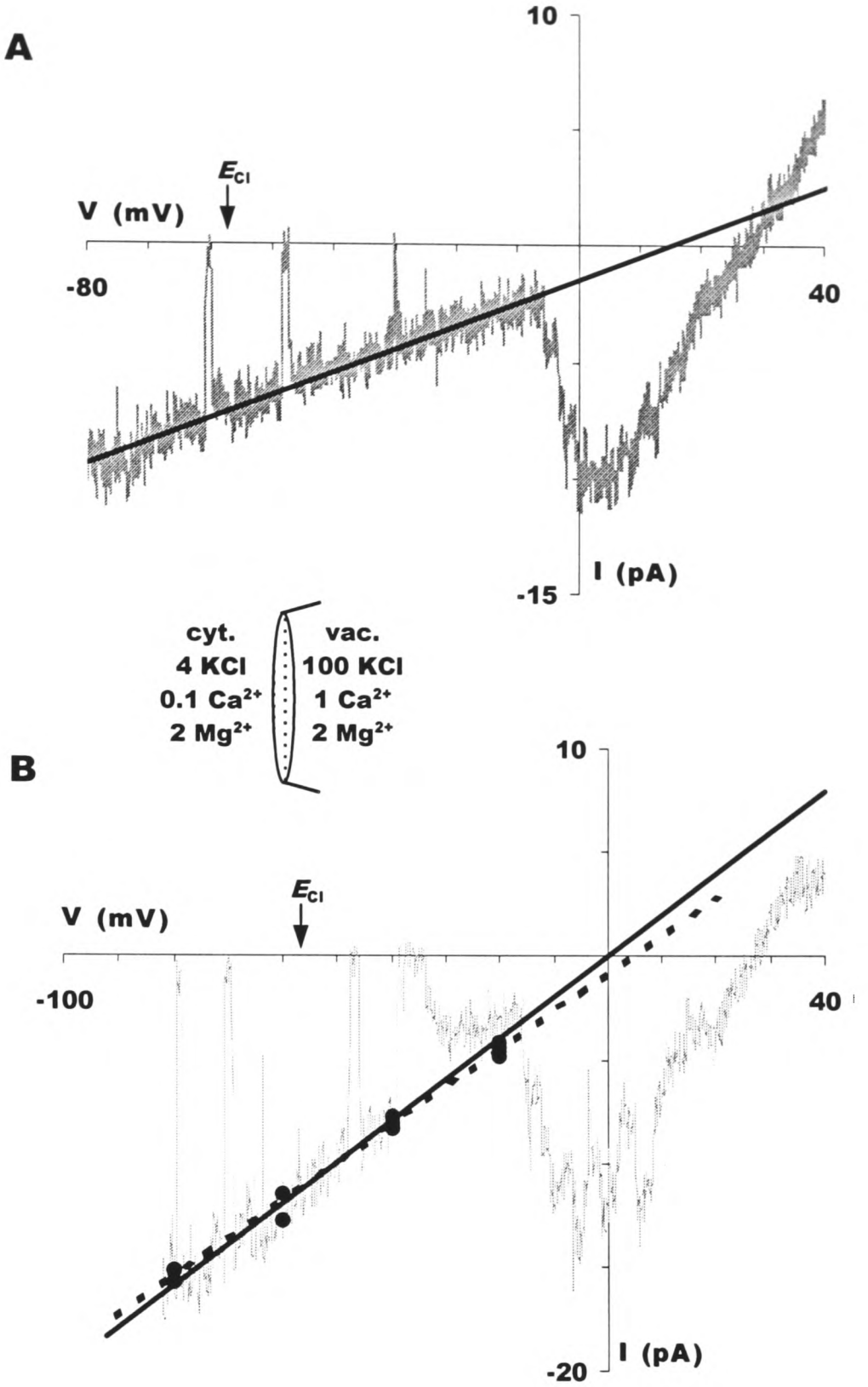


Figure 6.17. Single-channel current-voltage plots of the Ca^{2+}-activated currents (see Figure 6.15). Two distinct current amplitudes were observed (**A**,**B**). Voltage ramps were stepped from -100 mV to +100 mV in 750 ms (immediately from the holding potential of 0 mV). Leak currents were subtracted, and above potentials of -20 mV a drastic increase in the current amplitude was observed in all recordings due to the opening of a multitude of channels. The single-channel ramp was therefore fitted with a straight line below -20 mV and extrapolated (solid line) to obtain the reversal potential. In **B**) the single-channel amplitudes obtained from Figure 6.16 are plotted and fitted with a straight line (dashed line). The Nernst potential for Cl^-, E_{Cl}, is indicated. The cartoon indicates concentrations in mM

clear Cl^- selectivity could be found. Table 6.1 gives a summary of all types of channels found.

6.2.2.3 Whole-vacuole recordings with 1 µM free cytosolic Ca^{2+}

With free Ca^{2+} of about 1 µM on the cytosolic side of the membrane, large outward-rectifying currents could be observed (Figure 6.18), similar to the macroscopic currents seen with 1 mM free Ca^{2+} (Figure 6.4). These currents were slowly activating over a time course of about 1 s, and were only seen at membrane potentials above 20 mV in symmetrical 100 mM KCl solutions. The instantaneous currents also showed a slight outward-rectification at very positive membrane potentials. Changing to asymmetric solutions with 200 mM KCl on the cytosolic side did not alter the instantaneous currents (Figure 6.18.B and Figure 6.19.A). In contrast, the activation of the time-dependent currents seemed to be shifted towards positive potentials, and the voltage for half-maximal activation could be calculated for 200 mM KCl to be 98 mV. The outward-current amplitudes were much smaller in 200 mM KCl, being only 40% of those observed in 100 mM KCl at +140 mV.

The ionic selectivity of the time-dependent outward current was determined by tail-current recordings in asymmetric solutions. As Figure 6.20.A shows, 200 mM KCl on the cytosolic side gave a reversal potential close to the predicted E_K of -16.4 mV. Similarly, changing to 4 mM KCl (Figure 6.20.B) shifted the reversal potential positive to +35 mV. This indicated a high selectivity for K^+ over Cl^- for this slowly activating outward current.

In five whole-vacuolar recordings, regular current oscillations occurred at positive membrane potentials, usually immediately after obtaining the whole-vacuole configuration. Figure 6.21.A shows a typical recording in symmetrical 100 mM KCl

Table 6.1. Summary of all channel types observed

Name	Conductance	Selectivity	Voltage range[a]	Cyt. Ca^{2+}	KCl (mM)[b]	*n*[c]	Figure[d]	Remarks
KVIH1	35 pS	K^+	-/+	1 mM	100	5	9	
KVIH2	98 pS	K^+	-/+	1 mM	200	1	10	
KVIH3	10 pS	K^+	-/+	1 mM	100	3	11	
KVIH4	130 pS	K^+	-/+	1 mM	100	1	13	
ORH1	61 pS	K^+(?)	+	1 mM	100	3	14	slow activating
ORH1 (?)	199 pS	K^+(?)	(-)/+	0.1 mM	4	1	17	cyt. out
ORH2	99 pS	K^+(?)	(-)/+	0.1 mM	4	1	17	cyt. out
LOR1	170 pS	K^+ (Cl^-?)	+	1 µM	200	1	32	
KVI1	7 pS	K^+ (Ca^{2+})	-/+	1 µM	200	2	35	
KVI2	2-3 pS	K^+ (Ca^{2+})	-/+	1 µM	200	2	35	
KS1	108 pS	K^+	-/+	1 µM	200	5	39	after depol.
KS2	86 pS	K^+	-/+	1 µM	200	1	42	after hyperpol.

[a] Voltage range over which channel was active
[b] Bath solution in which the slope conductance was determined, with 100 mM KCl in the pipette and vacuolar-side-out configuration unless otherwise stated
[c] Number of observations
[d] Figure number in this chapter

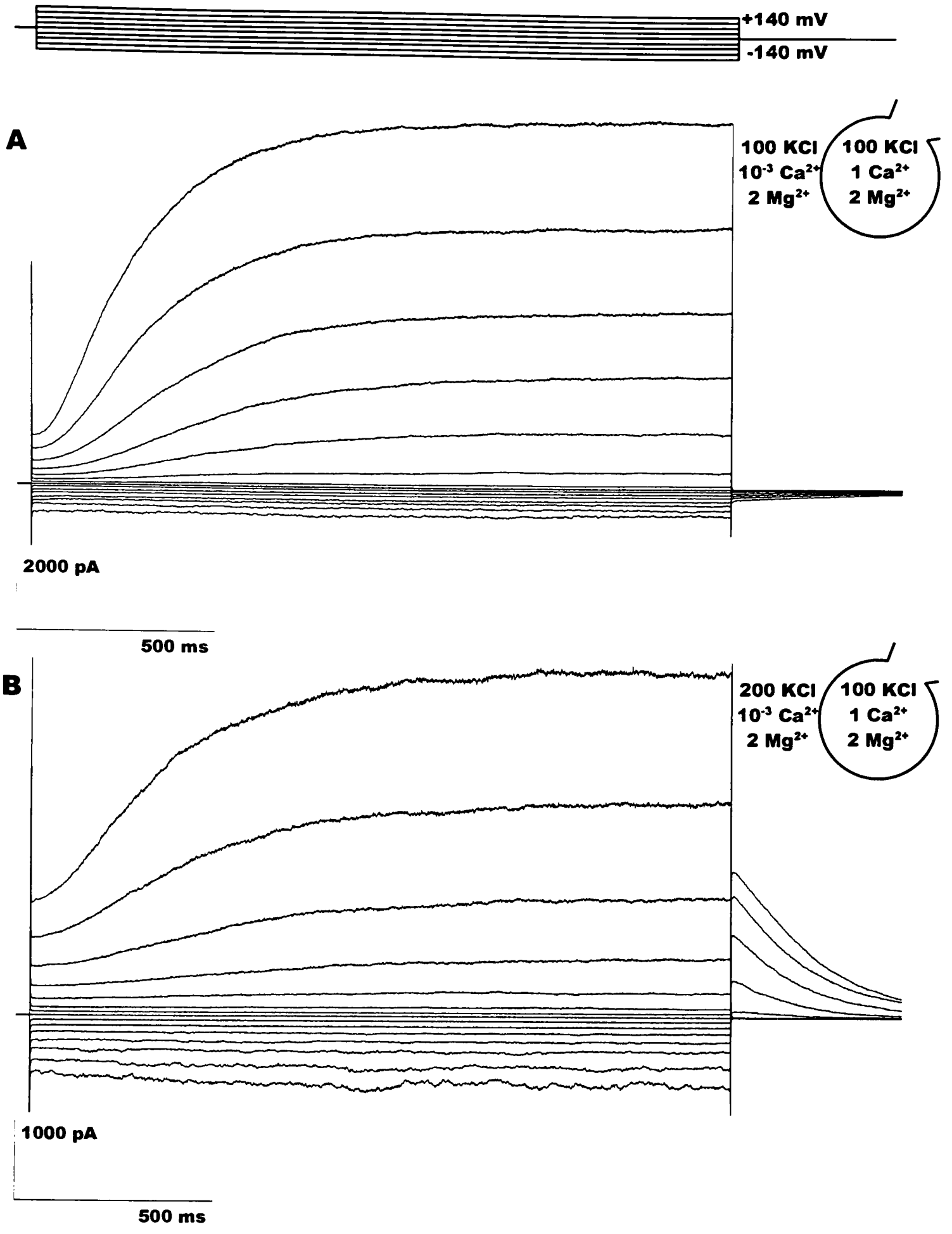


Figure 6.18. Whole-vacuole currents during voltage steps from -140 to +140 mV at 1 μM cytoplasmic Ca^{2+} (~60 μm vacuole diameter). **A**) 100 mM KCl in bath (solution J) and pipette (solution E). **B**) Bath solution changed to 200 mM KCl (solution L). The cartoons indicate concentrations in mM

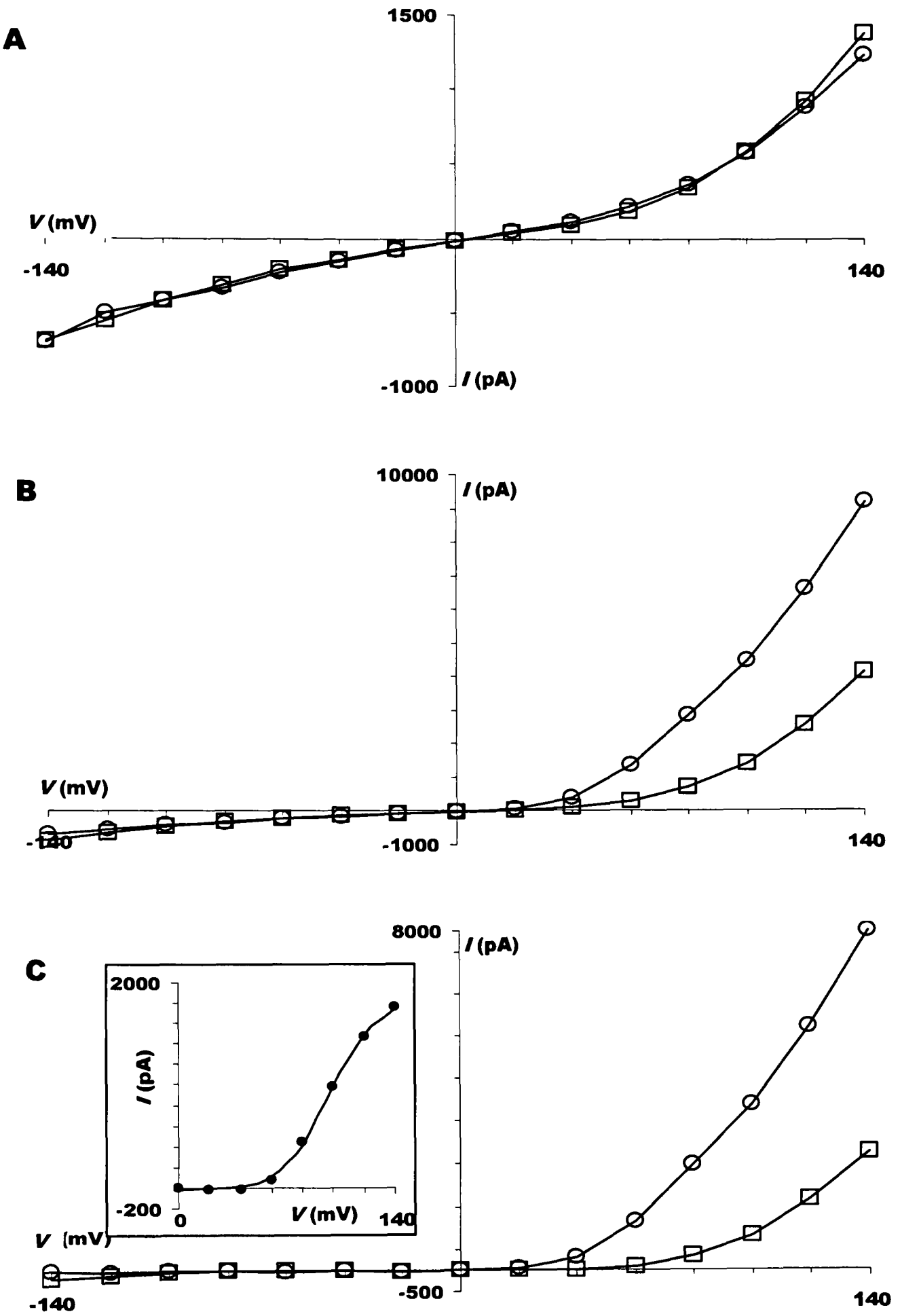


Figure 6.19. Current-voltage plot for the currents in Figure 6.18. The instantaneous currents (**A**), steady-state currents (**B**) and the difference between steady-state and instantaneous currents (**C**) were plotted against the membrane potential. Symbols: 100 mM KCl (○), 200 mM KCl (❑). The inset in part C shows the activation curve in 200 mM KCl. It was derived from the remaining currents after the end of the test pulse, plotted against the voltage during the test pulse. The line is a best fit to a Boltzmann function $I = (I_{max} - I_{min})/(1 + \exp((V_{½} - V)/k))) + I_{min}$ to the data, with a maximum current I_{max} of 1842 pA, a minimum current I_{min} of -15 pA, a voltage for half-maximal activation $V_{½}$ of 98 mV and a constant k of 14.9 mV

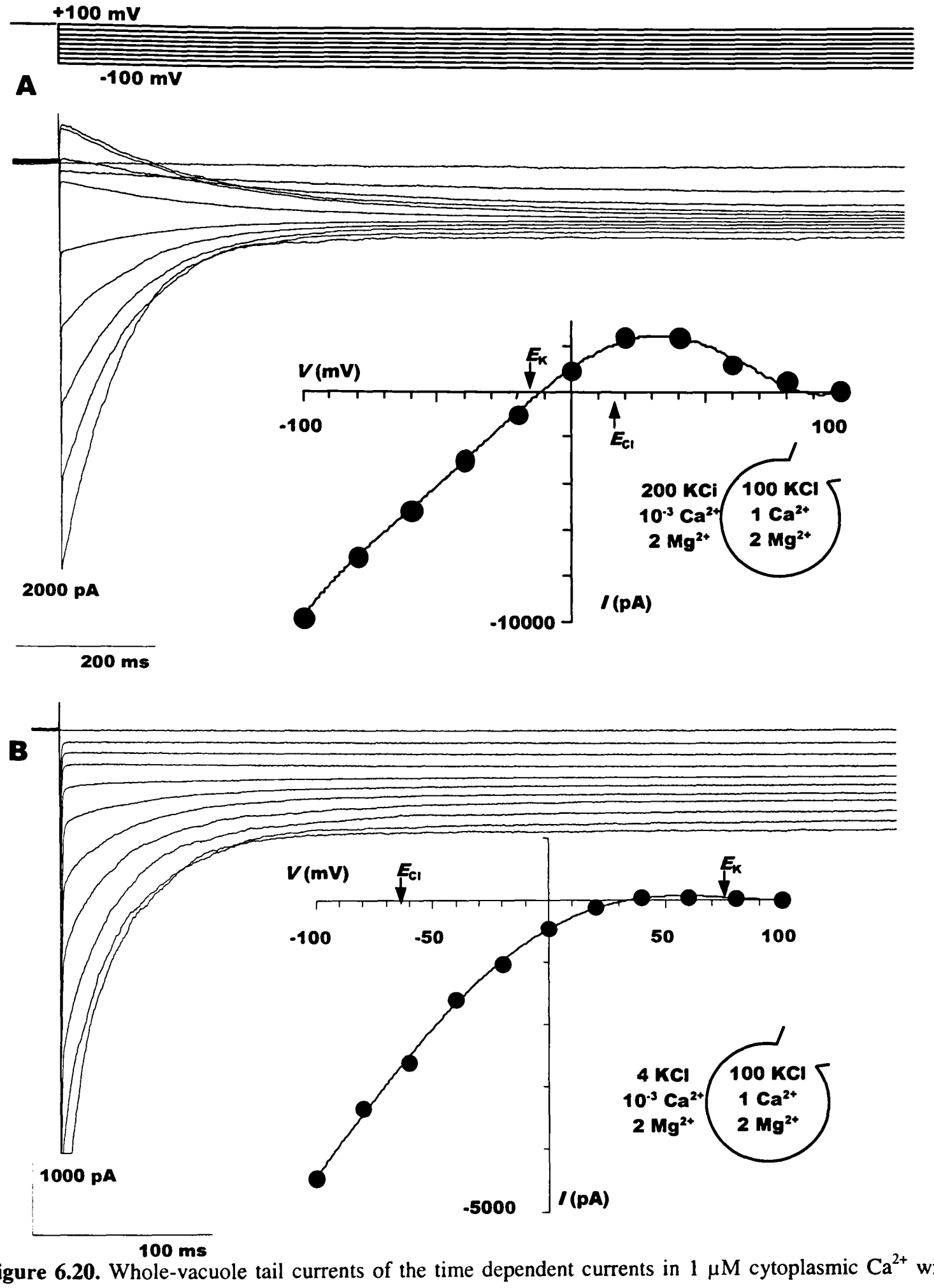


Figure 6.20. Whole-vacuole tail currents of the time dependent currents in 1 μM cytoplasmic Ca^{2+} with asymmetric KCl concentrations (with 100 mM KCl on the vacuolar side, solution E). **A**) 200 mM KCl on the cytoplasmic side (solution L). **B**) 4 mM KCl on the cytoplasmic side (solution K). Tail currents were obtained after stepping from a +100 mV prepulse (5 s) to membrane potentials ranging from -100 to +100 mV. Current-voltage plots were constructed after subtracting the steady-state current from the initial current, as derived from fitting the traces with single exponentials. The Nernst potentials for K^+, E_K, and Cl^-, E_{Cl}, were as shown. The cartoons indicate concentrations in mM

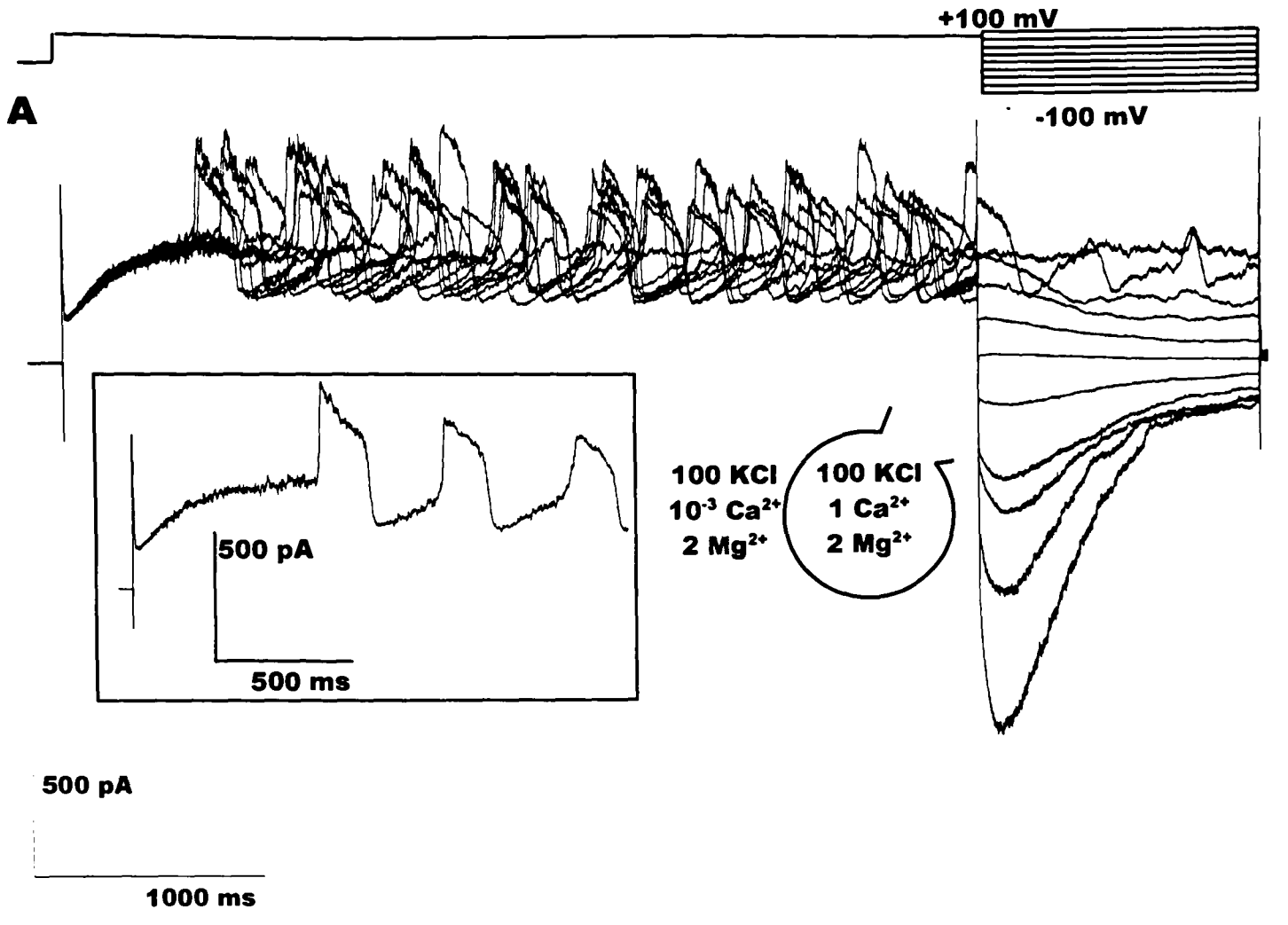


Figure 6.21. Current oscillations during tail-current recordings (vacuole diameter ~50 μm). **A)** Whole-vacuole current oscillations immediately after breaking the seal in symmetrical 100 mM KCl (cytoplasmic side: solution J; vacuolar side: solution E). The inset shows a single trace with three individual spikes. **B)** Whole-vacuolar recordings 17 min after seal break. No further oscillations were observed. The cartoons indicate concentrations in mM

solutions. At membrane potentials of +100 mV, initially a slowly activating outward current appeared. About 0.5 to 1 s after the onset of the command pulse, a sudden outward-current jump of about 500 pA occurred. The current slowly decreased over the course of a few hundred ms and then suddenly fell again by about 500 pA. This type of oscillation had a periodicity around 1 Hz. The tail-currents recorded in the presence of current oscillations did not show a sharp onset, but took several hundred ms to peak. These oscillations were usually rather ephemeral and disappeared within a few minutes of recording.

Figure 6.21.B shows the tail-current recordings after the current oscillations had disappeared. The inwardly directed tail currents at negative membrane potentials showed a sharp onset, were of much larger amplitude and showed a single exponential time course. At positive test pulses of +20 mV and +40 mV the tail-current amplitude was actually considerably larger than the amplitude during the activating pulse of +100 mV (see also Figure 6.20.A), a prominent feature that was seen in all similar recordings. As the current-voltage plots of the tail currents show (Figure 6.22), the time-dependent outward current was highly selective for K^+ over Cl^-, following closely the Nernst potential for K^+, similar to Figure 6.20. The following section will characterise the outward-current oscillations in more detail.

6.2.2.4 Whole-vacuolar-current oscillations observed with 1 µM free Ca^{2+}

This section will describe a variety of recordings of a single vacuole in different solutions during which outward-current oscillations were observed. Figure 6.23 shows a series of recordings in different solutions, in order of perfusion. Immediately after going from the vacuole-attached to the whole-vacuole configuration in symmetrical 100 mM KCl, regular oscillations could be seen at +100 mV (Figure

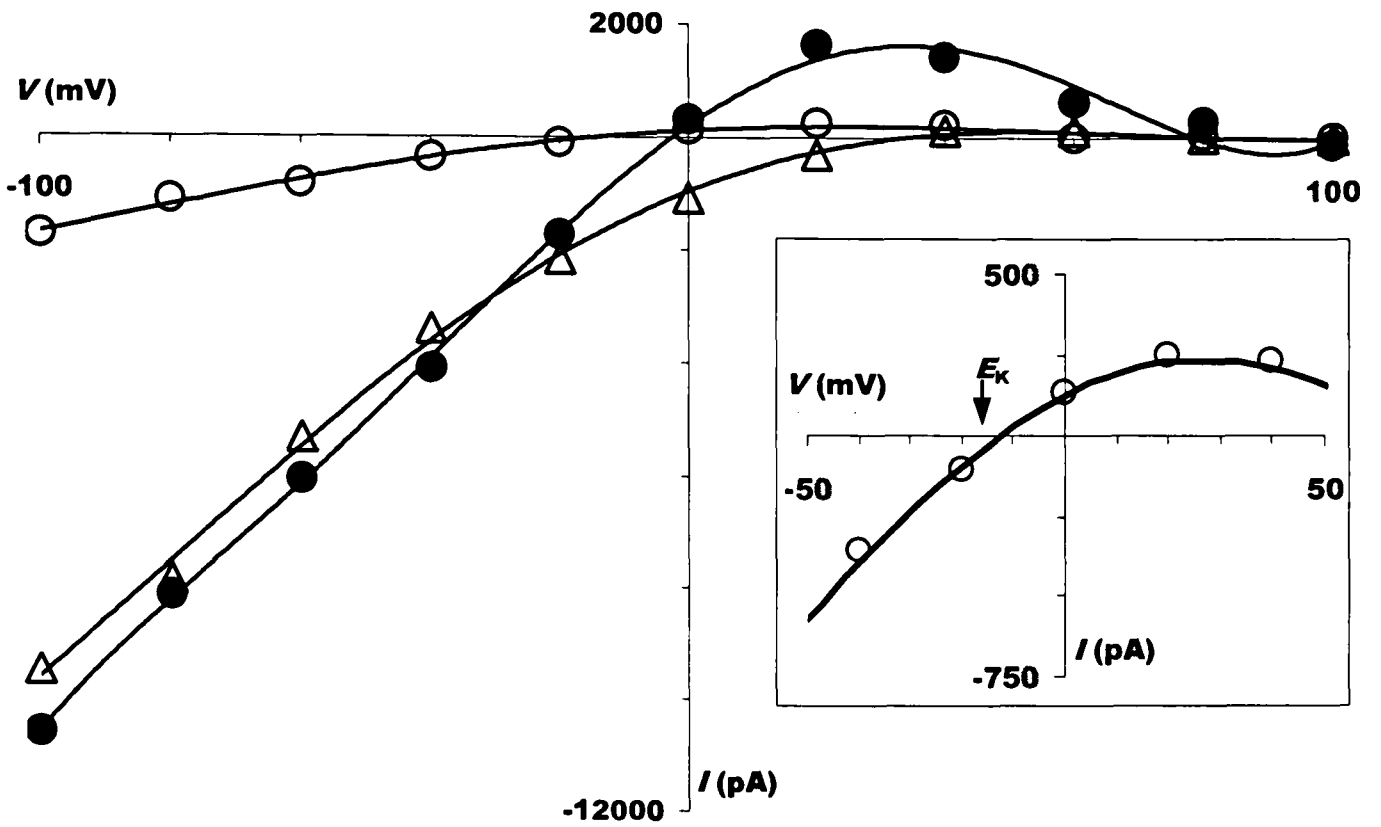


Figure 6.22. Current-voltage plots of tail currents after current oscillations had disappeared (see Figure 6.21). Symbols: 100 mM KCl (●, solution J), 200 mM KCl (○, solution L), 4 mM KCl (Δ, solution K) on the cytoplasmic side, with 100 mM KCl (solution E) on the vacuolar side. Inset shows the 200 mM KCl plot on a larger scale. Tail-currents were obtained after stepping from a +100 mV pre-pulse to membrane potentials ranging from -100 to +100 mV. Current-voltage plots were constructed after subtracting the steady-state current from the initial current, as derived from fitting the traces with single exponentials. The data points were fitted with higher-order polynomials

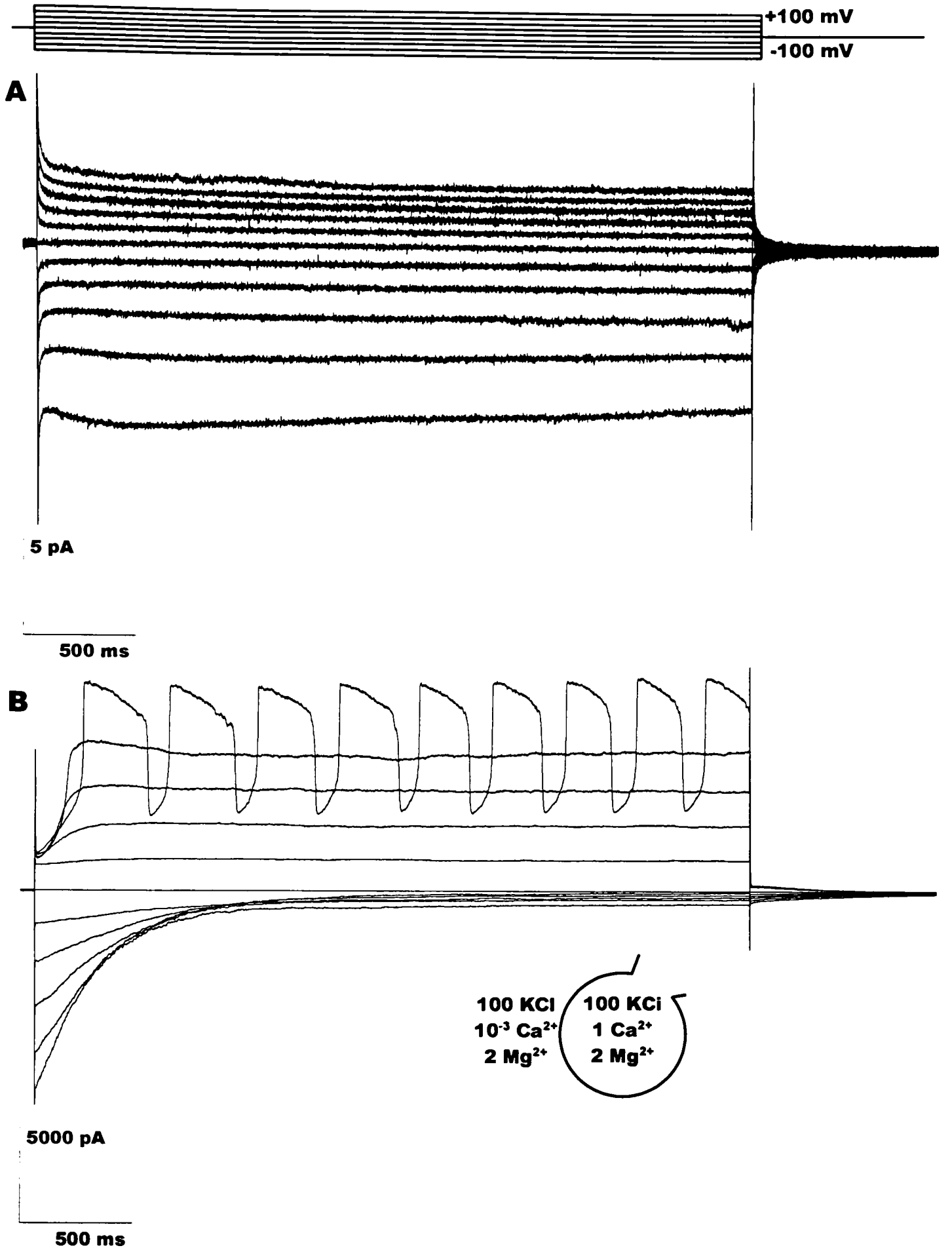


Figure 6.23. Series of recordings from one vacuole (~80 μm diameter) during which current oscillations were observed. The pipette contained 100 mM KCl (solution E), and the bath was continuously perfused with various KCl concentrations and 1 μM free Ca2+. The holding potential was 0 mV for all recordings. The cartoons indicate concentrations in mM. **A**) Vacuole-attached recording with 100 mM KCl in the bath (solution J). **B**) Whole-vacuolar currents immediately after seal break, in 100 mM KCl (solution J). R_s had not been compensated. Figure continued on the following page

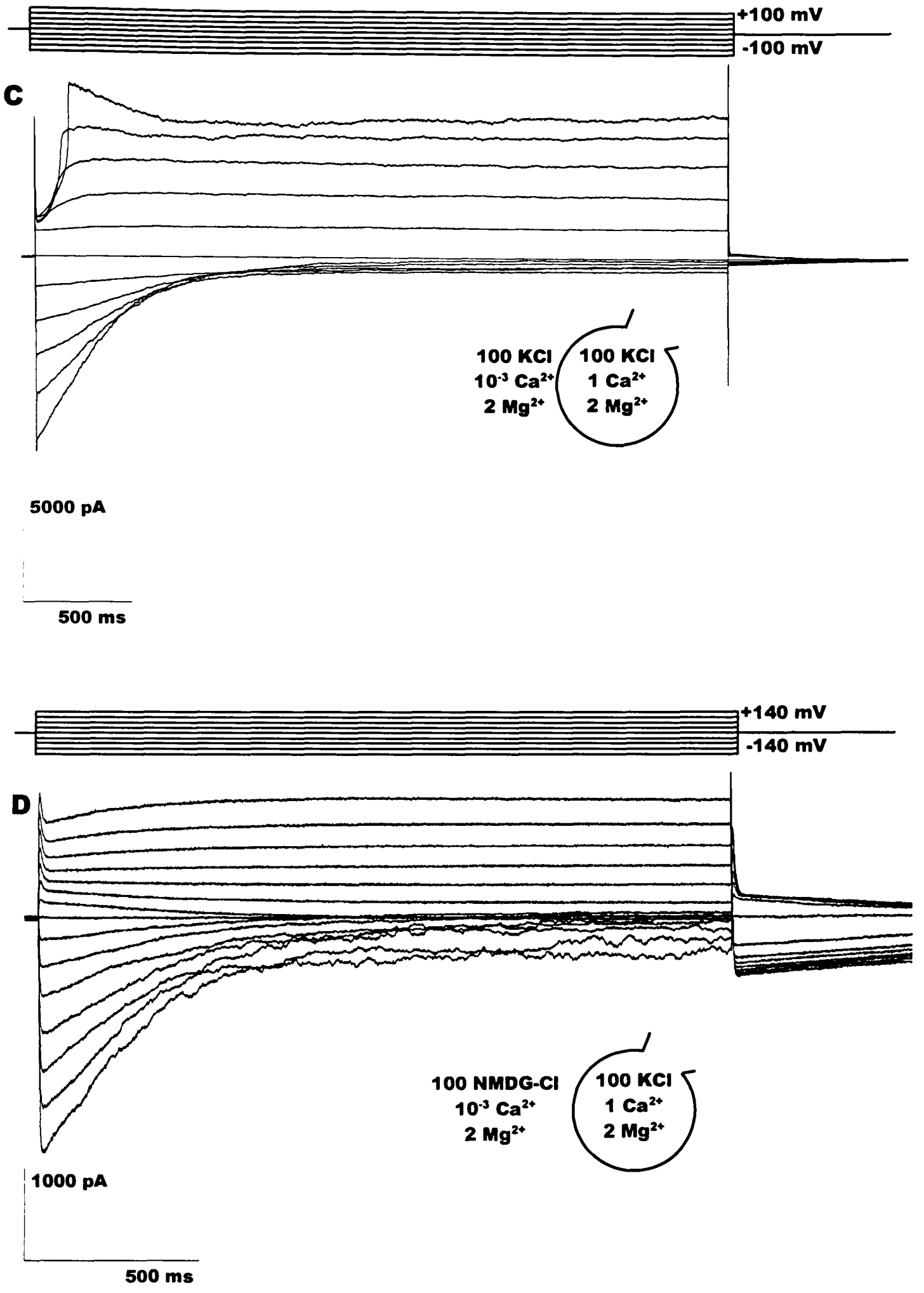


Figure 6.23. Continued from previous page. C) Whole-vacuolar currents 3 min after seal break, in 100 mM KCl (solution J). R_s of 3 MΩ was compensated by 50%. D) Whole-vacuolar currents 54 min after seal break, perfused with 100 mM NMDG-Cl (solution M). Figure continued on the following page

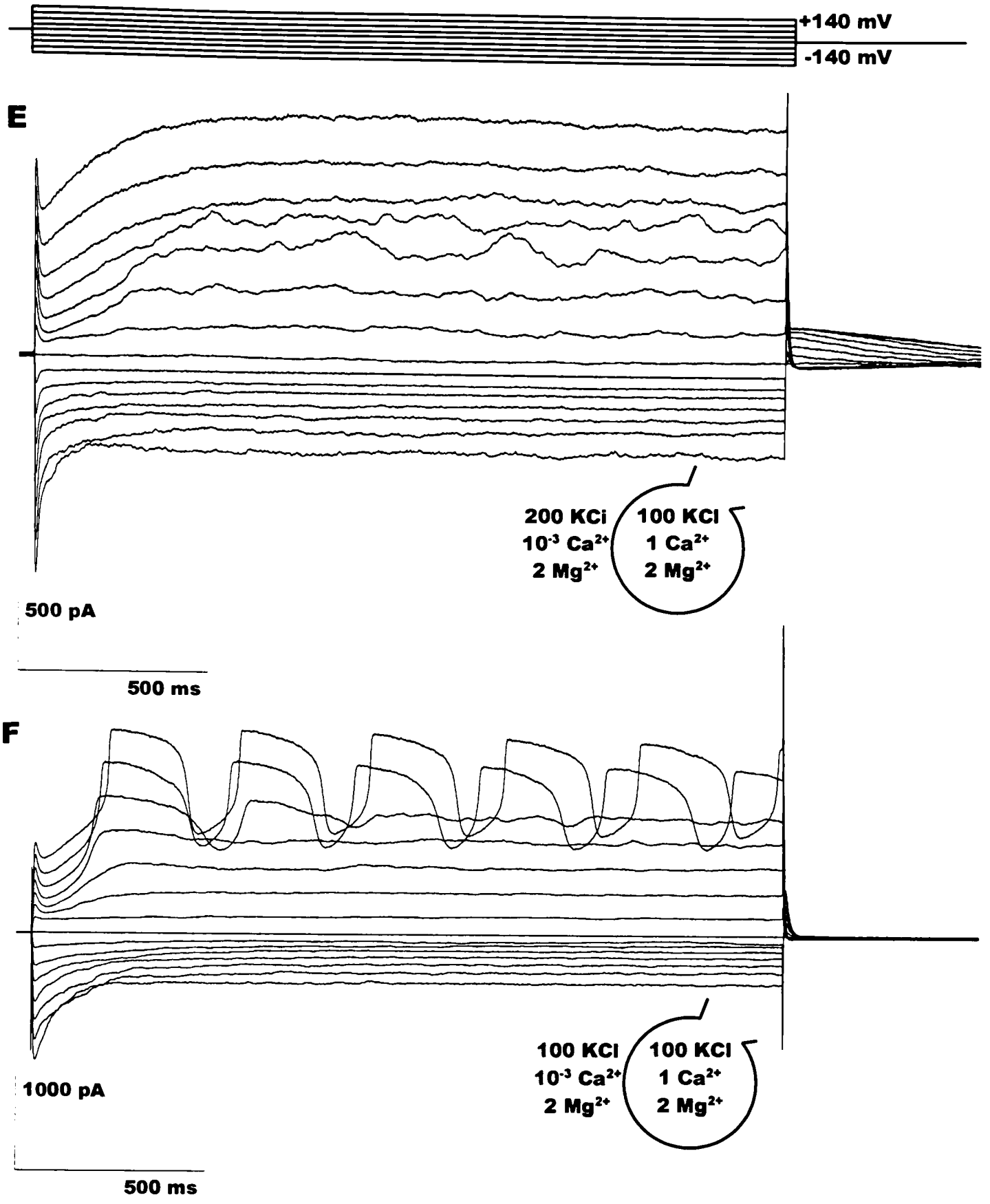


Figure 6.23. Continued from previous page. **E)** Whole-vacuolar currents 69 min after seal break, perfused with 200 mM KCl (solution L). **F)** Whole-vacuolar currents 84 min after seal break, changed back to 100 mM KCl (solution J). R_s had increased to 25 MΩ, and was 50% compensated. Figure continued on the following page

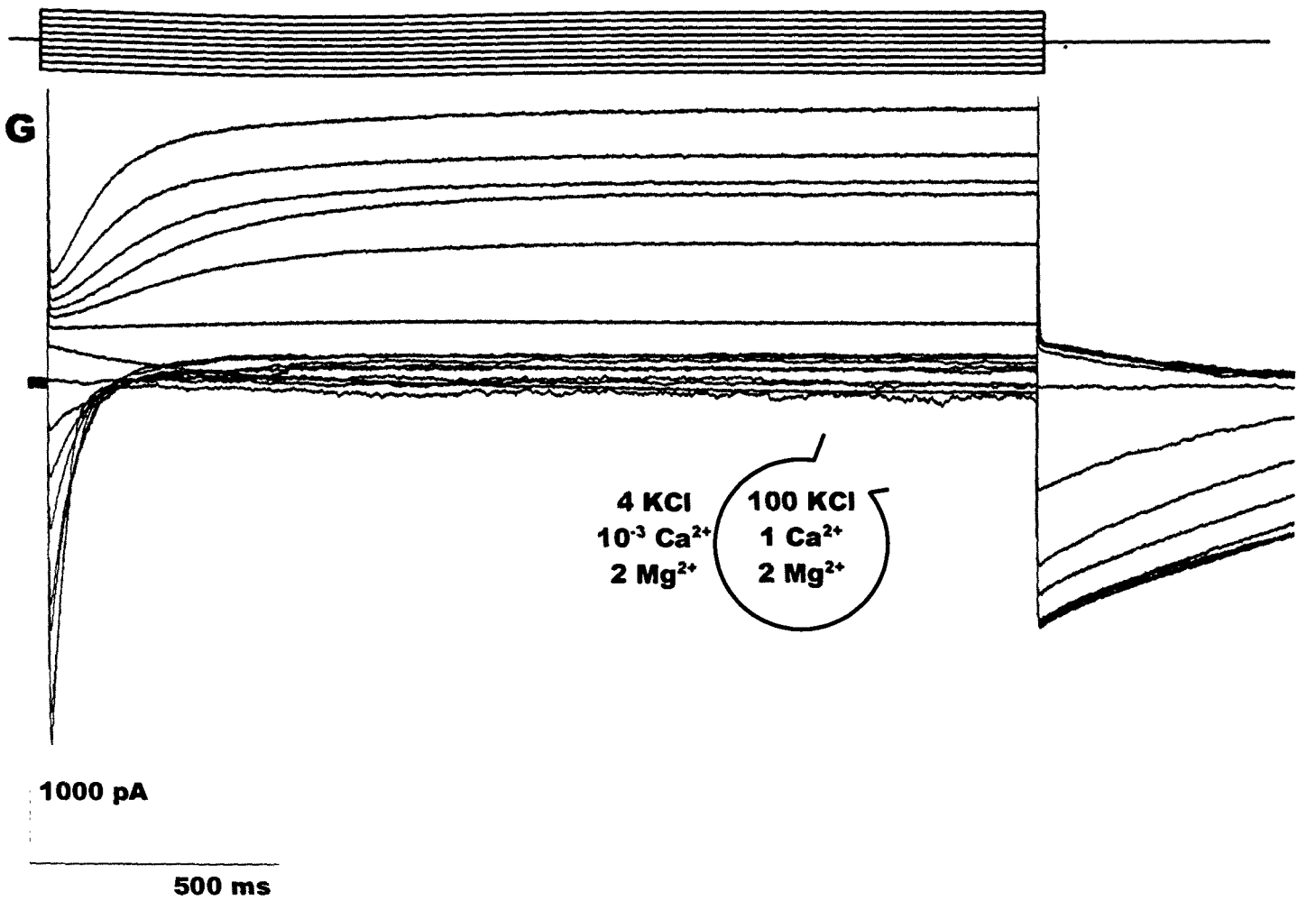


Figure 6.23. Continued from previous page. G) Whole-vacuolar currents 103 min after seal break, perfused with 4 mM KCl (solution N).

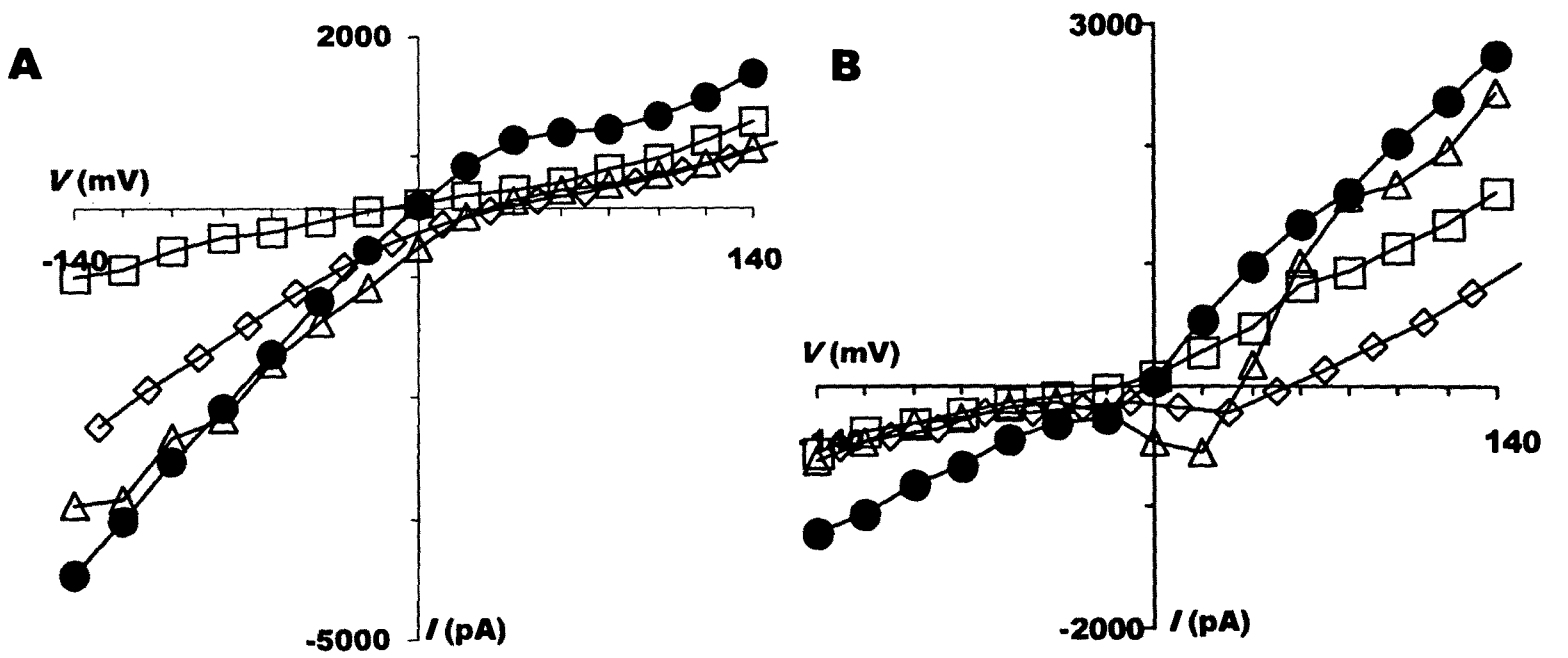


Figure 6.24. Current-voltage plots for the instantaneous (**A**) and steady-state (**B**) currents taken from Figure 6.23.C, D, E and G. Symbols: 100 mM KCl (●), 100 mM NMDG-Cl (◊), 200 mM KCl (❑), 4 mM KCl (Δ)

6.23.B). After 3 min these oscillations had subsided, but the outward currents still showed a characteristic initial sharp rise at positive membrane potentials (Figure 6.23.C). Perfusion with 100 mM NMDG-Cl drastically reduced the time-dependent outward currents, whereas large inactivating inward currents could still be observed (Figure 6.23.D). With 200 mM KCl these inward currents were much reduced, while the time-dependent outward currents became more pronounced (Figure 6.23.E). After changing back to 100 mM, the current oscillations reappeared at membrane potentials of +100 mV to +140 mV (Figure 6.23.F). After finally changing to 4 mM KCl in the bath, both the slowly activating outward currents, as well as the deactivating inward currents, became more pronounced (Figure 6.23.G).

Figure 6.24 shows the current-voltage plots of the instantaneous and steady-state currents with different KCl gradients. In 100 mM KCl the instantaneous currents were linear at negative potentials. At positive potentials, however, the current-voltage relationship was highly non-linear, with amplitudes almost levelling off between +40 and +80 mV, before increasing again at higher potentials. With 4 mM KCl the instantaneous inward currents were unchanged, while in 100 mM NMDG-Cl, and even more so in 200 mM KCl, the currents were much reduced. The instantaneous outward currents were of similar amplitudes in 200 mM KCl, 100 mM NMDG-Cl and 4 mM KCl. In all solutions the reversal potential followed E_K, indicating selectivity for K^+ over Cl^-. The steady-state currents showed outward rectification in 100 mM KCl, and at about -20 mV the inward currents showed a slightly increase, indicating activation of the currents at this potential. With 4 mM KCl and 100 mM NMDG-Cl these inward currents were much more pronounced, and the reversal currents again followed E_K.

Tail currents of the slowly activating outward current were recorded in 100 mM KCl, 200 mM KCl and 100 mM NMDG-Cl (Figure 6.25). As the current-voltage plot of the tail-current amplitudes in Figure 6.26 shows, the reversal potentials closely followed E_K, indicating high selectivity for K^+ over Cl^-.

Figure 6.27 illustrates the effect of the holding potential on these currents. Following a holding potential of 0 mV, stepping to voltages between -140 mV and +140 mV in 100 mM KCl showed slowly deactivating inward currents at negative membrane potentials (Figure 6.27.A). At positive membrane potentials, a time-dependent activation of outward current was observed, with currents rising more sharply at potentials above +60 mV, resulting in a distinct peak, before decreasing again and levelling off towards a constant steady-state current. Stepping from a more negative holding potential of -60 mV (Figure 6.27.B) abolished the deactivating inward currents, while the peak amplitudes and characteristics of the outward currents remained unchanged. When the holding potential was +60 mV (Figure 6.27.C), large inward currents could be observed at very negative test pulses, which initially increased for about 200 ms before deactivating and decreasing towards a steady-state level. The peak amplitudes of the outward currents were greatly reduced, with peak levels hardly greater than the steady-state current amplitudes.

Figure 6.28 summarises the current-voltage characteristics of these currents. The instantaneous outward currents showed a notable dependence on the holding potential. At a holding potential of -60 mV they were largely linear, but at 0 mV they were non-linear, levelling off between +60 and +80 mV before increasing again at more positive potentials. At +60 mV holding potential this effect became even more pronounced, with current amplitudes decreasing at test pulses above +80 mV. Also, at

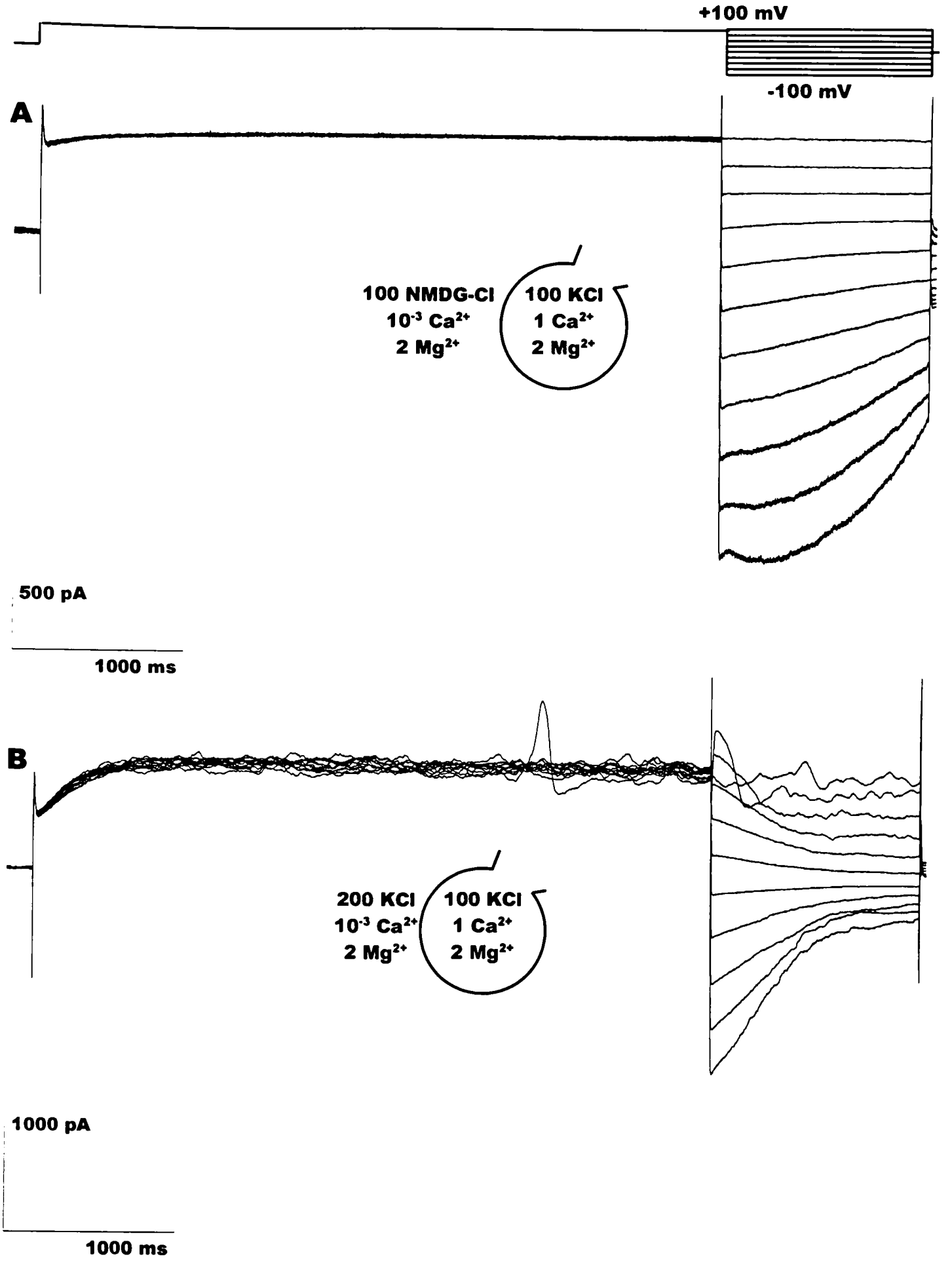


Figure 6.25. Whole-vacuolar tail currents in 1 μM cytoplasmic Ca^{2+} under asymmetric and symmetric KCl concentrations (with 100 mM KCl on the vacuolar side, solution E). **A**) 100 mM NMDG-Cl on the cytoplasmic side (solution M). **B**) 200 mM KCl on the cytoplasmic side (solution L). Tail currents were obtained after stepping from a +100 mV pre-pulse to membrane potentials ranging from -100 to +100 mV. The cartoons indicate concentrations in mM. Figure continued on following page

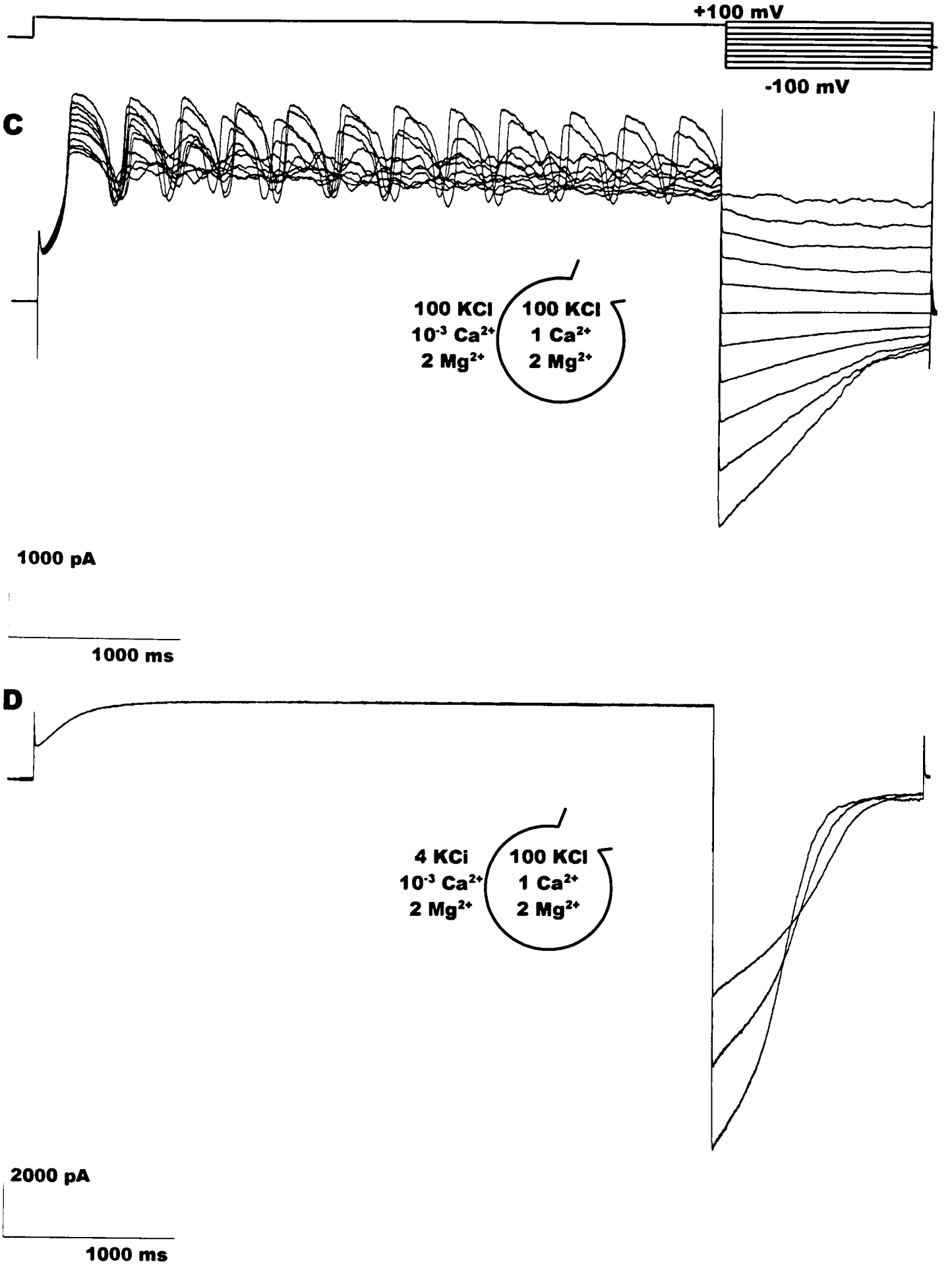


Figure 6.25. Continued from previous page. **C**) 100 mM KCl on the cytoplasmic side (solution J). **D**) 4 mM KCl on the cytoplasmic side (solution K). The seal was lost after the first three sweeps

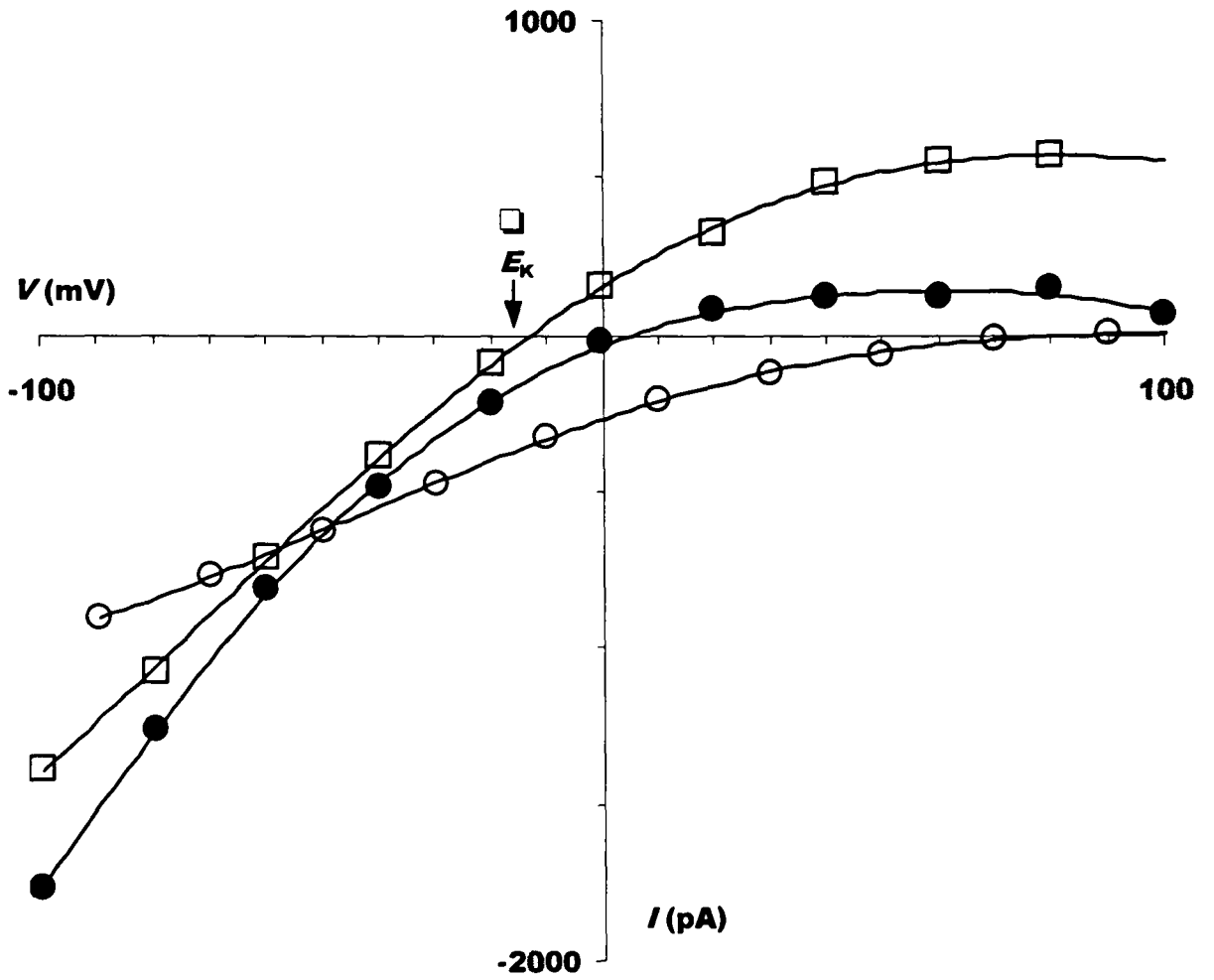


Figure 6.26. Tail-current-voltage plot for Figure 6.25. Current-voltage plots were constructed after subtracting the steady-state current from the initial current, as derived from fitting the traces with single exponentials. The lines are higher-order polynomials fitted to the data points. Symbols: 100 mM KCl (●), 200 mM KCl (❑), 100 mM NMDG-Cl (○)

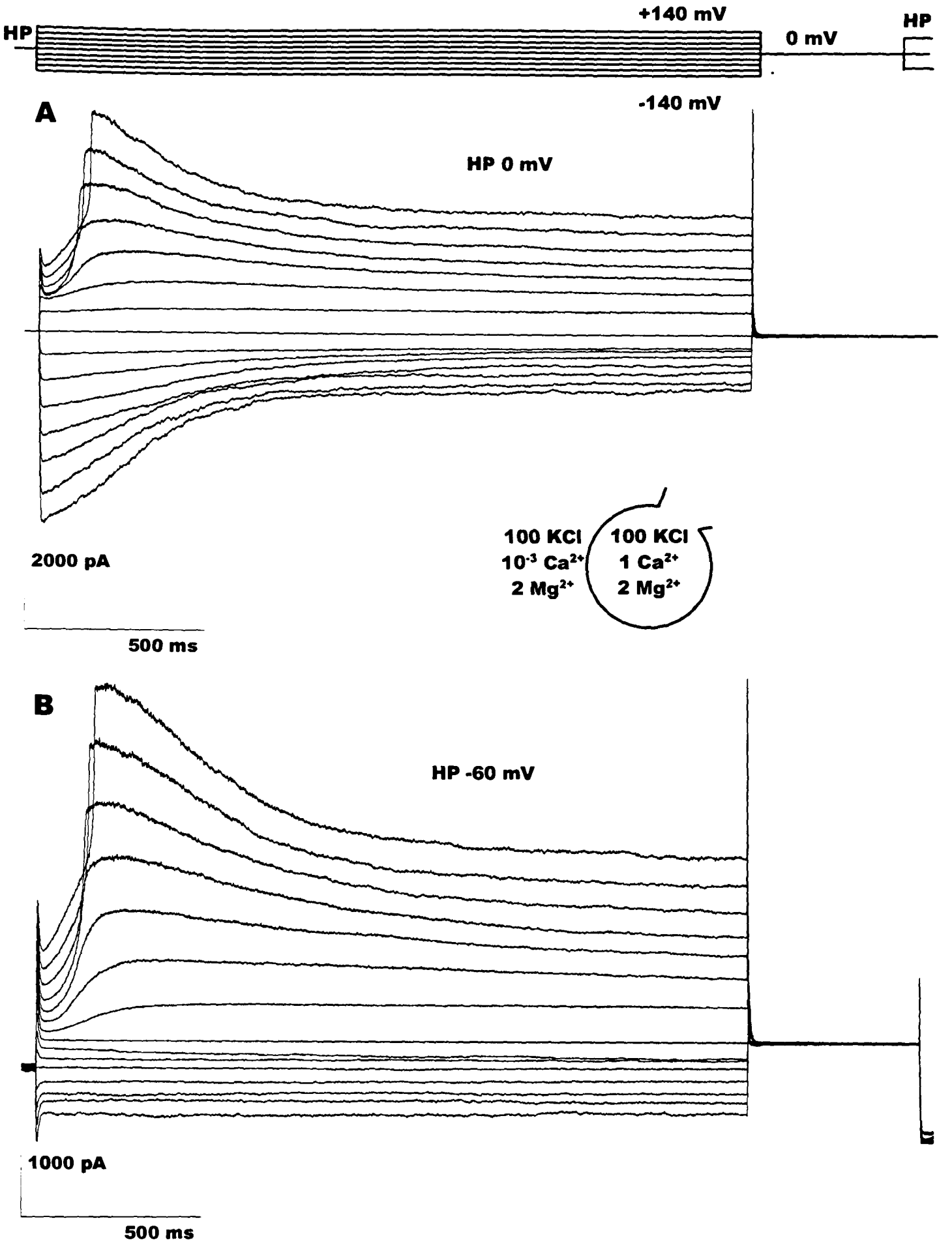


Figure 6.27. Effect of the holding potential (HP) on the oscillations. Recordings under symmetrical 100 mM KCl concentrations (solution J on cytoplasmic and solution E on vacuolar side). **A**) Holding potential 0 mV **B**) Holding potential -60 mV. Figure continued on the following page

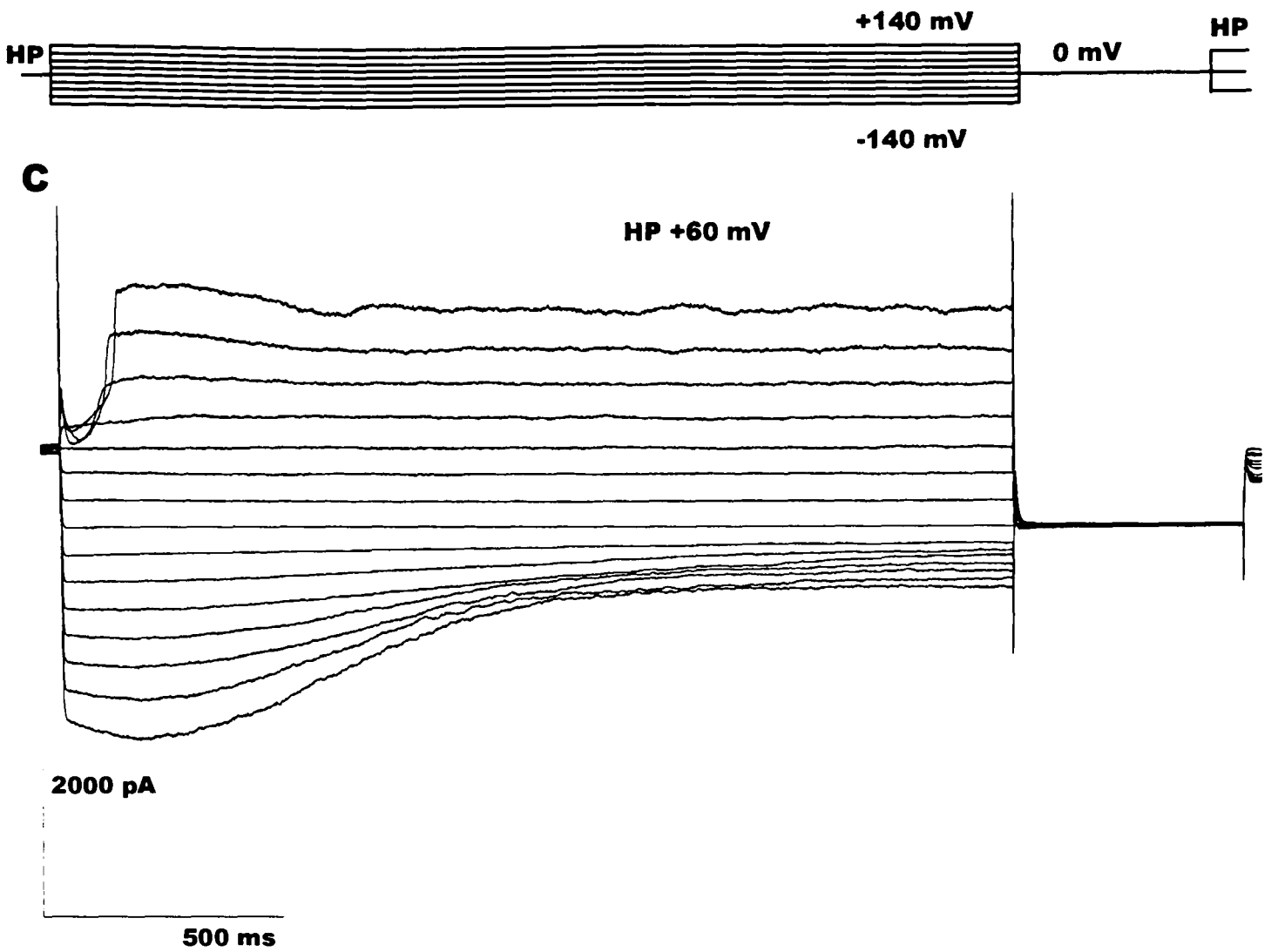


Figure 6.27. Continued from previous page. **C**) Holding potential +60 mV

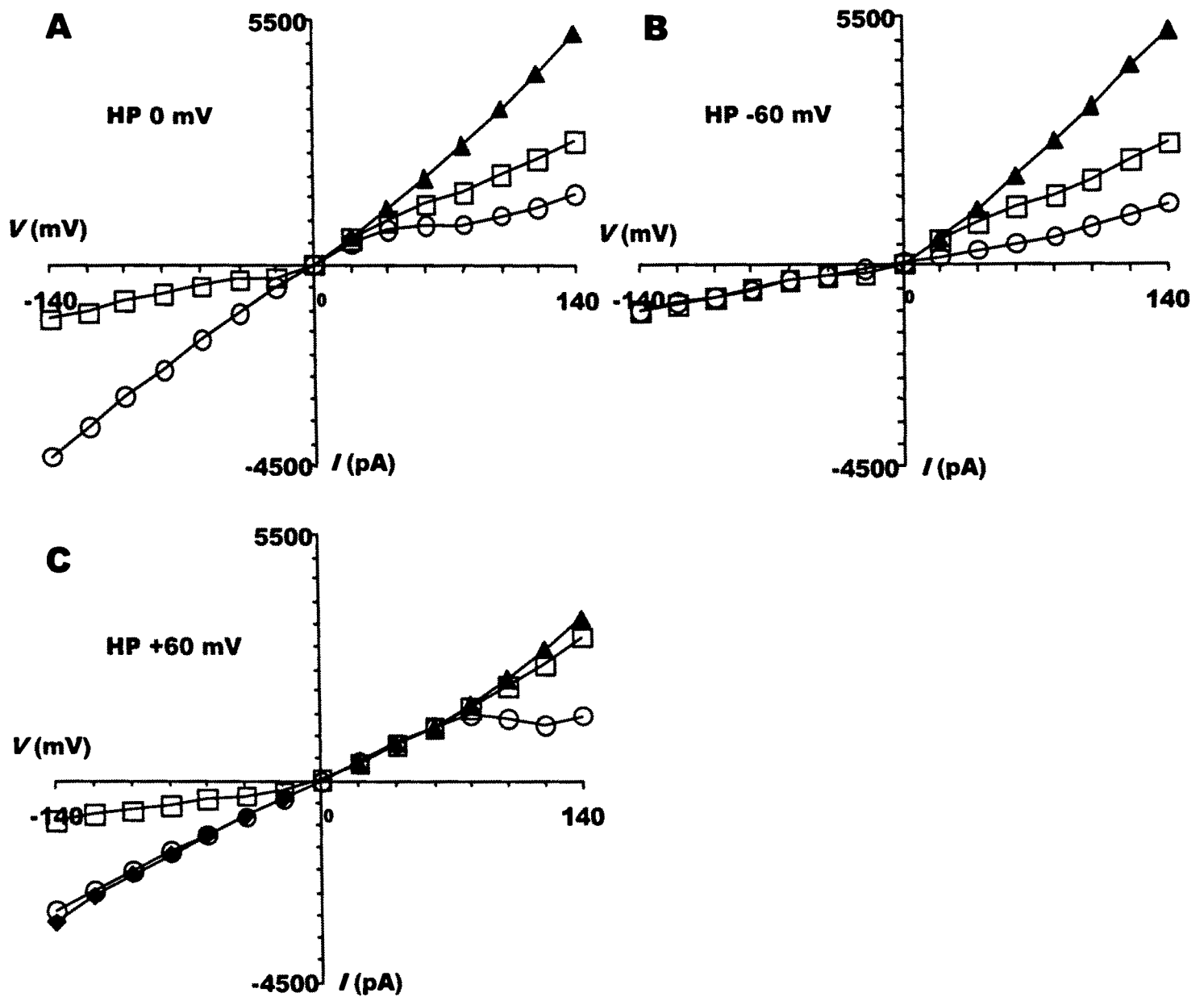


Figure 6.28. Effect of holding potential on the current-voltage relationship, as derived from Figure 6.27. **A**) Holding potential 0 mV, **B**) holding potential -60 mV, and **C**) holding potential +60 mV. Symbols indicate current amplitudes at different time points: initial currents (○), steady-state currents (❑), maximum currents at positive membrane potentials (▲), and minimum currents at negative membrane potentials (◆)

+60 mV holding potential the peak amplitudes of both the inward, as well as the outward, currents were reduced by about 30% compared to 0 mV holding potential, while the steady-state currents remained unchanged over the whole voltage range and showed a slight outward rectification.

Figure 6.29 shows two recordings at a holding potential of -60 mV with asymmetric solutions. With 100 mM NMDG-Cl replacing the cytosolic KCl, the time-dependent outward currents were greatly reduced and only a small time-dependent current component could be observed. In contrast, changing the cytosolic KCl concentration to 4 mM led to large time-dependent currents, which were inwardly directed negative of +40 mV, and outwardly above this potential. Also, the onset of the outward currents showed a biphasic behaviour.

The current-voltage plot of the instantaneous currents (Figure 6.30.A) shows that they were identical for 100 mM NMDG-Cl and 4 mM KCl, but were only about half of the amplitudes observed in 100 mM KCl over the whole voltage range tested. Figure 6.30.C shows the current-voltage relationship of the time-dependent current component. In 100 mM KCl and 4 mM KCl, it activated above -40 mV. This should reflect the actual activation-threshold potential, since at the holding potential of -60 mV no deactivating inward currents could be observed, indicating that all channels were closed at this holding potential. The reversal potentials followed E_K, demonstrating a high selectivity for K^+ over Cl^-. In 100 mM NMDG-Cl, the current amplitudes were much smaller and activated only above -20 mV. The reversal potential of +80 mV was shifted strongly towards E_K.

Figure 6.31 shows the activation curves that could be derived from the recordings in Figure 6.23 under asymmetric conditions for the time-dependent

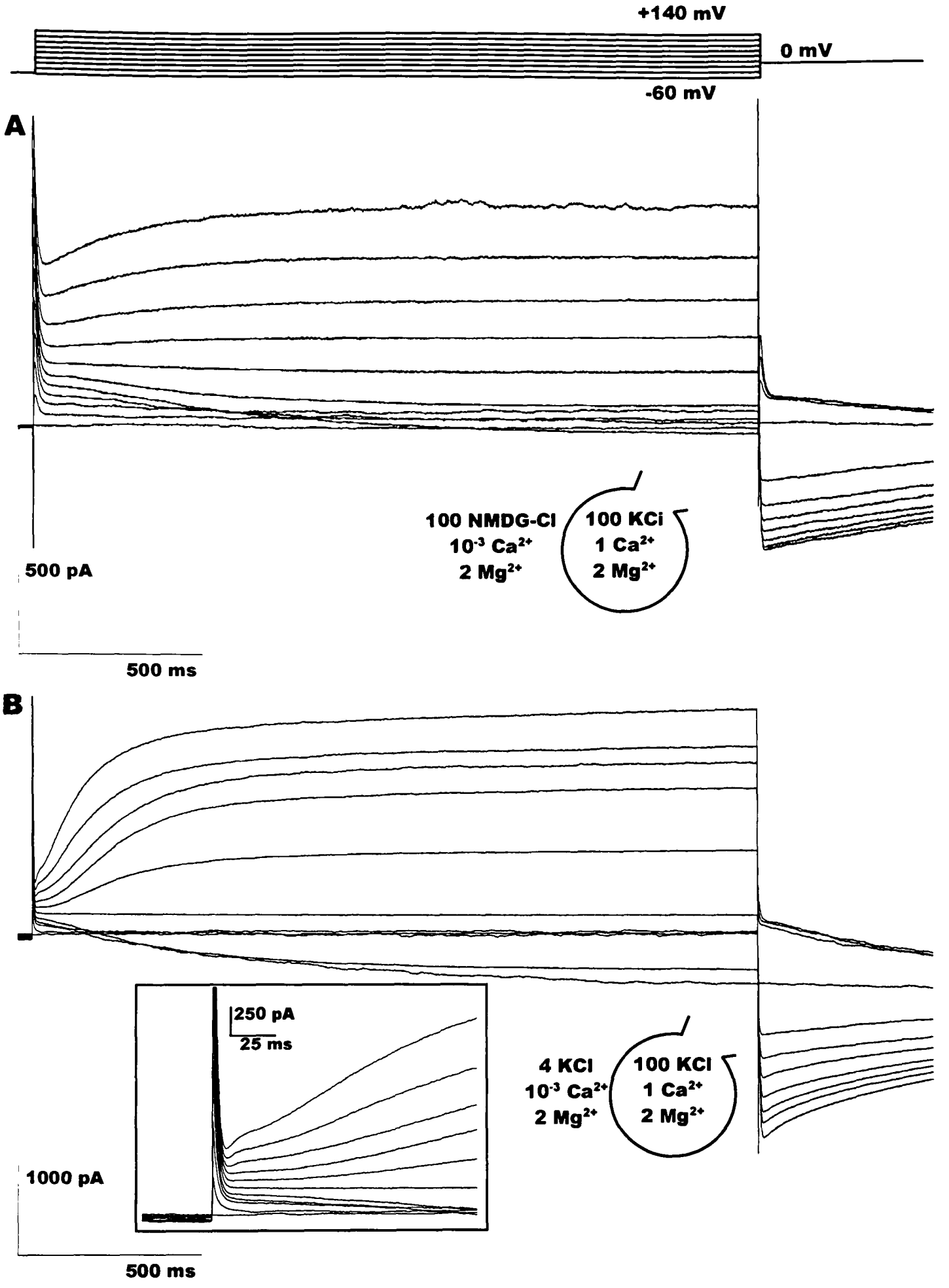


Figure 6.29. Effect of a negative holding potential of -60 mV on the currents under asymmetric KCl concentrations. **A**) 100 mM NMDG-Cl (solution M) on the cytoplasmic side and **B**) 4 mM KCl (solution K) on the cytoplasmic side, with 100 mM KCl (solution E) on the vacuolar side. The inset shows enlarged traces of the test-pulse onset showing biphasic activation. The cartoons indicate concentrations in mM

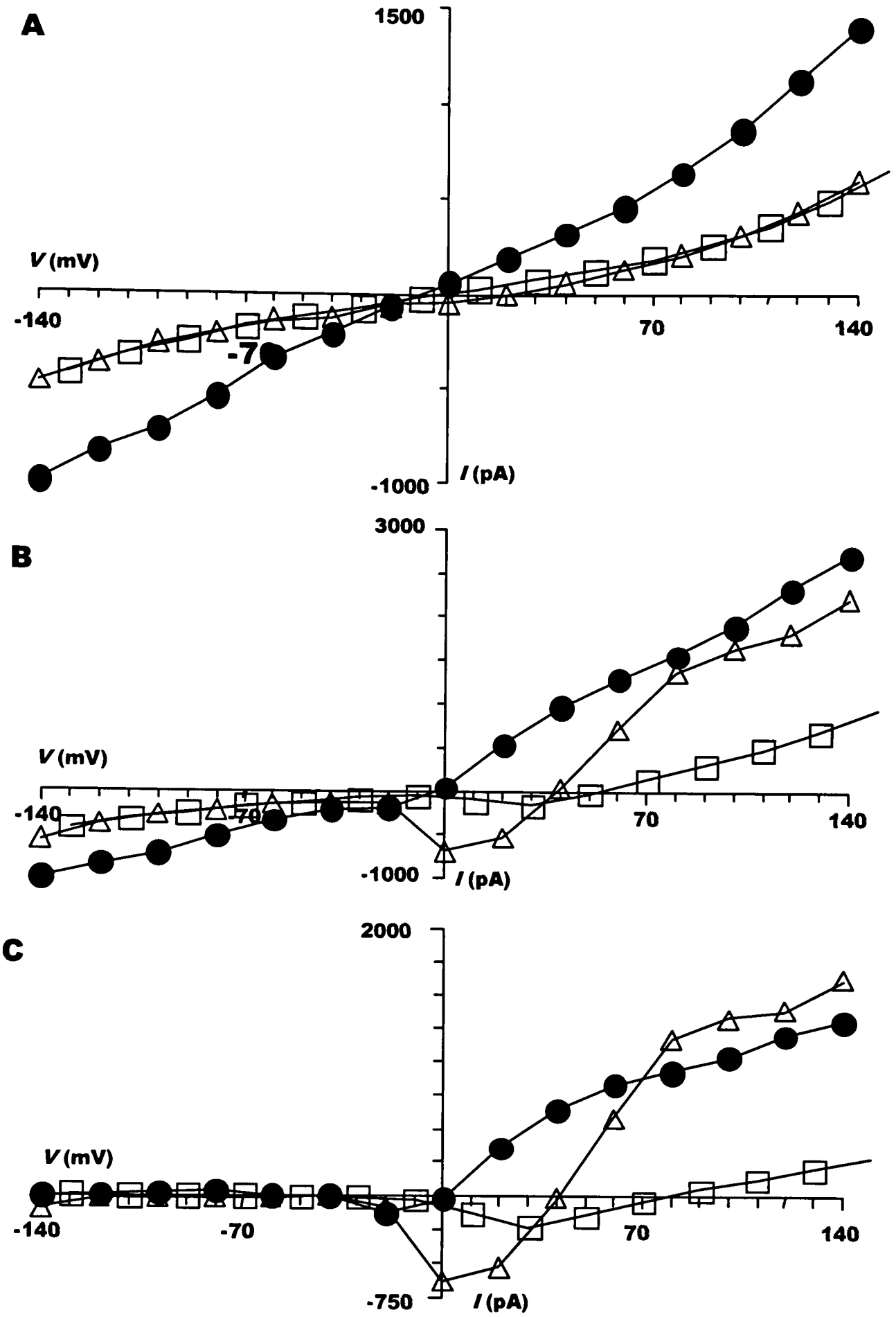


Figure 6.30. Current-voltage plot of the currents at -60 mV holding potential. The current-voltage plots were constructed by plotting the current amplitudes obtained from Figure 6.9.B and 6.11 against the membrane potential of the test pulse. **A**) Instantaneous currents, **B**) steady-state currents, and **C**) the difference after subtracting the instantaneous currents from the steady-state currents. Symbols: 100 mM KCl, (●, solution J), 4 mM KCl (Δ, solution K), 100 mM NMDG-Cl (❑, solution M)

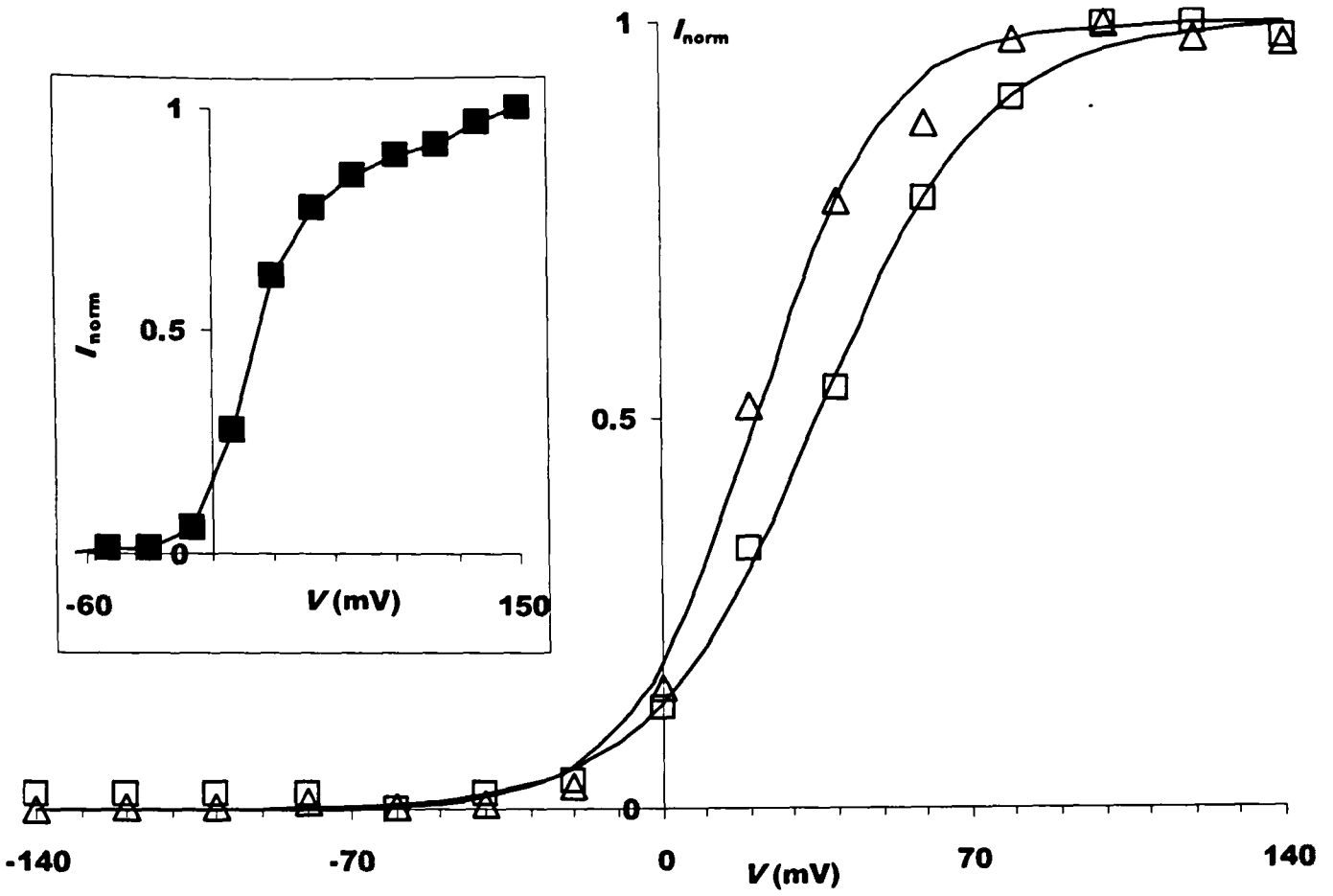


Figure 6.31. Activation of the time-dependent current under asymmetric conditions. Activation curves were constructed from recordings in Figure 6.23.E (❑, 200 mM KCl on the cytoplasmic side), Figure 6.23.G (Δ, 4 mM KCl on the cytoplasmic side) and Figure 6.23.D (inset, 100 mM NMDG-Cl on the cytoplasmic side). The current amplitude immediately after the end of the test pulse was derived by fitting single exponentials to the remaining currents and extrapolating the curve back to 1 ms after the test pulse. The current amplitude at this time point is proportional to the number of open channels at the end of the test pulse. The current amplitudes were normalised according to the function $I_{norm} = (I - I_{min})/(I_{max} - I_{min})$, with I_{min} and I_{max} being the observed minimum and maximum current amplitudes. The activation curves at 200 mM KCl and 4 mM KCl could be fitted according to the Boltzmann function $I_{norm} = 1/\{1 + \exp[V_{½} - V)/k]\}$, with the constant k (19.1 mV for 200 mM KCl and 14.8 mV for 4 mM KCl) and the voltage of half-maximal activation $V_{½}$ (35.6 mV for 200 mM KCl and 21.6 mV for 4 mM KCl) as fitted parameters. The activation curve for 100 mM NMDG-Cl could not be fitted with a Boltzmann function due to an additional linear component at positive membrane potentials.

outward currents. In 4 mM and 200 mM KCl, the activating threshold was negative of -20 mV. The voltage for half-maximum activation was +22 mV for 4 mM KCl and +36 mV for 200 mM KCl. In 100 mM NMDG-Cl similar activation characteristics to 4 mM KCl could be observed, but an additional linear component was seen at higher voltages, so the activation parameters could not be properly estimated.

6.2.2.5 Single channels with 1 μM cytosolic free Ca^{2+}

A number of different single-channel conductances were observed in a total of 37 patches with approximately 1 μM free Ca^{2+} on the cytosolic side. One patch showed a large single-channel conductance opening only at positive membrane potentials above +60 mV (Figure 6.32). A voltage ramp under asymmetric conditions with 200 mM KCl on the vacuolar side revealed a reversal potential of +5.5 mV, i.e. 10.9 mV negative of the reversal potential for K^+, E_K. According to the Goldman-Hodgkin-Katz (GHK) voltage equation, $E_{rev} = RT/F \times \ln((P_K[K^+]_o + P_K[Cl^-]_i)/(P_K[K^+]_I + P_K[Cl^-]_o))$, the permeability ratio for Cl^- over K^+ could be calculated as P_{Cl}/P_K = 0.47 (with the reversal potential E_{rev}, the K^+ permeability P_K, the Cl^- permeability P_{Cl}, and $[K^+]_i$, $[K^+]_o$, $[Cl^-]_i$, $[Cl^-]_o$ being the internal and external K^+ and Cl^- activities, respectively). This calculation was made under the simplified assumptions of independent movement of ions, a constant electrical field across the pore, and no permeation by Ca^{2+} or Mg^{2+}.

This channel had very low open probabilities even at very positive membrane potentials, with a *P*(open) at +100 mV of only 0.012. The slope conductance measured with 200 mM KCl on the vacuolar side was about 170 pS between -60 and -80 mV. Unfortunately, no recordings under symmetrical conditions could be made.

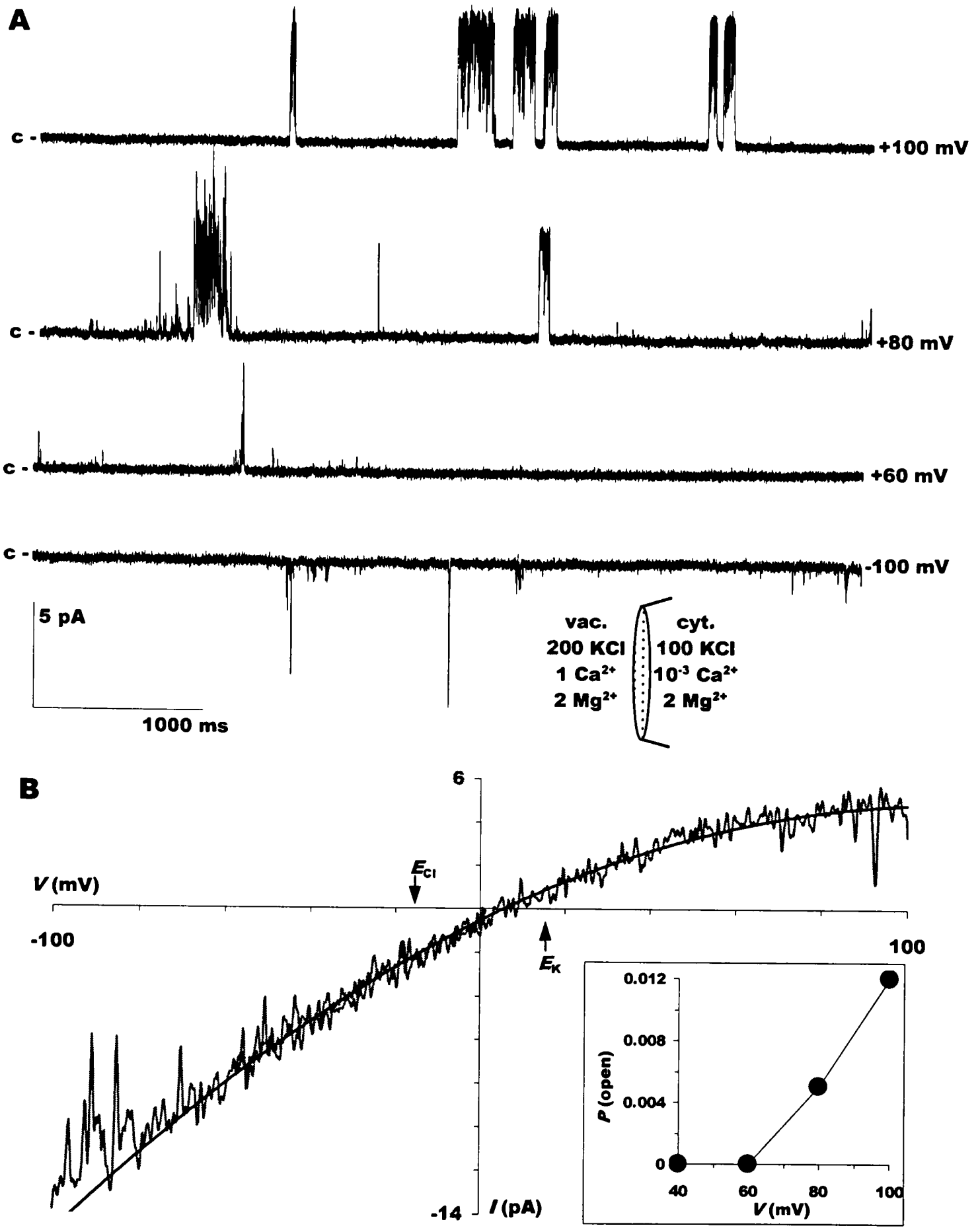


Figure 6.32. Single-channel recordings of LOR1. **A**) Single-channel recordings of a large ion channel with asymmetric KCl concentrations in vacuolar-side-out configuration (cyt.: 100 mM KCl, solution J; vac.: 200 mM KCl, solution G). **B**) Current-voltage plot constructed from a voltage ramp (from +100 mV to -100 mV in 25 ms). The reversal potential E_{rev} (+5.5 mV) and the Nernst potentials for K^+ (E_K = 16.4 mV) and Cl^- (E_{Cl} = -16.1 mV) are indicated. The smooth line is a higher order polynomial fitted to the data. The inset shows the open probability *P* (open), as derived from 1 min recordings, as a function of the membrane potential. The cartoon indicates concentrations in mM

This channel will be referred to as LOR1 (for large conductance, outward-rectifying channel).

Two small channel conductances were observed in one patch at both positive and negative membrane potentials with asymmetric KCl solutions (Figure 6.33). While in the vacuolar-attached configuration (Figure 6.33.A), this patch showed single-channel currents with a slope-conductance of 7 pS at -60 mV and +60 mV, and the current amplitudes reversed close to E_K (Figure 6.34). This indicated a high selectivity for K^+ over Cl^-, assuming vacuolar KCl concentrations to be around 100 mM. This channel type will be referred to as KVI1 (for K^+-selective, voltage-independent channel).

After excising the patch to obtain the vacuolar-side-out configuration (Figure 6.33.B), single-channel events were still observed at both positive and negative membrane potentials, and the currents reversed around E_K. However the observed single-channel amplitudes were much smaller than in the vacuole-attached recordings and had a slope conductance of about 3 pS at -60 mV and +60 mV (Figure 6.34). This type of channel will be referred to as KVI2. No single-channel events could be recorded after changing to 100 mM KCl on the vacuolar side.

Two very similar channels were observed simultaneously in another patch in 200 mM KCl (Figure 6.35). One channel had a slope conductance of about 7 pS at -80 mV and +80 mV. The smaller channel showed a slope conductance of about 2 pS at -80 mV and 3.3 pS at +80 mV. Both channels reversed slightly positive of E_K, indicating K^+ permeability with a smaller Ca^{2+} permeability (Figure 6.35.B). The same results were obtained for the larger channel in voltage-ramp recordings with this patch (data not shown).

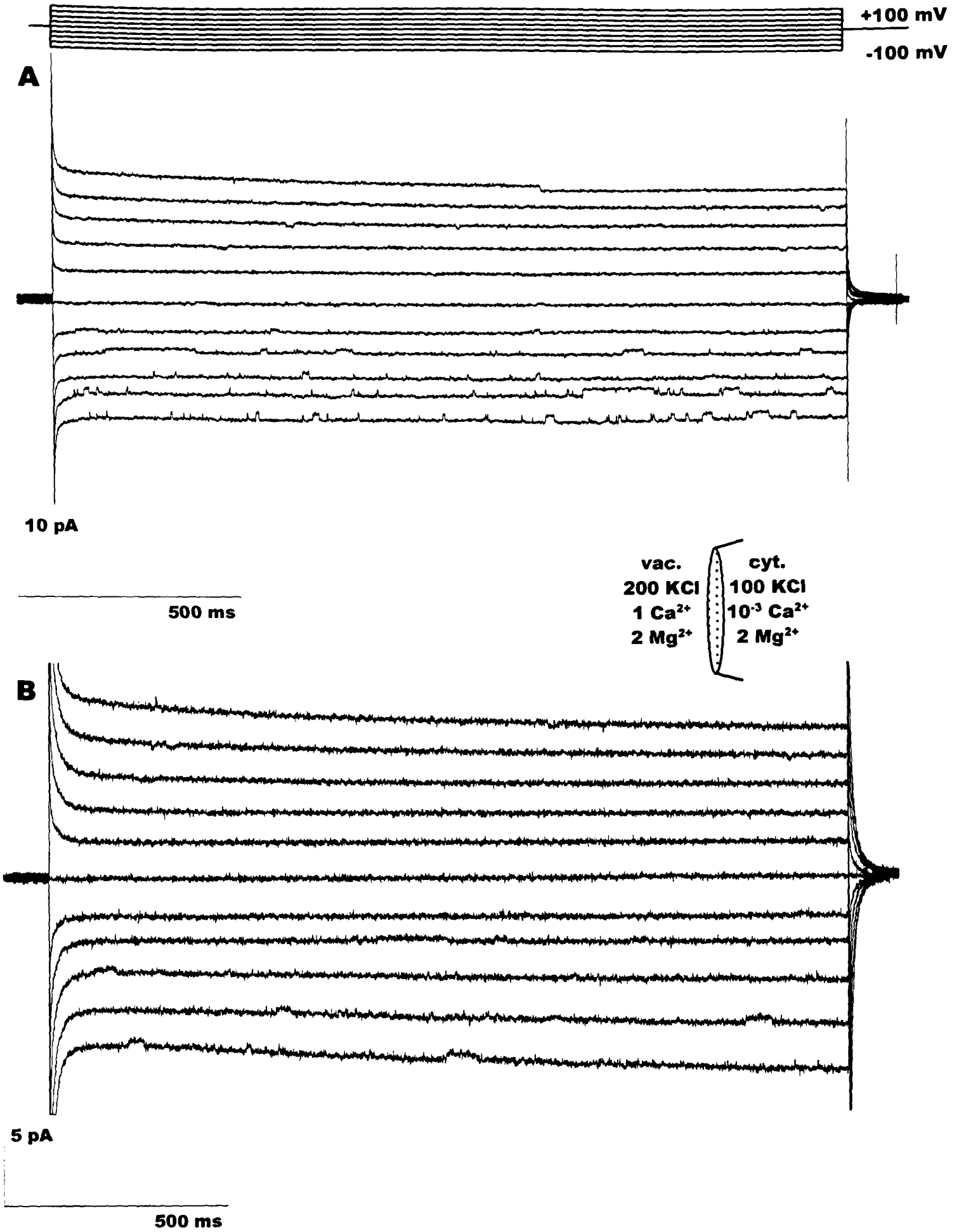


Figure 6.33. Single-channel recording in the vacuole-attached (**A**) and vacuolar-side-out configuration (**B**) with asymmetric KCl concentrations (cyt.: 100 mM KCl, solution J; vac.: 200 mM KCl, solution G). The cartoon indicates concentrations in mM

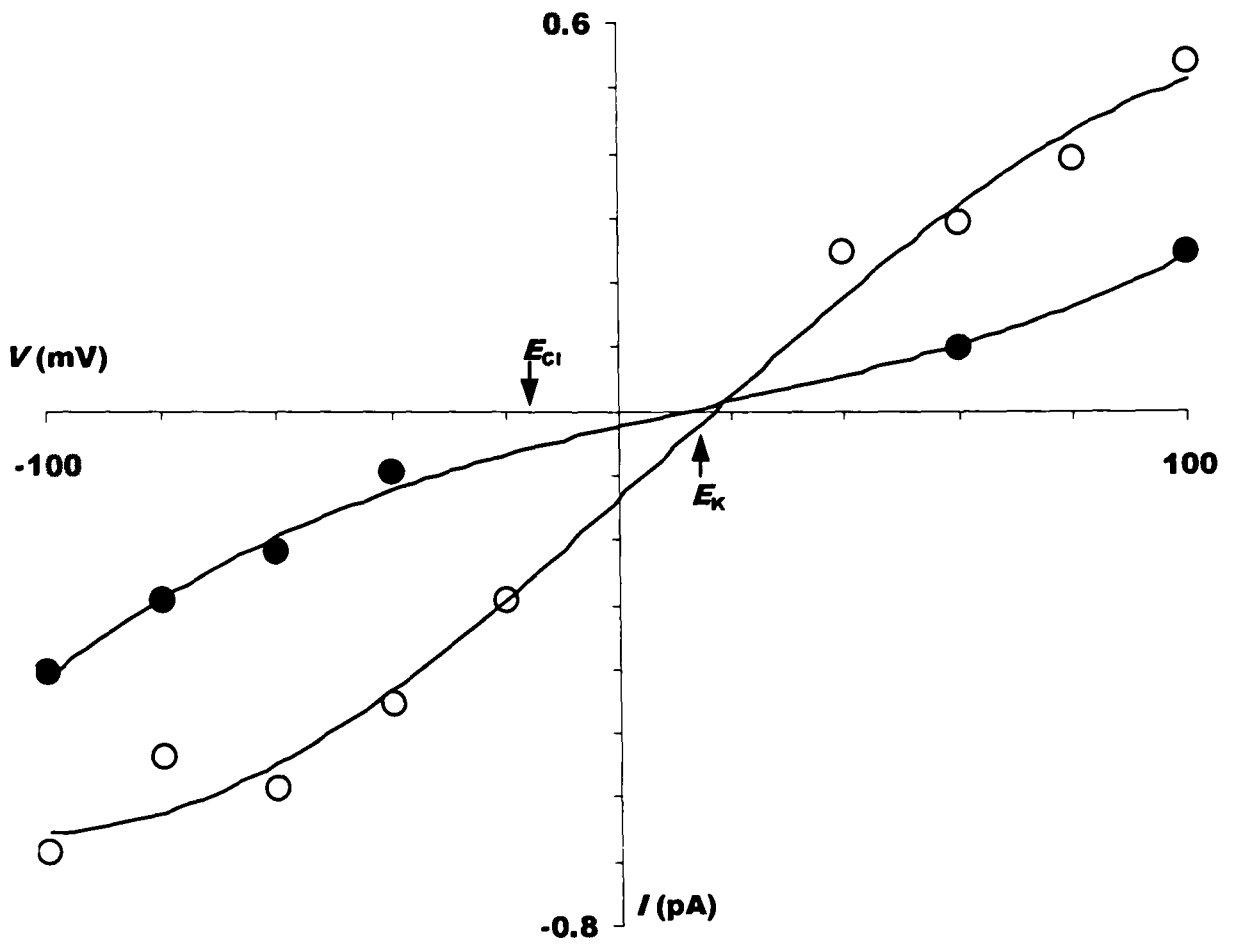


Figure 6.34. Current-voltage plots of the single-channel amplitudes derived from Figure 6.34. Symbols: vacuole-attached (○), vacuolar-side-out configuration (●). The lines are higher-order polynomials fitted to the data. The Nernst potentials for Cl^- (E_{Cl}) and K^+ (E_K) are indicated.

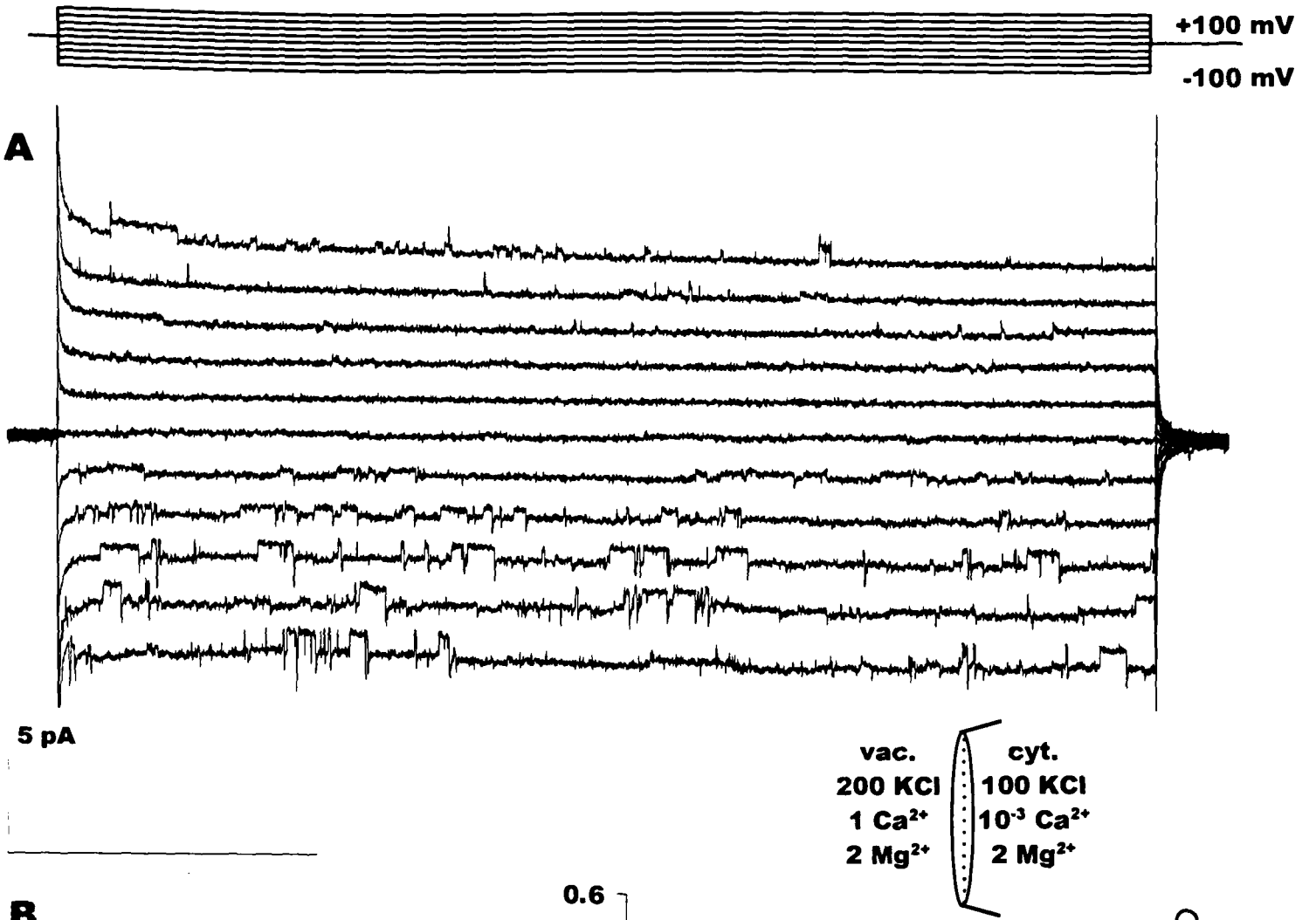


Figure 6.35. Single-channel activities of KVI1 (~7 pS) and KVI2 (~2 pS). **A**) Single-channel recordings during voltage steps from -100 to 100 mV with increments of 20 mV (cyt.: 100 mM KCl, solution J; vac.: 200 mM KCl, solution G). **B**) Current-voltage plot of the single-channel amplitudes observed. Two clearly distinguishable amplitude populations could be observed (○, ❑). The Nernst potentials for K^+ (E_K) and Cl^- (E_{Cl}) are indicated. The smooth lines are higher-order polynomials fitted to the data. The cartoon indicates concentrations in mM

In a total of 11 patches, slowly activating background currents could be observed immediately after the seal formation in both the vacuole-attached and vacuolar-side-out configurations. Figure 6.36.A shows a typical recording in the vacuole-attached configuration, with 100 mM KCl in the pipette and 200 mM KCl in the bath. At membrane potentials negative of -20 mV, a slowly activating inward current could be observed which took more then 1 s to reach its steady-state amplitude at -100 mV. Conversely, at positive membrane potentials, deactivation of the outward currents occurred. After excising the patch to obtain the vacuolar-side-out configuration, these characteristics remained unaltered (Figure 6.36.B, C). The amplitude of the time-dependent component (i.e. the difference between the instantaneous and steady-state currents) was 1.4 pA at -100 mV, but no single-channel activity could be observed.

These currents were difficult to analyse, since they usually could not be observed beyond a few minutes, or were obscured by other single-channel activity. Figure 6.37 shows the results from tail-current measurements on four individual patches under asymmetric KCl concentrations where no single-channel activity could be observed. The currents reversed at small negative potentials between 0 and -10 mV. One successful measurement could be performed where the initial vacuolar KCl concentration of 200 mM was exchanged with a K^+-gluconate-based solution with 100 mM K^+ and 10 mM Cl^-. Despite the steep Cl^--gradient, the reversal potential remained almost unchanged. Similarly, subsequently changing the vacuolar KCl concentration to 100 mM resulted in only a small shift in reversal potential. This indicated that this current was not carried by Cl^-. While the Nernst potentials for K^+ (+16.4 mV in 200 mM KCl) and Ca^{2+} (+85 mV) under these conditions were much

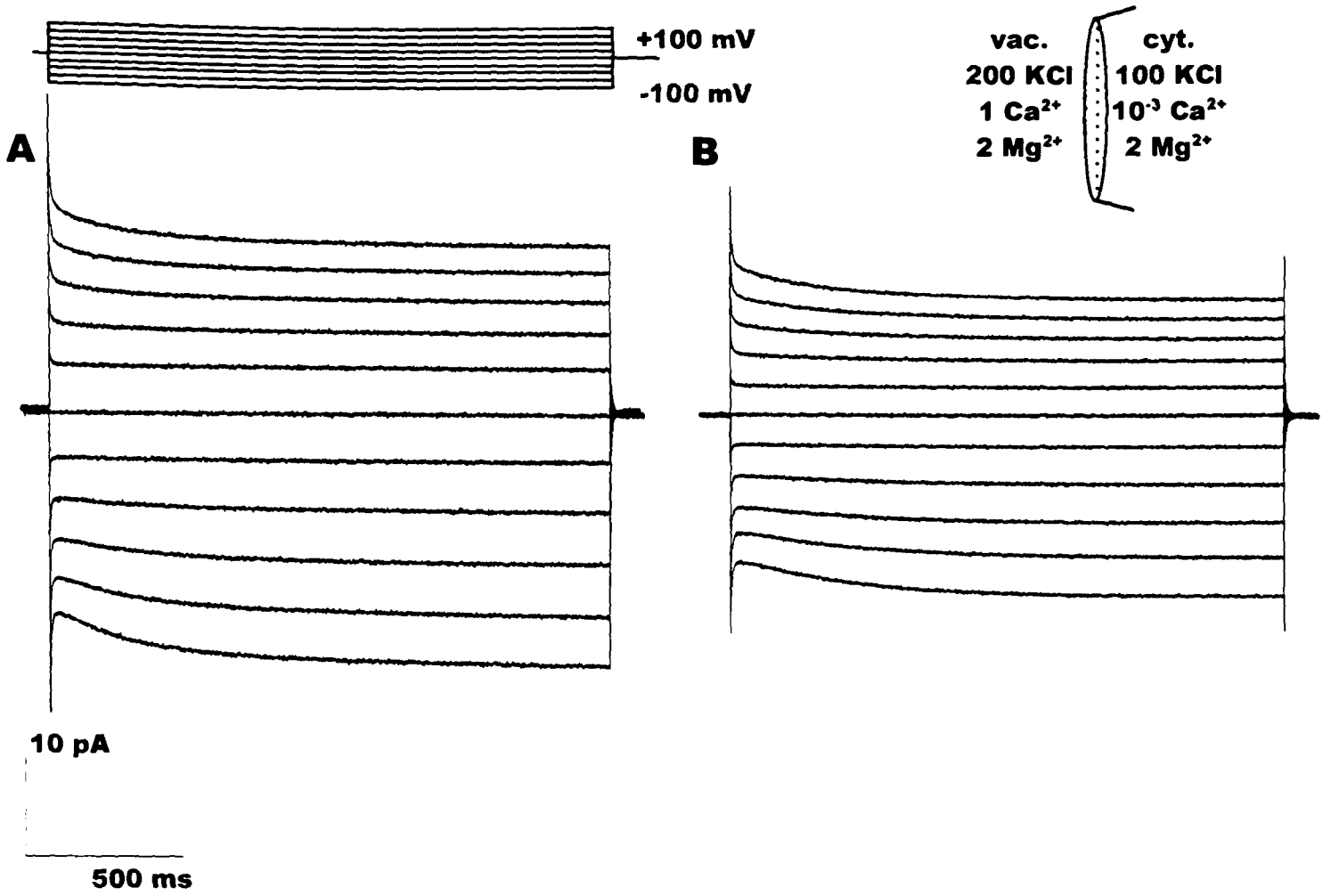


Figure 6.36. Small time-dependent inward-currents. **A**) Vacuole-attached and **B**) vacuolar-side-out patch with 200 mM KCl (solution G) on the vacuolar side. Slowly activating currents were observed at negative membrane potentials, while positive membrane potentials caused deactivation of currents. **C**) Current-voltage relationship of the instantaneous currents (○) and of the steady-state currents (❑). The cartoon indicates concentrations in mM

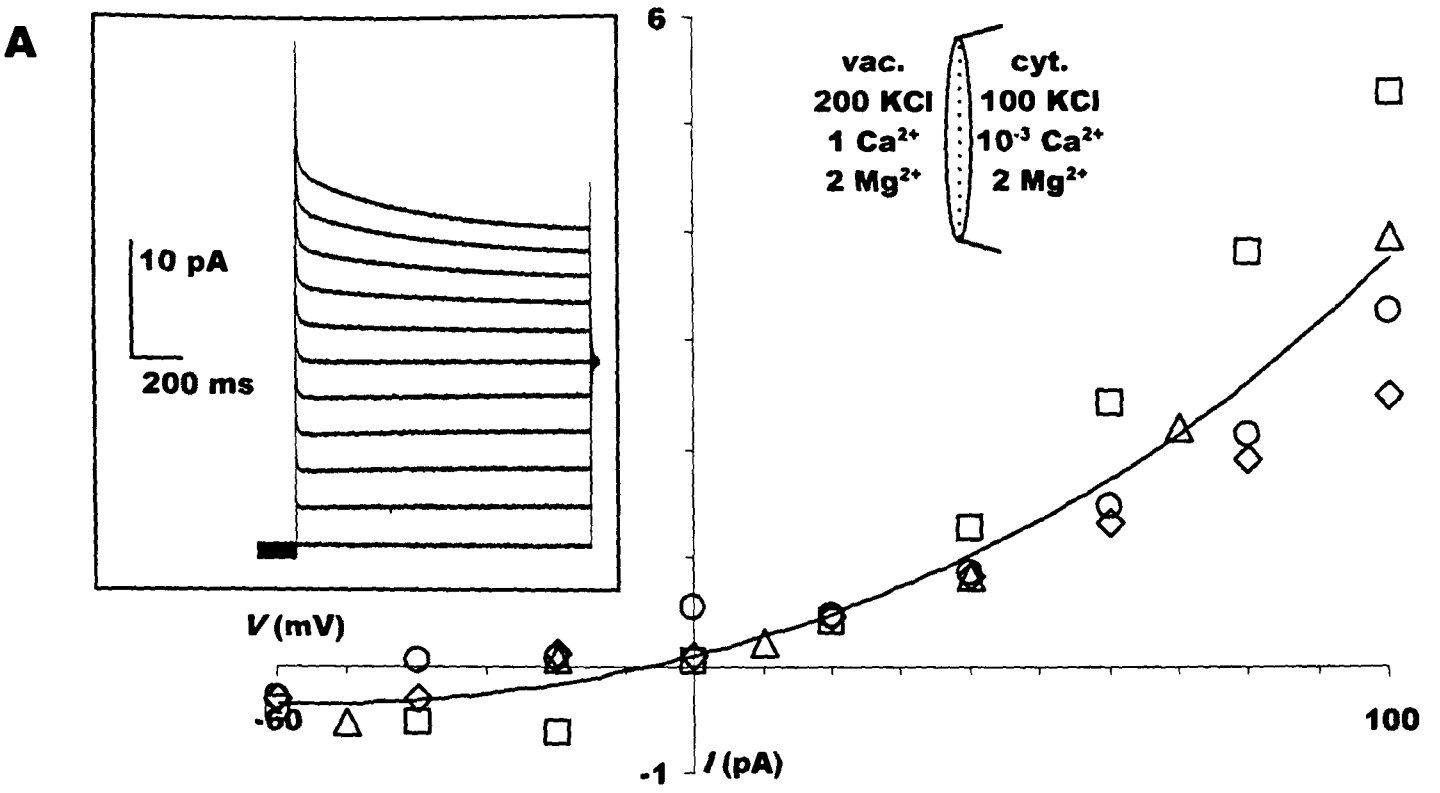


Figure 6.37. Tail currents of the small currents in asymmetric solutions. **A)** Tail currents were obtained by stepping from an activating pulse of -100 mV to membrane potentials between -100 mV and +110 mV (see inset). Single exponentials were fitted to the tail currents and the steady-state currents were subtracted from the extrapolated current amplitude at the onset of the tail current. The plot shows data obtained from four patches with 200 mM KCl on the vacuolar side (solution G) and 100 mM KCl on the cytoplasmic side (solution E). A higher-order polynomial was fitted to the data to estimate the reversal potential (-6.3 mV). The cartoon indicates concentrations in mM. **B)** Current-voltage relationship of the tail currents from a single patch where the vacuolar concentrations were changed from 200 mM KCl (○, solution G) to 100 mM K^+/ 10 mM Cl^- (❑, solution I) or to 100 mM KCl (Δ, solution E). The corresponding reversal potentials were shifted from -6.3 mV to -0.5 mV and -4.4 mV, respectively

more positive then the reversal potentials observed, the Nernst potential for Mg^{2+} was -2.4 mV, which was close to those observed. It therefore seems possible that this background current was mainly carried by Mg^{2+}, but this would require further experiments to establish unequivocally.

While a number of patches did not show any single-channel activity initially, with time, and often after prolonged depolarisations, a multitude of single channels became active. This was generally accompanied by a significant drop in the seal resistance and larger noise amplitudes. Figure 6.38 shows a typical recording where initially no single-channel activity was observed in 200 mM KCl. After depolarising the patch at +100 mV for 4 minutes, the current amplitude suddenly increased several-fold and saturated the amplifier input (Figure 6.38.B). Subsequently, at small negative membrane potentials, at least two individual channels were found to be active in the patch (Figure 6.38.C). At positive and more negative membrane potentials, no single-channel events could be isolated due to the large noise. The amplitude histogram in Figure 6.39.A shows three distinct current amplitudes at -30 mV could be separated, indicating single-channel amplitudes between 4.3 pA and 5 pA. The voltage-ramp experiments in Figure 6.39 show that in 200 mM KCl the reversal potential was very close to E_K. This indicated a high selectivity for K^+ over Cl^-. When the external KCl concentration was shifted to 4 mM KCl, the reversal potential was shifted negative accordingly, but at +3 mV was considerably positive of E_K (-78 mV). Since E_{Cl} (+56.4 mV) and E_{Ca} (+85 mV) were both positive, it could not be determined which of the two caused this positive shift. The observed slope conductance in the voltage-ramp experiments was 106 pS at -50 mV and 103 pS at +50 mV in 200 mM KCl. Figure 6.40 shows another example of this type of channel with initially no single-channel

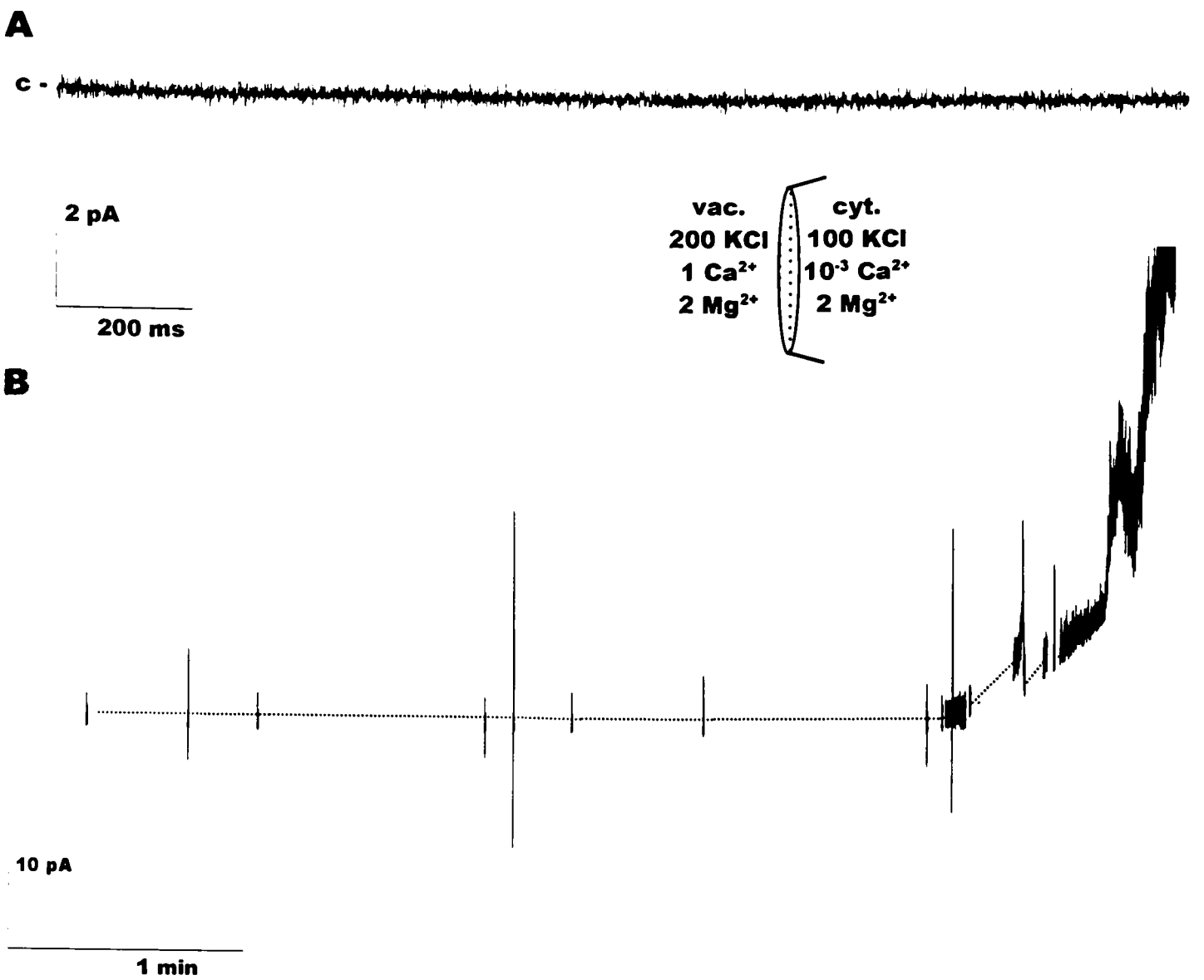
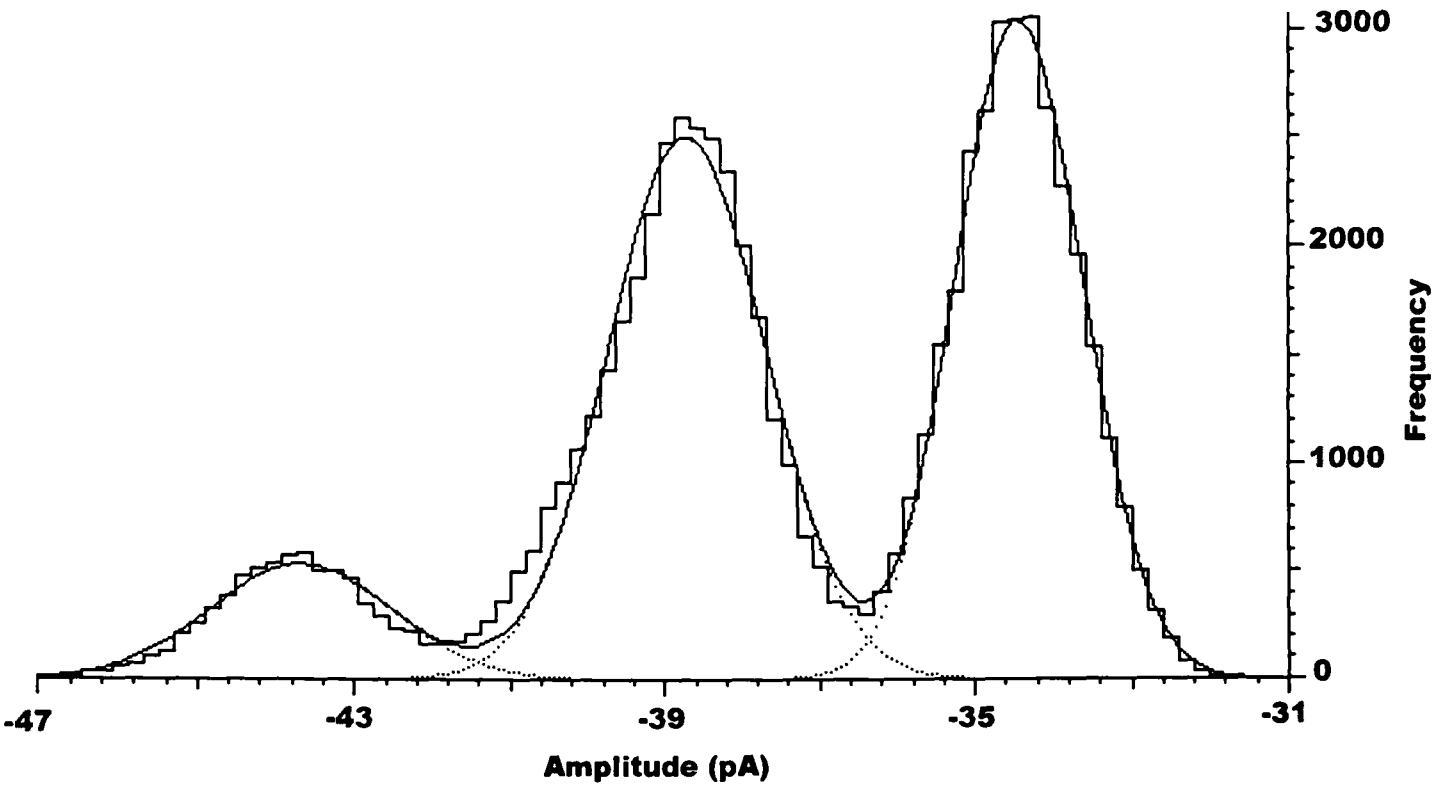


Figure 6.38. Single-channels appearing after prolonged depolarisation. **A**) No single-channel activity could be observed at any voltage (recording shown at -20 mV) immediately after obtaining the vacuolar-side-out configuration with a seal resistance of 20 GΩ (cyt.: 100 mM KCl, solution J; vac.: 200 mM KCl, solution G). The cartoon indicates concentrations in mM. **B**) Event-driven recording over 5 min at +100 mV holding potential. Actual recordings were only made when the current exceeded a certain threshold, with the interpolations indicated by the dotted lines. After about 4 min, the current increased dramatically and went off scale. **C**) Appearance of multiple channel activities, as indicated for -30 mV holding potential. The seal resistance had dropped to ~1 GΩ. The closed state is indicated by (c)



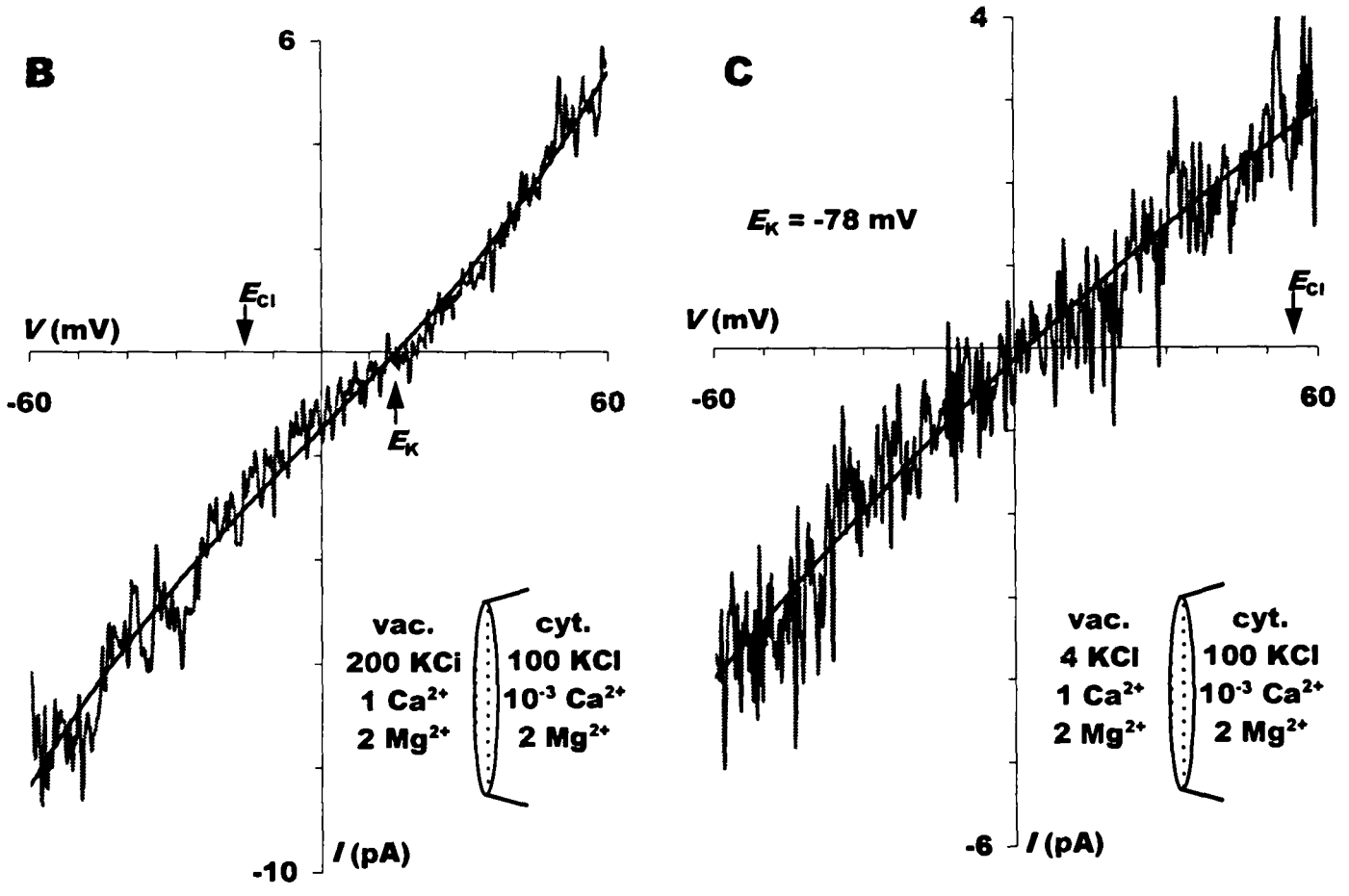


Figure 6.39. Single-channel activity of KS1 after prolonged depolarisations. **A**) Amplitude histogram of Figure 6.38.C. The histogram was fitted with a third-order Gaussian function, as indicated by the smooth lines, using the pCLAMP software package. The means obtained for the three distributions were -43.7 pA, -38.7 pA and -34.4 pA. **B**) Current-voltage plot constructed from a voltage ramp in 200 mM KCl (solution G) and **C**) in 4 mM KCl (solution F). Ramps were stepped from -60 mV to 60 mV in 20 ms. The Nernst potentials for K^+ (E_K) and Cl^- (E_{Cl}) are indicated. The smooth lines are higher-order polynomials fitted to the data. The cartoons indicate concentrations in mM

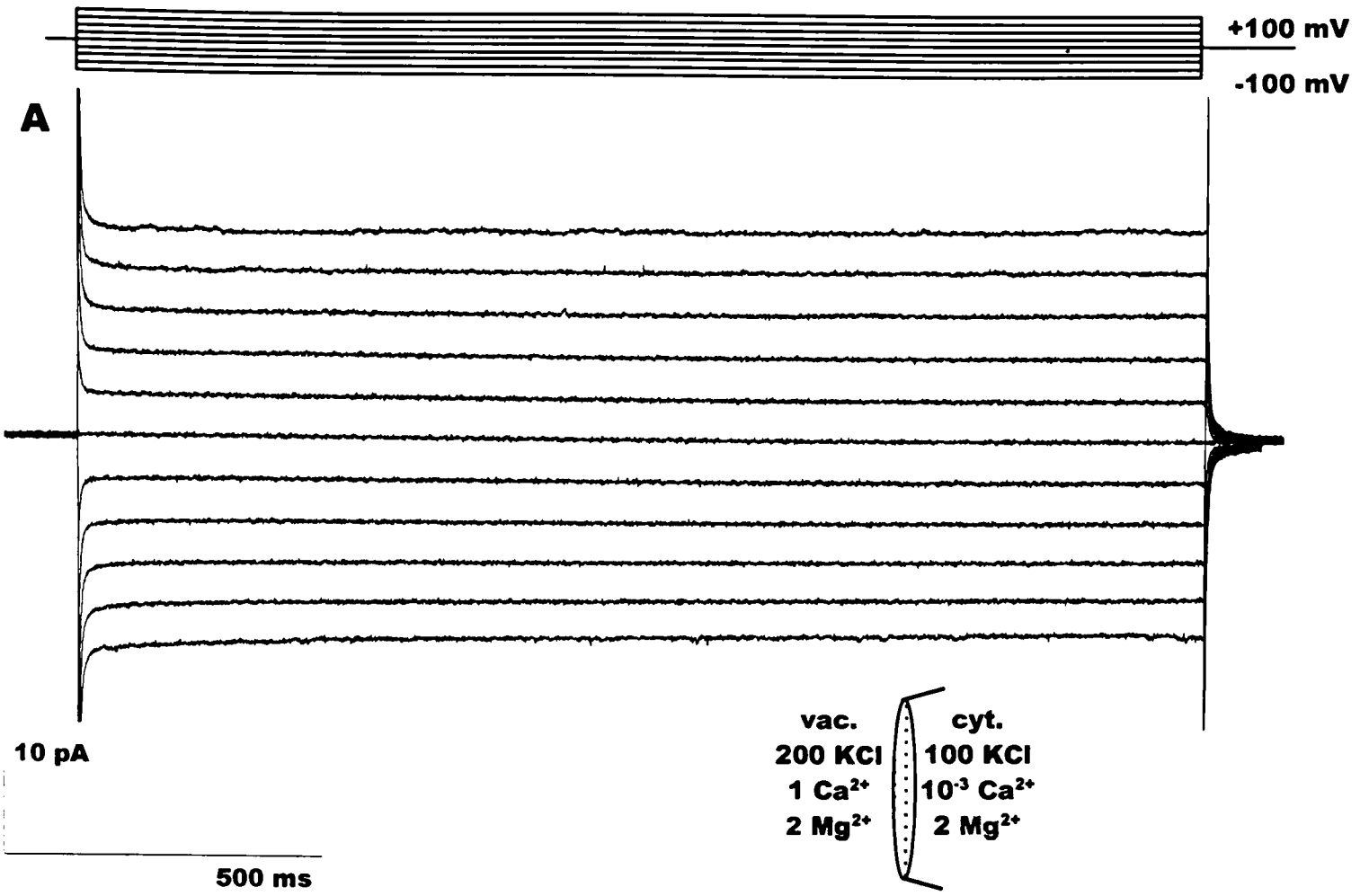


Figure 6.40. Single-channel activity of KS1 appearing after prolonged depolarisation. **A**) No single-channel activity could be observed at any voltage immediately after obtaining the vacuolar-side-out configuration (cyt.: 100 mM KCl, solution J; vac.: 200 mM KCl, solution G). **B**) Appearance of multiple channel activities after prolonged depolarisation for several minutes to up to +200 mV. The cartoon indicates concentrations in mM

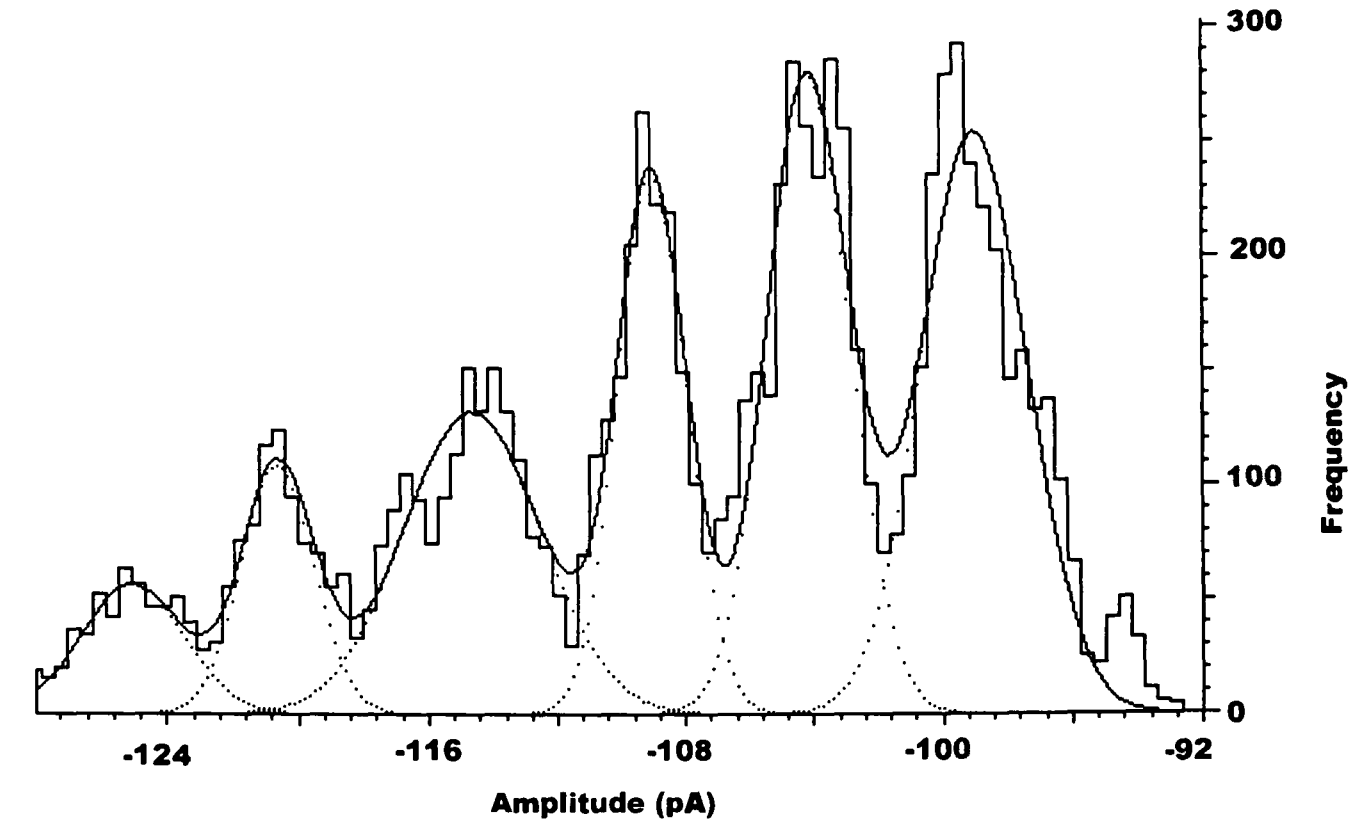
activity, but after waiting for 7 minutes, with intermittent depolarisations up to +200 mV, a multitude of channels appeared (Figure 6.40.B and Figure 6.41.A). These channels had a slope conductance of 110 pS at -30 mV and reversed close to E_K (Figure 6.41.B). This type of channel was recorded in five patches, and it will be referred to as KS1 (for K^+-conducting "sleeper" channel).

In one experiment, single-channel amplitudes appeared after hyperpolarising the patch for 10 min to -100 mV. At least two individual channels could be observed at -10 mV in 200 mM KCl (Figure 6.42.A). The voltage ramps showed that the current amplitudes reversed close to E_K in 200 mM KCl, and the reversal potential was shifted negative in 4 mM KCl. This indicated a high selectivity for K^+ over Cl^-. The slope conductance was 88 pS at -50 mV and 85 at +50 mV. This type of channel will be referred to as KS2.

Thus, as with the recordings at high cytosolic Ca^{2+}, at 1 μM Ca^{2+} a number of channels were also found to be active in the tonoplast membrane of *M. crystallinum*. However, none has yet shown any specificity for Cl^-. Table 6.1 lists all channel types found under the different conditions.

6.2.2.6 Recordings with 100 nM cytosolic Ca^{2+}

The lowest concentration of free Ca^{2+} tested was around 100 nM. At this low Ca^{2+} concentration in the bath, the success rate for obtaining a good seal was very low, and the recordings were not very stable in the whole-vacuole configuration. Only one experiment with successful perfusion could be performed (Figure 6.43). The whole-vacuole configuration was obtained in asymmetric KCl solutions, with 200 mM KCl on the cytosolic side. Large instantaneous outward and inward currents could be observed, with no time-dependent currents at any membrane potential. The



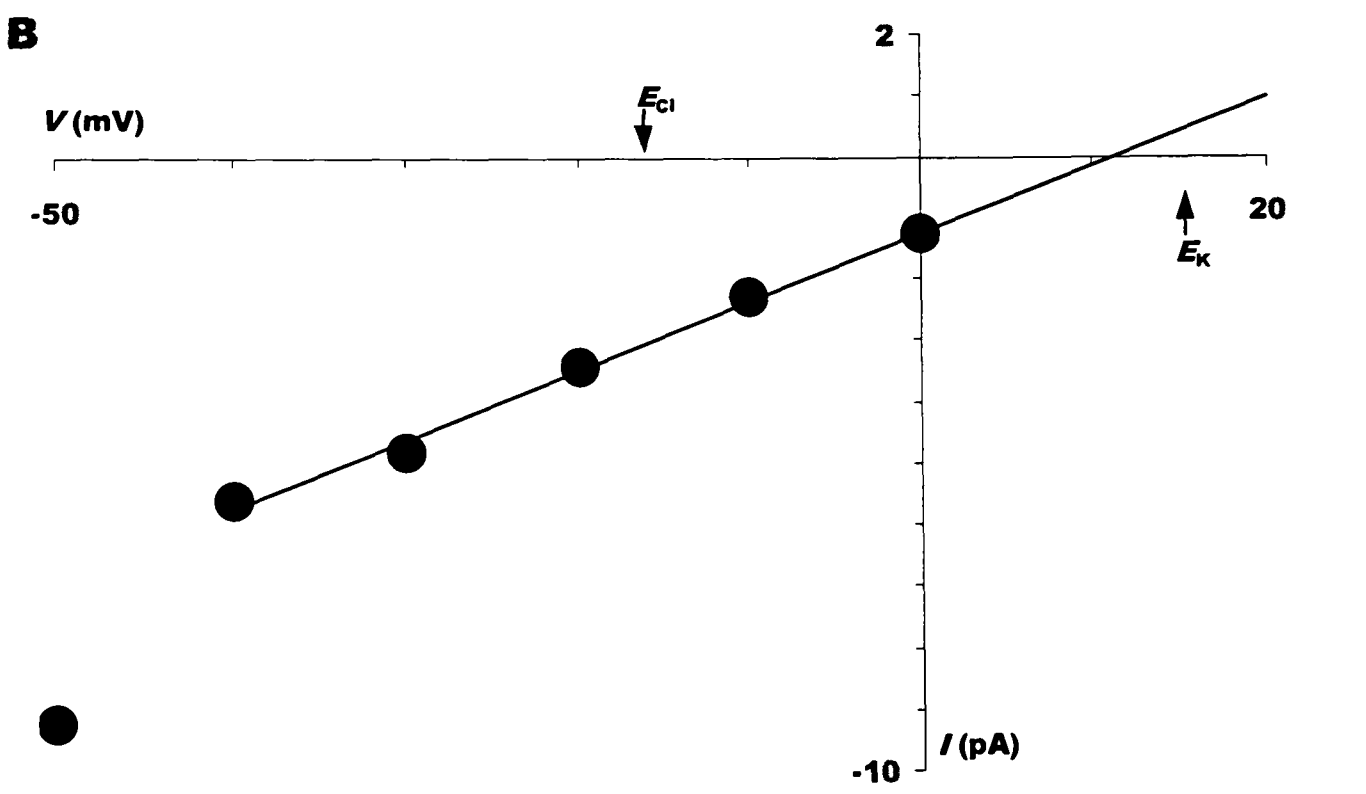


Figure 6.41. Single-channel activity of KS1 appearing after prolonged depolarisations. **A**) Amplitude histogram of Figure 6.40.B. The histogram was fitted with a sixth-order Gaussian function, as indicated by the smooth lines, using the pCLAMP software package. The means obtained for the six distributions were amplitudes of -125.2 pA, -120.6 pA, -114.6 pA, -109.0 pA, -104.2 pA and -99.0 pA. **B**) Current-voltage plot constructed from several amplitude histograms obtained at various membrane potentials. The Nernst potentials for K^+ (E_K) and Cl^- (E_{Cl}) are indicated. The data between -40 and 0 mV were fitted with a straight line

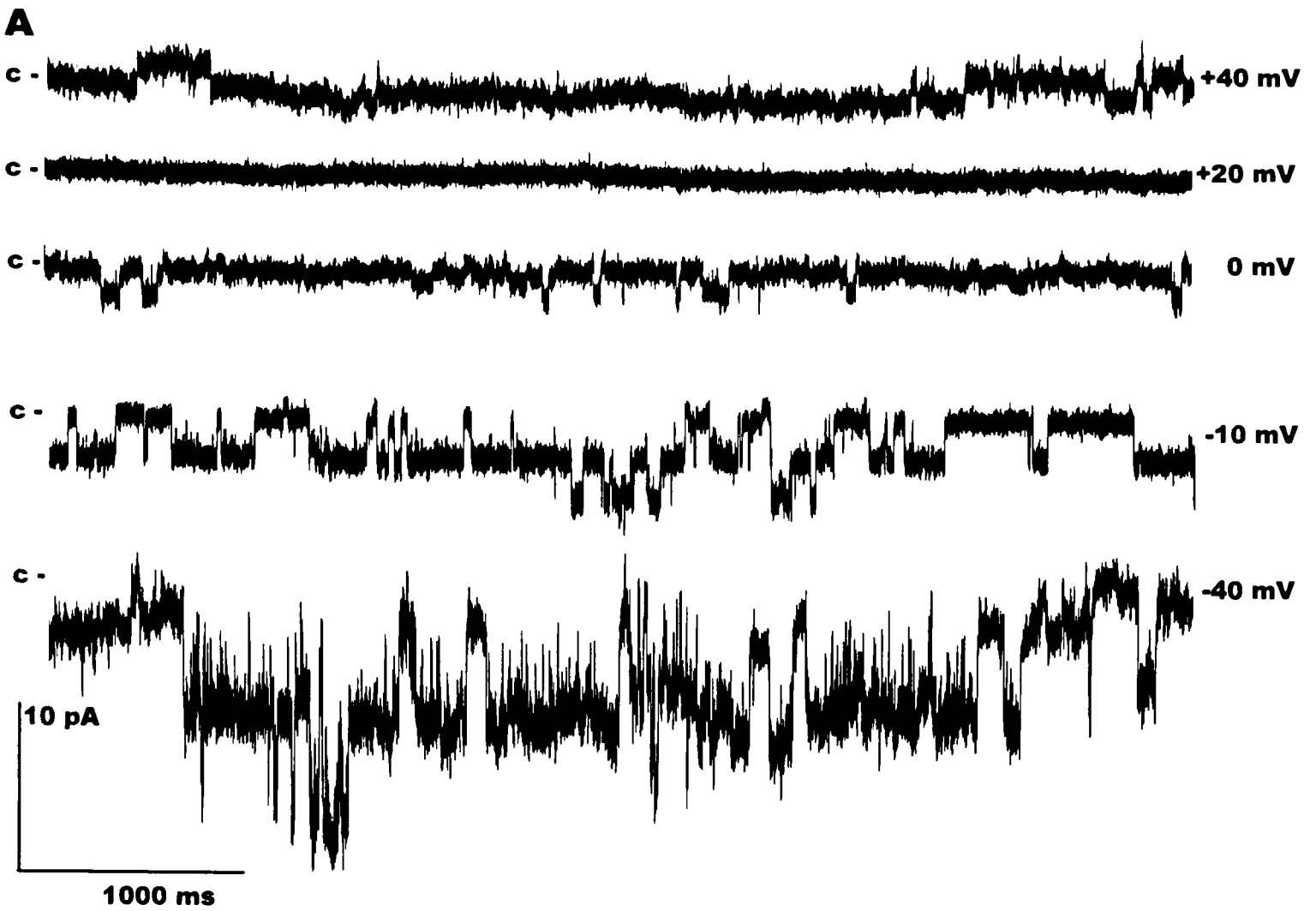


Figure 6.42. Single-channel activity of KS2 appearing 10 min after continuous hyperpolarisation at -100 mV. **A**) Single-channel activity appearing after no activity was seen immediately after obtaining the vacuolar-side-out configuration (cyt.: 100 mM KCl, solution J; vac.: 200 mM KCl, solution G). The closed state is indicated by (c). **B**) Current-voltage plot constructed from a voltage ramp in 200 mM KCl (solution G) and **C**) in 4 mM KCl (solution F). Ramps were stepped from -100 mV to 100 mV in 25 ms. The Nernst potentials for K^+ (E_K) and Cl^- (E_{Cl}) are indicated. The smooth lines are higher-order polynomials fitted to the data. The cartoons indicate concentrations in mM

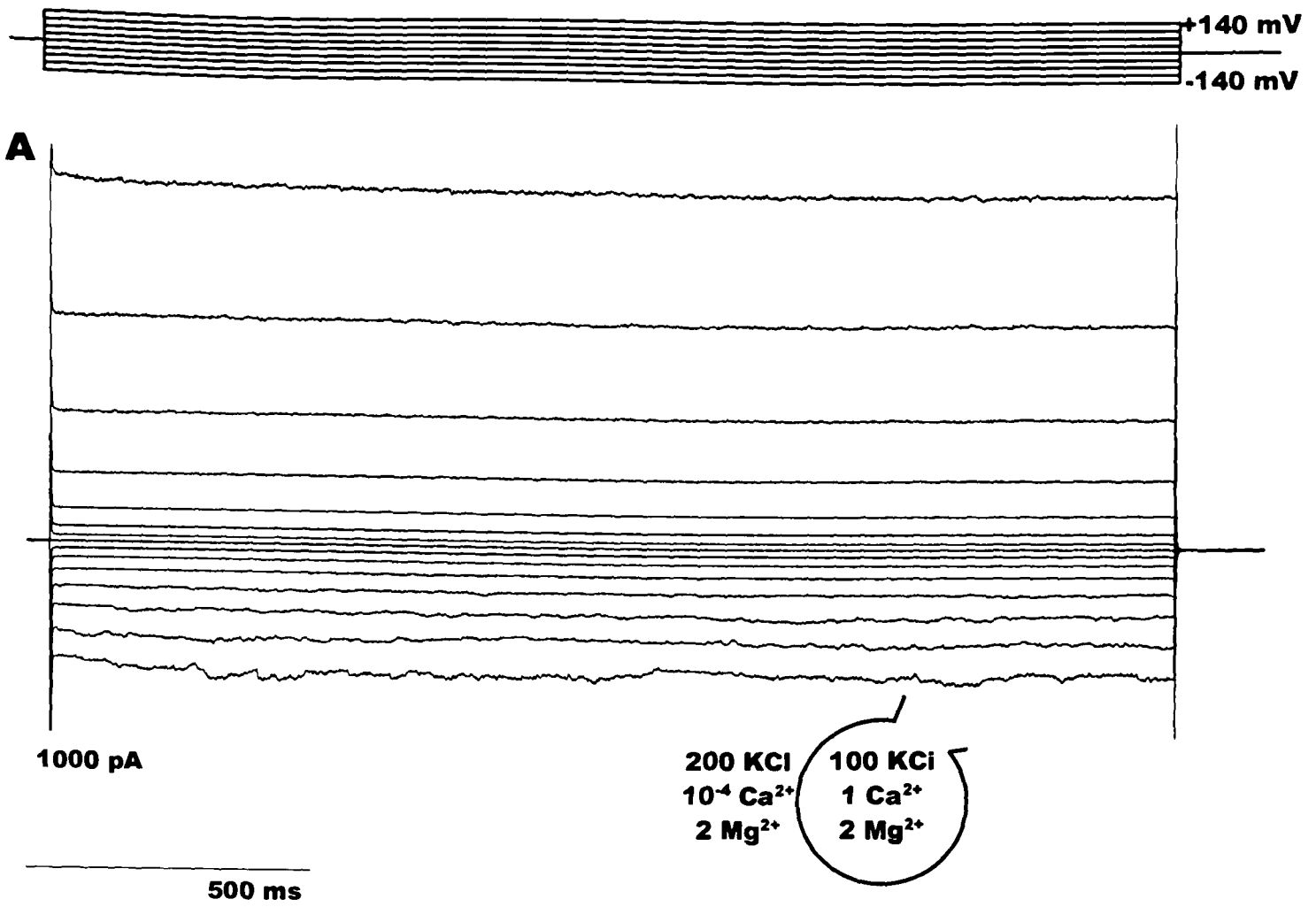


Figure 6.43. Whole-vacuole currents at low cytoplasmic Ca^{2+} (100 nM). The vacuolar diameter was ~60 μm. From a holding potential of 0 mV, the membrane potential was stepped from -140 mV to +140 mV in 20 mV steps (100 mM KCl, solution E, at the vacuolar side. **A**) 15 min after obtaining the whole vacuole configuration and perfusing the cytoplasmic side with 200 mM KCl (solution Q). **B**) After perfusing the cytoplasmic side with 100 mM K^+ / 10 mM Cl^- (solution S). The cartoons indicate concentrations in mM. Figure continued on the following page

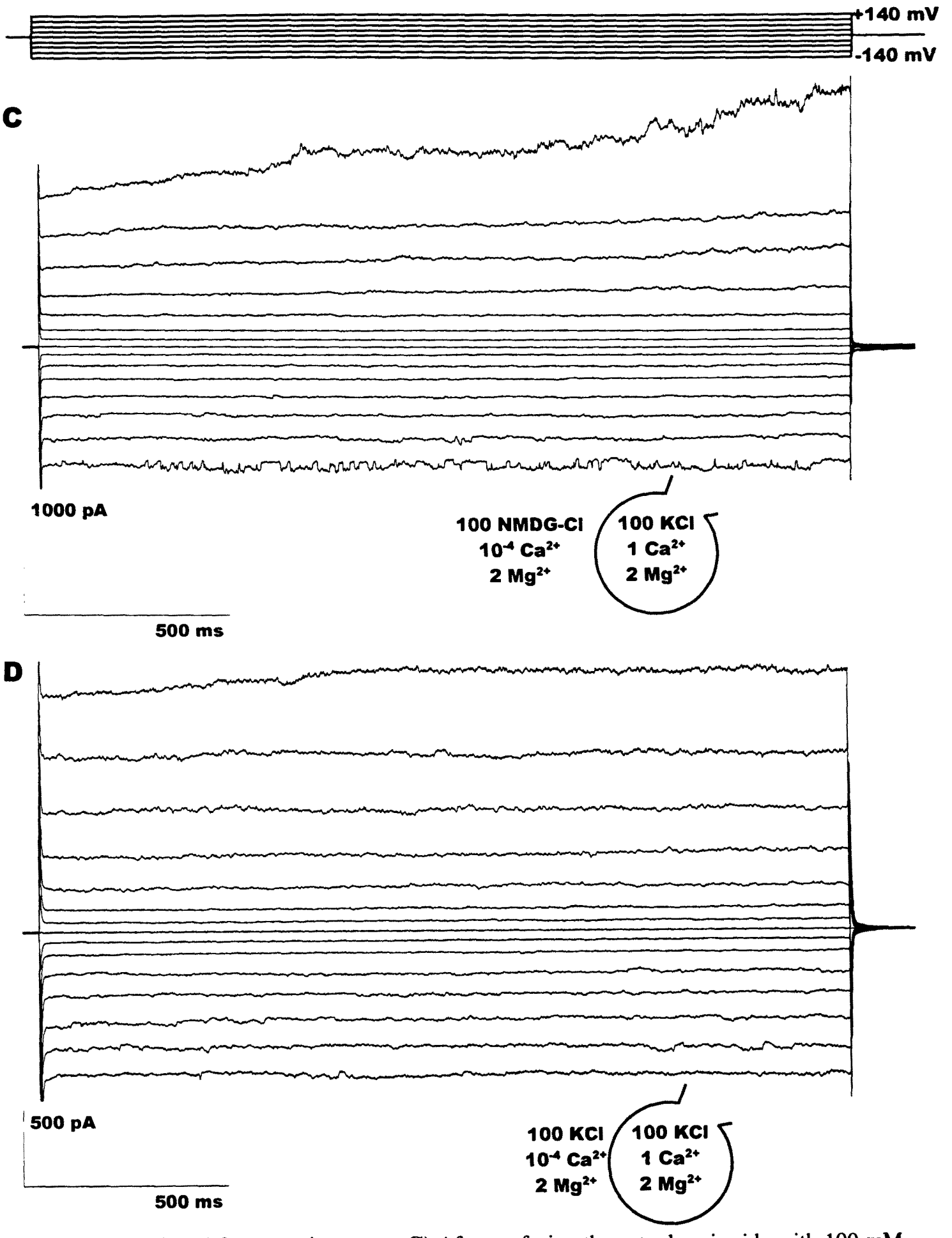


Figure 6.43. Continued from previous page. **C**) After perfusing the cytoplasmic side with 100 mM NMDG-Cl (solution R). **D**) After perfusing the cytoplasmic side with 100 mM KCl (solution O). The cartoons indicate concentrations in mM. Figure continued on the following page

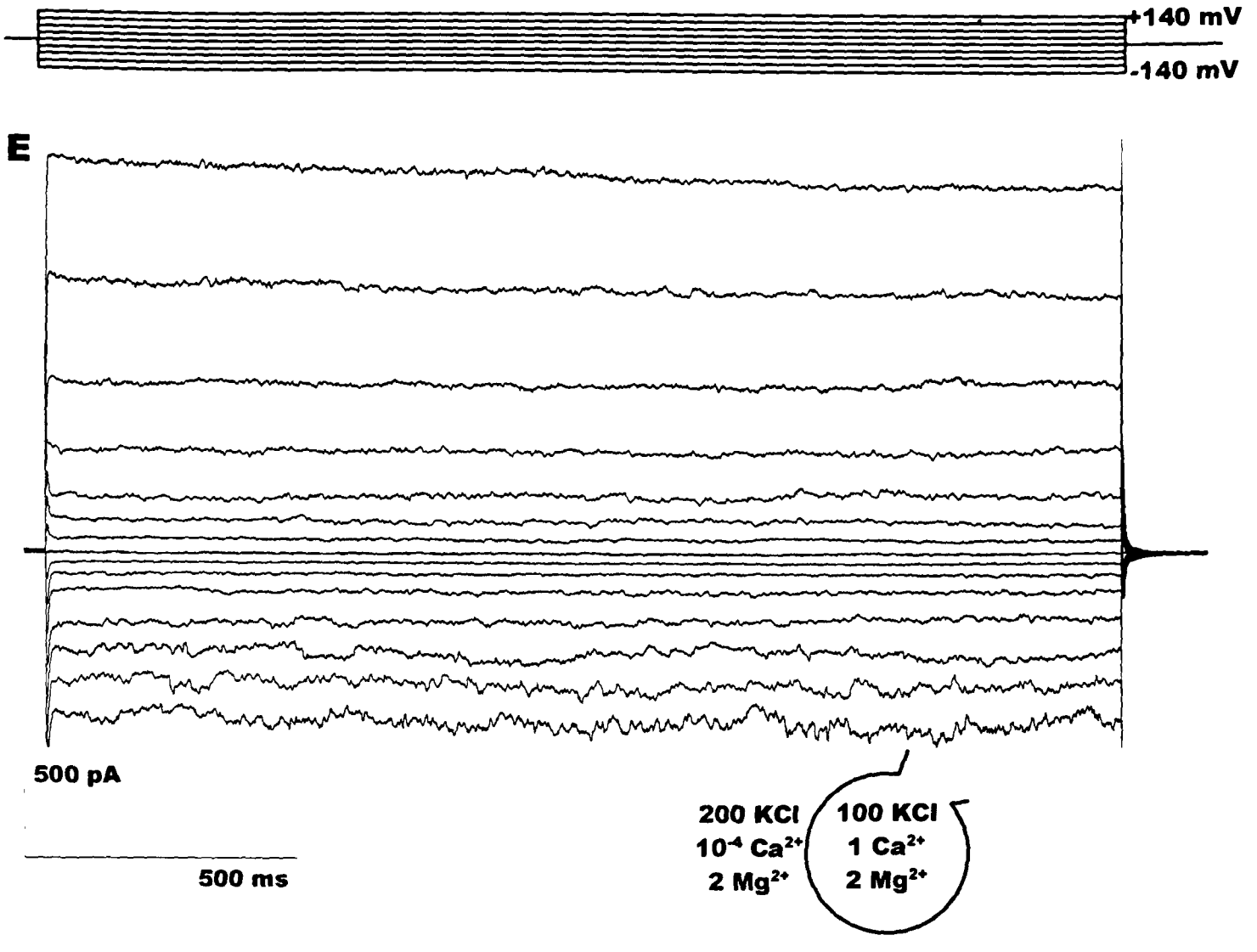


Figure 6.43. Continued from previous page. E) Whole-vacuole recordings after changing the cytoplasmic side back to 200 mM KCl (solution Q). The cartoon indicates concentrations in mM

currents reversed around +40 mV immediately after obtaining the whole-vacuole configuration, but 15 min later the reversal potential was shifted less positive towards +16 mV (data not shown), indicative of the exchange of the vacuolar solution with the pipette. When the cytosolic side was again perfused with 200 mM KCl after 70 min, the reversal potential had shifted further negative towards -5.5 mV. When exactly the vacuolar lumen was equilibrated with the pipette was difficult to determine. However, the relative shifts of reversal potentials under different ionic conditions should still give an indication which of the ions might be carrying the current. In all solutions tested (200 mM KCl, 100 mM K^+/10 mM Cl^-, 100 mM NMDG-Cl and 100 mM KCl), the instantaneous character of the currents was similar. Given the instantaneous nature of these currents, tail-current experiments could not be performed.

Figure 6.44 summarises the current-voltage relationships for these currents under different ionic concentrations. The overall current-voltage relationship was similar in all three solutions, but with the steep inwardly directed Cl^- gradient in 100 mM K^+/10 mM Cl^- the outward currents increased, while the inward currents remained unchanged. This is consistent with Cl^- carrying part of the outward current. On the other hand, with the steep inwardly directed K^+ gradient the inward currents increased, without an increase in outward currents, indicating K^+ also being a charge carrier. Similarly, the reversal potentials measured were always intermediate between the Nernst potentials for K^+ and Cl^-. At high K^+ (200 mM KCl), the reversal potential tended to be closer to E_K, while at low K^+ concentrations it was closer to E_{Cl}. The very positive Nernst potential of +134 mV for Ca^{2+} seemed to have hardly any effect in any of the measurements. The permeability ratios for K^+ and Cl^- were calculated to be P_{Cl}/P_K = 0.47 in 200 mM KCl and P_{Cl}/P_K = 1.69 in 100 mM K/ 10 mM Cl^-,

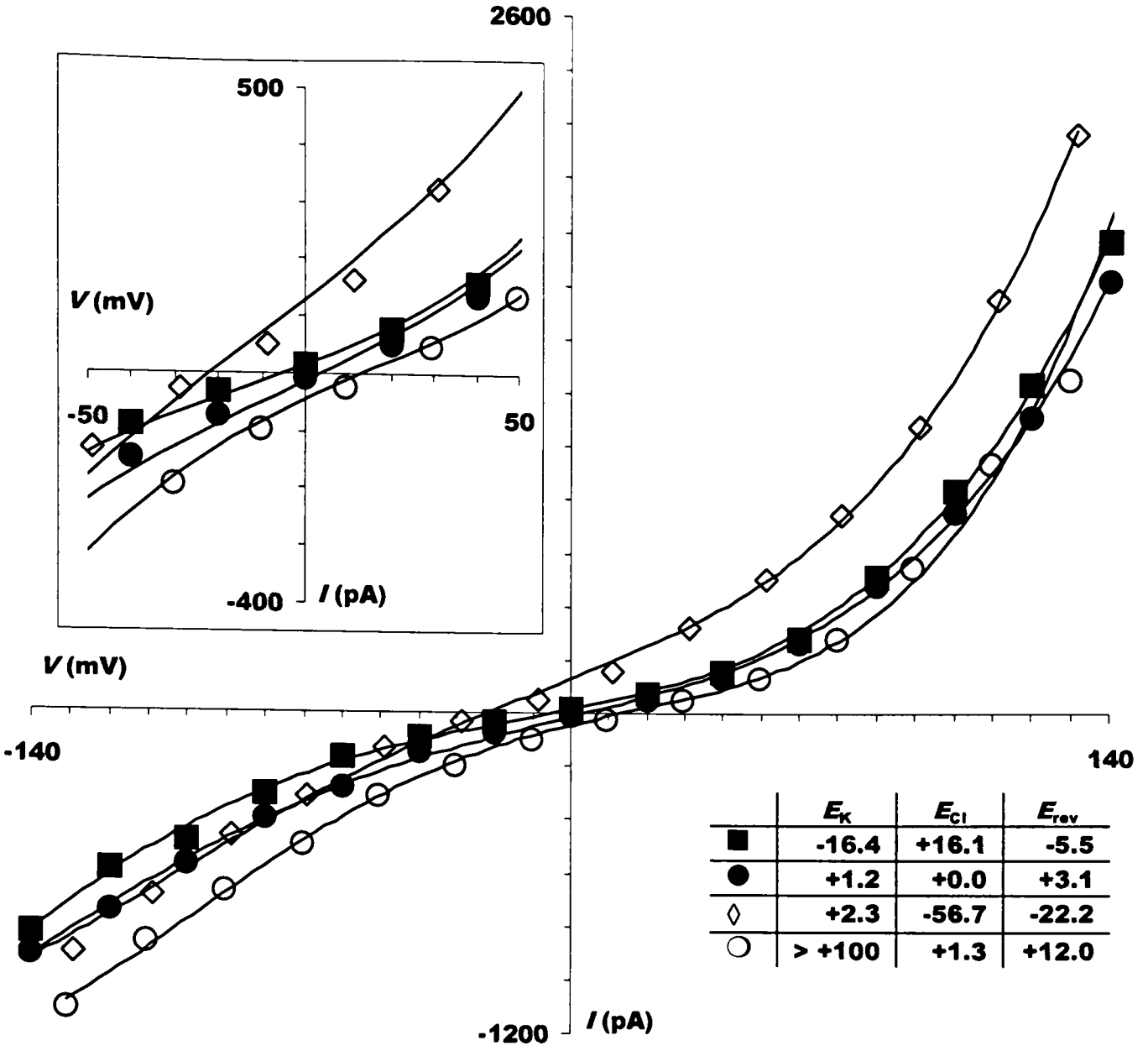


Figure 6.44. Current-voltage plots of the whole-vacuole currents at low Ca^{2+} (100 nM). Current-voltage plots were constructed from Figure 6.44.B to E, with 100 mM KCl (solution E) on the vacuolar side. Symbols for cytoplasmic KCl concentrations: 200 mM KCl (■), 100 mM KCl (●), 100 mM K^+ / 10 mM Cl^- (◊), 100 mM NMDG-Cl (○). The inset shows the same plot on a larger scale to show the reversal potentials. The Nernst potentials for K^+ (E_K) and Cl^- (E_{Cl}) and the observed reversal potentials E_{rev} are indicated in mV. The Nernst potential for Ca^{2+}, E_{Ca}, was +134 mV for all recordings. For 100 mM NMDG-Cl, without any K^+, E_K could not be calculated, but should have considerably exceeded +100 mV

respectively, according to the GHK voltage-equation (see section 6.2.2.5, page 134). The value for 200 mM KCl should be the more reliable, since it was determined 70 min after the experiment was started, thus being more likely to be fully equilibrated. The measurement in 100 mM K^+/10 mM Cl^- was made 32 min after obtaining the whole-vacuole configuration, and therefore might not have been fully equilibrated.

The leak currents through the seal could not be subtracted from these instantaneous currents, and might well have influenced the reversal potential. But they should be non-selective for K^+ over Cl^-, and therefore always have a reversal potential halfway between E_K and E_{Cl}. The fact that in 100 mM NMDG-Cl the observed reversal potential was quite close to E_{Cl}, with very positive E_K and E_{Ca} (and hence very positive reversal potentials for the leak currents) points to a high Cl^- selectivity. Unfortunately, this was the only whole-vacuole recording at low cytosolic Ca^{2+} where the seal lasted long enough to give a reasonable equilibration of the vacuolar lumen and to allow the exchange of the cytosolic bath solutions. Single-channel recordings were attempted, but generally resulted in unstable recordings and low seal resistances. Figure 6.15 shows one of six successful seals, but in none of these experiments were single-channel events observed.

6.2.3 Patch-clamp recordings with NMDG-Cl-based solutions

To eliminate any K^+ currents, whole-vacuole recordings were performed with $NMDG^+$ (*N*-methyl-D-glucamine), which is membrane-impermeant (Cheffings *et al.*, 1997), substituting for K^+ as the major cation. Figure 6.45 shows a typical recording (out of a total of six) with symmetrical 100 mM NMDG-Cl solutions. Immediately after obtaining the whole-vacuole configuration large, slowly activating outward currents could be observed at positive membrane potentials. At negative membrane

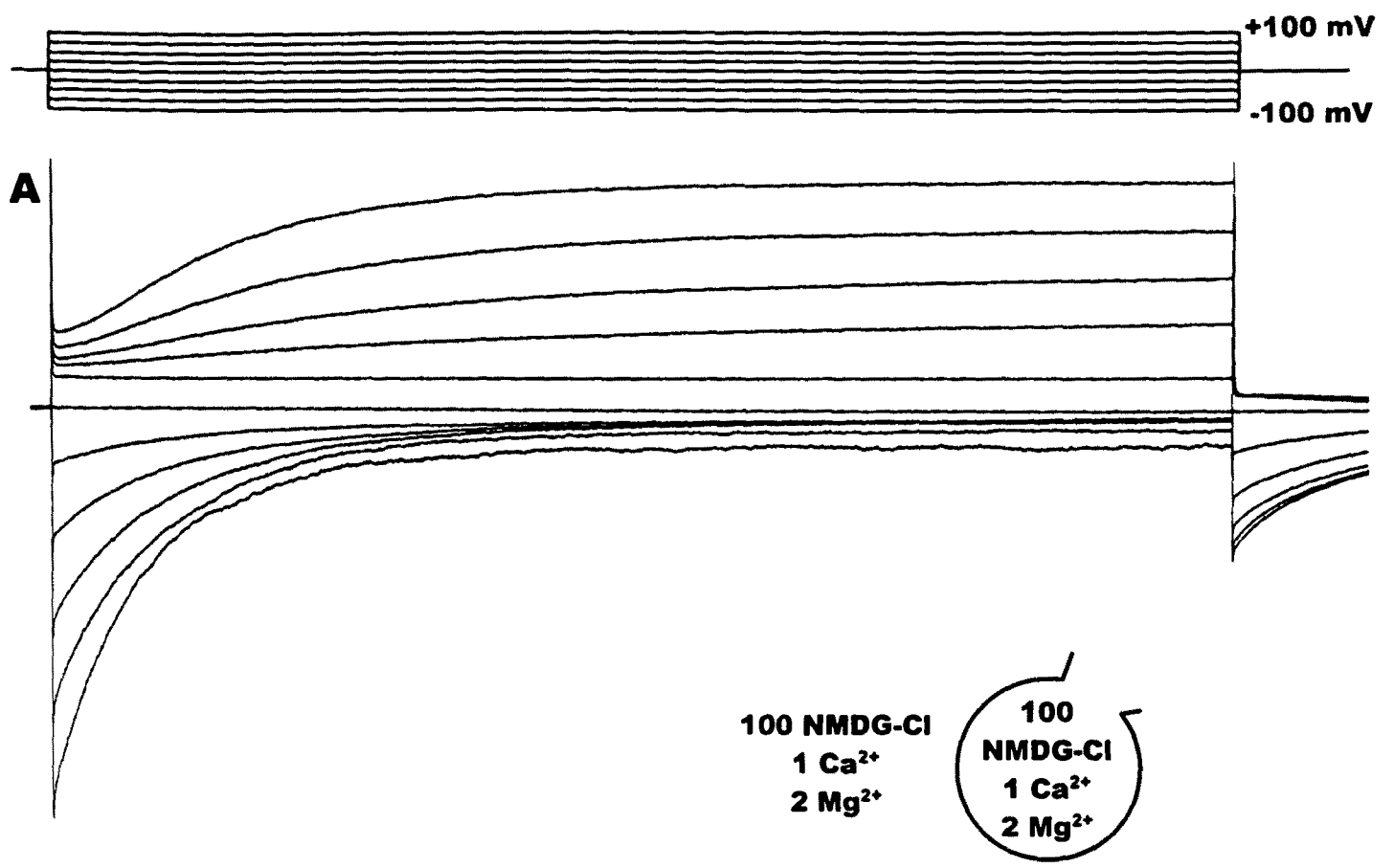


Figure 6.45. Whole-vacuole currents in symmetrical 100 mM NMDG-Cl solutions (solution H on both sides). **A**) Immediately after obtaining the whole-vacuole configuration. **B**) 20 min after obtaining the whole-vacuole configuration. The cartoon indicates concentrations in mM

potentials, large instantaneous currents of several nA amplitude inactivated within 0.5 s. After 20 min, the time-dependent currents were reduced to less than 30% of the original values, while the time-independent amplitudes remained largely unchanged. Figure 6.46 shows a recording immediately after obtaining the whole-vacuole configuration at a holding potential of -50 mV. No inactivating inward currents could be observed, and the time-dependent outward currents were activated positive of 0 mV, indicating the strong outward rectification of this current.

Figure 6.47 shows recordings of tail currents immediately after and 25 min after, obtaining the whole-vacuole configuration. Immediately after obtaining the whole-vacuole configuration, large inward currents could be observed at negative test pulses, saturating the amplifier input. After 25 min, the inward-current amplitudes were reduced by more than 30%. Also, the activation during the prepulse was now much slower and the prepulse amplitude reduced. The reversal potential had shifted from about +40 mV to about +20 mV (Figure 6.48). This showed that even after 25 min the vacuolar lumen was still not equilibrated with the pipette solution, since the symmetrical solutions should have generated a reversal potential of 0 mV. The deviation towards positive reversal potentials could be due to cations, probably K^+, still being left in the vacuole. However, since there was no K^+ in the bath, the observed outward currents could not have been carried by K^+.

During one recording it was possible to change the cytosolic (bath) NMDG-Cl concentration from 100 mM to 20 mM and back (Figure 6.49). Whereas the reversal potential was not affected by this change, the amplitude of the steady-state outward currents was increased by about 50% in 20 mM NMDG-Cl. This would be in line with Cl^- currents being enhanced by the steep inwardly directed Cl^- gradient. However, the

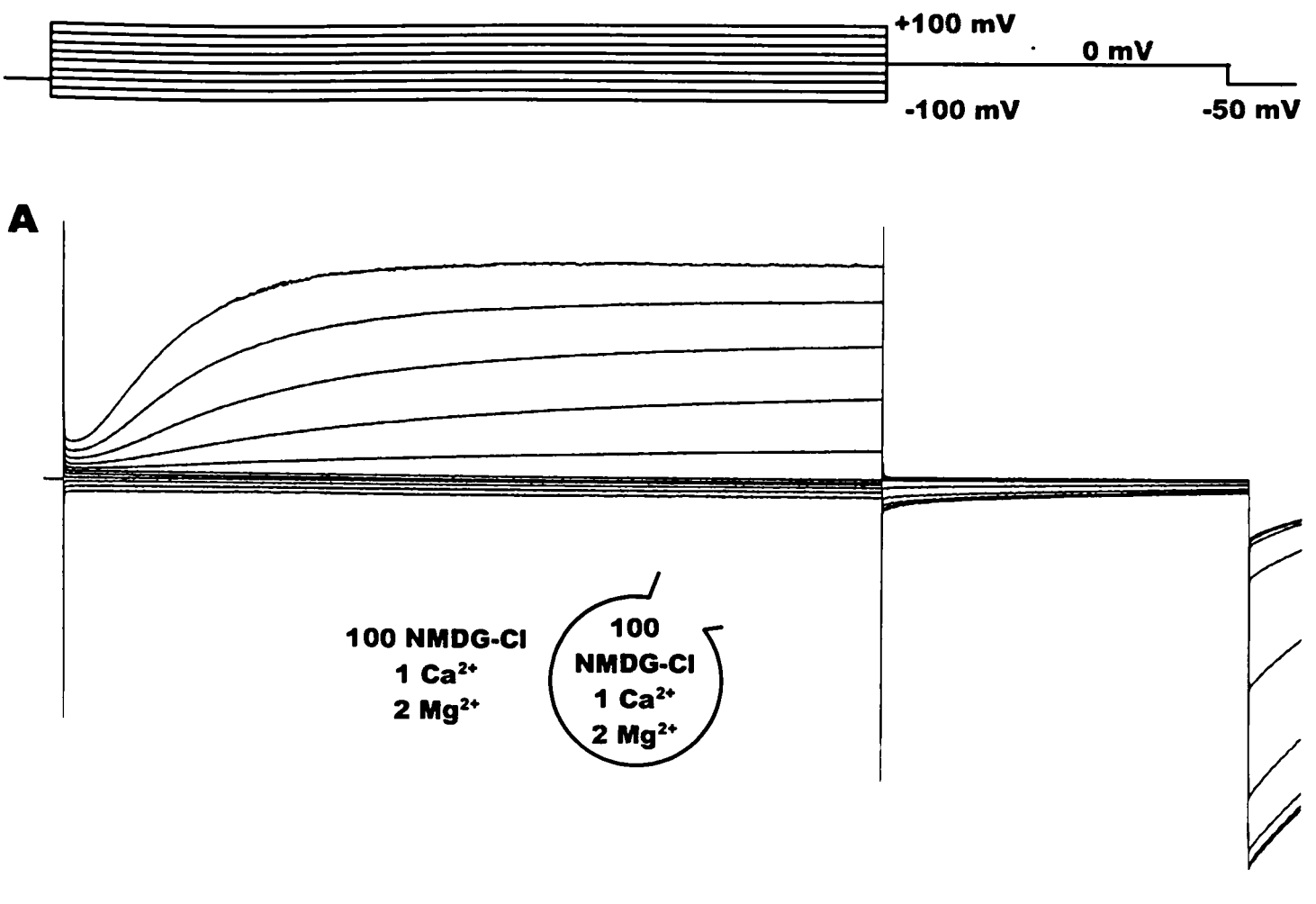


Figure 6.46. Whole-vacuolar currents in symmetrical 100 mM NMDG-Cl (solution H) at -50 mV holding potential. **A**) From a holding potential of -50 mV, the pipette potential was stepped to values from -100 to +100 mV in 20 mV increments. After the test pulse, the potential was stepped to 0 mV. **B**) Current-voltage plots of the instantaneous (○) and steady-state currents (❑). The instantaneous currents were subtracted from the steady-state currents to reveal the time-dependent current (Δ). The cartoon indicates concentrations in mM

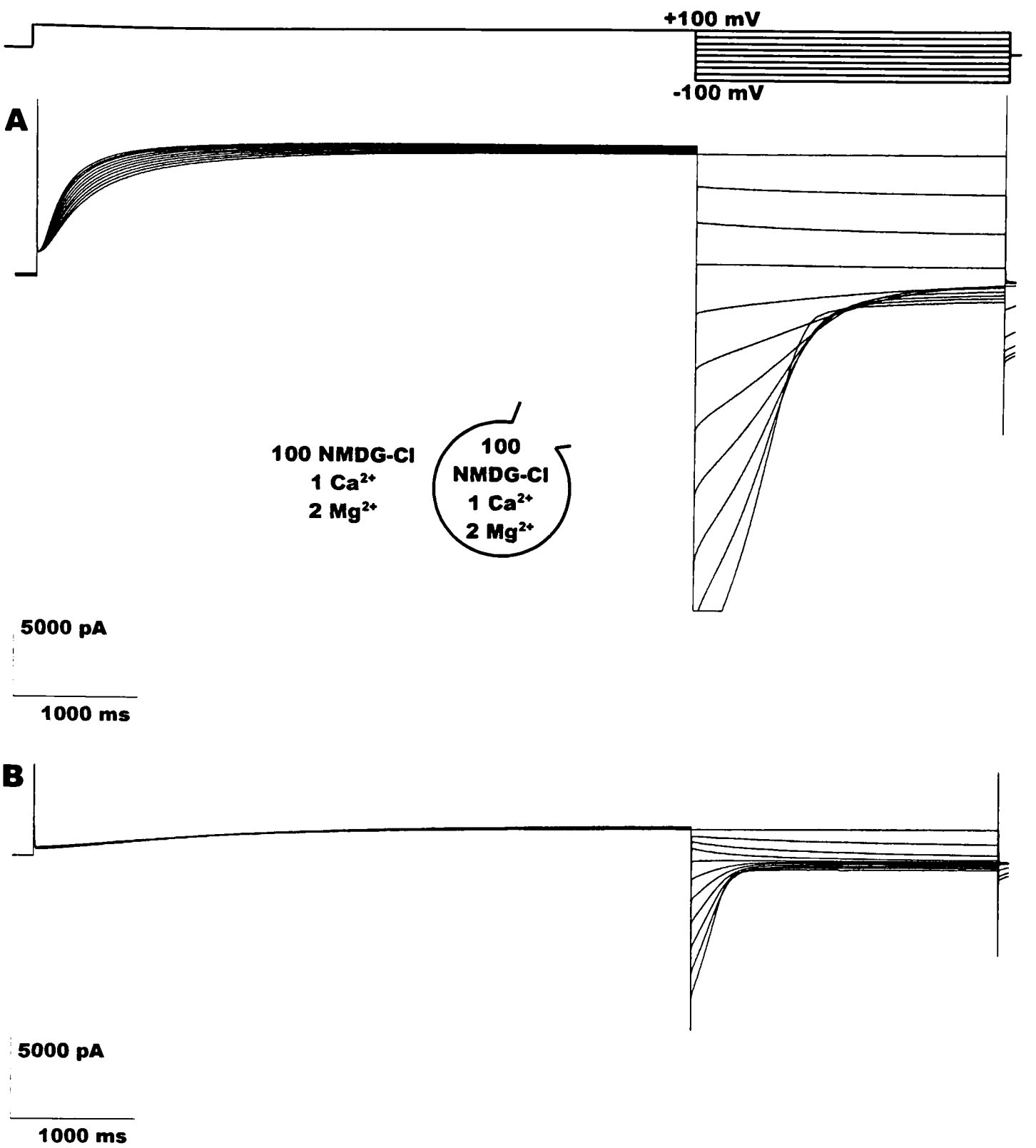


Figure 6.47. Whole-vacuole tail currents in symmetrical 100 mM NMDG-Cl solutions (solution H on both sides). The membrane potential was stepped from an activating prepulse of +100 mV to a membrane potential from -100 mV to +100 mV. **A**) Tail currents immediately after obtaining the whole-vacuole configuration. Note that at a test pulse of -100 mV and -80 mV the inward currents initially exceeded the maximum current limit of the amplifier. **B**) Tail currents 20 min after obtaining the whole-vacuole configuration. The cartoon indicates concentrations in mM

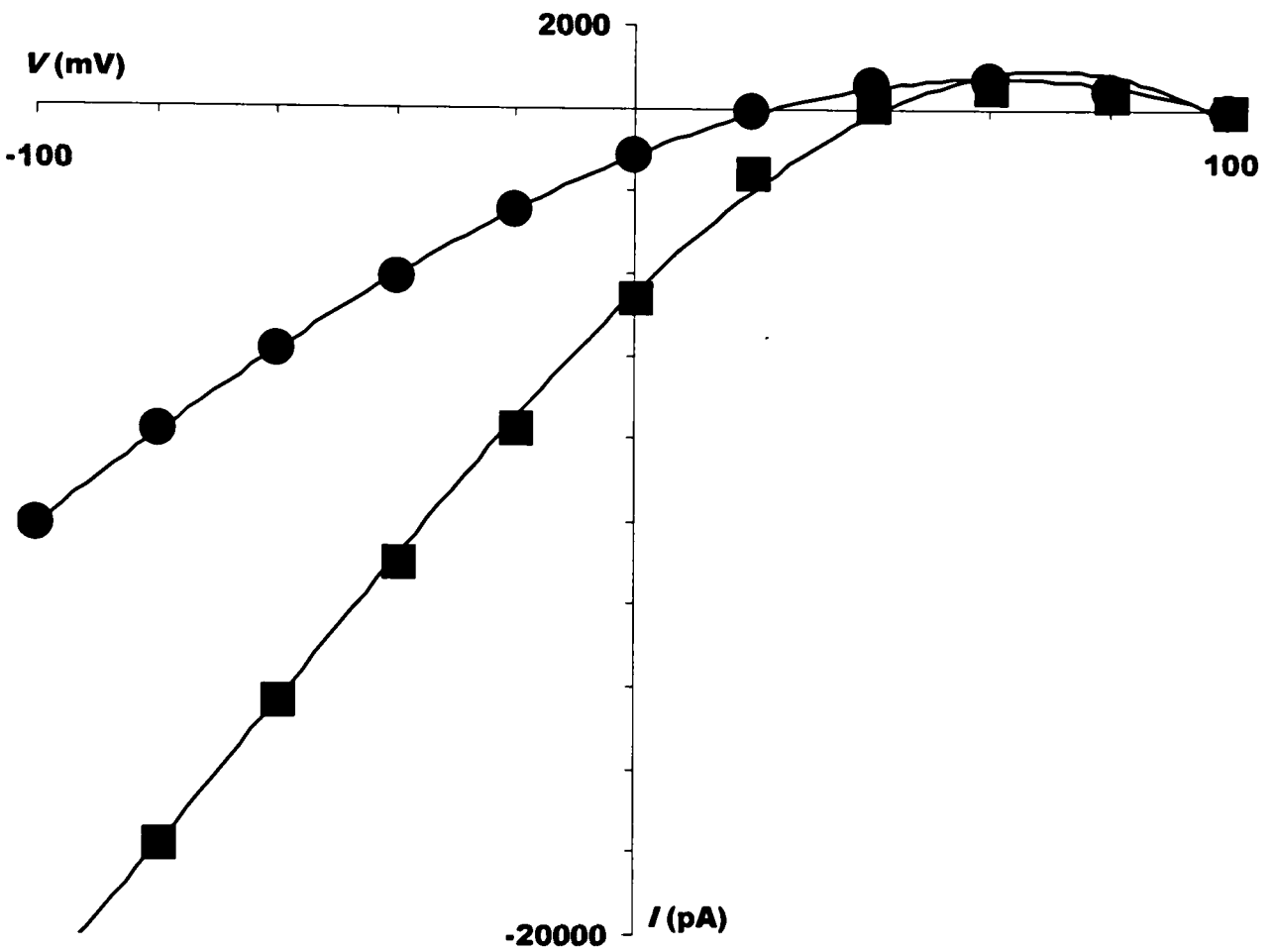


Figure 6.48. Current-voltage plot of the tail currents from Figure 6.47. The amplitudes of the tail currents for the recordings immediately after obtaining the whole-vacuole configuration (■) were obtained by subtracting the currents at the end of the test pulse from the currents at the beginning of the test pulse. For the recordings 20 min later (●), the tail currents were fitted with single exponentials and extrapolated back to the amplitude at the very beginning of the test pulse and the steady-state current subtracted from this. The lines are higher-order polynomial fitted to the data

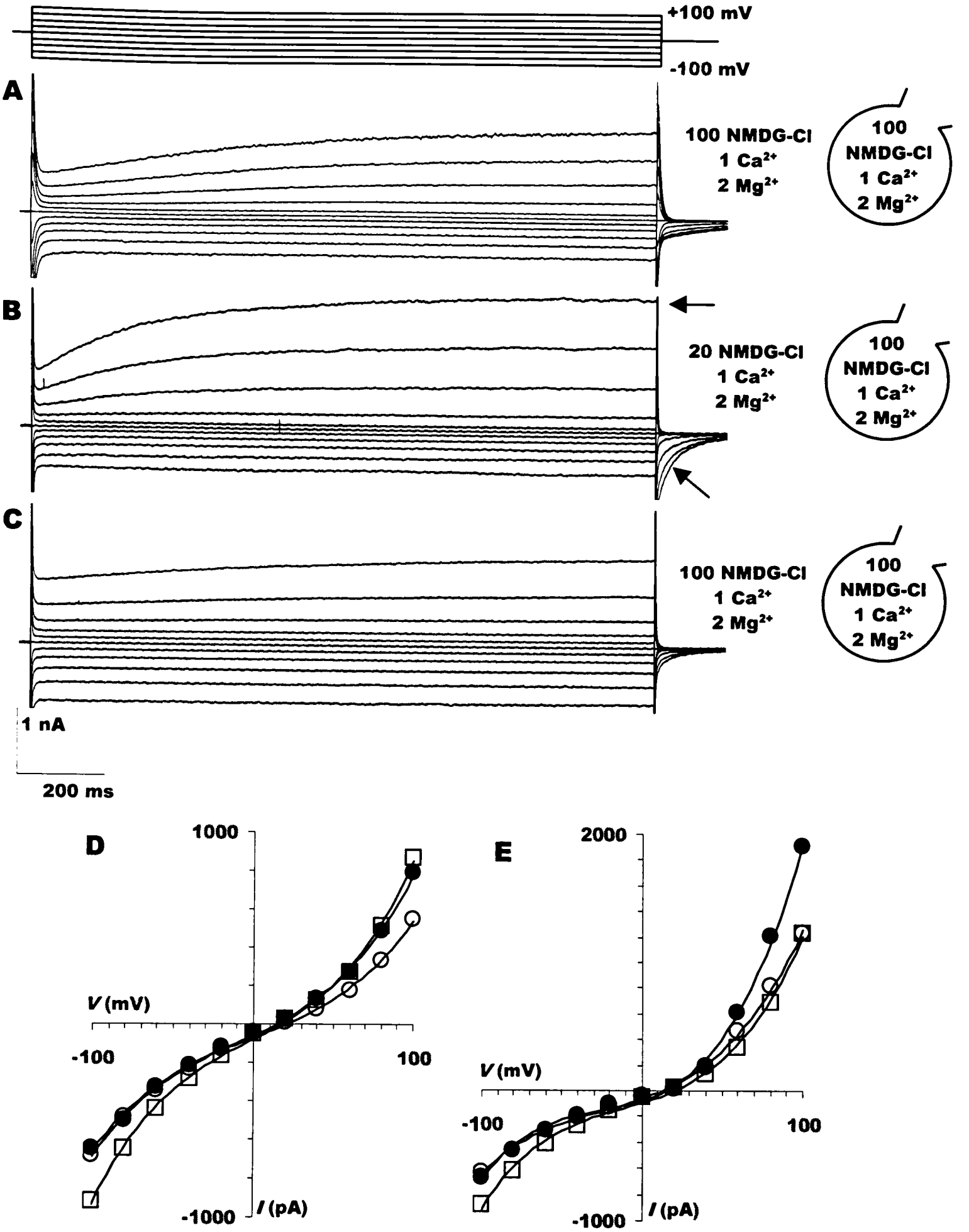


Figure 6.49. Whole-vacuole recordings under asymmetric NMDG-Cl concentrations. **A**) Recordings in symmetrical 100 mM NMDG-Cl (solution H) 25 min after obtaining the whole-vacuole configuration. **B**) Recordings after perfusion of the cytoplasmic side with 20 mM NMDG-Cl (as solution H, but with 20 mM NMDG-Cl), after 42 min. Note the increase in outward current and also tail-current amplitude, indicated by the arrows. **C**) Recordings after changing back to 100 mM NMDG-Cl (70 min). **D**) Current-voltage plot of the instantaneous and **E**) of the steady-state currents. Symbols: (○) 100 mM NMDG-Cl, 25 min; (●) 20 mM NMDG-Cl, 42 min; (❑) 100 mM NMDG-Cl, 70 min. The cartoons indicate concentrations in mM

tail currents after positive test pulses also increased (Figure 6.49.B). This suggests that the observed amplitude increase was due to an increase in the ionic permeability, rather than to the Cl^- inward-gradient providing a stronger driving force.

With the cytosolic side Ca^{2+}-free, no time-dependent currents could be observed (Figure 6.50); the instantaneous currents observed showed slight inward rectification. Only one successful recording was obtained under these conditions, without any solution changes, making it impossible to characterise these currents further.

6.3 Discussion

This study has provided a broad overview of the electrophysiological characteristics of vacuoles from leaf mesophyll cells of *Mesembryanthemum crystallinum*. The problems associated with the large vacuole diameter and the relatively low sealing rate led to a low number of replicates being obtained for some experiments. The recordings with NMDG-Cl were especially hampered by the long diffusion time, since the vacuolar cations had to be completely replaced by $NMDG^+$, and even low amounts of K^+ in the vacuole still resulted in a considerable driving force for this ion, given its complete absence on the cytosolic side. That the equilibration times observed were even lower than the estimates calculated according to the method of Pusch and Neher (1988) was due to the different methods employed. Their work on small animal cells determined the diffusion times of individual ions. This was accomplished by measuring the reversal potentials for defined K^+ or Na^+ currents as a function of the intracellular concentration, or by following the diffusion of fluorescent molecules of different molecular weight. In the present study, the time

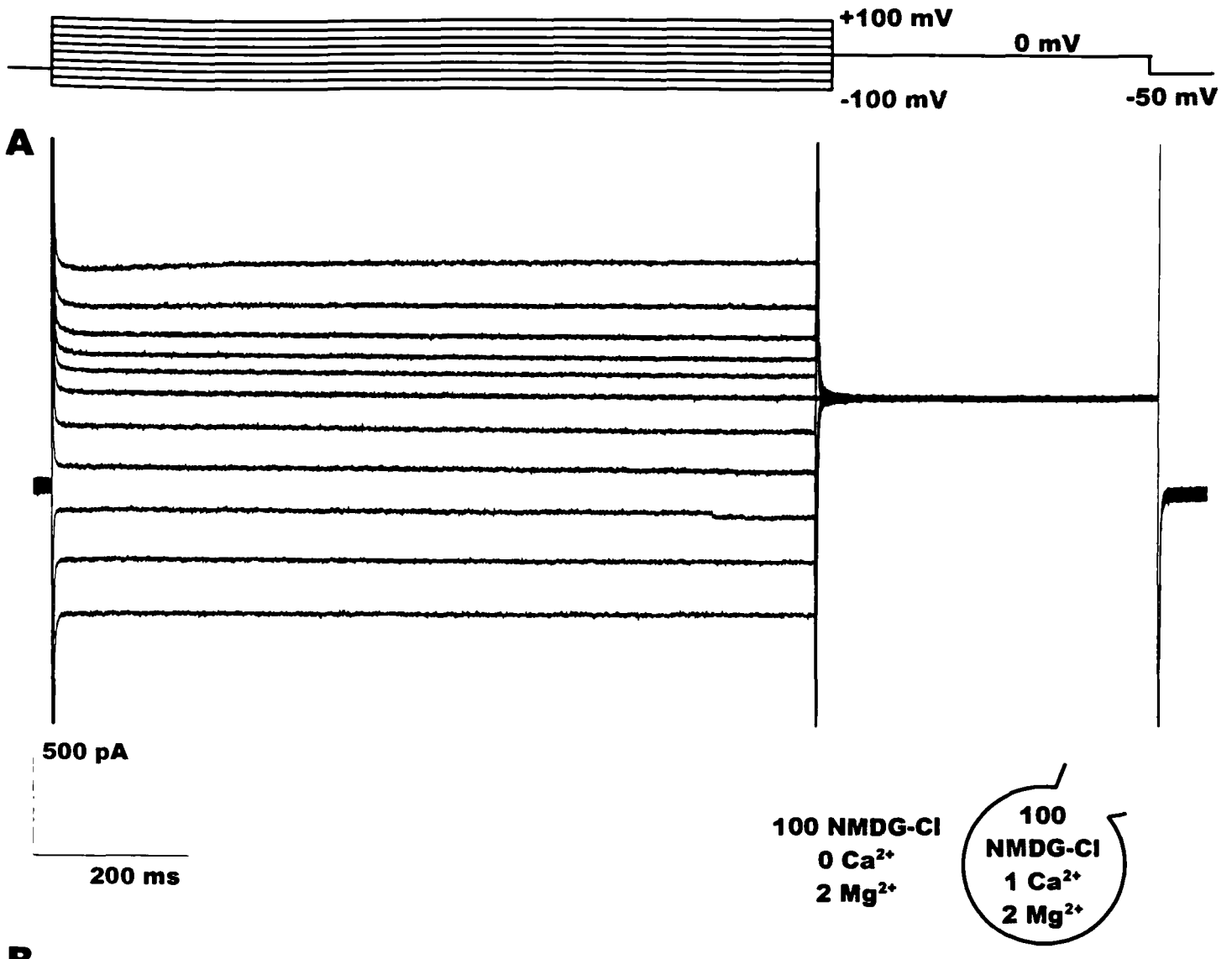


Figure 6.50. Whole-vacuole currents in 100 mM NMDG-Cl with low Ca^{2+} on the cytoplasmic side. The vacuole was perfused with solution H, but with Ca^{2+} substituted by 5 mM EGTA, thereby giving a nominally Ca^{2+}-free 100 mM NMDG-Cl solution on the cytoplasmic side (solution H at the vacuolar side). **A**) From a holding potential of -50 mV, the pipette potential was stepped to values from -100 to +100 mV in 20 mV increments. After the test pulse, the potential was stepped to 0 mV. **B**) Current-voltage plots of the instantaneous (○) and steady-state currents (❑). The cartoon indicates concentrations in mM

course of the free-running membrane potential was taken as an indicator of ion equilibration, which was determined by all ionic species in the vacuole. Since the diffusion of ions larger than K^+ is much slower, the total time course of equilibration was bound to be longer. A good agreement between the time course of vacuolar diffusion and that predicted from the relationship of Pusch and Neher (1988) was, however, reported for the diffusion of endogenous betacyanins from red beet vacuoles into the pipette by Meissner (1996). Thus, care had to be taken to allow sufficient time for large vacuoles to equilibrate with the pipette solution. This further reduced the number of successful recordings since many vacuoles were lost after a few minutes of perfusion. Macropatches therefore proved to be a valuable alternative for recording macroscopic currents, allowing better control of the solutions on both sides of the membrane, and improved electrophysiological characterisation. However, the actual size of the macropatch area was difficult to control, and no reliable protocol could be found to maintain reproducible patch sizes. Furthermore, large patches were mainly obtained in the vacuolar-side-out configuration, because the extra step of obtaining the whole-vacuole configuration before proceeding to cytosolic-side-out patches reduced the success rate considerably. While this technique has been widely used on larger animal cells (Hilgemann, 1994; Hilgemann, 1995), only two studies on plant vacuoles have employed large patches (Cheffings *et al.*, 1997; Pottosin *et al.*, 1997).

The macroscopic currents of *M. crystallinum* vacuoles with high cytosolic $[Ca^{2+}]_{cyt}$ were dominated by large, slow-activating, outward-rectifying currents. This type of current appears to be ubiquitous in vacuoles of higher plants and has been reported in many studies (Hedrich and Neher, 1987; Schulz-Lessdorf and Hedrich, 1995; Barkla and Pantoja, 1996; Allen *et al.*, 1998). Due to its slow activation, it is

commonly referred to as the SV current (slow-activating vacuolar current). It is selective for K^+ under high-K^+ conditions, but at low K^+ becomes permeable for other ions. A significant anion permeability has been suggested in initial studies on SV channels (Hedrich and Neher, 1987; Hedrich and Kurkdjian, 1988). However, recent studies have shown that this type of current is highly selective for cations by carefully taking into account all present ions (Ward and Schroeder, 1994; Allen and Sanders, 1996). It was shown that the SV channel has a significant permeability for Ca^{2+} and Mg^{2+}.

The channel type underlying the macroscopic currents is ORH1 (Figure 6.14), which shows the same rectification and time-dependent activation seen in the macropatch and whole-vacuole recordings. With a single-channel conductance of about 60 pS at positive membrane potentials, this is well within the range of 26 to 280 pS reported for other SV channels (summarised in Schulz-Lessdorf and Hedrich, 1995). It was unclear why these channels were not observed more frequently in single-channel recordings, despite their prominence in the macropatches. Also, after excising a macropatch, SV currents were usually smaller than in the previous vacuole-attached configuration. One reason might be the loss of a vacuolar factor, which reduces the single-channel activity, similar to a vacuolar factor that regulates SV-channel activity in *Vigna unguiculata* seedlings (Maathuis and Prins, 1991).

The SV-type currents were activated by high $[Ca^{2+}]_{cyt}$, a prominent feature of all SV-type currents. However, very similar SV-type currents could also be observed at 1 μM $[Ca^{2+}]_{cyt}$ in *M. crystallinum* vacuoles (Figure 6.18). This Ca^{2+} concentration required for channel activation is quite low compared with other studies, in which SV currents were activated by $[Ca^{2+}]_{cyt}$ well above 1 μM, such as in *Vicia faba* (Allen and

Sanders, 1996) or *Hordeum vulgare* (Pottosin *et al.*, 1997). On the other hand, in *Beta vulgaris*, SV-type currents were also partially activated at 0.1 μM $[Ca^{2+}]_{cyt}$ (Schulz-Lessdorf and Hedrich, 1995).

Periodic outward-current oscillations were a prominent feature observed at positive membrane potentials with 1 μM $[Ca^{2+}]_{cyt.}$. Similar current oscillations were also observed in K_2-malate based solutions with vacuoles from *M. crystallinum* leaf mesophyll cells (personal communication, Omar Pantoja, UNAM, Mexico). This indicated that Cl^- was not involved in this phenomenon. It was difficult to assess the origin and physiological relevance of these observations. The fact that they were observed only at 1 μM $[Ca^{2+}]_{cyt}$ indicates that oscillations might depend on a specific physiological state of the membrane. In plants, fast oscillations of the plasma-membrane potential and of ionic fluxes with similar frequencies have been shown in models of the electrocoupling of guard-cell ion-transporters under physiological conditions, but the underlying assumptions and conditions were very different (Gradmann *et al.*, 1993; Gradmann and Hoffstadt, 1998).

Furthermore, the large currents involved, together with an insufficiently compensated series resistance R_s (R_s being the sum of the reference electrode resistance and the access resistance R_a) of between 3 to 15 MΩ, lead to insufficient voltage control will create artefacts under these conditions. This is due to the actual membrane voltage deviating significantly from the imposed command potential as it changes with the current amplitude (Armstrong and Gilly, 1992). With large outward currents, the actual membrane potential might be considerably less then the imposed command voltage. With the patch-clamp technique, the voltage drop generated by the current flowing through R_s can not be separated from the command potential, which is

measured over the total resistance R_{total}, with $R_{total} = R_m + R_s$ (R_m being the actual membrane resistance). This implies that the membrane voltage, defined by the voltage drop across R_m, could not be considered to be truly "clamped" to a constant potential. The fact that most oscillations were only seen immediately after obtaining the whole-vacuole configuration, with R_s not compensated, or after a drastic increase in R_s during recordings, points to an involvement of R_s. But even after compensating R_s effectively to 1.5 MΩ, a characteristic peak with a sharp onset could be seen, so other factors need to be taken into account.

Given that the Nernst potential for Ca^{2+} lies around +85 mV at 1 μM $[Ca^{2+}]_{cyt}$, close to the potentials at which current oscillations occur, Ca^{2+} currents might play a role. For example, the oscillations observed in Figure 6.23.B were generated at a command potential of +100 mV. The actual membrane potential at the start could be calculated to be 4.5 mV lower (with R_s being 3 MΩ, and an initial outward current of 1.5 nA). With increasing outward currents the voltage drop across R_s becomes bigger and hence the membrane potential lower. With a current of 5 nA, the voltage drop would be 15 mV, thereby lowering the actual membrane potential to +85 mV, the Nernst potential for Ca^{2+}. Further current increases would reduce the membrane potential even further, thereby reversing the Ca^{2+} driving force inward, while still maintaining large K^+ outward currents. Assuming a sizeable Ca^{2+} permeability of the SV channel, Ca^{2+} would start flowing inward, thereby transiently increasing the local $[Ca^{2+}]_{cyt}$ around the SV channel. This could lead to activation of SV channels, which in turn would increase the K^+-outward currents. This would hyperpolarise the membrane further, and together with the increased SV-channel activity, Ca^{2+}-inward currents would increase.

This series of events would provide a positive feedback mechanism once the membrane potential drops below the reversal potential for Ca^{2+}. This feedback loop would stop once all channels were activated and the amplitude saturated. The accompanying hyperpolarisation (10 nA currents would lead to a 30 mV shift towards a less positive membrane potential) would induce deactivation of the SV channels, thereby reducing the K^+-outward current as well as the Ca^{2+}-inward current. This would lead to an increase in the actual membrane potential, reducing the Ca^{2+}-inward currents and thereby the local $[Ca^{2+}]_{cyt}$ around the SV channel. This would further reduce SV-channel activity, and with it $[Ca^{2+}]_{cyt}$, providing another positive feedback mechanism with opposite direction. If the activation/deactivation by $[Ca^{2+}]_{cyt}$ is much faster than the voltage-dependent deactivation, this process could rapidly reduce the outward-current.

The speed of the voltage clamp plays a critical role here if these fast feedback processes can escape the voltage control of the amplifier, leading to even bigger changes in membrane potential. And with a large R_a the speed is much reduced, promoting the generation of oscillations. With reasonably fast voltage-control the feedback mechanism might be suppressed, resulting in slowly developing steady-state currents.

While this proposed mechanism is purely hypothetical, it can explain the oscillations adequately taking into account a minimum of known factors. Since 1 μM $[Ca^{2+}]_{cyt}$ is at the low end of the activation range of Ca^{2+} concentrations for the SV channel, a large fraction of the channels might not be activated. Furthermore, assuming a fast Ca^{2+}-dependent activation, this might also explain the observed overshoot of tail currents. At membrane potentials below the Nernst potential for

Ca^{2+}, E_{Ca}, Ca^{2+}-inward currents would locally increase the $[Ca^{2+}]_{cyt}$, thereby activating SV channels. Positive of E_{Ca}, the lack of Ca^{2+}-inward currents reduces the local $[Ca^{2+}]_{cyt}$, thus leading to smaller outward currents. Therefore, the activating prepulse at +100 mV had a smaller current amplitude than at membrane potentials below +80 mV (see Figure 6.21).

This hypothesis would explain the observed current oscillations as a mere artefact due to the combination of properties of the SV channel, the recording conditions, large currents and a large, uncompensated R_s. The very positive membrane potentials under which this phenomenon was observed makes a physiological relevance even more unlikely, given the small or negative membrane potential generally observed across the tonoplast (Bates *et al.*, 1982; Bethmann *et al.*, 1995).

The macroscopic currents seen in NMDG-Cl-based solutions at 1 mM $[Ca^{2+}]_{cyt}$ also had the characteristics of typical SV-currents, despite the absence of K^+ (Figure 6.45). But as noted already, the large inward currents and the positively shifted reversal potential during perfusion indicate insufficient vacuolar perfusion, with vacuolar cations not being quantitatively replaced. Given the high permeability of SV channels for Ca^{2+} and Mg^{2+} (Ward and Schroeder, 1994;Allen and Sanders, 1996; Pottosin *et al.*, 1997), outward currents observed in the absence of K^+ are likely to be SV currents carried by Ca^{2+} and Mg^{2+}. Very similar SV-type currents were reported by Ward and Schroeder (1994) with $CaCl_2$ replacing KCl on both sides of the membrane. These currents showed a very high selectivity for Ca^{2+} over Cl^-. In the present study, no tail-current recordings were obtained under asymmetric Cl^- or Ca^{2+} concentration, hence permeabilities could not be assigned for the NMDG-Cl-based recordings in *M. crystallinum*.

The increasing outward current in the presence of an inwardly directed NMDG-Cl gradient would be in line with a greater driving force for Cl^- (Figure 6.49). However, the fact that the deactivating currents after the test pulse were much increased and were all inwardly directed points to more activation of the outward-rectifying currents under these conditions.

It has been shown for a number of large organic cations that they are permeable inhibitors of SV channels (personal communication by Igor Pottosin, University of Colima, Mexico). The observed current increase might therefore be due to less inhibition of SV channels at lower $NMDG^+$ concentrations. Slow binding and inhibition by $NMDG^+$ would also explain the observed "run-down" of the current amplitudes during perfusion with NMDG-Cl based solutions. This run-down was not seen in KCl-based recordings. A similar reduction was seen in other experiments when the vacuolar solution was changed from 100 mM KCl to 100 mM NMDG-Cl (Figure 6.30). In contrast, 4 mM KCl did not lead to a significant reduction. This suggests an inhibitory effect of $NMDG^+$, rather than Cl^-, on the outward currents. While on the basis of these few experiments a Cl^- current cannot be absolutely ruled out, it seems most likely that the observed slow-activating outward currents are of the cation-selective SV-type.

At a low $[Ca^{2+}]_{cyt}$ of 100 nM, the whole-vacuolar currents resembled the FV-type (fast-activating vacuolar) currents seen in other studies under similar conditions. This type of current activates both at positive and negative membrane potentials, with an area of higher resistance between -20 and +20 mV, and is selective for K^+ (Hedrich and Neher, 1987; Allen and Sanders, 1996; Allen *et al.*, 1998). Due to the instantaneous activation of this current, the selectivity was difficult to determine, with

leak currents dominating the reversal potential. But the shift towards E_{Cl}, despite the large positive Nernst potentials for K^+ and Ca^{2+}, indicated a Cl^- selectivity of the leak currents. A more reliable way to determine the ion selectivity would be single-channel analysis at low $[Ca^{2+}]_{cyt.}$. But vacuolar-side-out patches could not be obtained due to the low Ca^{2+} in the pipette lowering the seal rate (Maathuis *et al.*, 1997). Only five patches could be obtained in the cytosolic-side-out configuration, and no clear single-channel events could be detected. The nature of the observed Cl^- conductance could therefore not be further specified. There have been no other studies reporting Cl^- channels under similar conditions.

Despite a considerable number of different single-channel types being observed in this study, no obvious Cl^- channel could be found. Only one recording showed a channel, LOR1, with a significant permeability for ions other than K^+ (Figure6.32). However, the observed reversal potential negative of E_K could be due to either Cl^- or Mg^{2+}. Since this channel did not seem to have any permeability for Ca^{2+}, a general permeability for divalent cations is perhaps less likely. This non-selective, 170 pS channel was seen only at very positive membrane potentials and with rather low open probabilities, putting its physiological role in doubt. At +80 mV (an unphysiological potential), it would only mediate Cl^- efflux from the vacuole. No further characterisation was possible, But it is conceivable that the gating might be regulated by other factors, thereby opening the channel at lower membrane potentials.

A similarly large channel was also seen in vacuoles from tobacco cell suspension cells by Ping *et al.* (1992) in $CaCl_2$-based solutions. It was only short lasting, with a conductance of 110 pS, and was highly selective for Cl^- over Ca^{2+}.

However, this channel was seen only at negative membrane potentials, and might therefore represent a different type.

All other channels observed in the present work showed rather high K^+ selectivities. Ca^{2+} permeabilities were not quantified, but some channels also showed clear shifts in the reversal potential towards E_{Ca} (KIV1, KIV2), even with high KCl. Given the heterogeneity of the recording conditions, and with some channels being recorded under highly asymmetric conditions only, it is difficult to compare these results with other studies. One of the voltage-independent K^+-selective channels might be of the VK type, which is activated by μM to mM $[Ca^{2+}]_{cyt}$ and has a reported conductance of about 70 pS (Ward and Schroeder, 1994; Allen and Sanders, 1996). KVIH2, KS1 and KS2 show conductances and selectivities in a similar range. Other channels, such as the small KVI1, KVI2 and KVIH3 channels might have significant Ca^{2+} permeabilities, especially at low KCl concentrations. However, no similar channel types could be found in the literature. Most vacuolar Ca^{2+} channels described have either much larger conductances, or show strong voltage dependence (Johannes *et al.*, 1992; Allen and Sanders, 1994).

While this study has provided an initial characterisation of the electrophysiological features of the *Mesembryanthemum crystallinum* leaf mesophyll tonoplast, it has failed to give clear evidence for the presence of Cl^--conducting channels. One obvious reason for the absence might be the loss of a cytosolic regulatory factor when isolating vacuoles. For example, in *Vicia faba* guard-cell vacuoles, Cl^--specific currents and single channels could only be observed after activation by a Ca^{2+}-dependent protein kinase (Pei *et al.*, 1996). Based on previous

electrophysiological characterisations of *Vicia faba* vacuoles, the authors managed to eliminate all FV, VK and SV currents that might otherwise mask any Cl^- current.

In order to test for current activation by protein kinases in *M. crystallinum*, it will be essential to use macropatches, since the success rate of whole-vacuole perfusion was generally very low. Other reports of vacuolar Cl^- currents have been rare. Malate-conducting anion channels have been shown to be highly selective for malate over Cl^- (Cerana *et al.*, 1995; Cheffings *et al.*, 1997). Also, *M. crystallinum* plants have not been electrophysiologically characterised under salt stress, which could regulate vacuolar Cl^- currents as a stress response. Attempts to patch-clamp vacuoles from salt-treated plants failed initially, because the lower-density vacuoles did not settle to the bottom of the recording chamber. Using glycerol rather than mannitol as an osmoticum reduced the specific density of the medium, hence improving the settling of vacuoles, but successful perfusion could not be accomplished.

Based on this initial characterisation, future work could usefully focus on regulatory factors that might activate Cl^- currents, and also on the impact of salt stress on the Cl^- conductivity of the tonoplast membrane. This should be done primarily at the single-channel or the macropatch level, since the power of the patch-clamp technique is limited by the large size of the intact vacuoles of *M. crystallinum*.

Chapter 7

General discussion

The aim of this work was to characterise the Cl^--uptake mechanism of vacuoles from leaf mesophyll cells of *Mesembryanthemum crystallinum*. Of particular physiological interest was the question whether passive transport would be sufficient, or whether active transport is required, to explain the accumulation of vacuolar Cl^- concentrations between 700 mM in mesophyll cells and up to 1 M in epidermal bladder cells *in vivo* (Adams *et al.*, 1998). The answer to this will provide important insight into the role of vacuolar Cl^- transport in salt tolerance in plants.

In isolated tonoplast vesicles of leaf mesophyll cells of *M. crystallinum*, Cl^- uptake could be demonstrated directly using the Cl^--sensitive fluorescent dye lucigenin. No evidence was found to support the existence of an ATP-dependent Cl^- uptake mechanism. Also, despite showing good V-type H^+-ATPase and Na^+/H^+ antiport activities, the isolated vesicles did not show any signs of Cl^- uptake by a putative Cl^-/H^+ antiport mechanism. This negative evidence obviously does not rule out the existence of a vacuolar H^+/Cl^- antiporter in *M. crystallinum*. Proteolysis, or the loss of functional subunits during the isolation of tonoplast vesicles, could have easily rendered the transporter inactive. Furthermore, the role of regulatory factors, such as cytosolic Ca^{2+}, or activation by phosporylation by protein kinases, was not explored further in this study. To maintain cellular Cl^- homeostasis, especially under salt stress, physiological regulators are likely to be important, so this might be an interesting question for future studies.

The fact that the observed Cl^- uptake was mediated neither *via* a putative Cl^--ATPase, nor *via* an H^+/Cl^- antiporter, makes a passive mechanism of transport likely. Very similar characteristics of vacuolar Cl^- transport in terms of its saturating concentration-dependence and its voltage-dependence were found in red beet (Pope and Leigh, 1988, 1990). These characteristics could be described by a three-state model for carrier-type reaction kinetics, also being consistent with channel mediated Cl^- transport (Pope *et al.*, 1990).

On the basis of the vacuolar Cl^--transport rates obtained in the present study, an approximate estimate of the expected currents can be made. Assuming an uncoupled Cl^- flux of around 31 nmol m^{-2} s^{-1}, the equivalent current density would be about 3 mA m^{-2} (multiplying the flux with the Faraday constant). For a whole vacuole with a diameter of 80 µm, this would be only about 60 pA, or about 1 fA for an average-sized vesicle with a diameter of 320 nm. These are current amplitudes well below the detection limit of the patch-clamp technique. It should therefore not be surprising that currents resembling the Cl^- uptake fluxes in vesicles could not be resolved in the patch clamp-recordings.

On the other hand, the low Cl^- transport rates observed raise the question whether they are sufficient to explain the vacuolar accumulation of Cl^- *in vivo*. On a whole vacuole basis (80 µm diameter), a flux of 31 nmol m^{-2} s^{-1} is equivalent to 6.3×10^{-17} mol $vacuole^{-1}$ s^{-1}. Assuming a doubling of the Cl^- transport rate with inside positive membrane potentials, and a further 60% increase under salt stress, the Cl^--transport rate might be increased to about 2×10^{-16} mol $vacuole^{-1}$ s^{-1}. With such a Cl^--uptake rate it would need around 3 years to accumulate 700 mM Cl^- in the large vacuolar lumen of mesophyll cells from *M. crystallinum*, a plant whose life cycle can

be completed in less than one hundred and fifty days. This suggests that *in vivo* the Cl^- uptake will have to be considerably upregulated, or that another Cl^- transport system might exist, which could not be detected in tonoplast vesicles. The fact that very similar Cl^- transport rates were measured for the uptake of $^{36}Cl^-$ in isolated barley vacuoles (Martinoia *et al.*, 1986) indicates that the low transport rates might not just be due to the detection method employed or loss of function during the vesicle preparation. It might rather suggest that isolated tonoplast membranes have low Cl^- transport rates in general. Since such a low transport rate cannot explain the observed accumulation, other Cl^- uptake mechanisms might exist that could not be detected in isolated vacuoles or tonoplast vesicles. In other electrophysiological studies on isolated vacuolar membrane of higher plants where Cl^- channel activity was reported, it lasted either only for a very short period (Ping *et al.*, 1992), or could be seen only after activation *via* a protein kinase (Pei *et al.*, 1996). This shows that vacuolar Cl^- channels are subject to tight physiological control by cytoplasmic factors, which could leave the Cl^- channels inactive in isolated tonoplast preparations.

Further studies on vacuolar Cl^- transport in *M. crystallinum* should therefore focus on investigating physiological factors that can activate vacuolar Cl^- channels. Using a wide range of cytoplasmic Ca^{2+} concentrations in the present studies represented a first attempt, but did not lead to detection of a distinct Cl^--selective channel. Another potential regulation mechanism is activation *via* a Ca^{2+}-dependent protein kinase (CDPK), which was shown to activate vacuolar Cl^- channels in *Vicia faba* (Pei *et al.*, 1996). With the imminent cloning and functional expression of a putative CDPK in *M. crystallinum* (personal communication, John Cushman, University of Arizona, USA), a species-specific kinase will be available. Other

regulatory factors to study will be cytosolic and vacuolar pH, since it was shown in the vesicle transport studies that pH directly affected vacuolar Cl^- uptake. Also, activation by calmodulin, dephosphorylation, or nucleotide binding should be explored.

In order to study the regulation of macroscopic currents in *M. crystallinum* vacuoles, it will be important to develop the macropatch technique further to obtain cytosolic-side out patches effectively. This will allow the fast perfusion of the cytoplasmic side of the membrane, which is essential to study the effect of regulatory factors. Alternatively, methods to reduce the vacuolar size or to break vacuoles of *M. crystallinum* into smaller vesicles need to be developed.

While this study did not find any evidence for the existence of H^+-coupled Cl^- uptake, the existence of such a transporter *in vivo* cannot be ruled out. A promising approach to answer the question whether active Cl^- uptake is needed to explain the observed Cl^- accumulation *in vivo* would be the use of ion-selective microelectrodes to determine Cl^- concentrations in the cytoplasm and vacuole. Impaling cells with Cl^--sensitive microelectrodes and determining the trans-tonoplast membrane-potential in *M. crystallinum* should give clear answers about the Cl^- gradients involved and about the role of the vacuolar membrane potential as a possible driving force for Cl^- uptake (Miller, 1995). Care should be taken for the fact that Cl^--selective micro electrodes poorly discriminate between NO_3^- and Cl^- (Miller, 1995), with intracellular NO_3^- concentrations up to 200 mM measured in *M. crystallinum* (Adams *et al.*, 1992).

Using this approach in glycophytes revealed only small tonoplast membrane potentials that could not account for the measured distribution of vacuolar and cytoplasmic Cl^- (Trebacz *et al.*, 1994; Bethmann *et al.*, 1995). However, the measured

Cl^- concentrations in the earlier microelectrode studies were generally low in both cytoplasm and vacuole. This approach has not been used so far on plants under salt stress conditions or in halophytes, where the total Cl^- concentrations in the whole cell usually reach several hundred mM. Estimates of cytoplasmic Cl^- concentrations under salt stress are mainly based on less reliable methods. In phloem exudate of barley, believed to reflect cytosolic ion concentrations, Cl^- concentrations of up to 50 mM were measured under salt stress (Munns *et al.*, 1986). Also, X-ray studies on salt-adapted tobacco cells revealed a cytosolic Cl^- concentration around 100 mM, and 600 mM in the vacuole (Binzel *et al.*, 1988). Other estimates for cytosolic Cl^- concentrations in halophytes indicated similar values (Flowers *et al.*, 1986). In isolated *M. crystallinum* chloroplasts, Cl^- concentrations were between 40 and 60 mM after prolonged salt stress (Demmig and Winter, 1986). Measuring the protein biosynthesis activity of a *in vitro* translation system from *Suaeda maritima* (a halophyte) revealed an optimum NaCl concentration around 100 mM, while in a similar system from wheat germ under identical conditions no activity could be detected above 80 mM NaCl (Flowers and Dalmond, 1992). This indicates that such high cytosolic Cl^- concentrations are not likely to be toxic in halophytes.

Based on those figures, cytosolic concentrations up to 100 mM Cl^- in the cytoplasm could be realistic in halophytes such as *M. crystallinum*. To allow the passive accumulation of 700 mM Cl^- in the vacuole, a tonoplast potential of around -50 mV would be required. So far, no reliable measurements for the vacuolar membrane potential of *M. crystallinum* exist. Measurements on glycophytes range from about 0 mV up to -60 mV (Bates *et al.*, 1982; Miller and Smith, 1992; Trebacz *et al.*, 1994; Bethmann *et al.*, 1995), so a vacuolar membrane potential of -50 mV

would be within the range observed. A passive uptake of Cl^- driven by the negative tonoplast membrane potential could therefore be feasible, but so far the thermodynamic evidence is only circumstantial. Direct measurements of the cytosolic and vacuolar Cl^- concentrations are needed, as well as reliable measurements of the trans-tonoplast potential.

The fact that only severe salt treatments significantly increased the vacuolar Cl^- uptake rates suggests that the basic transport capacity might be sufficient to cope with moderate salt stress. Also, the V-type H^+-ATPase activity showed an increase only under more severe salt treatment in the present study. Sufficient vacuolar ion-transport rates and H^+-pump activities to cope with salt stress, without the need for increased activities have also been found for in the halophyte *Suaeda maritima* (Maathuis *et al.*, 1992). Similarly, a recent study by Ratajczak *et al.* (1994) failed to detect any increases V-type H^+-ATPase activity in *M. crystallinum* under salt stress, but saw an increased in V-ATPase activity with progressing plant age. On the other hand, a number of studies have reported several-fold higher activities (Struve *et al.*, 1985; Barkla *et al.*, 1995; Tsiantis *et al.*, 1996; Vera-Estrella *et al.*, 1997). Also, the vacuolar Na^+/H^+-antiport activity was shown to increase under salt treatment in *M. crystallinum* (Barkla *et al.*, 1995). It remains unknown what causes this stark contrast in the different studies. Well defined growth conditions and standardised protocols for salt treatment, such as suggested by Adams *et al.* (1998), will certainly help to compare the results from different studies on the physiology of salt stress.

At the end of this thesis, a number of questions still remain unanswered. No evidence for active or H^+-coupled Cl^- transport could be found at the tonoplast, whereas all the data are in accordance with passive, membrane-potential-driven Cl^-

uptake. However, the actual mechanism still needs to be determined directly. Lucigenin as a Cl^--sensitive indicator has proven to be a powerful tool to study Cl^- transport, and complemented by macropatch and single-channel recordings on *M. crystallinum* vacuoles, it will provide the means for further investigations. Also, the observed low transport rates could indicate loss of Cl^- transport activity in isolated tonoplast vesicles and possibly also in isolated vacuoles. In future, studies on intact cells might also be feasible and would avoid possible loss of activity. The development of Cl^--sensitive, ratiometric dyes will be essential to allow such measurements (Jayaraman *et al.*, 1998). Alternatively, determining the actual Cl^- concentration gradients within the cell and reliably measuring the trans-tonoplast membrane-potential should unequivocally determine the thermodynamic requirements of vacuolar Cl^- accumulation in *M. crystallinum*.

References

Adams, P., Nelson, D. E., Yamada, S., Chmara, W., Jensen, R. G., Bohnert, H. J. and Griffiths, H., 1998. Growth and development of *Mesembryanthemum crystallinum* (Aizoaceae). *New Phytologist* **138**(2), 171-190.

Adams, P., Thomas, J. C., Vernon, D. M., Bohnert, H. J. and Jensen, R. G., 1992. Distinct cellular and organismic responses to salt stress. *Plant and Cell Physiology* **33**(8), 1215-1223.

Alexandre, J. and Lassalles, J. P., 1991. Hydrostatic and osmotic-pressure activated channel in plant vacuole. *Biophysical Journal* **60**(6), 1326-1336.

Allen, G. J. and Sanders, D., 1994. Two voltage-gated, calcium release channels coreside in the vacuolar membrane of broad bean guard cells. *Plant Cell* **6**(5), 685-694.

Allen, G. J. and Sanders, D., 1996. Control of ionic currents in guard cell vacuoles by cytosolic and luminal calcium. *Plant Journal* **10**(6), 1055-1069.

Allen, G. J., Sanders, D. and Gradmann, D., 1998. Calcium-potassium selectivity: kinetic analysis of current-voltage relationships of the open, slowly activating channel in the vacuolar membrane of Vicia faba guard-cells. *Planta* **204**(4), 528-541.

Amtmann, A., Laurie, S., Leigh, R. and Sanders, D., 1997. Multiple inward channels provide flexibility in Na^+/K^+ discrimination at the plasma membrane of barley suspension culture cells. *Journal of Experimental Botany* **48**(SISI), 481-497.

Armstrong, C. M. and Gilly, W. F., 1992. Access resistance and space clamp problems associated with whole-cell patch clamping. *Methods in Enzymology* **207**, 100-122.

Ayala, F., O'Leary, J. W. and Schumaker, K. S., 1996. Increased vacuolar and plasma membrane H^+-ATPase activities in *Salicornia bigelovii* Torr. in response to NaCl. *Journal of Experimental Botany* **47**(294), 25-32.

Ballesteros, E., Blumwald, E., Donaire, J. P. and Belver, A., 1997. Na^+/H^+ antiport activity in tonoplast vesicles isolated from sunflower roots induced by NaCl stress. *Physiologia Plantarum* **99**(2), 328-334.

Barkla, B. J. and Pantoja, O., 1996. Physiology of ion-transport across the tonoplast of higher-plants. *Annual Review of Plant Physiology and Plant Molecular Biology* **47**, 159-184.

Barkla, B. J., Zingarelli, L., Blumwald, E. and Smith, J. A. C., 1995. Tonoplast Na^+/H^+ antiport activity and its energization by the vacuolar H^+-ATPase in the halophytic plant *Mesembryanthemum crystallinum* L. *Plant Physiology* **109**(2), 549-556.

Bates, G. W., Goldsmith, M. H. M. and Goldsmith, T. H., 1982. Separation of tonoplast and plasma-membrane potential and resistance in cells of oat coleoptiles. *Journal of Membrane Biology* **66**(1), 15-23.

Bazzanella, A., Lochmann, H., Tomos, A. D. and Bachmann, K., 1998. Determination of inorganic cations and anions in single plant cells by capillary zone electrophoresis. *Journal of Chromatography a* **809**(1-2), 231-239.

Begenisich, T. and Melvin, J. E., 1998. Regulation of chloride channels in secretory epithelia. *Journal of Membrane Biology* **163**(2), 77-85.

Beilby, M., 1982. Cl^- channels in *Chara*. *Philosophical Transactions of the Royal Society of London Series B* **299**, 435-445.

Beilby, M. and Walker, N., 1981. Chloride transport in *Chara*. I. Kinetics and current-voltage curves for a probable proton symport. *Journal of Experimental Botany* **32**, 43-54.

Bennett, A. B. and Spanswick, R. M., 1983. Optical measurements of ΔpH and $\Delta\Psi$ in corn root membrane- vesicles - Kinetic analysis of Cl^- effects on a proton-translocating ATPase. *Journal of Membrane Biology* **71**(1-2), 95-107.

Bertl, A., Blumwald, E., Coronado, R., Eisenberg, R., Findlay, G., Gradmann, D., Hille, B., Kohler, K., Kolb, H. A., Macrobbie, E., Meissner, G., Miller, C., Neher, E., Palade, P., Pantoja, O., Sanders, D., Schroeder, J., Slayman, C.,

Spanswick, R., Walker, A. and Williams, A., 1992. Electrical measurements on endomembranes. *Science* **258**(5084), 873-874.

Bethmann, B., Thaler, M., Simonis, W. and Schönknecht, G., 1995. Electrochemical potential gradient of H^+, K^+, Ca^{2+}, and Cl^- across the tonoplast of the green alga *Eremosphaera viridis*. *Plant Physiology* **109**(4), 1317-1326.

Binzel, M. L., Hess, F. D., Bressan, R. A. and Hasegawa, P. M., 1988. Intracellular compartmentation of ions in salt adapted tobacco cells. *Plant Physiology* **86**(2), 607-614.

Biwersi, J., Tulk, B. and Verkman, A. S., 1994. Long-wavelength chloride-sensitive fluorescent indicators. *Analytical Biochemistry* **219**(1), 139-143.

Biwersi, J. and Verkman, A. S., 1991. Cell-permeable fluorescent indicator for cytosolic chloride. *Biochemistry* **30**(32), 7879-7883.

Blake-Kalff, M. M. A. and Coleman, J. O. D., 1996. Detoxification of xenobiotics by plant cells: Characterisation of vacuolar amphiphilic organic anion transporters. *Planta* **200**(4), 426-431.

Bohnert, H. J., Nelson, D. E. and Jensen, R. G., 1995. Adaptations to environmental stresses. *Plant Cell* **7**(7), 1099-1111.

Bolter, B., Soll, J., Schulz, A., Hinnah, S. and Wagner, R., 1998. Origin of a chloroplast protein importer. *Proceedings of the National Academy of Sciences of the United States of America* **95**(26), 15831-15836.

Bowman, E. J., Siebers, A. and Altendorf, K. H., 1988. Bafilomycins - a class of inhibitors of membrane ATPases from microorganisms, animal-cells, and plant-cells. *Proceedings of the National Academy of Sciences of the United States of America* **85**(21), 7972-7976.

Bradford, M. M., 1976. A rapid and sensitive method for the quantitation of microgram quantities of protein utilising the principle of dye-binding. *Analytical Biochemistry* **72**, 248-256.

Brearley, J., Venis, M. A. and Blatt, M. R., 1997. The effect of elevated CO_2 concentrations on K^+ and anion channels of *Vicia faba* L. guard cells. *Planta* **203**(2), 145-154.

Bremberger, C., Haschke, H. P. and Lüttge, U., 1988. Separation and purification of the tonoplast ATPase and pyrophosphatase from plants with constitutive and inducible Crassulacean acid metabolism. *Planta* **175**(4), 465-470.

Bremberger, C. and Lüttge, U., 1992. Dynamics of tonoplast proton pumps and other tonoplast proteins of *Mesembryanthemum crystallinum* L. during the induction of Crassulacean acid metabolism. *Planta* **188**(4), 575-580.

Buyse, G., Trouet, D., Voets, T., Missiaen, L., Droogmans, G., Nilius, B. and Eggermont, J., 1998. Evidence for the intracellular location of chloride channel (CIC)- type proteins: Co-localization of CIC-6a and CIC-6c with the sarco/endoplasmic-reticulum Ca^{2+} pump SERCA2b. *Biochemical Journal* **330**(Pt2), 1015-1021.

Canut, H., Brightman, A., Boudet, A. M. and Morre, D. J., 1990. Tonoplast vesicles of opposite sidedness from soybean hypocotyls by preparative free-flow electrophoresis. *Plant Physiology* **94**(3), 1149-1156.

Cerana, R., Giromini, L. and Colombo, R., 1995. Malate-regulated channels permeable to anions in vacuoles of *Arabidopsis thaliana*. *Australian Journal of Plant Physiology* **22**(1), 115-121.

Chao, A. C. and Mochizuki, H., 1992. Niflumic and flufenamic acids are potent inhibitors of chloride secretion in mammalian airway. *Life Sciences* **51**(18), 1453-1457.

Chao, A. C., Widdicombe, J. H. and Verkman, A. S., 1990. Chloride conductive and cotransport mechanisms in cultures of canine tracheal epithelial cells measured by an entrapped fluorescent indicator. *Journal of Membrane Biology* **113**(3), 193-202.

Cheffings, C. M., Pantoja, O., Ashcroft, F. M. and Smith, J. A. C., 1997. Malate transport and vacuolar ion channels in CAM plants. *Journal of Experimental Botany* **48**(SISI), 623-631.

Chifflet, S., Torriglia, A., Chiesa, R. and Tolosa, S., 1988. A method for the determination of inorganic phophate in the presence of labile organic phophate and high concentrations of protein: Application to lens ATPases. *Analytical Biochemistry* **168**, 1-4.

Cho, M. H. and Spalding, E. P., 1996. An anion channel in *Arabidopsis* hypocotyls activated by blue light. *Proceedings of the National Academy of Sciences of the United States of America* **93**(15), 8134-8138.

Coleman, H. A., 1986. Chloride currents in *Chara* - a patch-clamp study. *Journal of Membrane Biology* **93**(1), 55-61.

Coleman, J. O. D., Blake-Kalff, M. M. A. and Davies, T. G. E., 1997. Detoxification of xenobiotics by plants: Chemical modification and vacuolar compartmentation. *Trends in Plant Science* **2**(4), 144-151.

Cosgrove, D. J. and Hedrich, R., 1991. Stretch-activated chloride, potassium, and calcium channels coexisting in plasma-membranes of guard-cells of *Vicia-faba* L. *Planta* **186**(1), 143-153.

Crawford, R. M. M., 1989. *Studies in plant survival: Ecological case histories of plant adaptation to adversity.* Oxford, Blackwell Scientific Publications.

Cushman, J. C. and Bohnert, H. J., 1997. Molecular genetics of crassulacean acid metabolism. *Plant Physiology* **113**(3), 667-676.

Davies, J. M., 1997. Vacuolar energization: Pumps, shunts and stress. *Journal of Experimental Botany* **48**(308), 633-641.

Davies, J. M. and Sanders, D., 1995. ATP, pH and Mg^{2+} modulate a cation current in *Beta vulgaris* vacuoles - a possible shunt conductance for the vacuolar H^{+}-ATPase. *Journal of Membrane Biology* **145**(1), 75-86.

Davis-Kaplan, S. R., Askwith, C. C., Bengtzen, A. C., Radisky, D. and Kaplan, J., 1998. Chloride is an allosteric effector of copper assembly for the yeast

multicopper oxidase Fet3p: An unexpected role for intracellular chloride channels. *Proceedings of the National Academy of Sciences of the United States of America* **95**(23), 13641-13645.

Demmig, B. and Winter, K., 1986. Sodium, potassium, chloride and proline concentrations of chloroplasts isolated from a halophyte, *Mesembryanthemum crystallinum*. *Planta* **168**(3), 421-426.

Dietrich, P. and Hedrich, R., 1994. Interconversion of fast and slow gating modes of GCAC1, a guard-cell anion channel. *Planta* **195**(2), 301-304.

Dietrich, P. and Hedrich, R., 1998. Anions permeate and gate GCAC1, a voltage-dependent guard cell anion channel. *The Plant Journal* **15**(4), 479-487.

Duax, W. L., Griffin, J. F., Langs, D. A., Smith, G. D., Grochulski, P., Pletnev, V. and Ivanov, V., 1996. Molecular structure and mechanisms of action of cyclic and linear ion transport antibiotics. *Biopolymers* **40**(1), 141-155.

Eleno, N., Marin, J. J. G. and Boyd, C. A. R., 1992. DIDS shows substrate-like behaviour for the bile acid transporter of human placental basal membrane vesicles. *Journal of Physiology* **452**, 59P.

Elias, H., Henning, A. and Schwartz, D. E., 1971. Stereology: Applications to biochemical research. *Physiological Reviews* **51**, 158-200.

Elzenga, J. T. and Van Volkenburgh, E., 1997a. Kinetics of Ca^{2+}- and ATP-dependent, voltage-controlled anion conductance in the plasma membrane of mesophyll cells of *Pisum sativum*. *Planta* **201**(4), 415-423.

Elzenga, J. T. M. and Van Volkenburgh, E., 1997b. Characterization of a light-controlled anion channel in the plasma membrane of mesophyll cells of pea. *Plant Physiology* **113**(4), 1419-1426.

Evetts, V. (1998). Carboxylate transport at the vacuolar membrane of the CAM plant *Kalanchoe daigremontiana*. *St. Hugh's College*. Oxford, University of Oxford, 204.

Falke, L. C., Edwards, K. L., Pickard, B. G. and Misler, S., 1988. A stretch-activated anion channel in tobacco protoplasts. *FEBS Letters* **237**(1-2), 141-144.

Faraday, C. D. and Spanswick, R. M., 1995. Differential stimulation by Cl^- of H^+ transport and ATPase activity in purified plasma membrane vesicles from maize (*Zea mays* L.) roots. *Journal of Experimental Botany* **46**(290), 1169-1176.

Felle, H. H., 1994. The H^+/Cl^- symporter in root-hair cells of *Sinapis alba*. An electrophysiological study using ion-selective microelectrodes. *Plant Physiology* **106**(3), 1131-1136.

Fischer, K., Weber, A., Brink, S., Arbinger, B., Schunemann, D., Borchert, S., Heldt, H. W., Popp, B., Benz, R., Link, T. A., Eckerskorn, C. and Flügge, U. I., 1994. Porins from plants - molecular-cloning and functional characterization of 2 new members of the porin family. *Journal of Biological Chemistry* **269**(41), 25754-25760.

Flowers, T., Troke, P. and Yeo, A., 1977. The mechanism of salt tolerance in halophytes. *Annual Review of Plant Physiology* **28**, 875-884.

Flowers, T. J. and Dalmond, D., 1992. Protein synthesis in halophytes - the influence of potassium, sodium and magnesium invitro. *Plant and Soil* **146**(1-2), 153-161.

Flowers, T. J., Hajibagheri, M. A. and Clipson, N. J. W., 1986. Halophytes. *Quarterly Review of Biology* **61**(3), 313-337.

Flowers, T. J. and Yeo, A. R., 1995. Breeding for salinity resistance in crop plants: Where next? *Australian Journal of Plant Physiology* **22**(6), 875-884.

Fricke, W., Leigh, R. A. and Tomos, A. D., 1994. Concentrations of inorganic and organic solutes in extracts from individual epidermal, mesophyll and bundle-sheath cells of barley leaves. *Planta* **192**(3), 310-316.

Fuks, B. and Homble, F., 1995. A voltage-dependent porin-like channel in the inner envelope membrane of plant chloroplasts. *Journal of Biological Chemistry* **270**(17), 9947-9952.

Garlid, K. D., Orosz, D. E., Modriansky, M., Vassanelli, S. and Jezek, P., 1996. On the mechanism of fatty acid-induced proton transport by mitochondrial uncoupling protein. *Journal of Biological Chemistry* **271**(5), 2615-2620.

Garrill, A., Tyerman, S. D. and Findlay, G. P., 1994. Ion channels in the plasma membrane of protoplasts from the halophytic angiosperm *Zostera muelleri*. *Journal of Membrane Biology* **142**(3), 381-393.

Gaxiola, R. A., Rao, R., Sherman, A., Grisafi, P., Alper, S. L. and Fink, G. R., 1999. The *Arabidopsis thaliana* proton transporters, AtNhx1 and Avp1, can function in cation detoxification in yeast. *Proceeding of the National Academy of Science* **96**(4), 1480-1485.

Gaxiola, R. A., Yuan, D. S., Klausner, R. D. and Fink, G. R., 1998. The yeast CLC chloride channel functions in cation homeostasis. *Proceedings of the National Academy of Sciences of the United States of America* **95**(7), 4046-4050.

Grabov, A., Leung, J., Giraudat, J. and Blatt, M. R., 1997. Alteration of anion channel kinetics in wild-type and *abi*1-1 transgenic *Nicotiana benthamiana* guard cells by abscisic acid. *Plant Journal* **12**(1), 203-213.

Gradmann, D., Blatt, M. R. and Thiel, G., 1993. Electrocoupling of ion transporters in plants. *Journal of Membrane Biology* **136**(3), 327-332.

Gradmann, D. and Hoffstadt, J., 1998. Electrocoupling of ion transporters in plants: Interaction with internal ion concentrations. *Journal of Membrane Biology* **166**(1), 51-59.

Greenway, H. and Munns, R., 1980. Mechanisms of salt tolerance in nonhalophytes. *Annual Reviews in Plant Physiology* **31**, 149-190.

Hajibagheri, M. A. and Flowers, T. J., 1989. Quantitative ion localization within *Suaeda maritima* cortical-cells using the combined techniques of freeze-substitution and X-ray- microanalysis. *Biochemical Society Transactions* **17**(2), 369-371.

Hall, M. A., Ed. 1976. *Plant structure, function and adaptation*. London, Macmillan Press.

Hamill, O. P., Marty, A., Neher, E., Sakmann, B. and Sigworth, F. J., 1981. Improved patch-clamp techniques for high-resolution current recording from cells and cell-free membrane patches. *Pflügers Archiv-European Journal of Physiology* **391**(2), 85-100.

Hare, P. D., Cress, W. A. and Van Staden, J., 1998. Dissecting the roles of osmolyte accumulation during stress. *Plant Cell and Environment* **21**(6), 535-553.

Hechenberger, M., Schwappach, B., Fischer, W. N., Frommer, W. B., Jentsch, T. J. and Steinmeyer, K., 1996. A family of putative chloride channels from *Arabidopsis* and functional complementation of a yeast strain with a CLC gene disruption. *Journal of Biological Chemistry* **271**(52), 33632-33638.

Hedrich, R., 1994. Voltage-dependent chloride channels in plant-cells - Identification, characterization, and regulation of a guard-cell anion channel. *Current Topics in Membranes* **42**, 1-33.

Hedrich, R. and Kurkdjian, A., 1988. Characterization of an anion-permeable channel from sugar beet vacuoles: Effect of inhibitors. *EMBO Journal* **7**(12), 3661-3666.

Hedrich, R., Marten, I., Lohse, G., Dietrich, P., Winter, H., Lohaus, G. and Heldt, H. W., 1994. Malate-sensitive anion channels enable guard-cells to sense changes in the ambient CO_2 concentration. *Plant Journal* **6**(5), 741-748.

Hedrich, R. and Neher, E., 1987. Cytoplasmic calcium regulates voltage-dependent ion channels in plant vacuoles. *Nature* **329**(6142), 833-836.

Heiber, T., Steinkamp, T., Hinnah, S., Schwarz, M., Flügge, U. I., Weber, A. and Wagner, R., 1995. Ion channels in the chloroplast envelope membrane. *Biochemistry* **34**(49), 15906-15917.

Heinemann, S. H.,1995. Guide to data acquisition and analysis. In: *Single-Channel Recording*. B. Sakman and N. E. New York, Plenum Press, 53-91.

Hilgemann, D. W., 1994. Channel-like function of the Na,K pump probed at microsecond resolution in giant membrane patches. *Science* **263**(5152), 1429-1432.

Hilgemann, D. W.,1995. The giant membrane patch. In: *Single-Channel Recording*. B. Sakman and N. E. New York, Plenum Press, 307-327.

Hinnah, S. C., Hill, K., Wagner, R., Schlicher, T. and Soll, J., 1997. Reconstitution of a chloroplast protein import channel. *EMBO Journal* **16**(24), 7351-7360.

Hörtensteiner, S., Vogt, E., Hagenbuch, B., Meier, P. J., Amrhein, N. and Martinoia, E., 1993. Direct energization of bile acid transport into plant vacuoles. *Journal of Biological Chemistry* **268**(25), 18446-18449.

Ibarz, E., Palmgren, M. G., Palazon, J., Pinol, M. T. and Serrano, R., 1994. Activation of plant plasma membrane H^+-ATPase by the non-ionic detergent Brij 58. *Biochimica et Biophysica Acta* **1196**(1), 93-96.

Illsley, N. P. and Verkman, A. S., 1987. Membrane chloride transport measured using a chloride-sensitive fluorescent-probe. *Biochemistry* **26**(5), 1215-1219.

Iwasaki, I., Arata, H., Kijima, H. and Nishimura, M., 1992. 2 types of channels involved in the malate ion-transport across the tonoplast of a crassulacean acid metabolism plant. *Plant Physiology* **98**(4), 1494-1497.

Jabs, T., Tschope, M., Colling, C., Hahlbrock, K. and Scheel, D., 1997. Elicitor-stimulated ion fluxes and $O2^-$ from the oxidative burst are essential components in triggering defense gene activation and phytoalexin synthesis in parsley. *Proceedings of the National Academy of Sciences of the United States of America* **94**(9), 4800-4805.

James-Kracke, M. R., 1992. Quick and accurate method to convert BCECF fluorescence to pH-i: Calibration in three different types of cell preparations. *Journal of Cellular Physiology* **151**(3), 596-603.

Jayaraman, S., Biwersi, J. and Verkman, A. S., 1998. Synthesis of cell-permeable dual-wavelength chloride sensitive fluorescent indicators for ratio imaging. *FASEB Journal* **12**(4 Pt1 SS), 2166.

Jentsch, T. J. and Günther, W., 1997. Chloride channels: An emerging molecular picture. *Bioessays* **19**(2), 117-126.

Jentsch, T. J., Günther, W., Pusch, M. and Schwappach, B., 1995. Properties of voltage-gated chloride channels of the ClC gene family. *Journal of Physiology-London* **482P**, S 19-S 25.

Johannes, E., Brosnan, J. M. and Sanders, D., 1992. Parallel pathways for intracellular Ca^{2+} release from the vacuole of higher-plants. *Plant Journal* **2**(1), 97-102.

Johannes, E., Crofts, A. and Sanders, D., 1998. Control of Cl^- efflux in *Chara corallina* by cytosolic pH, free Ca^{2+}, and phosphorylation indicates a role of plasma membrane anion channels in cytosolic pH regulation. *Plant Physiology* **118**(1), 173-181.

Kaestner, K. H. and Sze, H., 1987. Potential-dependent anion transport in tonoplast vesicles from oat roots. *Plant Physiology* **83**(3), 483-489.

Karniski, L. P., 1989. Activation of chloride-hydroxide exchange by *p*-chloromercuribenzoic acid in rabbit renal brush-border membranes. *Journal of Membrane Biology* **112**(1), 59-66.

Kearns, A., Cole, L., Hawes, C. R. and Evans, D. E., 1998. Establishment of low extracellular pH is essential for uptake of the fluorescent anionic dye hydroxypyrenetrisulfonate by suspension- cultured carrot cells. *Plant Physiology and Biochemistry* **36**(12), 879-887.

Keller, B. U. and Hedrich, R., 1992. Patch clamp technique to study ion channels from organelles. *Methods in Enzymology* **207**, 673-680.

Klein, M., Martinoia, E. and Weissenbock, G., 1997. Transport of lucifer yellow CH into plant vacuoles - evidence for direct energization of a sulphonated substance and implications for the design of new molecular probes. *FEBS Letters* **420**(1), 86-92.

Klink, R., Haschke, H. P., Kramer, D. and Lüttge, U., 1990. Membrane particles, proteins and ATPase activity of tonoplast vesicles of *Mesembryanthemum crystallinum* in the C-3 and CAM state. *Botanica Acta* **103**(1), 24-31.

Kourie, J. I., 1996. Oscillation of membrane currents during the action potential in *Chara corallina*: Modification and significance for repolarisation of the

membrane potential and salt sensitivity. *Australian Journal of Plant Physiology* **23**(3), 361-369.

Lambert, R. W., Bradley, M. E. and Mircheff, A. K., 1991. pH-sensitive anion exchanger in rat lacrimal acinar cells. *American Journal of Physiology* **260**(3 PART 1), G517-G523.

Linder, B. and Raschke, K., 1992. A slow anion channel in guard-cells, activating at large hyperpolarization, may be principal for stomatal closing. *FEBS Letters* **313**(1), 27-30.

Loew, L. M.,1993. Potentiometric membrane dyes. In: *Fluorescent and luminescent probes for biological activity*. W. T. Mason. London, San Diego, Academic Press, 151-160.

Ludewig, U., Pusch, M. and Jentsch, T. J., 1996. Two physically distinct pores in the dimeric CIC-0 chloride channel. *Nature* **383**(6598), 340-343.

Ludewig, U., Pusch, M. and Jentsch, T. J., 1997. Independent gating of single pores in CLC-0 chloride channels. *Biophysical Journal* **73**(2), 789-797.

Lurin, C., Geelen, D., Barbier-Brygoo, H., Guern, J. and Maurel, C., 1996. Cloning and functional expression of a plant voltage-dependent chloride channel. *Plant Cell* **8**(4), 701-711.

Lüttge, U., 1993. The role of crassulacean acid metabolism (CAM) in the adaptation of plants to salinity. *New Phytologist* **125**(1), 59-71.

Lüttge, U., Fischer, E. and Steudle, E., 1978. Membrane potentials and salt distribution in epidermal bladders and photosynthetic tissue of *Mesembryanthemum crystallinum* L. *Plant, Cell and Environment* **1**, 121-129.

Lüttge, U. and Ratajczak, R., 1997. The physiology, biochemistry and molecular biology of the plant vacuolar ATPase. *Advances in Botanical Research Incorporating Advances in Plant Pathology* **25**, 253-296.

Lutz, W. K., Wipf, H.-K. and Simon, W., 1970. Alkalikationen-Spezifität und Träger-Eigenschaften der Antibiotica Nigericin und Monesin. *Helvetica Chimica Acta* **53**(7), 1741-1746.

Maathuis, F. J. M., Flowers, T. J. and Yeo, A. R., 1992. Sodium chloride compartmentation in leaf vacuoles of the halophyte *Suaeda maritima* (L.) Dum. and its relation to tonoplast permeability. *Journal of Experimental Botany* **43**(254), 1219-1223.

Maathuis, F. J. M. and Prins, H. B. A., 1991. Inhibition of inward rectifying tonoplast channels by a vacuolar factor: Physiological and kinetic implications. *Journal of Membrane Biology* **122**(3), 251-258.

Maathuis, F. J. M., Taylor, A. R., Assmann, S. M. and Sanders, D., 1997. Seal-promoting solutions and pipette perfusion for patch clamping plant cells. *Plant Journal* **11**(4), 891-896.

MacRobbie, E. A. C., 1998. Signal transduction and ion channels in guard cells. *Philosophical Transactions of the Royal Society of London Series B-Biological Sciences* **353**(1374), 1475-1488.

MacRobbie, E. A. C. and Burman, T. G., 1989. Chloride fluxes during osmoregulation in *Chara*. *Journal of Experimental Botany* **40**(214), 551-558.

Marten, I., Busch, H., Raschke, K. and Hedrich, R., 1993. Modulation and block of the plasma membrane anion channel of guard cells by stilbene derivatives. *European Biophysics Journal* **21**(6), 403-408.

Martinoia, E., Schramm, M. J., Kaiser, G., Kaiser, W. M. and Heber, U., 1986. Transport of anions in isolated barley vacuoles: I. Permeability to anions and evidence for a chloride uptake system. *Plant Physiology* **80**(4), 895-901.

Meissner, S. T., 1996. Analysis of patch-clamp methods using vacuoles from red beet (*Beta vulgaris*) storage tissue seal resistance estimates, a resistance network model, exchange times in whole-vacuole configuration. *Plant Physiology* **111**(2 SS), 422.

Meyer, K., Ackermann, A., Fromter, E. and Korbmacher, C., 1996. Cell swelling activates ATP-dependent voltage-gated Cl^- channels in M-1 mouse cortical collecting duct (CCD) cells. *Kidney International* **50**(5), 1812.

Middleton, R. E., Pheasant, D. J. and Miller, C., 1996. Homodimeric architecture of a CIC-type chloride ion channel. *Nature* **383**(6598), 337-340.

Miller, A. J., 1995. Ion-selective microelectrodes for measurement of intracellular ion concentrations. *Methods in Cell Biology* **49**, 275-291.

Miller, A. J. and Smith, S. J., 1992. The mechanism of nitrate transport across the tonoplast of barley root cells. *Planta* **187**(4), 554-557.

Miller, A. J., Walker, D. J. and Leigh, R. A., 1995. Potassium homeostasis in barley root-cells - Measurements with triple-barreled ion-selective microelectrodes. *Journal of Cellular Biochemistry*(S19A SIA), 152-152.

Miszalski, Z., Slesak, I., Niewiadomska, E., Baczek-Kwinta, R., Lüttge, U. and Ratajczak, R., 1998. Subcellular localization and stress responses of superoxide dismutase isoforms from leaves in the C_3-CAM intermediate halophyte *Mesembryanthemum crystallinum* L. *Plant Cell and Environment* **21**(2), 169-179.

Müller, M. L., Irkenskiesecker, U., Rubinstein, B. and Taiz, L., 1996. On the mechanism of hyperacidification in lemon - Comparison of the vacuolar H^+-ATPase activities of fruits and epicotyls. *Journal of Biological Chemistry* **271**(4), 1916-1924.

Munns, R., 1993. Physiological processes limiting plant-growth in saline soils - some dogmas and hypotheses. *Plant Cell and Environment* **16**(1), 15-24.

Munns, R., Fisher, D. B. and Tonnet, M. L., 1986. Sodium ion and chloride transport in the phloem from leaves of sodium chloride-treated barley. *Australian Journal of Plant Physiology* **13**(6), 757-766.

Nelson, D., Koukoumanos, M. and Bohnert, H., 1999. *Myo*-inositol-dependent sodium uptake in ice plant. *Plant physiology* **119**, 165-172.

Nett, W. and Deitmer, J. W., 1996. Simultaneous measurements of intracellular pH in the leech giant glial cell using 2',7'-bis-(2-carboxyethy])-5,6-carboxyfluorescein and ion-sensitive microelectrodes. *Biophysical Journal* **71**(1), 394-402.

Niu, X., Bressan, A., Hasegawa, P. M. and Pardo, J. M., 1995. Ion homeostasis in NaCl stress environments. *Plant Physiology* **109**(3), 735-742.

Noh, B. and Spalding, E. P., 1998. Anion channels and the stimulation of anthocyanin accumulation by blue light in *Arabidopsis* seedlings. *Plant Physiology* **116**(2), 503-509.

O'Leary, J. W.,1985. Saline environments and halophytic crops. In: *Arid Lands - Today and tomorrow*. E. E. Whitehead, C. F. Hutchinson, B. N. Timmermann and R. G. Varady. London, Belhaven Press.

Palmgren, M. G., Sommarin, M., Ulvskov, P. and Larsson, C., 1990. Effect of detergents on the proton-ATPase activity of inside-out and right-side-out plant plasma membrane vesicles. *Biochimica et Biophysica Acta* **1021**(2), 133-140.

Pantoja, O., Dainty, J. and Blumwald, E., 1989. Ion channels in vacuoles from halophytes and glycophytes. *FEBS Letters* **255**(1), 92-96.

Pantoja, O., Dainty, J. and Blumwald, E., 1992a. Cytoplasmic chloride regulates cation channels in the vacuolar membrane of plant cells. *Journal of Membrane Biology* **125**(3), 219-229.

Pantoja, O., Gelli, A. and Blumwald, E., 1992b. Characterization of vacuolar malate and K^+ channels under physiological conditions. *Plant Physiology* **100**(3), 1137-1141.

Parker, D. R., Norvell, W. A. and Chaney, R. L.,1995. GEOCHEM-PC: A chemical speciation program for IBM and compatible personal computers. In: *Chemical equilibrium and reaction models*. R. H. Loeppert, A. P. Schwab and S. Goldberg, Soil Science Society of America/American Society of Agronomy; SSSA. **SP42**.

Pei, Z. M., Ghassemian, M., Kwak, C. M., McCourt, P. and Schroeder, J. I., 1998. Role of farnesyltransferase in ABA regulation of guard cell anion channels and plant water loss. *Science* **282**(5387), 287-290.

Pei, Z. M., Kuchitsu, K., Ward, J. M., Schwarz, M. and Schroeder, J. I., 1997. Differential abscisic acid regulation of guard cell slow anion channels in *Arabidopsis* wild-type and *abi1* and *abi2* mutants. *Plant Cell* **9**(3), 409-423.

Pei, Z. M., Ward, J. M., Harper, J. F. and Schroeder, J. I., 1996. A novel chloride channel in *Vicia faba* guard cell vacuoles activated by the serine/threonine kinase, CDPK. *EMBO Journal* **15**(23), 6564-6574.

Ping, Z., Yabe, I. and Muto, S., 1992. Identification of K^+, Cl^-, and Ca^{2+} channels in the vacuolar membrane of tobacco cell-suspension cultures. *Protoplasma* **171**(1-2), 7-18.

Plant, P. J., Gelli, A. and Blumwald, E., 1994. Vacuolar chloride regulation of an anion-selective tonoplast channel. *Journal of Membrane Biology* **140**(1), 1-12.

Plasek, J. and Sigler, K., 1996. Slow fluorescent indicators of membrane potential: A survey of different approaches to probe response analysis. *Journal of Photochemistry and Photobiology B Biology* **33**(2), 101-124.

Pope, A. J., Jennings, I. R., Sanders, D. and Leigh, R. A., 1990. Characterization of Cl^- transport in vacuolar membrane-vesicles using a Cl^- sensitive fluorescent probe: Reaction kinetic-models for voltage-dependence and concentration-dependence of Cl^- flux. *Journal of Membrane Biology* **116**(2), 129-137.

Pope, A. J. and Leigh, R. A., 1987. Some characteristics of anion transport at the tonoplast of oat roots, determined from the effects of anions on pyrophosphate-dependent proton transport. *Planta* **172**(1), 91-100.

Pope, A. J. and Leigh, R. A., 1988. The use of a chloride-sensitive fluorescent-probe to measure chloride transport in isolated tonoplast vesicles. *Planta* **176**(4), 451-460.

Pope, A. J. and Leigh, R. A., 1990. Characterization of chloride transport at the tonoplast of higher plants using a chloride-sensitive fluorescent probe - Effects of other anions, membrane-potential, and transport inhibitors. *Planta* **181**(3), 406-413.

Pottosin, II and Schönknecht, G., 1995. Patch-clamp study of the voltage-dependent anion channel in the thylakoid membrane. *Journal of Membrane Biology* **148**(2), 143-156.

Pottosin, II, Tikhonova, L. I., Hedrich, R. and Schönknecht, G., 1997. Slowly activating vacuolar channels can not mediate Ca^{2+}-induced Ca^{2+} release. *Plant Journal* **12**(6), 1387-1398.

Prabhananda, B. S. and Ugrankar, M. M., 1991. Nigericin-mediated H^+, K^+ and Na^+ transports across vesicular membrane - T-jump studies. *Biochimica et Biophysica Acta* **1070**(2), 481-491.

Pusch, M. and Neher, E., 1988. Rates of diffusional exchange between small cells and a measuring patch pipette. *Pflügers Archiv-European Journal of Physiology* **411**(2), 204-211.

Ramahaleo, T., Alexandre, J. and Lassalles, J. P., 1996. Stretch activated channels in plant cells: A new model for osmoelastic coupling. *Plant Physiology and Biochemistry* **34**(3), 327-334.

Ratajczak, R., 1994. The nonionic detergent Brij-58 conserves the structure of the tonoplast H^+-ATPase of *Mesembryanthemum crystallinum* L during solubilization and partial purification. *Botanica Acta* **107**(4), 201-209.

Ratajczak, R., Hille, A., Mariaux, J. B. and Lüttge, U., 1995. Quantitative stress responses of the V_0V_1-ATPase of higher plants detected by immuno-electron microscopy. *Botanica Acta* **108**(6), 505-513.

Ratajczak, R., Richter, J. and Lüttge, U., 1994. Adaptation of the tonoplast V-type H^+-ATPase of *Mesembryanthemum crystallinum* to salt stress, C_3-CAM transition and plant age. *Plant Cell and Environment* **17**(10), 1101-1112.

Rausch, T., Kirsch, M., Löw, R., Lehr, A., Viereck, R. and An, Z., 1996. Salt stress responses of higher plants: The role of proton pumps and Na^+/H^+-antiporters. *Journal of Plant Physiology* **148**(3-4), 425-433.

Rea, P. A., Li, Z. S., Lu, Y. P., Drozdowicz, Y. M. and Martinoia, E., 1998. From vacuolar GS-X pumps to multispecific ABC transporters. *Annual Review of Plant Physiology and Plant Molecular Biology* **49**, 727-760.

Rea, P. A. and Sanders, D., 1987. Tonoplast energization - 2 H^+ pumps, one membrane. *Physiologia Plantarum* **71**(1), 131-141.

Rockel, B., Lüttge, U. and Ratajczak, R., 1998. Changes in message amount of V-ATPase subunits during salt-stress induced C_3-CAM transition in *Mesembryanthemum crystallinum*. *Plant Physiology and Biochemistry* **36**(8), 567-573.

Rosenberg, L. A., Padgett, P. E., Assmann, S. M., Walling, L. L. and Leonard, R. T., 1997. Identification of mRNAs and proteins in higher plants using probes from the Band 3 anion transporter of mammals. *Journal of Experimental Botany* **48**(309), 857-868.

Sakmann, B. and Neher, E., Eds., 1995. *Single-channel recording*. New York, Plenum Press.

Sanders, D., 1980. The mechanism of Cl^- transport at the plasma membrane of *Chara corallina*. I. Cotransport with H^+. *Journal of Membrane Biology* **53**, 129-141.

Sanders, D.,1994. Proton-coupled chloride transport in plant cells. In: *Advances in Comparative and Environmental Physiology: Electrogenic Cl^- Transporters in Biological Membranes*. G. A. Gerencser. Berlin, Heidelberg, Springer Verlag. **19,** 81-107.

Schachtman, D. P., Kumar, R., Schroeder, J. I. and Marsh, E. L., 1997. Molecular and functional characterization of a novel low-affinity cation transporter (LCT1) in higher plants. *Proceedings of the National Academy of Sciences of the United States of America* **94**(20), 11079-11084.

Scherman, D. and Henry, J. P., 1980. Oxonol-V as a probe of chromaffin granule membrane potentials. *Biochimica et Biophysica Acta* **559**, 150-166.

Schmidt, C., Schelle, I., Liao, Y. J. and Schroeder, J. I., 1995. Strong regulation of slow anion channels and abscisic-acid signalling in guard-cells by

phosphorylation and dephosphorylation events. *Proceedings of the National Academy of Sciences of the United States of America* **92**(21), 9535-9539.

Schmidt, C. and Schroeder, J. I., 1994. Anion selectivity of slow anion channels in the plasma-membrane of guard-cells - large nitrate permeability. *Plant Physiology* **106**(1), 383-391.

Schönknecht, G., Hedrich, R., Junge, W. and Raschke, K., 1988. A voltage-dependent chloride channel in the photosynthetic membrane of a higher plant. *Nature* **336**(6199), 589-592.

Schroeder, J. I., 1995. Anion channels as central mechanisms for signal transduction in guard cells and putative functions in roots for plant-soil interactions. *Plant Molecular Biology* **28**(3), 353-361.

Schroeder, J. I. and Keller, B. U., 1992. 2 types of anion channel currents in guard-cells with distinct voltage regulation. *Proceedings of the National Academy of Sciences of the United States of America* **89**(11), 5025-5029.

Schroeder, J. I., Schmidt, C. and Sheaffer, J., 1993. Identification of high-affinity slow anion channel blockers and evidence for stomatal regulation by slow anion channels in guard cells. *Plant Cell* **5**(12), 1831-1841.

Schulz-Lessdorf, B. and Hedrich, R., 1995. Protons and calcium modulate SV-type channels in the vacuolar-lysosomal compartment: Channel interaction with calmodulin inhibitors. *Planta* **197**(4), 655-671.

Schumaker, K. S. and Sze, H., 1986. Calcium transport into the vacuole of oat roots: Characterization of H^+/Ca^{2+} exchange activity. *Journal of Biological Chemistry* **261**(26), 12172-12178.

Schumaker, K. S. and Sze, H., 1987. Decrease of pH gradients in tonoplast vesicles by NO_3^- and Cl^-: Evidence for proton-coupled anion transport. *Plant Physiology* **83**(3), 490-496.

Schwappach, B., Stobrawa, S., Hechenberger, M., Steinmeyer, K. and Jentsch, T. J., 1998. Golgi localization and functionally important domains in the NH_2 and

COOH terminus of the yeast CLC putative chloride channel Gef1p. *Journal of Biological Chemistry* **273**(24), 15110-15118.

Schwartz, A., Ilan, N., Schwarz, M., Scheaffer, J., Assmann, S. M. and Schroeder, J. I., 1995. Anion-channel blockers inhibit S-type anion channels and abscisic acid responses in guard cells. *Plant Physiology* **109**(2), 651-658.

Schwiebert, E. M., Morales, M. M., Devidas, S., Egan, M. E. and Guggino, W. B., 1998. Chloride channel and chloride conductance regulator domains of CFTR, the cystic fibrosis transmembrane conductance regulator. *Proceedings of the National Academy of Sciences of the United States of America* **95**(5), 2674-2679.

Skerrett, M. and Tyerman, S. D., 1994. A channel that allows inwardly directed fluxes of anions in protoplasts derived from wheat roots. *Planta* **192**(3), 295-305.

Smith, J. A. C., Uribe, E. G., Ball, E., Heuer, S. and Lüttge, U., 1984. Characterization of the vacuolar ATPase activity of the crassulacean- acid-metabolism plant *Kalanchoe daigremontiana*. Receptor modulating. *European Journal of Biochemistry* **141**(2), 415-420.

Spurr, A. R., 1969. A low-viscosity epoxy resin embedding medium for electron microscopy. *Journal for Ultrastructure Research* **26**, 31-43.

Stein, W. D., 1990. *Channels, carriers, and pumps: An introduction to membrane transport*. San Diego, London, Academic Press.

Struve, I. and Lüttge, U., 1987. Characteristics of magnesium-ATP-dependent electrogenic proton transport in tonoplast vesicles of the facultative crassulacean acid metabolism plant *Mesembryanthemum crystallinum* L. *Planta* **170**(1), 111-120.

Struve, I., Weber, A., Lüttge, U., Ball, E. and Smith, J. A. C., 1985. Increased vacuolar ATPase activity correlated with crassulacean acid metabolism induction in *Mesembryanthemum crystallinum* and *Kalanchoe blossfeldiana* cultivar Tom Thumb. *Journal of Plant Physiology* **117**(5), 451-468.

Swanson, S. J., Bethke, P. C. and Jones, R. L., 1998. Barley aleurone cells contain two types of vacuoles: characterization of lytic organelles by use of fluorescent probes. *Plant Cell* **10**, 685-698.

Terry, B. R., Tyerman, S. D. and Findlay, G. P., 1991. Ion channels in the plasma-membrane of *Amaranthus* protoplasts - one cation and one anion channel dominate the conductance. *Journal of Membrane Biology* **121**(3), 223-236.

Thiel, G., 1995. Dynamics of chloride and potassium currents during the action potential in *Chara* studied with action potential clamp. *European Journal of Biophysics* **24**, 85-92.

Thiel, G. and Dityatev, A. E., 1998. Transient activity of excitatory Cl^- channels in *Chara*: Evidence for quantal release of a gating factor. *Journal of Membrane Biology* **163**(3), 183-191.

Thiel, G., Homann, U. and Gradmann, D., 1993. Microscopic elements of electrical excitation in *Chara*: transient activity of Cl^- channels in the plasma membrane. *Journal of Membrane Biology* **134**, 53-66.

Thomine, S., Zimmermann, S., Guern, J. and Barbier Brygoo, H., 1995. ATP-dependent regulation of an anion channel at the plasma membrane of protoplasts from epidermal cells of *Arabidopsis* hypocotyls. *Plant Cell* **7**(12), 2091-2100.

Trebacz, K., Simonis, W. and Schönknecht, G., 1994. Cytoplasmic Ca^{2+}, K^+, Cl^- and NO_3^- activities in the liverwort *Concephalum conicum* L. at rest and during action potentials. *Plant Physiology* **106**(3), 1073-1084.

Tsiantis, M. S., Bartholomew, D. M. and Smith, J. A. C., 1996. Salt regulation of transcript levels for the c subunit of a leaf vacuolar H^+-ATPase in the halophyte *Mesembryanthemum crystallinum*. *Plant Journal* **9**(5), 729-736.

Tyerman, S. D., 1992. Anion channels in plants. *Annual Review of Plant Physiology and Plant Molecular Biology* **43**, 351-373.

Tyerman, S. D. and Findlay, G. P., 1989. Current-voltage curves of single chloride channels which coexist with two types of potassium channel in the tonoplast of *Chara corallina*. *Journal of Experimental Botany* **40**(210), 105-118.

Ullrich, C. I. and Novacky, A. J., 1990. Extracellular and intracellular pH and membrane-potential changes induced by K^+, Cl^-, $H_2PO_4^-$, and NO_3^- uptake and fusicoccin in root hairs of *Limnobium stoloniferum*. *Plant Physiology* **94**(4), 1561-1567.

Van den Wijngaard, P. W. J. and Vredenberg, W. J., 1997. A 50-picosiemens anion channel of the chloroplast envelope is involved in chloroplast protein import. *Journal of Biological Chemistry* **272**(47), 29430-29433.

Vasseur, M., Frangne, R. and Alvarado, F., 1993. Buffer-dependent pH sensitivity of the fluorescent chloride-indicator dye SPQ. *American Journal of Physiology* **264**(1 PART 1), C27-C31.

Vera-Estrella, R., Barkla, J. B., Bohnert, H. and Pantoja, O., 1997. Adaptation mechanisms of cell suspensions from the halophyte *Mesembryanthemum crystallinum* to salinity. *Plant Physiology* **114**(3 SS), 1669-1669.

Verkman, A. S. and Biwersi, J., 1995. Chloride-sensitive fluorescent indicators. *Methods in Neuroscience* **27**, 328-339.

Verkman, A. S., Takla, R., Sefton, B., Basbaum, C. and Widdicombe, J. H., 1989. Quantitative fluorescence measurement of chloride transport mechanisms in phospholipid-vesicles. *Biochemistry* **28**(10), 4240-4244.

Ward, J. M. and Schroeder, J. I., 1994. Calcium-activated K^+ channels and calcium-induced calcium release by slow vacuolar ion channels in guard cell vacuoles implicated in the control of stomatal closure. *Plant Cell* **6**(5), 669-683.

Weber, W. M., Liebold, K. M., Reifarth, F. W. and Clauss, W., 1995. The Ca^{2+}-induced leak current in *Xenopus* oocytes is indeed mediated through a Cl^- channel. *Journal of Membrane Biology* **148**(3), 263-275.

White, P. J. and Smith, J. A. C., 1989. Proton and anion transport at the tonoplast in crassulacean-acid-metabolism plants: Specificity of the malate-influx system in *Kalanchoe daigremontiana*. *Planta* **179**(2), 265-274.

Wilson, C. and Shannon, M. C., 1995. Salt-induced Na^+/H^+ antiport in root plasma-membrane of a glycophytic and halophytic species of tomato. *Plant Science* **107**(2), 147-157.

Winter, K., 1973. CO_2-Fixierungsreaktion bei der salzpflanze *Mesembryanthemum crystallinum* unter variierten Außenbedingungen. *Planta* **114**, 75.

Winter, K. and Lüttge, U., 1979. C_3-Photosynthese und Crassulaceen-Säurestoffwechsel bei *Mesembryanthemum crystallinum* L. *Berichte der Deutschen Botanischen Gesellschaft* **92**, 117-132.

Yamashita, K., Kasai, M., Yamamoto, Y. and Matsumoto, H., 1994. Stimulation of plasma-membrane H^+-transport activity in barley roots by salt stress - possible role of increase in chloride permeability. *Soil Science and Plant Nutrition* **40**(4), 555-563.

Yeo, A., 1998. Molecular biology of salt tolerance in the context of whole-plant physiology. *Journal of Experimental Botany* **49**(323), 915-929.

Zimmermann, S., Frachisse, J. M., Thomine, S., Barbier-Brygoo, H. and Guern, J., 1998. Elicitor-induced chloride efflux and anion channels in tobacco cell suspensions. *Plant Physiology and Biochemistry* **36**(9), 665-674.

Zimmermann, S., Thomine, S., Guern, J. and Barbier-Brygoo, H., 1994. An anion current at the plasma-membrane of tobacco protoplasts shows ATP-dependent voltage regulation and is modulated by auxin. *Plant Journal* **6**(5), 707-716.